1954

A study of the deformation texture and its variation in cold drawn nickel rods

Krishan Kumar Tangri

A STUDY OF THE DEFORMATION TEXTURE AND ITS VARIATION IN COLD DRAWN NICKEL RODS

A Dissertation

Presented to

the Faculty of the Graduate School

University of Missouri

In Partial Fulfillment

of the Requirements for the Degree

Doctor of Philosophy

---

by

Krishan Kumar Tangri

July 1954

ACKNOWLEDGEMENTS

The author would like to thank the International Nickel Company for support of the research fellowship under which this work was conducted and to express his gratitude to Mr. F. E. Allen of the Educational Service, for his aid in procuring the samples of nickel examined and for furnishing the analysis of the metal.

He is also indebted to the following:

Professor A. V. Kilpatrick, of the Mechanical Engineering Department, of the Missouri School of Mines and Metallurgy, for machining the spherical x-ray diffraction specimens.

Mr. Oliver F. Rhea, of the Mechanical Engineering Department, of the Missouri School of Mines and Metallurgy, for machining the 'spherical-specimen mount' and the 'disc-specimen mount'.

Mr. R. G. Knickerbocker, Chief of Minerals Technology Division of U. S. Bureau of Mines, Rolla, Missouri, for permission to use the 'Tukon Hardness Tester' in the experimental station of the U. S. Bureau of Mines at Rolla, Missouri.

The author would also like to acknowledge the aid and advice given by Dr. D. S. Eppelsheimer, Professor of Metallurgical Engineering, and to thank him for his enthusiasm and for the manner in which he made available his vast familiarity with the literature.

TABLE OF CONTENTS

LIST OF TABLES

LIST OF FIGURES

FIGURE PAGE

FIGURE PAGE

FIGURE PAGE

FIGURE PAGE

FIGURE PAGE

CHAPTER I

INTRODUCTION

The production of rods by cold drawing is a development of recent years as compared to other methods of fabrication. Though a good many investigations correlating the observed mechanical properties to the mill practices employed have been reported, the results nevertheless are more of a qualitative and empirical nature. It is well known that the physical properties of a metal product are related to its deformation textures which are characteristic of the metal and the fabricating method used. Thus a study of the deformation textures of cold-drawn rods, specially by x-ray diffraction techniques, should provide a much more precise and direct correlation of the mechanical properties of the product and the mill practice.

A. THE PROBLEM

Statement of the problem. This study was undertaken (1) to determine the textures developed in nickel during cold drawing, (2) to determine whether the effect of cold drawing is uniformly distributed over the cross-section of the drawn rod, and (3) to develop a satisfactory explanation of the observed deformation textures of cold drawn nickel.

Importance of the study. The presence of preferred orientation in a metal, its magnitude and variation, can cause marked changes in its mechanical properties and corrosion resistance. The only in-

vestigations reported in the literature on deformation textures of cold drawn nickel wires date back to early nineteen twenties. Because of the inherent limitations of the photographic techniques employed for texture studies in those early days, detailed and quantitatively reliable data can not be procured from such investigations. Furthermore, no work on the deformation textures of cold-drawn rods, as contrasted to the textures of cold drawn wires, has been encountered in the published literature.

It is known that in the case of cold-drawn wires, the tensile strength of the center portion of the wire is greater than that of the wire as a whole. This is a direct consequence of the characteristics of plastic flow in the cold drawing process and the deformation textures developing thereof. It seems reasonable to assume that in the case of a cold-drawn rod, because of its much greater cross-sectional area, there would exist a variation in texture and thereby a variation in the mechanical properties of its different concentric layers.

Thus it is evident that a study of the deformation textures and texture variation in a cold drawn rod should make possible a better understanding of the cold drawing process, and thereby a better control on the mill practice to produce a cold-drawn rod with the desired physical properties in the most economical way.

B. OUTLINE OF THE STUDY

The following material presented in this thesis is divided into four sections, review of the literature; previous history of the metal

investigated; experimental determination of pole figures and theoretical interpretation of texture data; and determination of variation in deformation and the resulting deformation texture in a cold drawn metal.

A description of the metal investigated is given in chapter III and the preparation and x-ray examination of specimens for pole figure work is discussed in chapter IV. Experimental determination of thickness of the metal layer disturbed during the preparation of x-ray specimens is dealt with in Appendix I. A detailed description of the construction and use of a new specimen mount for pole figure determination is given in Appendix II. The results of the experimental work for pole figure determination is presented in chapter V and a theoretical consideration of the fibre textures of cold drawn nickel are discussed in chapter VI. Validity of the pole figure data for drawn metal is considered in chapter VII.

Chapter VIII deals with the experimental determination of variation in deformation and deformation textures in cold drawn nickel, The effect of annealing at various temperatures on the distribution of texture is also discussed. A detailed description of the x-ray technique used for the study of the variation in texture is given in Appendix III.

Chapter IX is devoted to the study of variation in hardness on the cross-section of the cold-drawn nickel rods. Macrographs of the various cold drawn rods are also included in this chapter. A study of microstructures at various distances from the fibre axis on the cross-section of cold drawn and subsequently annealed nickel rods

is reported in chapter X. Limitations of the pole figure method for orientation studies in metals showing inhomogeneous texture is discussed in Appendix IV.

CHAPTER II

REVIEW OF THE LITERATURE

The literature on nickel, cold drawing methods, pole figure techniques, and x-ray techniques is much too voluminous to permit a complete coverage of even one of these topics. Only a brief sketch of the cold drawing method and a short summary of the more important basic papers on pole figures, x-ray techniques, deformation textures, etc. which are directly related to the problem studies can be given.

A. LITERATURE OF THE COLD DRAWING PROCESS

Historical background of the cold-drawing process. It is a matter of record that the die block method for drawing wires was in operation as early as the Eighth Century, and it is well known that wire drawing on a commercial scale was being practiced in Europe as early as the Thirteenth Century.

The first wire drawn in this country was in New England in 1775, and from that date to about 1860, the materials used for wire were wrought iron, copper, brass, bronze, etc. It was at about this time that Bernard Lauth patented a cold rolling process for wrought iron. By this method, rounds larger than wire sizes were cold finished by passing a hot rolled bar, cleaned of scale, repeatedly through rolls, effecting a light reduction in each pass, until the desired size was obtained. The resultant product, generally speaking, was quite similar to the present cold-drawn bar product in appearance,

finish, size, accuracy and physical characteristics.

But, as a commercial production method, cold rolling is a comparatively slow and cumbersome process. In around 1900, after the similarity in the general characteristics of cold-rolled shafting and cold-drawn wire products became fully recognized, it followed that producers of cold-rolled shafting developed cold drawing methods, patterned after wire drawing practices to accommodate bar sizes.

Cold-drawing process. Bars, rods, wires and shapes with a bright clean surface, accurate dimensions and varying tensile strength are usually obtained by cold drawing. Generally, such a bar is first hot worked down to a certain size and then cold finished.

In the drawing process the metal is pulled by tension force through a tapered die. A compression force originates between the working surface of the die and the metal, and this is the actual forming stress. Regarding the cold-drawing practice itself, the order of major operations follows: (a) pickling; (b) washing with water and liming; (c) pointing; (d) cold drawing; (e) straightening. Each of these steps will be discussed very briefly.

The purpose of acid pickling is to remove the hot rolling scale which if allowed to remain on the bar would mar the cold-drawn finish and damage the dies. After proper pickling, the material is washed thoroughly with a water stream. Though washing with water dilutes any free acid present on the material, yet there would be some free acid remaining which if not removed would cause subsequent pitting and

corrosion, both of which would be objectionable in a cold-drawn product. Consequently the material, after washing, is dipped into a slaked lime emulsion which serves a two-fold purpose. First, any free acid present is neutralized, and second, the lime forms a porous surface layer which serves as an ideal base for the lubricant.

One end of the rod is then pointed so that it can be introduced into the die and attached to the pulling head. The pointing is usually done in swagers with conical or cylindrical dies, and in forging rolls or in presses equipped with swaging dies. The actual drawing operation consists of pulling or drawing the pickled and limed hot-rolled bars through a die by means of a so-called draw bench mechanism.

The cold-drawn products are usually straightened to meet the exacting straightness requirements. For cold-drawn rounds, by far the most popular type of straightening is the Medart. Briefly, this machine is a cross roll type consisting of one concave and one straight roll. The bar to be straightened is fed horizontally between the cross rolls which if set to give sufficient pressure to straighten, propel it through the rolls at a feed per bar revolution dependent upon the bar size and angle of the rolls. Not only is the bar straightened to fairly close accuracy but it is also polished to some extent due to the burnishing or wiping action of the rolls. Moreover, straightening also decreased the magnitude of the residual stresses (Fig. 1), there-

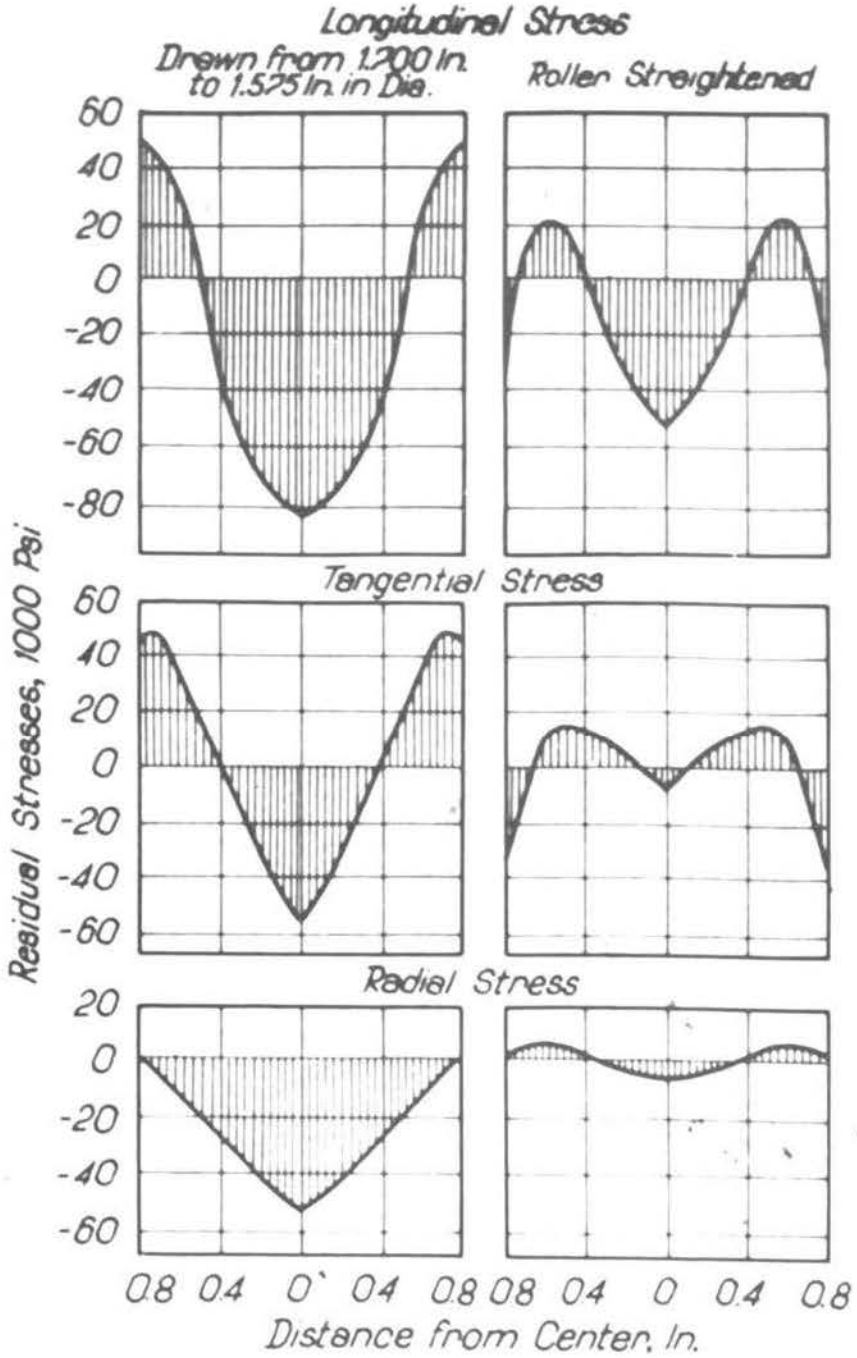

FIGURE 1. Residual stresses in drawn bessemer steel rods before and after straightening. (Sachs and Van Horn).

by decreasing the tendency for cracking[1].

Development of compressive stresses in the drawing process. In the drawing process the stress directly caused by the applied force is that of tension. However, this tensile stress is usually smaller than the reactive compressive stresses developed in directions perpendicular to that of the applied force. The metal then flows under the continued action of tensile and compressive stresses. It is for this reason that the drawing process is classified as an Indirect-Compression-type-working method.

Another characteristic of such indirect-compression-type-working processes is the large variations in the stresses over the volume of the deformed article. Thus, in almost all drawing processes the applied forces create tensions of considerable magnitude in the vicinity of the locations where they attack. "With increasing distance from these locations", according to Sachs[2], "the compressive stresses become more and more predominant and the tensile stresses fade out entirely at the edges of the regions that are being deformed".

The distribution of stresses in the most common of the drawing processes, the drawing of rod or wire, is shown in figure 2. The applied force in this case is tension and it creates longitudinal, or

---

1 G. Sachs, and Van Horn, Practical Metallurgy, (A.S.M. Publication, 1940), p. 388.

2 G. Sachs, Fundamentals of the Working of Metals, (London: Pergamon Press, 1954), p. 90.

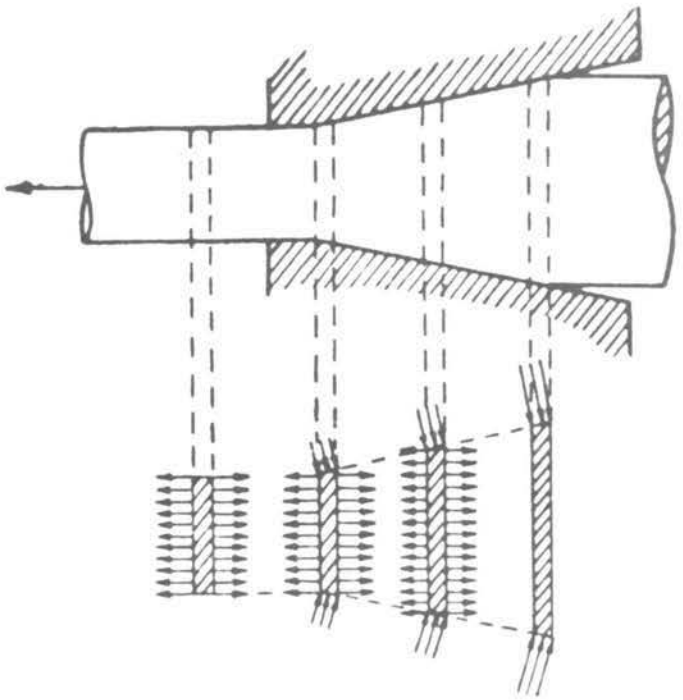

FIGURE 2. Distribution of stresses in different sections of a drawn rod (Sachs).

axial, tensile stresses in the metal on the exit side of the drawing die. Within the drawing die the tension is supplemented by radial compressive stresses and, as a consequence of the decrease in dimensions in all directions, also by circumferential compressive forces. Towards the entry side of the drawing die, the tensions in the metal decrease while the compressive stresses increase correspondingly. Directly at the entry the tensions fade out entirely and compressive stresses perform the entire work of deforming the metal.

Distribution of deformation in the drawing process. Scientific investigations of the forming processes began with the work of Tresca[3] and Obermayer[4], in the second half of the preceeding century, on the discharge of plastic substances through orfices. Significantly, the flow of material was first investigated in a comparitively simple way by means of the imbedded strata, whereas measurements of the deforming forces with the facilities then available presented much greater difficulties. Similar test methods have been applied in many cases, even in the most recent investigations.

Theoretical investigations of the deformation of a body were

---

3 H. Tresca, Memoires sur l'ecoulement des corps solides; Ann. du conservatoire des arts et metiers, 1865; Comptes rendus, 1867.

4 A. V. Obermayer, Versuche uber den Ausfluss plastischen Tones; Ber. d. Kaiserl. Akad. d. Wissensch., Wein 1868, p. 737.

conducted by Unkel in 1928[5, 6]. According to him, the deformation of a body element bounded by mutually perpendicular surfaces can be resolved into a deformation normal to the bounding surfaces of the element and additional shear deformations. If the boundaries are so selected that two opposite limiting surfaces lie perpendicular to a direction of principal stress, as is the case, if a limiting surface lies in a plane of symmetry, then shear deformations are possible only in the planes which are normal to the limiting surfaces.

In each continuous forming process, moreover, the same curvature must exist after the forming in all cross-sections lying perpendicular to the axis of the bar; because all fibres certainly undergo the same overall extension in the direction of the axis of the bar. Accordingly, if a cross-section is curved after forming, the condition of deformation existing at each point of the bar thereby is determined. Siebel[7] has investigated the distortion to which a co-ordinate, constructed of unit intervals in the longitudinal and transverse sections, is subjected during deformation. He concluded that the deformation during the forming process occurs as a simple elongation, corresponding in amount to the reduction of cross-sectional area of the bar, only in

---

5 H. Unkel, Uber die Fleissbewegung in Plastischem Material (Berlin: J. Springer, 1928).

6 H. Unkel, "Einiges uber die fleissbewegung beim Pressen von Stangen und Rohren sowie beim Ziehen", Z. Metallk., Vol. 20 (1928), p. 323.

7 E. Siebel, "The plastic forming of metals", Steel, Vol. 94 (1934), No. 12, p. 28.

the direct vicinity of the axis of the bar. All body elements not lying at the axis of the bar must indeed undergo the same elongation in the direction of the axis, because of the cohesion of the material; but additional displacements (shear deformations) parallel to the axis nevertheless occur, which usually have their highest values at the points where the direct effect of the forming tool is applied. Elongation and additional shear deformation at each particle produce a total deformation which differs in magnitude and direction from that of a particle at the axis of the bar.

The extent of the shear deformation has been revealed by experiments with assembled wires [8] and rods [9] consisting of two sections split through the center and the interface marked with a grid. Siebel [9] carried out the drawing tests on copper rods with varying die angle and varying reduction of cross-sectional area, in order to acquire an insight into the manner in which the relations of deformation are affected by these two factors, and to derive some conclusions regarding the condition of deformation which exists at higher degrees of deformation. Figs. 3-8 show the photographs (double magnification) of the separate halves of the rods after the test. Summarizing in his own words:

---

8 G. I. Taylor and H. Quinney, "The distortion of wires on passing through a draw plate", J. Inst. Metals (London), Vol. 49 (1932), pp. 187-202.

9 E. Siebel, "The plastic forming of metals", Steel, No. 12, pp. 28-30, No. 13, p. 38.

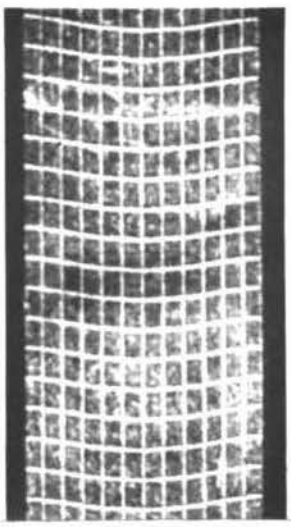

FIG. 3.

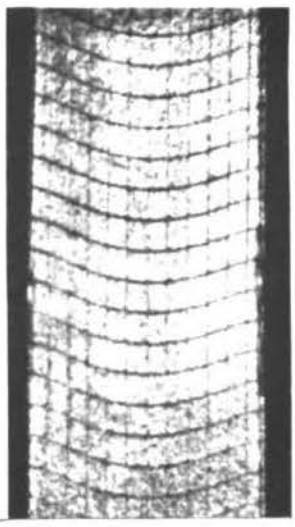

FIG. 4.

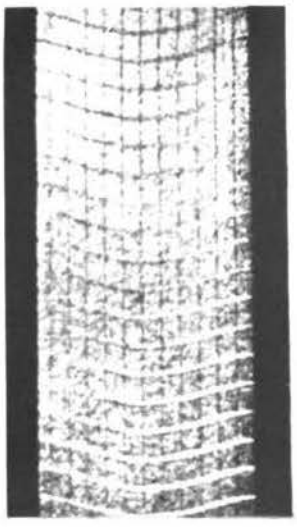

FIG. 5.

FIGURES 3, 4 and 5. Drawing tests on copper bars with 27.8 per cent reduction of area with die opening angles of 12, 24 and 40 degrees respectively.

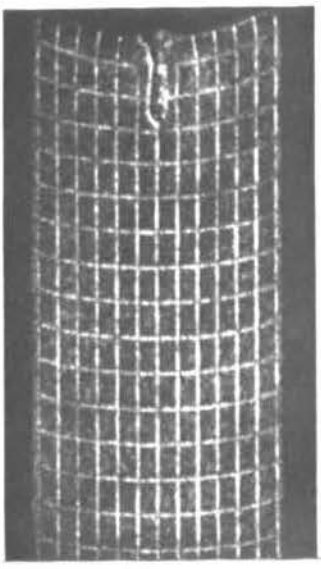

FIG. 6.

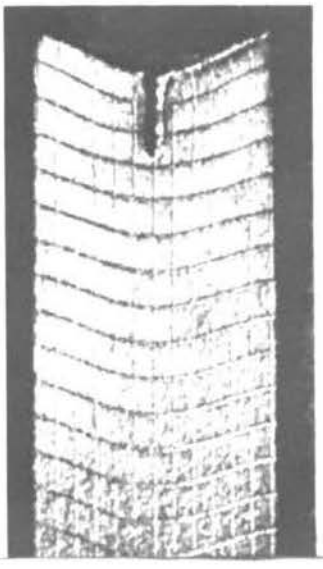

FIG. 7.

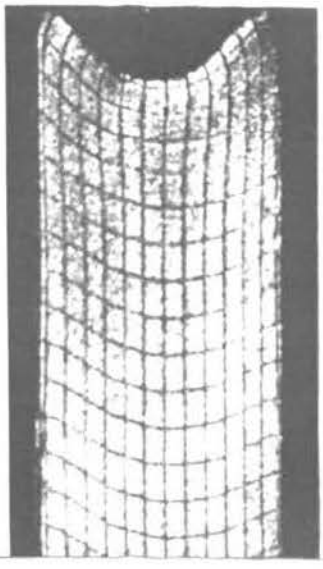

FIG. 8.

FIGURES 6, 7 and 8. Drawing tests on copper bars with 36.2 per cent reduction of area with die opening angles of 12, 24 and 40 degrees respectively.

> "It appears that the total deformations first increase with increasing distance from the central axis, where pure elongation prevails. With severe reduction of area and small opening angles of the dies (Fig. 123) [Fig. 6 in this text], the deformations increase up to the edge, but otherwise a decrease is observed in the outer zone (Figs. 120-122, 124 and 125) [Figs. 3-5, 7 and 8 in this text]. If the die angle increases, the elongation remaining unaltered, the additional shear deformations are increased; that is, the internal forming losses become higher".

Another interesting phenomenon which occurred in drawing through the 40-degree die deserves mention. Whereas the network of lines in all other draws was reproduced on the opposing surfaces by the pressure in the die, this was the case only at the edge zones in the 40-degree die. This was attributed to the fact that, because of the small effective die area, the effect of pressure does not penetrate deeply, which also has been shown by Pomp, Siebel and Hondremont [10]. Therefore, only the outer zones are deformed by the pressure of the walls of the die, while the central zone no longer is subjected to compressive stress.

B. LITERATURE OF THE TEXTURES RESULTING FROM THE DRAWING PROCESS

When a polycrystalline metal is plastically deformed, the lattice orientation in individual grains is altered toward a preferred orientation in which certain lattice directions are aligned with the principal directions of flow in the metal. The progress of this reorientation is gradual; and may not be completed until the metal has received reductions of 90% or more. The nature of the

---

10 A. Pomp, E. Siebel and E. Hondremont, "Uber den Kraft- und Arbeitsbedarf beim Kaltziehen von Drahten", Mitt. K. W. Inst. Eisenforsch., Vol. 11 (1929), p. 53.

preferred orientation, or "deformation texture", that is finally reached and the manner in which it is reached are characteristic of the metal and of the nature of the flow which is related to the way in which the metal was stressed.

Textures of drawn f.c.c. metals. The texture of a drawn metal is frequently described as "fibre texture" because it resembles the arrangement in natural fibrous materials. In the ideal case it consists simply of orientations having a definite crystallographic direction parallel to the wire axis. Deviations from an ideal texture are common and may have the nature of (1) a scatter about the ideal position or a random orientation superimposed upon the ideal texture, (2) a "double fibre texture", in which two different crystal directions are found in the axial position; and (3) a structure in which surface layers are disturbed by friction or other external factors[11].

Due to the disturbance of the surface layers as mentioned above, wires drawn through dies exhibit zonal structures in which the grains become more perfectly oriented as the center of the wire is approached. In an investigation made by Schmid and Wassermann[12], this effect has been strikingly displayed by the x-ray patterns of hard-drawn copper wire, taken after etching away successive layers

---

11 C. S. Barrett, Structure of Metals, (New York: McGraw-Hill Book Company, 1943), p. 382.

12 E. Schmid and G. Wassermann, Z. Physik, Vol. 42 (1927), p. 779.

from the surface. In the outermost skin of the wire, the effect of the die was to keep the grains with a [111] axis nearly parallel to the direction of drawing. Slightly below this the flow was distinctly conical, while the innermost portion again had a perfect fibre structure with [111] accurately in line with the axis of the wire. It was also found that the tensile strength of the center position was greater than that of the wire as a whole.

The wire texture in face-centered cubic metals is usually a double fibre texture with [111] and [100] parallel to the wire axis, i.e., that crystallites have either [111] or [100] parallel to the axis of the wire and have random orientations around this axis. The percentage of crystals in these two positions differ from metal to metal, as shown by the measurements of Schmid and Wassermann[13, 14], summarized in Table I. Lead[15] and Platinum[16] resemble Aluminum, with a single [111] texture. Brass containing more than 10 per cent Zinc resembles Silver, as does also Bronze containing 5 per cent Tin and Copper containing 30 per cent Silver[17].

---

13 Loc. cit.

14 E. Schmid and G. Wassermann, Naturwissenschaft, Vol. 17 (1929), p. 321.

15 W. Hofmann, Z. Metallkunde, Vol. 29 (1937), p. 266.

16 Gilbert Greenwood, Z. Krist, Vol. 78 (1931), p. 250.

17 G. v. Göler and G. Sachs, Z. Physik, Vol. 41 (1927), pp. 873, 889.

TABLE I

DOUBLE FIBRE TEXTURE IN FACE-CENTERED CUBIC METALS

Metal	Percentage of crystals	
	with [100] parallel to the wire axis	with [111] parallel to the wire axis
Aluminum	0	100
Copper	40	60
Gold	50	50
Silver	75	25

Texture of drawn nickel. The first published investigation of the texture of drawn nickel wire was by Ettisch, Polanyi and Weisenberg[18] in 1921. They found that nickel has a double fibre texture with [111] and [100] parallel to the wire axis. In the year 1929, Mazza and Nasini[19], while working with pure commercial nickel cold-drawn wires of 1 mm. diameter, reported that the x-ray photograms did not show the characteristics of a wire-drawing structure. However, in the same year, the work of Greenwood[20] confirmed the results of Ettisch, Polanyi and Weissenberg. No study of the textures of drawn rods has been encountered in this literature survey.

C. LITERATURE OF THE DETERMINATION OF POLE FIGURES

It was Wever[21] who first suggested in 1924, that the description of the orientation of metal crystals in a polycrystalline material could be given by the "pole figure" method, which is commonly used in crystallography to represent crystal symmetry. The technique developed by him, though laborious and time consuming, made it possible to represent the orientations of all the crystals in the

---

18 Ettisch, M. Polanyi and K. Weissenberg, Z. Physik., Vol. 7 (1921), p. 181.

19 L. Mazza and A. G. Nasini, Phil. Mag., Vol. 7 (1929), p. 301.

20 Greenwood, Z. Krist., Vol. 72 (1929), p. 309.

21 F. Wever, "The structure of cubically crystallizing metals after rolling", Z. Physik., Vol. 28 (1924), pp. 69-90.

metal by means of showing the actual intensity distribution instead of merely designating the positions in which the majority of the crystals seemed to be located.

There were only minor changes in the pole figure techniques during the following years. Almost all pole figures were made by x-ray photographic techniques [22], or by optical methods [23] involving the development of crystallographic etch pits on polished metal specimens. The only changes in technique involved slight modifications of sample preparation, mounting, etc.

In 1948 two papers were published which introduced methods for the adaptation of the Geiger counter x-ray spectrometer for pole figure determinations [24, 25].

The method developed by Decker, Asp, and Harper [24] requires a thin sheet x-ray sample which is placed in a special sample mount such that the transmission intensities can be read with the sample at various positions. Correction of the data thus obtained, however, is necessary to take into account absorption change and change in dif-

---

22 C. S. Barrett, The Structure of Metals, (New York: McGraw-Hill Book Company, 1943), pp. 154-163.

23 Ibid., pp. 173-177.

24 B. F. Decker, E. T. Asp, and D. Harker, "Preferred orientation determination using a Geiger counter x-ray diffraction goniometer", J. App. Phy., Vol. 19 (1948), pp. 388-92.

25 J. T. Norton, "A technique for quantitative determination of textures of sheet metals", J. App. Phy., Vol. 19 (1948) pp. 1176-78.

fracting volume as the sample changes position with respect to the x-ray beam. Unfortunately, this transmission method does not allow the center of the pole figure to be determined.

The method developed by Norton[25] requires the use of cylindrical samples machined with their axes bearing different angular relations to the reference axis. Since all the samples are cylindrical and of the same diameter, there is no absorption correction to be applied. Although this method allows complete pole figure coverage the time necessary to prepare a number of delicate samples and its applicability to only sheet metals makes the method very limited in its application.

In 1949, Schulz[26] developed a reflection technique which allows coverage of the central portion of the pole figure but does not give reliable data for its outer regions. Thus, by use of the Schulz reflection method in conjunction with the Decker transmission method, it is possible to obtain complete pole figure coverage while retaining the advantages of a sheet sample which is easy to prepare. In another article published by Schulz[27] in the same year, he has shown that the thickness of the transmission sample can be so controlled that the intensity correction necessary in the Decker method may be eliminated.

---

26 L. G. Schulz, "A direct method of determining preferred orientation of a flat reflection sample using a Geiger counter x-ray spectrometer", J. App. Phy., Vol. 20 (1949) pp. 1030-33.

27 L. G. Schulz, "Determination of preferred orientation in a flat transmission sample using a Geiger counter x-ray spectrometer", J. App. Phy., Vol. 20 (1949), pp. 1033-36.

Williams and Eppelsheimer[28] have incorporated the best features of the specimen mounts developed by Decker and Schulz into a universal specimen mount, which materially aids in the manipulation of the specimen.

In April 1952, in a weekly conference with his graduate students, Dr. D. S. Eppelsheimer suggested that the possibilities of employing a spherical x-ray specimen to eliminate intensity corrections should be explored. This author, then proceeded, under Dr. Eppelsheimer's advice, to design a specimen mount that would enable complete pole figure coverage. A progress report[29] on the design of such a mount was submitted in April 1953, to Dr. D. S. Eppelsheimer and also a copy to International Nickel Company, who supported this work.

Later, in May 1953, Jetter and Borie[30] published a paper describing a more elaborate specimen mount for spherical specimens, based on principles essentially similar to the ones previously mentioned[29].

---

28 D. N. Williams and D. S. Eppelsheimer, "Universal specimen mount for pole figure determination using the Schulz-Decker Technique", Univ. of Mo. Tech. Series, Bulletin No. 79.

29 K. Tangri, "X-ray diffraction techniques for studies in texture variation in successive concentric layers of a drawn metal rod", Unpublished progress report submitted to Dr. D. S. Eppelsheimer, April 1953.

30 L. K. Jetter and B. S. Borie, Jr., "A Method for the Quantitative Determination of Preferred Orientation", J. App. Phy., Vol. 24 (1953), pp. 532-535.

D. LITERATURE OF THE ORIGIN OF TEXTURES

Many attempts have been made to rationalize the behaviour of the crystallites of a polycrystalline material when subjected to forces of deformation, and thereby develop a satisfactory explanation of the observed tendency of the crystallites to align themselves in certain preferred crystallographic directions under the influence of such forces.

In 1923, Mark [31] and others postulated that each grain in a polycrystalline material acts essentially like a single crystal. The basis of their explanation was the occurrence of bend slipping or "Biegegleitung". To explain the external changes in shape of the crystal resulting from the applies stress, it was assumed that the bending moments produced by the applied stress cause the slip plane to rotate in such a direction that the active slip direction approaches the direction of flow. The deformation texture is a direct result of this rotation of slip direction toward the flow direction. Most of the theories of deformation textures, while retaining this idea of slip rotation or bend slipping, have differed chiefly in the number of slip systems that are assumed to operate.

In 1930, Wever and Schmid [32] suggested that in the deformation

---

31 H. Mark, M. Polanyi, and E. Schmid, "Processes in the stretching of zinc crystals", Z. Physik, Vol. 12 (1923), pp. 58-72, 78-110, 111-116.

32 F. Wever and W. E. Schmid, "Texture of cold-deformed metals", Z. Metallkunde, Vol. 22 (1930), pp. 133-40.

of a polycrystalline aggregate by tension or compression, the slip starts at first on the planes of maximum resolved shear stress. At the same time, each crystallite rotates about an axis lying in the slip plane at right angles to the slip direction. This rotation brings the deformation axis in a plane of symmetry between two active slip systems. At this stage, as the resolved shear stresses for both systems are equal, a second slip system simultaneously begins to operate, thereby producing the following ideal end orientations: for tension, a [111] position in the wire axis, and for compression a [110] direction in the axis of compression. To idealize the complex deformation process of rolling the authors assumed that the rolling stresses can be approximated by tension in the rolling direction and compression along the rolling plane normal. Wever and Schmid called it "plane parallelepipedal deformation". This theory, though successful in explaining many of the observed deformation textures, was not able to predict the occurrence of [100] position for the wire axis in drawing, which is observed experimentally in certain metals.

Later in 1931, Boas and Schmid[33] proposed that it is necessary to assume at least three active slip systems to explain the origin of deformation textures. The three slip systems are those for which the resolved shear stresses are maximum. When the stable end orientation is reached, the rotations due to slip on these systems cancel each other. Thus the final deformation texture is that which

---

33 W. Boas and E. Schmid, "The interpretation of the deformation textures of metals", Z. tech. Physik, Vol. 12 (1931), p. 71.

is stable for slip on the three most favorable slip systems. This theory was successful in accounting for both the [100] and the [111] components of the tension textures and for the [110] compression textures of face-centered cubic metals. Plane parallelepipedal deformation, as suggested by Wever and Schmid was assumed to predict rolling textures. Furthermore, it was assumed that those slip systems in tension which do not lead to a further diminution of the sheet thickness, do not operate during the rolling process.

Taylor[34] developed a mathematical theory based on the assumption of perfectly homogeneous deformation of the aggregate. For homogeneous deformation--such as will let grains fit together after deformation and will produce the same change of shape in the grains as in the aggregate as a whole--a minimum of five slip systems are required to operate simultaneously, as shown by the analysis of Mises[35]. The active slip systems were calculated using the principle of virtual work which states that the minimum number will function which can produce the required change in shape. As mentioned above, this number is five, except for special orientations. Furthermore, only that group of five is chosen for which the total work of deformation is less than for any other group.

---

34 G. I. Taylor, "Mechanism of plastic deformation of crystals", Proc. Royal Soc. (London), Vol. A145 (1934), pp. 362-404.

35 R. v. Mises, Z. angew. Math. Mech., Vol. 8 (1928), p. 161.

Taylor's method of analysis, though successful in predicting the textures of face-centered cubic metals, is too complex and unwieldy for application to other crystal structures. A further disadvantage of this method is that homogeneous deformation rarely occurs in practice.

Pickus and Mathewson[36] have developed a theory of the origin of rolling textures requiring unequal participation of at least three of the most favorable slip systems resulting in end positions in which the functioning slip directions are symmetrically disposed about the direction of flow so that the resolved shear stresses for all operative slip systems are equal and the rotations of the crystals cancel out. The three operative slip systems are assumed to be those for which the product of the resolved shear stress and cosine of the angle between the slip direction and the flow direction are highest. The relative probability of occurrence of each of the end positions is considered to depend on the values of the product function at the end position. The observed rolling textures in face-centered cubic metals and also the relative frequency of their occurrence was found to be in reasonable agreement with the predictions of this theory.

Hibbard and Yen[37] developed a semi-graphical method of pre-

---

36 M. R. Pickus and C. H. Mathewson, "On the theory of the origin of rolling textures in face-centered cubic metals", J. Inst. Met., Vol. 64 (1939), pp. 237-60.

37 W. R. Hibbard and M. K. Yen., "Wire textures of copper and its binary and solid solution alloys with aluminum, nickel, and zinc", Trans. AIME, Vol. 175 (1948), pp. 126-140.

dicting end orientations in the metals of face-centered cubic, body-centered cubic, and hexagonal systems. They postulated that the active slip systems of the individual grains of a polycrystalline aggregate in a stable end orientation are symmetrical with respect to the stress axis. Furthermore, in the ideal texture the active slip directions of each grain should be suitably oriented with respect to the flow direction to produce the required flow. For example, in simple tension the slip direction must be within forty-five degrees of the flow direction so that the component of flow in the desired direction is greater than that in directions normal to this. They pointed out that the [112] end position, observed for a single f.c.c. crystal in tensile stress, could not be expected to be stable in drawn wires because it provides only two slip directions which are within forty-five degrees of the wire axis and lie in a plane containing this axis. This would result in a wire of eliptical rather than circular cross-section. On the other hand, the [111] end position, which is found to be stable in polycrystalline wires of f.c.c. metals, provide three slip directions within forty-five degrees of the wire axis, and is thus better suited to yield a wire of circular cross-section.

In recent years, Calnan and Clews have developed a graphical method for analyzing tension, compression and cold rolling textures of face-centered cubic [38],

---

38 E. A. Calnan and C. J. B. Clews, "Deformation textures in face-centered cubic metals", Phil. Mag., Vol. 41 (1950), pp. 1085-1100.

body-centered cubic [39], and closed-packed hexagonal [40] metals. The assumption that only the slip system or systems of maximum resolved shear stress operate at any one point in the deformation process, as first suggested by Wever and Schmid, has been retained in this method. The method, however, differs from all previous methods in that the number of slip systems operative at any point is considered not to be dependent solely on the actual position of the crystallite. To explain the means by which the most favorable system or systems can apparently withstand resolved shear stresses greater than the critical value until the resolved shear stress on less favorable systems reaches the critical value, it is assumed that the effective stress position may move away from the applied stress position without actual physical movement of the crystal due to lateral stresses from the grain boundaries. In this way the variation in textures in different metals of the same crystal class can be explained. A fixed axis of rotation, as suggested by Wever and Schmid, is not assumed. Instead, the rotation of the crystal is considered to follow the laws established for single crystals, thus the direction of rotation may vary considerably with the orientation of the crystallites within the unit triangle.

---

39 E. A. Calnan and C. J. B. Clews, "The development of deformation textures in metals. Part II. Body-centered cubic metals", Phil. Mag., Vol. 42 (1951), pp. 616-35.

40 E. A. Calnan and C. J. B. Clews, "The development of deformation textures in metals. Part III. Hexagonal structures", Phil. Mag., Vol. 42 (1951), pp. 919-31.

This method has been successful not only in predicting the deformation textures in metals of all three common lattice types, but also in explaining the variation in textures observed in different metals belonging to the same lattice type.

As is apparent from the lack of agreement among different investigators as to the exact mode of rotation of an individual grain in a polycrystalline aggregate and also the number of active slip systems which must operate to produce the deformation textures as observed experimentally, the theory of the origin of textures is still in its early stages.

CHAPTER III

DESCRIPTION OF THE METAL INVESTIGATED

In this chapter all available information about the previous work history of the metal, the mill practice to produce the required amount of cold reduction, and the chemical analysis is given. Photomicrographs at the mid-radius of the rods with varying amounts of cold reduction are included, and the variation in their grain size discussed.

A. MILL HISTORY OF THE NICKEL RODS

A 1-5/8" diameter rod of twelve foot length was taken from hot rolled stock, and centerless ground to 1.580" diameter in three passes. The rod was pointed, annealed, pickled in acid solution, limed and drawn to 1-15/32" diameter using forum 45 drawing oil. The rod was then pickled, roughed to 1-3/8" diameter, pickled, and finished at 1.298" diameter. At this point one third of the rod was cut off and designated item number three. Item three was pickled, roughed to 1-3/16" diameter, pickled, roughed to 1-1/16" diameter, pickled and finished to size at 1.001" diameter, having a 60.0 per cent cold reduction.

The balance of the rod after cutting was annealed, pickled, roughed to 1-3/16" diameter, pickled and finished at 1.122" diameter. This rod was then cut in half and designated item numbers one and two. Item two was pickled and finished to 1.001" diameter, having a 40.5

per cent cold reduction. Item one was annealed after cutting and finished to 1.001" diameter, having a cold reduction of 20.6 per cent. The surface of all three items was satisfactory.

All the three rods were drawn through dies with a twenty two degree included angle approach and a fifty degree included angle entry. All intermediate annealing was done in the Cold Draw continuous annealing furnace at 1700°F and at speeds ranging from eight to sixteen inches per minute.

B. COMPOSITION OF NICKEL RODS

An analysis of the nickel rods was furnished with the material. This analysis was run by the International Nickel Company. The results of the analysis are given in Table II.

C. MICROSTRUCTURE AND GRAIN SIZE OF COLD DRAWN NICKEL

Photomicrographs at the mid-radius of the three cold drawn nickel rods with 20.6 (item no. 1), 40.5 (item no. 2) and 60 (item no. 3) per cent cold reduction respectively were made, and the grain size in each case was studied.

Microstructure of cold drawn nickel. A typical microstructure in the transverse and longitudinal directions at the mid-radius of each of the three nickel rods is given in Figures 9 through 14. The samples were mechanically polished and etched in Merica's solution consisting of equal parts by volume of nitric acid (70 per cent) and acetic acid (50 per cent).

TABLE II

REPORTED ANALYSIS OF NICKEL RODS

Element	Percent
C	0.08
Mn	0.23
Fe	0.09
S	0.005
Si	0.02
Cu	0.05
Ni (by difference)	99.525

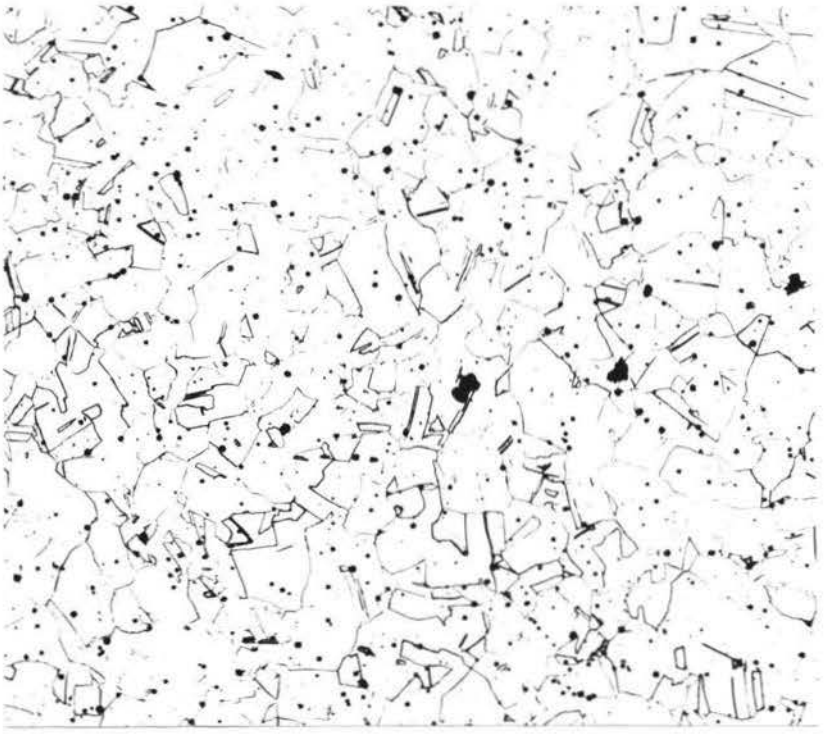

FIGURE 9. Transverse Section....x100

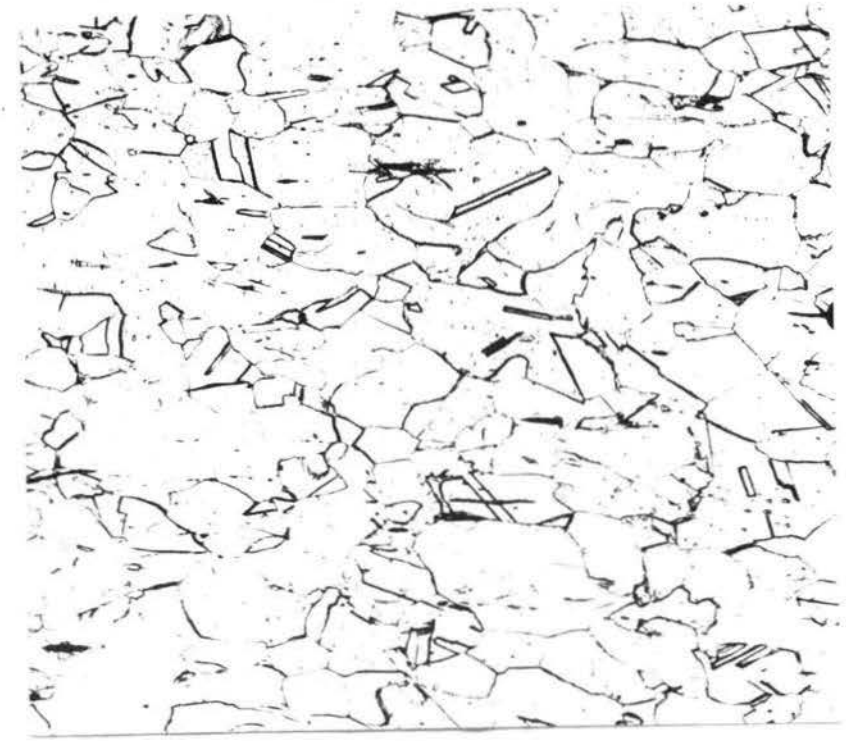

FIGURE 10. Longitudinal Section....x100

FIGURES 9 and 10. Photomicrographs at mid-radius of a 20.6 per cent cold drawn one inch diameter nickel rod.

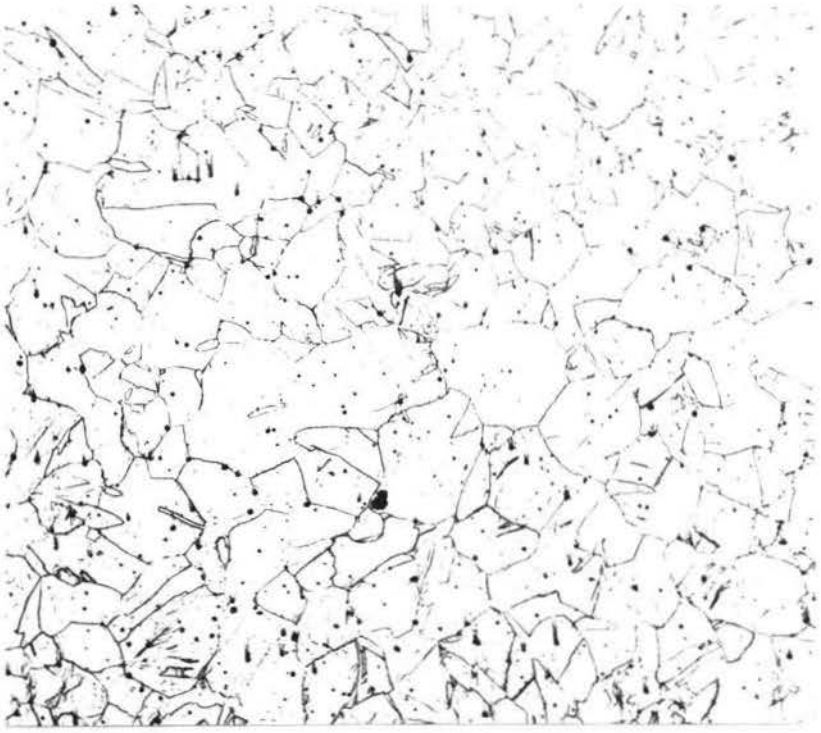

FIGURE 11. Transverse Section...x100

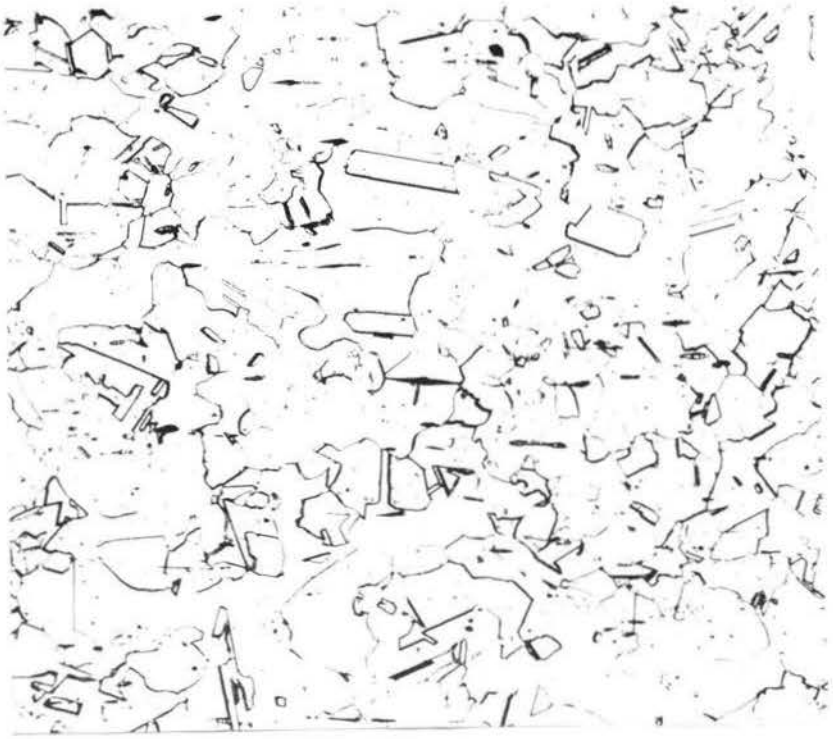

FIGURE 12. Longitudinal Section....x100

FIGURES 11 and 12. Photomicrographs at mid-radius of a 40.5 per cent cold drawn one inch diameter nickel rod.

FIGURE 13. Transverse Section....x100

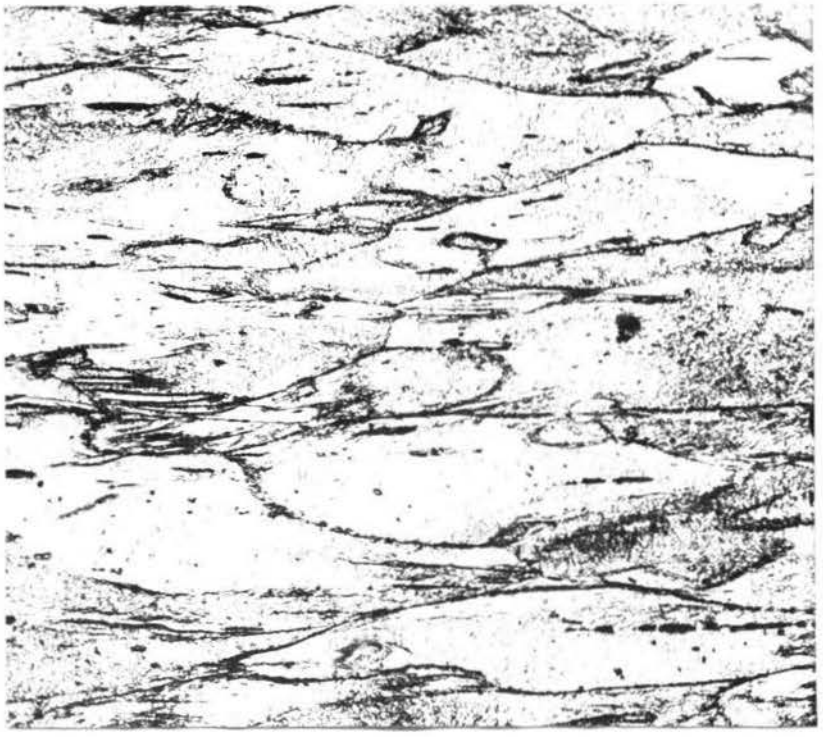

FIGURE 14. Longitudinal Section....x100

FIGURES 13 and 14. Photomicrographs at mid-radius of a 60 per cent cold drawn one inch diameter nickel rod.

Though the above etching solution gave the best results of all of those tried, still it was not entirely satisfactory as it seemed to develope only certain grain boundaries, probably only those separating grains with rather larger differences in orientation. This differential etching of different grain boundaries on the transverse section of the rod becomes more pronounced with progressively increasing cold work as is seen in Figures 9, 11 and 13 respectively. This seems to be a direct consequence of the fact that with increasing degree of drawing, the crystallites tend to align their [111] and [100] directions more and more along the fibre axis, thus decreasing the variation in orientation in a plane perpendicular to this axis. Though this phenomenon of differential etching of the different grain boundaries is also evidenced in the longitudinal sections of the 20.6 (item no. 1) and 40.5 (item no. 2) per cent cold drawn rods, as seen in Figures 10 and 12, yet it seems to be more or less random in nature in this direction.

Figures 9, 11 and 13, show the microstructure at the mid-radius of the transverse section of 20.6 (item no. 1), 40.5 (item no. 2) and 60 (item no. 3) per cent cold drawn nickel rods respectively at 100x. The first indication of deformation observable in the microstructure is given by the curvature of twin crystals, as seen in Figure 9. The curvature seems to increase with increasing amount of cold working as shown in Figures 9, 11 and 13. This indication is succeeded by the appearance of a secondary structure, consisting of groups of curved or wavy lines, within the grains themselves. The secondary structure is barely discernible in Figure 9, but becomes more prominent as we pass

to higher reductions as seen in Figures 11 and 13.

Figures 10, 12 and 14, show the microstructure at the mid-radius in the longitudinal direction of 20.6 (item no. 1), 40.5 (item no. 2), and 60 (item no. 3) per cent cold drawn nickel rods respectively at 100x. At a reduction of about 20 per cent, as in Figure 10, the direction of extension in cold drawing is apparent, in that the grains themselves show a prevailing direction of elongation. The elongation of the grains progressively increases with increasing amounts of reduction, as seen in Figures 12 and 14. The secondary structure within the grains of the microstructure in the longitudinal direction is shown only by the 60 per cent (item no. 3) cold reduced nickel, as seen in Figure 14.

The most difficult of the samples to prepare were the transverse and the longitudinal sections of the 60 per cent (item no. 3) cold drawn nickel. Their surfaces, as seen in Figures 13 and 14, show the effect of mechanical polishing even after repeated polishing and etching.

It will be noted from figures nine through fourteen, that the grain size in the 60 per cent (item no. 3) cold reduced rod is considerably larger than that of the 40.5 (item no. 2) and 20.6 (item no. 1) per cent cold reduced material. This apparent anomaly is due to the different work histories prior to cold drawing of the three samples as shown in the flow sheet of the mill practice. The 60 per cent (item no. 3) cold reduced rod was drawn from hot rolled and subsequently annealed stock which readily explains the large grain size of the finished product.

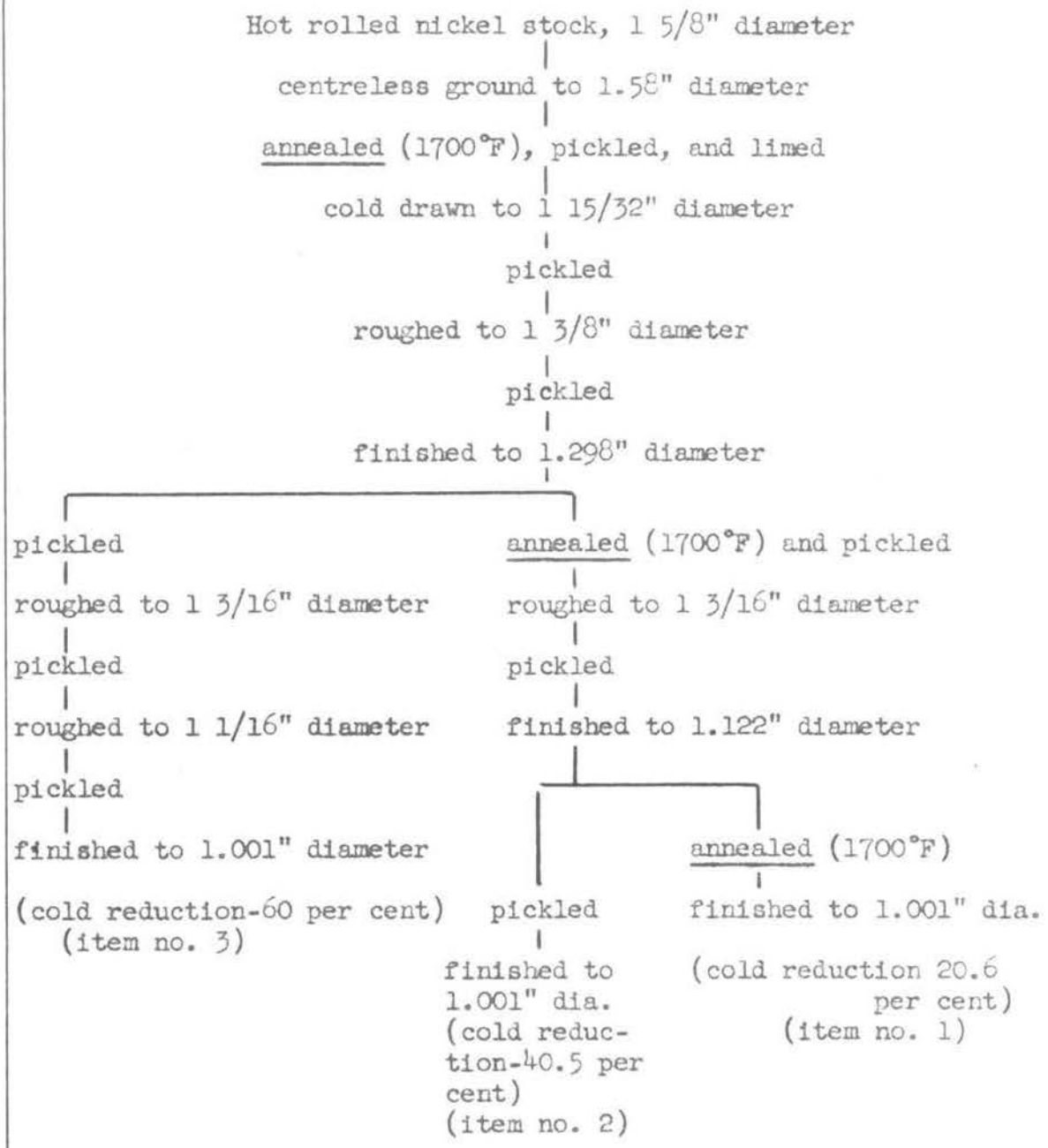

FIGURE 15. Flow sheet of cold-drawing operations to produce 1" diameter nickel rods with approximately 20, 40 and 60 per cent cold reduction.

During the production of the 60 per cent (item no. 3) cold drawn specimen, a portion of the hot rolled and subsequently annealed rod was cut after it had received approximately 25 per cent cold reduction. This portion of the rod, after an intermediate anneal, was used for drawing the 40.5 (item no. 2) and 20.6 (item no. 1) per cent cold reduced specimens. As is known, the annealing of a fairly cold worked material results in a much finer recrystallized grain structure. The whole rod after this intermediate anneal was cold reduced from a diameter of 1.187" to 1.122". At this stage the rod was cut into two parts. One of these was further cold drawn to produce the specimen with the 40.5 (item no. 2) percent cold reduction. The other half of the rod was given another intermediate anneal, after which it was drawn to effect a cold reduction of 20.6 per cent. Thus, it is evident from the above discussion that the intermediate anneals used at different stages of the mill practice prohibit any valid grain size comparison between the finished samples.

As the developement of deformation textures in polycrystalline aggregates is considered to be due to single and duplex slip rotations of the crystallites, the variation in grain size of the materials to which varying amounts of cold reductions were given, does not present a serious handicap as far as texture studies are concerned.

CHAPTER IV

THE PREPARATION AND X-RAY EXAMINATION OF SPECIMENS

Pole figures for the 20.6 (item no. 1), 40.5 (item no. 2) and 60 per cent (item no. 3) cold drawn nickel rods discussed in chapter III were determined using a new x-ray technique developed independently by this author and also by Jetter and Borie[41]. The unique feature of this technique is that a spherical x-ray diffraction specimen is employed.

This chapter deals with the experimental techniques involved in machining the spherical x-ray specimens, the determination of the depth to which the surface of the specimen was disturbed due to machining, and the removal of this disturbed metal by electro-etching. The basic principles of the new x-ray technique, and the x-ray examination of the specimens is also discussed. For convenience, much of the more detailed information about the x-ray technique for pole figure determination and the determination of the depth to which the metal gets disturbed due to machining, is placed in two of the appendixes.

A. PREPARATION OF X-RAY SPECIMENS

The above mentioned x-ray technique for pole figure determination requires the preparation of spherical specimens. Moreover, to avoid errors due to subsidiary surface textures which might form

---

41 L. K. Jetter and B. S. Borie, Jr., "A method for the Quantitative Determination of Preferred Orientation", J. Appl. Phy., Vol. 24 (1953), pp. 532-535.

during the machining of specimens, it was necessary to remove the layers of disturbed metal by etching.

Machining of spherical X-ray specimens. The spherical x-ray diffraction specimens were machined on a lathe. The set-up for machining is shown in Figure 16. An offset back tool post (1) was mounted onto the compound cross-slide (2) on a lathe. A bar handle (3) was fastened onto the compound cross-slide, which facilitated swinging the cross-slide around the trunnion pin (not seen in Figure 16).

To machine a true sphere, the trunnion pin on the cross-slide was brought directly under the spindle axis. This was easily done by mounting a dial indicator in the offset tool post, and swinging it to opposite sides of the rod which was held in the lathe chuck. When the trunnion pin was directly under the spindle axis, the dial indicator did not show any variation in its readings.

The tool was then set in the tool post at the center height of the rod. Light cuts were taken by allowing the rod to rotate around its fibre axis, and by swinging the compound cross-slide slowly at the same time. In the finishing cuts, approximately one thousandth of an inch of the metal was removed in each cut to avoid undue disturbance of the surface layers of the metal. Finally, a stem parallel to and centered on the fibre axis of the rod was machined on one side of the spherical specimen. With this technique spherical specimens of 1" diameter were machined from 1.001" diameter cold drawn nickel rods.

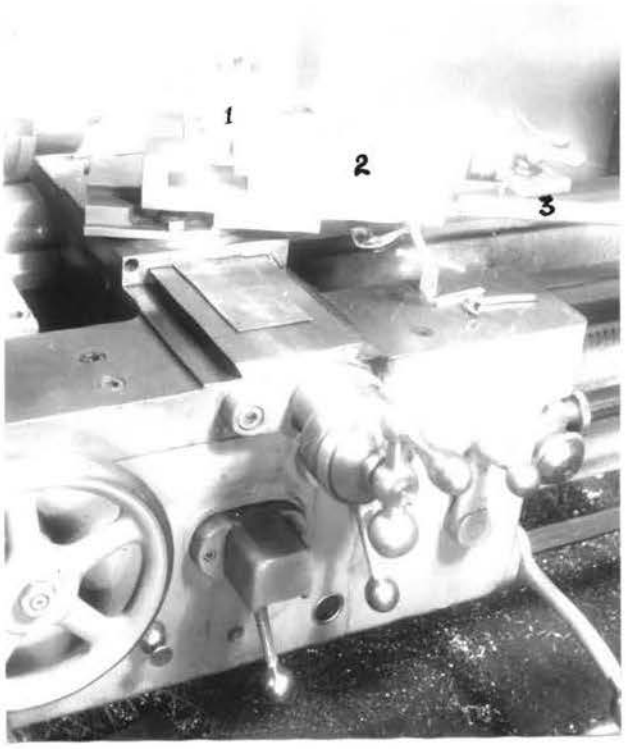

FIGURE 16. Set-up for machining spherical x-ray diffraction specimen.

Measurement of the thickness of the disturbed surface layer resulting from machining. An annealed sample of the 40.6 per cent (item no. 2) cold drawn nickel rod was subjected to a similar machining operation as that employed for the preparation of the x-ray diffraction specimens. Back-reflections patterns of the surface as machined, and after etching away successive surface layers were obtained by conventional methods with cobalt radiation. The back-reflection patterns showed a progressive decrease in the degree of diffuseness of the reflection spots as successive layers of the metal were etched away. The complete removal of the disturbed metal was indicated when no further change in the patterns was noticed on repeated etching treatments. The thickness of the disturbed surface layer resulting from this specific machining operation was thus found to be approximately equal to 0.0026 inches. A detailed discussion of this method is given in Appendix I.

Etching technique. The spherical specimens were electrolytically etched to remove the surface layer of disturbed metal. Many electrolytes were tried, but the most satisfactory results were obtained with a solution consisting of 390 c.c. of concentrated sulphuric acid and 290 c.c. of distilled water, as first suggested by Wensch[42]. The cathode used was in the form of a hollow sphere made

---

42 Glen W. Wensch, "Electrolytic Polishing of Nickel", Metals Progress, November, 1950, pp. 735-36.

out of stainless steel wire cloth. With a current density of 1.5 amperes per square inch, only eight to ten minutes were required to etch away 0.003 inches of the metal from the surface of the specimen. The specimen was continuously rotated during the etching operation and the temperature of the electrolyte was not allowed to rise above 95°F.

B. THE X-RAY TECHNIQUE FOR THE POLE FIGURE DETERMINATION

This technique permits complete pole figure coverage with the use of only one diffraction specimen. Because a spherical specimen is employed, the intensities of the reflections may be plotted directly on a stereographic net without geometry or absorption corrections.

Basic principles of the x-ray technique. Figure 17 shows the diffraction geometry for this technique and the relationship of specimen orientation to the position of the diffracting plane normal on a polar net. To vary the specimen orientation, two mutually perpendicular axes of rotation are provided. One axis is defined by a cylindrical stem appended to the spherical specimen. This axis is usually a principal direction of the specimen, as for example, the fibre axis in a drawn rod. The second axis, which is perpendicular to the first axis and is parallel to the spectrometer axis, passes through the center of the spherical specimen. It will be noted that rotation of the specimen on either of the two axes does not bring about any change in the diffraction geometry; hence, no intensity correction is required.

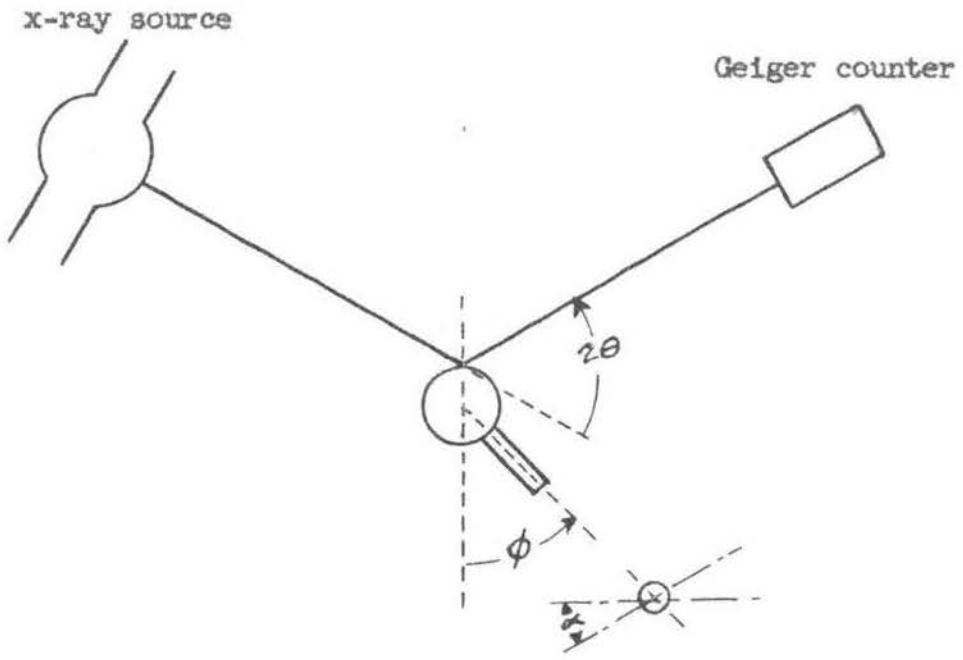

A.

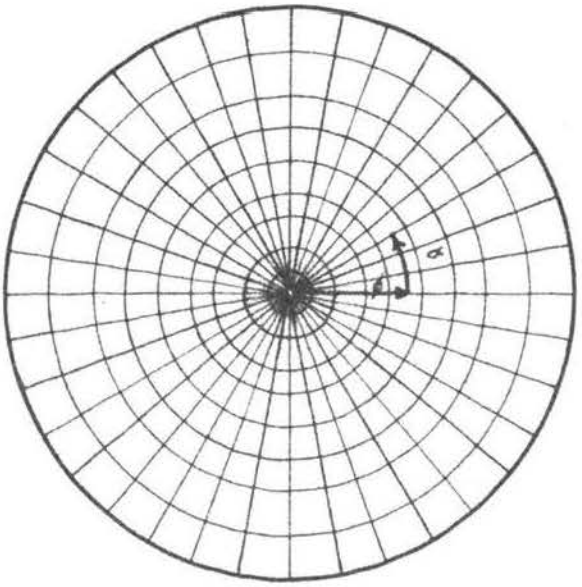

B.

FIGURE 17 (A and B). Diffraction geometry for the x-ray diffraction technique for pole figure determination and relationship of specimen orientation to position of diffracting plane normal on a polar net.

Figure 17B shows changes in the position of the diffracting plane normal on the polar net, corresponding to changes in the orientation of the specimen as seen in Figure 17A. For simplicity, the axis which allows angular changes around any of the concentric latitude circles in the polar net drawn on the projection plane will be referred to as the axis of rotation. The axis which allows angular changes which change the diameter of the concentric latitude circles will be referred to as the axis of revolution. Similarly, the angles α and ϕ, as seen in Figure 17, will be referred to as the angles of rotation and revolution.

A detailed discussion of the construction and use of the specimen mount--called hereafter the 'spherical specimen mount', based on the principles outlined above, is given in Appendix II.

Measurement of x-ray intensity. Measurements of the intensities of diffracted x-rays from the (111) and (100) planes were made at every ten degree interval of latitude on a polar stereographic net for the pole figure determination of each of the three cold drawn nickel samples. As the first order reflection from (100) planes in a face-centered cubic material does not appear on the x-ray patterns, second order reflections of these planes were used for the determination of 100 pole figures. As the orientation around the fibre axis in the ideal case of a drawn rod is supposed to be random, the specimen was rotated continuously at 60 rpm, while the angle of revolution was changed for settings of ten degree latitude intervals (see Appendix II for further details).

All x-ray examinations were made using iron k-alpha radiation from a North American Philips Geiger counter x-ray spectrometer.

Plotting the pole figures. The intensity contour system for presenting the data is used in this report. The maximum reflection intensity from the plane under investigation is taken as fifty intensity units and all intensity values are then expressed in terms of this base. The designation of the intensity contours is as follows: up to ten units--1, eleven to twenty--2, twenty one to thirty--3, thirty one to forty--4, and forty one to fifty--5.

CHAPTER V

THE FIBRE TEXTURE OF DRAWN NICKEL

The mechanical properties of a cold-formed metal are known to depend upon the orientation of the crystallites developed during the forming process. As the Youngs modulus of a face-centered cubic material is maximum in the [111] direction and a minimum in the [100] direction, the predominance of 111 texture in a cold drawn face-centered cubic metal would result in an increase in the modulus along the fibre axis. Thus a knowledge of the deformation textures developed during drawing, when correlated with the mill practice, would prove of great practical importance.

A. EXPERIMENTAL RESULTS

Spherical x-ray diffraction specimens from the 20.6 (item no. 1), 40.5 (item no. 2) and 60 (item no. 3) per cent cold drawn nickel rods were prepared as described in chapter IV. The diffracted intensities from the (111) and (100) planes of the spherical specimens were recorded using the new technique for pole figure determination as discussed in chapter IV and dealt in greater detail in appendix II. As the first order reflection from (100) planes in a face-centered cubic material does not exist, second order reflections were used.

111 and 100 pole figures of cold-drawn nickel. The 111 and 100 pole figures of the 20.6 (item no. 1), 40.5 (item no. 2) and 60 (item no. 3) per cent cold-drawn nickel are shown in Figures 18, 19 and 20

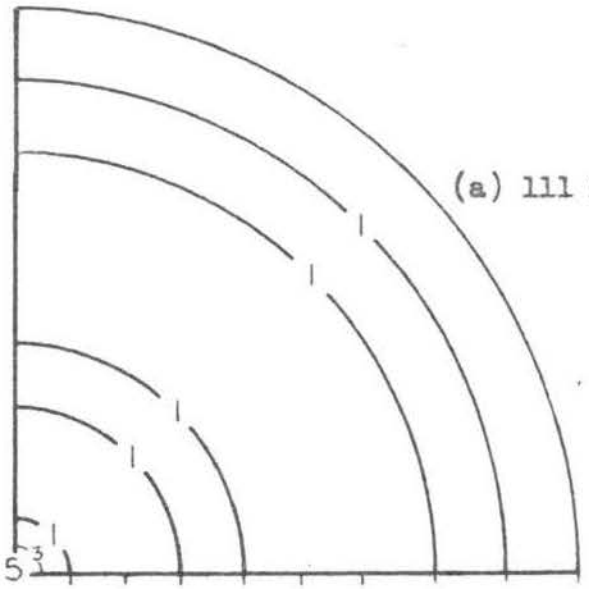

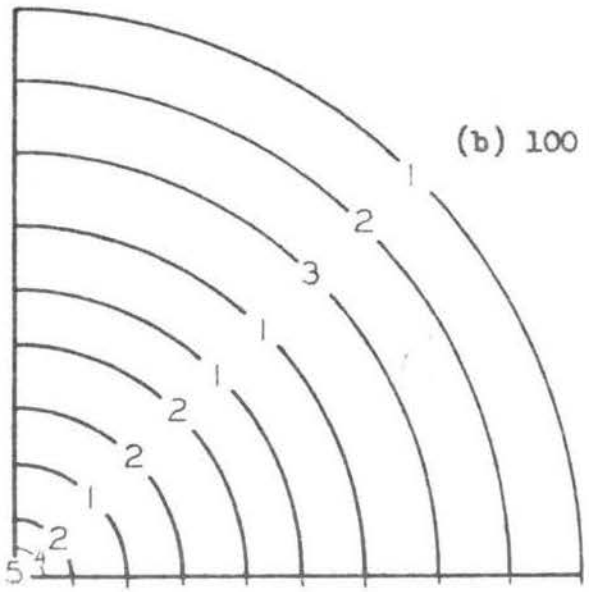

FIGURE 18. 111 and 100 pole figures of 20.6 per cent cold-drawn nickel.

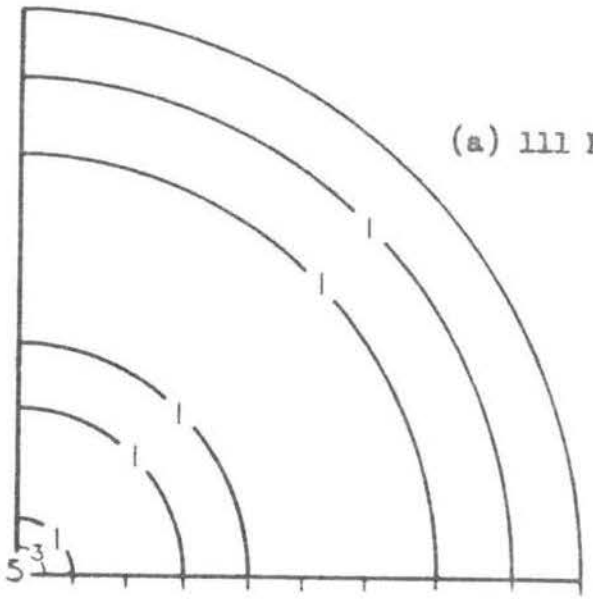

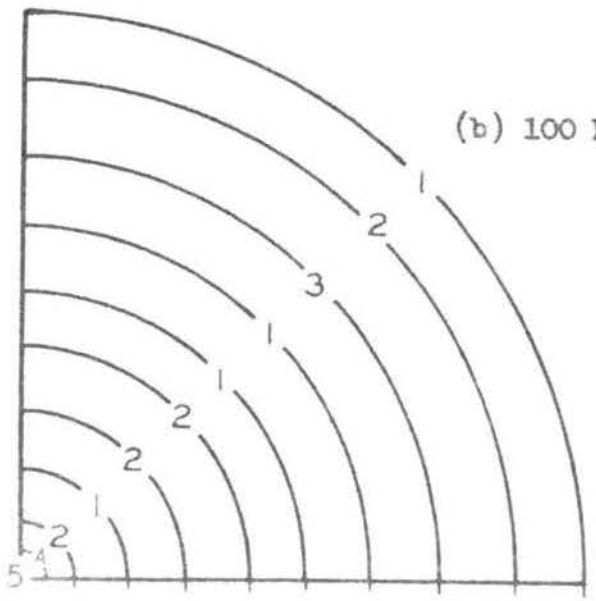

FIGURE 19. 111 and 100 pole figures of 40.5 per cent cold-drawn nickel.

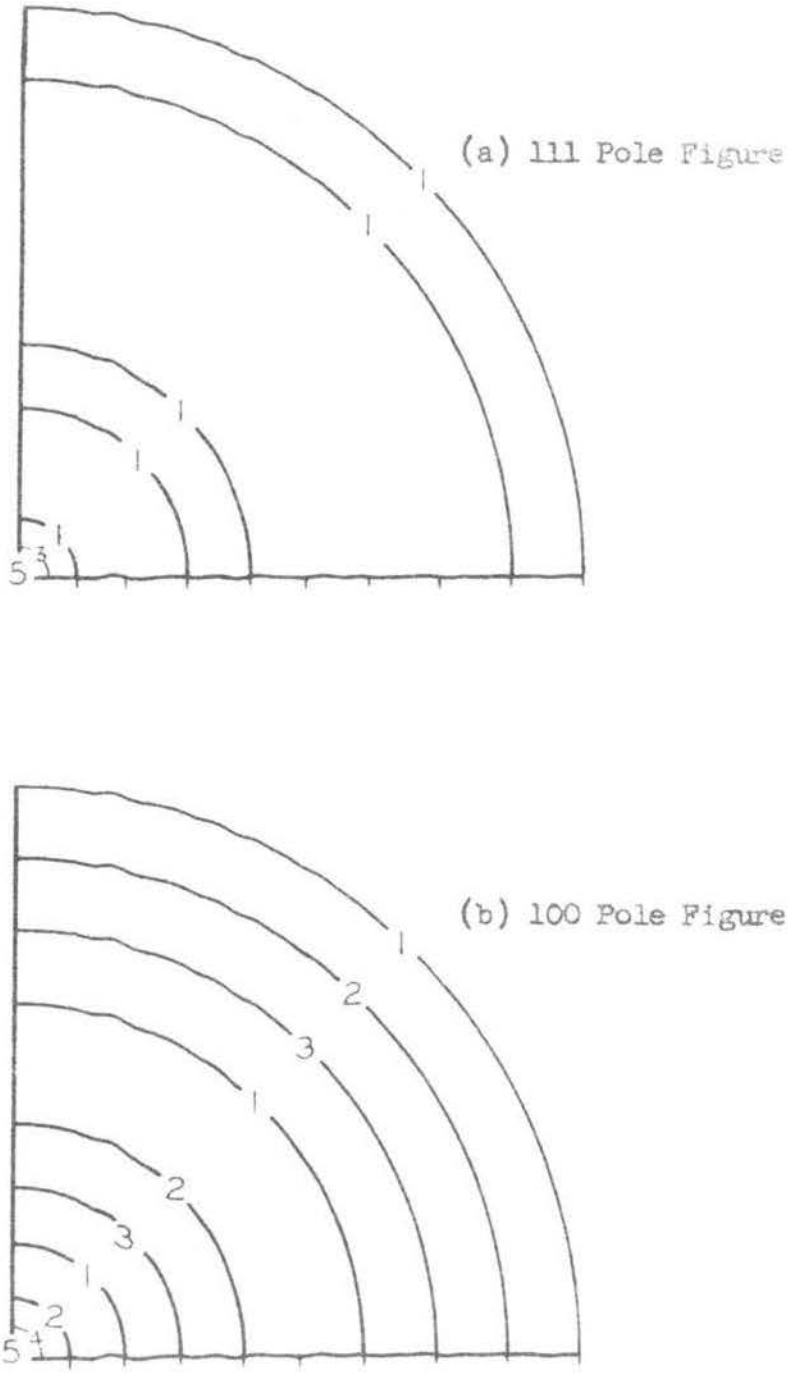

FIGURE 20. 111 and 100 pole figures of 60 per cent cold-drawn nickel.

respectively. The plane of the pole figure corresponds to a plane perpendicular to the fibre axis. It is assumed that the distribution of crystals with the favored direction (the direction that tends to align itself along the fibre axis during the drawing process) at any one angle of inclination around the fibre axis is uniform. Thus it is necessary to draw only one quadrant, as the pole figures consist of a series of concentric rings centered on the fibre axis.

From an examination of the 111 and 100 pole figures 18 through 20, it is evident that the degree of preferredness of the [111] direction is much greater than that of the [100] direction. As seen in the 111 pole figures 18a, 19a and 20a, a majority of the crystals align their [111] direction in the fibre axis, this number decreasing progressively as an inclination of about 10 degrees is reached. The areas 10-30 degrees and 40-70 degrees are devoid of any concentration of intensity. The occurrence of relatively small intensity in the regions 30-40 degrees and 70-80 degrees in the pole figures 18a and 19a, and 30-40 degrees and 80-90 degrees in the pole figure 20a should be noted. A similar tendency for such an intensity concentration in the regions 30-40 degrees and 70-80 degrees is also indicated by the 100 pole figures 18b, 19b and 20b. The shift of this intensity region in the 111 pole figures from 70-80 degrees to 80-90 degrees with increased amount of cold-reduction suggests that the alignment of some directions at these inclinations may be due to the effect of the radial compressive stress developed in the drawing process.

The concentration of intensity in the 100 pole figures, as in the 111 pole figures, is maximum at the fibre axis (figures 18b

through 20b). An area of zero intensity at 50 degrees is shown by the 60 per cent cold-drawn specimen only (figure 20b).

Relative diffracted intensity at the fibre axis. The pole figures 18 through 20, show that the diffracted intensity is a maximum at the fibre axis. But, due to the plotting method used, these pole figures do not indicate the relative strength of the reflection from a particular family of planes for the specimens with varying amount of cold reduction. The maximum calculated relative intensities of the (111) planes and also of the (100) planes are listed in table III. It is seen that the (111) intensity for the 20.6 (item no. 1) per cent cold drawn nickel increases to twice as much with a 20 per cent increase in cold reduction. Further cold drawing does not seem to increase the intensity to any appreciable extent, as shown in table III. The intensity of 2(100) reflection does not show any significant change with increasing cold work, however, there is a slight tendency for its decrease at higher reductions.

Diagramatic representation of the texture data for drawn materials. The pole figure method for representing the texture data for drawn materials is not very satisfactory for the following reasons. Though a pole figure shows the relative concentration of different orientations, the relative percentage of crystals with a particular crystallographic direction at various angles to the fibre axis cannot be indicated in an easily understandable manner. Moreover, interpretation of pole figures requires a thorough understanding of the principles of stereographic projection. An attempt to represent the

TABLE III

RELATIVE DIFFRACTED INTENSITY AT THE FIBRE AXIS

Per Cent Cold Reduction	Relative Intensity of (111) Maximum	Relative Intensity of 2(100) Maximum
20.6	48	100
40.5	95	100
60	100	93

texture data for drawn materials in a simpler yet more readily understandable form was made as follows: The sum of all the diffracted intensities from the plane under investigation is taken as hundred intensity units and all intensity values are then expressed in terms of this base. These values are then represented to a suitable scale by lines emanating from the center of a quadrant of a circle at required angles to the fibre axis, as shown in Figures 21 through 26. The vertical radius of the quadrant is considered to represent the fibre axis. Thus, if the preferred orientation of the crystallites in the body of the drawn rod is assumed as uniform, such a diagram would readily indicate the relative percentage of crystals with a particular crystallographic direction aligned at various angles to the fibre axis. The data for drawing 111 and 100 diagrams for various cold drawn nickel rods is listed in tables IV and V respectively.

It is very evident from Figures 21 through 26, that the 111 texture approaches the ideal end orientation with increasing amounts of cold drawing, whereas, the pronounced scatter of the 100 texture is not appreciably affected even after heavy reduction. Thus it is seen that cold-drawn nickel has a double fibre texture with [$\bar{1}$11] and [$\bar{1}$00] parallel to the wire axis--the 111 texture being more predominant.

TABLE IV

RELATIVE PERCENTAGE OF CRYSTALS WITH [111] DIRECTION AT VARIOUS ANGLES (ϕ) TO THE FIBRE AXIS IN 20.6 (ITEM NO. 1), 40.5 (ITEM NO. 2) and 60 (ITEM NO. 3) PERCENT COLD DRAWN NICKEL RODS

ϕ	Percent crystals in		
	20.6% cold drawn	40.5% cold drawn	60% cold drawn
0	43	58	56
5	27	31	30
10	14	6	7
15	5	--	--
20	2	0	0
30	1	1	3
40	2	1	1
50	2	0	0
60	3	0	0
70	1	1	0
80	0	2	2
90	0	0	1

TABLE V

RELATIVE PERCENTAGE OF CRYSTALS WITH [100] DIRECTION AT VARIOUS ANGLES (ϕ) TO THE FIBRE AXIS IN 20.6 (ITEM NO. 1), 40.5 (ITEM NO. 2) and 60 (ITEM NO. 3) PERCENT COLD DRAWN NICKEL RODS

ϕ	Percent crystals in		
	20.6% cold drawn	40.5% cold drawn	60% cold drawn
0	25	26	23
5	19	20	16
10	11	7	7
15	6	--	--
20	4	3	2
30	4	7	10
35	--	--	12
40	6	7	7
50	7	3	0
60	6	5	1
70	4	12	10
80	3	6	8
90	5	4	4

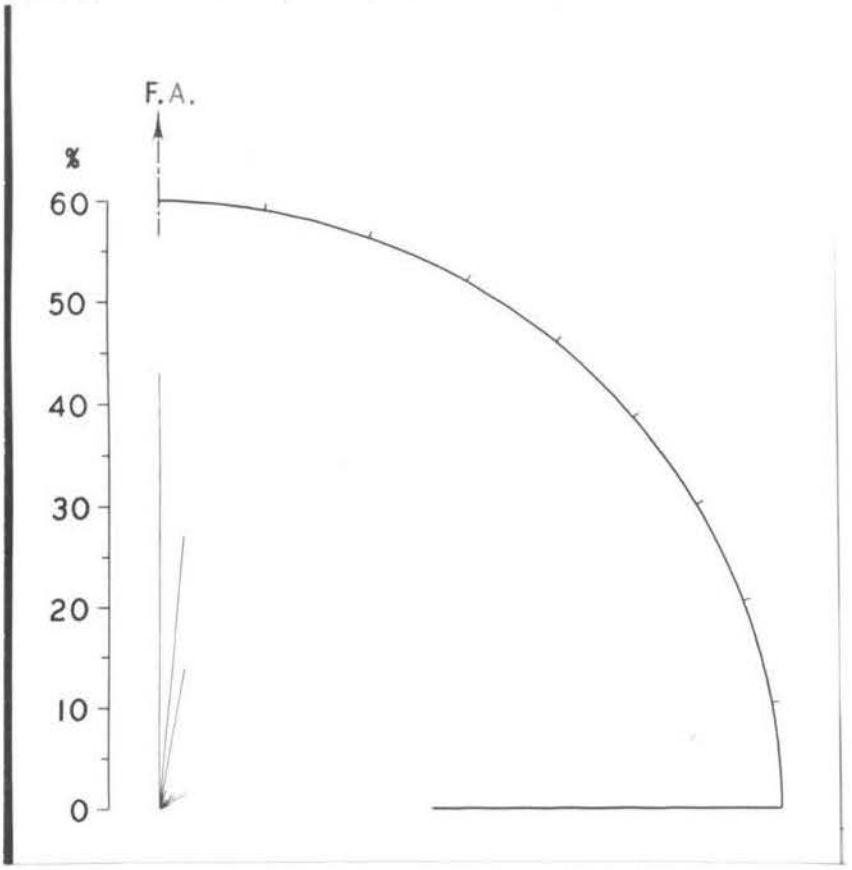

FIGURE 21. Percentage of crystals with [111] direction at various angles to the fibre axis of a 20.6 percent cold-drawn nickel rod.

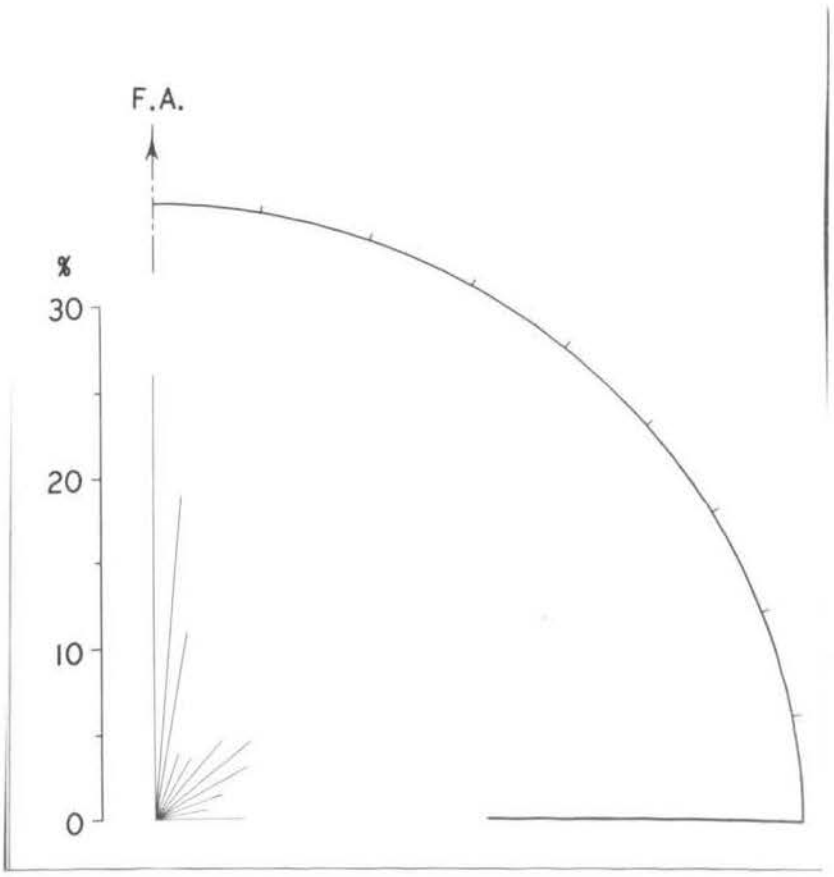

FIGURE 22. Percentage of crystals with [100] direction at various angles to the fibre axis of a 20.6 percent cold-drawn nickel rod.

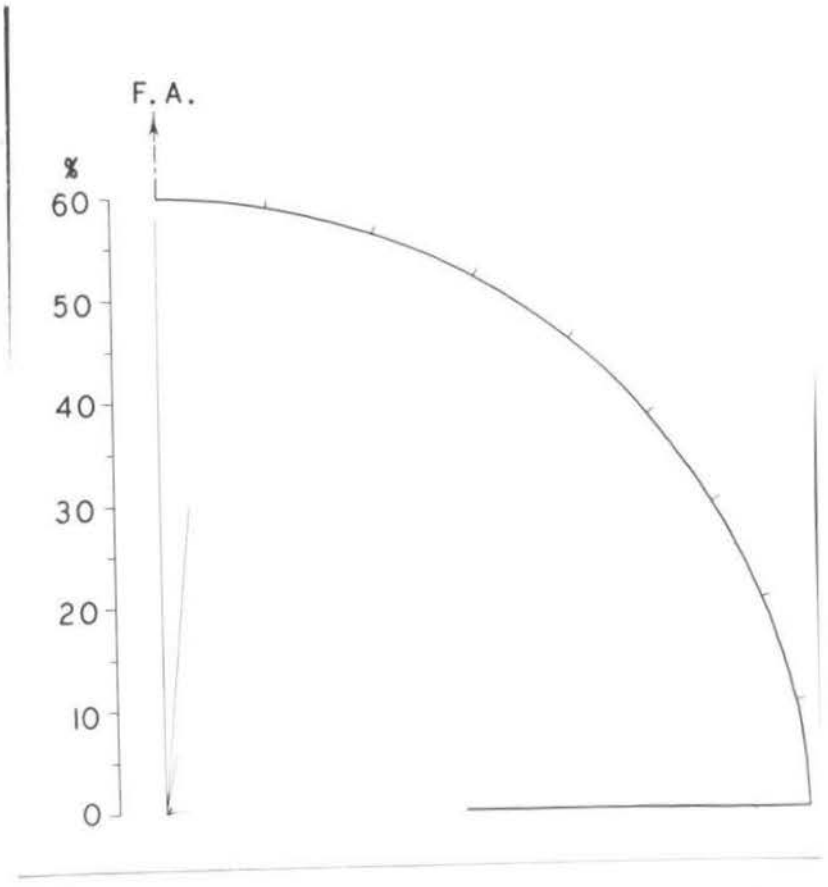

FIGURE 23. Percentage of crystals with [111] direction at various angles to the fibre axis of a 40.5 percent cold-drawn nickel rod.

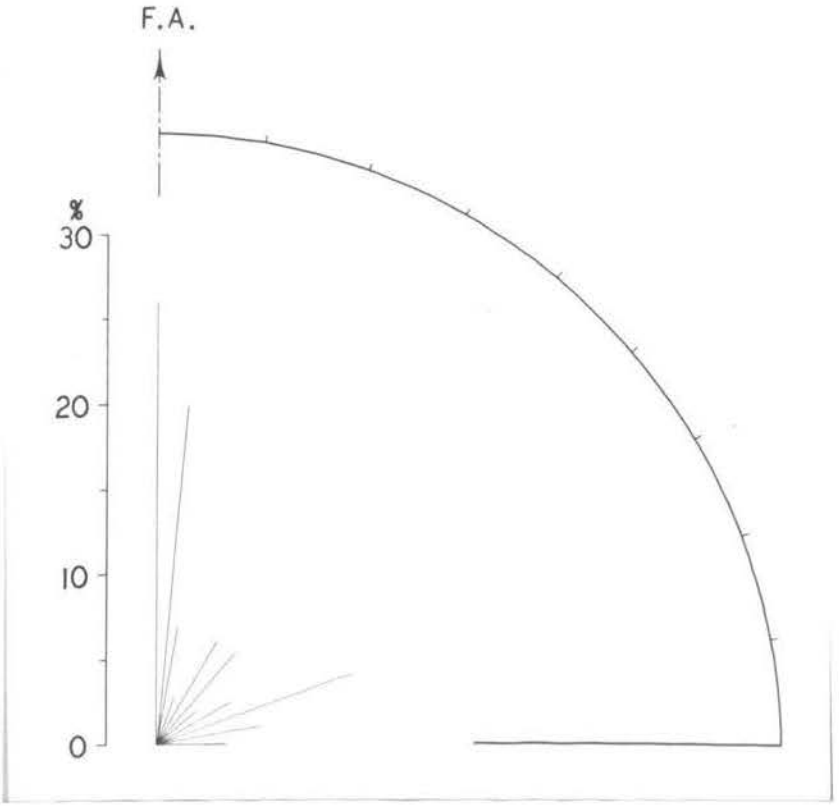

FIGURE 24. Percentage of crystals with [100] direction at various angles to the fibre axis of a 40.5 percent cold-drawn nickel rod.

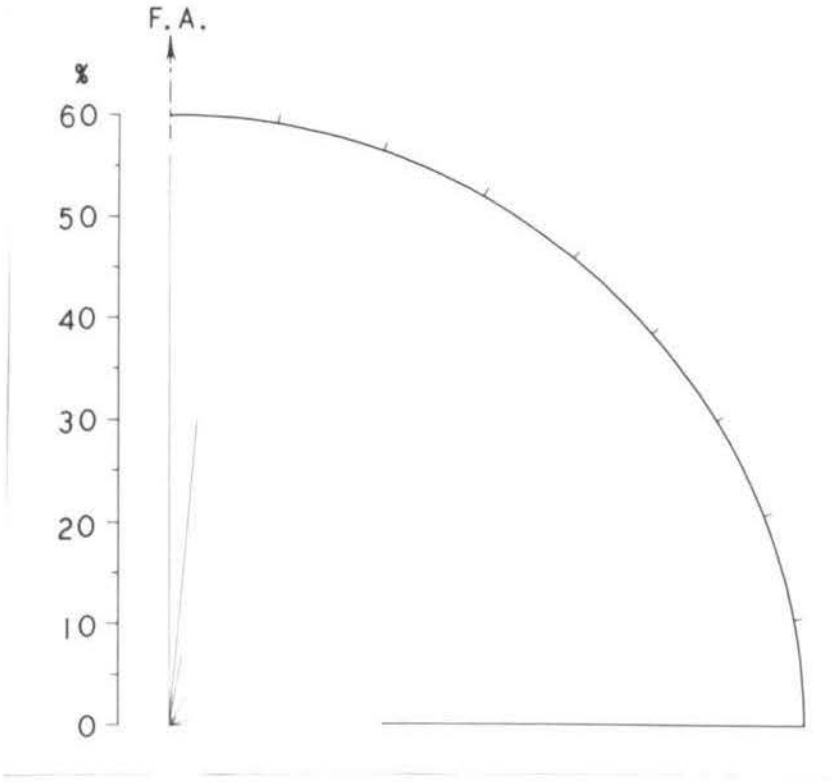

FIGURE 25. Percentage of crystals with [111] direction at various angles to the fibre axis of a 60 percent cold-drawn nickel rod.

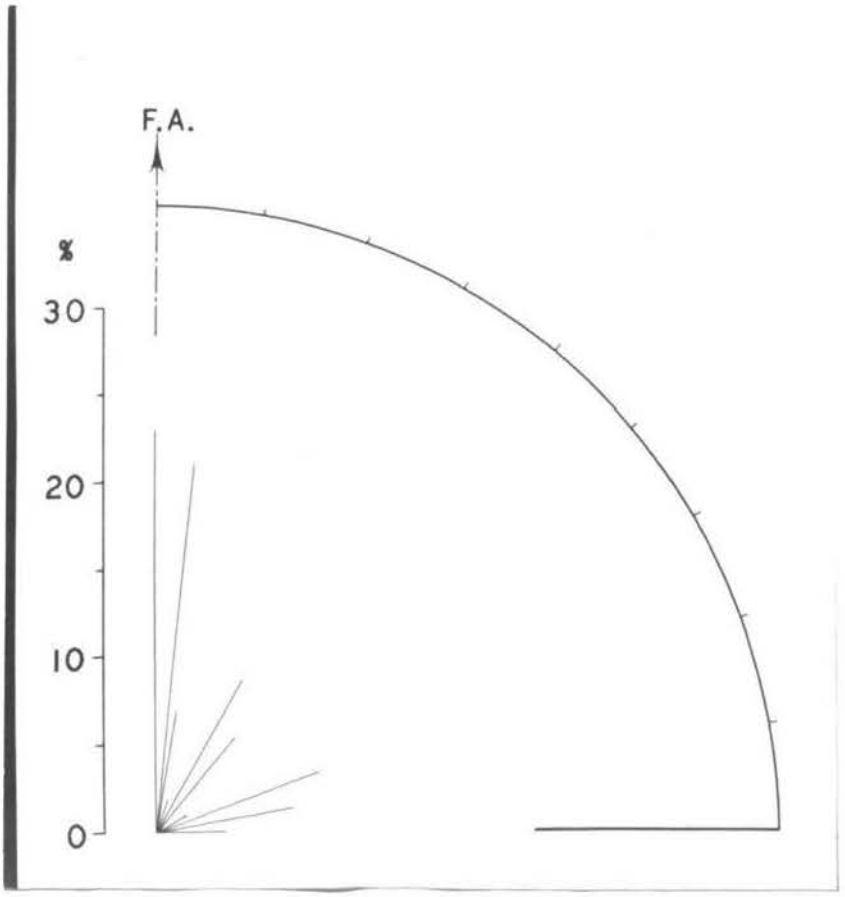

FIGURE 26. Percentage of crystals with [100] direction at various angles to the fibre axis of a 60 percent cold-drawn nickel rod.

CHAPTER VI

THEORETICAL CONSIDERATIONS OF THE FIBRE TEXTURE OF COLD-DRAWN NICKEL

As described in chapter V, cold-drawn nickel rods possess a double fibre texture with [111] and [100] parallel to the rod axis. In the following pages a theoretical explanation of the development of this double fibre texture is given. This treatment is based on the basic principles for the analysis of deformation textures, as developed by Calnan and Clews [43], and referred to hereafter as "Calnan and Clews Method".

Though a few other methods of analysing deformation textures, as discussed in chapter II, have also been successful in predicting the occurrence of both [111] and [100] directions in the rod axis, no other method except that of Calnan and Clews satisfactorily explains the textures developed in metals of all the three common lattice types and specially that of the close-packed hexagonal metals. In view of this outstanding advantage, Calnan and Clews method has been given preference in this thesis.

A. MAIN CONCEPTS OF THE CALNAN AND CLEWS METHOD

In the Calnan and Clews method of texture analysis it is

---

43 E. A. Calnan and C. J. B. Clews, "Deformation textures in face-centered cubic metals", Phil. Mag., Vol. 41 (1950), pp. 1085-1100.

assumed that inhomogeneous deformation is occurring. It is further assumed that only the slip system or systems of maximum resolved shear stress operate at any one point in the deformation process and that multiple slip occurs only when the stress is such as to give equal resolved shear stresses simultaneously on all of the operative slip planes. The explanation of the means by which the most favorable system or systems may withstand resolved shear stresses greater than critical value until the resolved shear stress on less favorable system reaches the critical value is based on the assumption that the effective stress--Te, may move away from the applied stress--Ta, without actual physical movement of the crystal due to lateral stresses from the grain boundaries.

The rotation of the crystal in a polycrystalline aggregate is supposed to follow the laws established for single crystals. Thus, during slip on a single slip system, the slip plane normal rotates toward the stress axis in compression and the slip direction rotates toward the stress axis in tension. Duplex slip will produce rotation of the great circle joining the two slip plane normals toward the stress axis in compression and the great circle joining the two slip directions toward the stress axis in tension. Whereas, the single and duplex slip tends to produce a deformation texture, multiple slip is necessary for maintaining the end orientation and also a common surface between adjacent grains. To study the effect of simultaneous operation of single, duplex and multiple slip a unit ~~of~~ triangle of the stereographic plot of the crystal is used. It is assumed that single slip occurs within the area of the unit triangle, whereas duplex

and multiple slip occurs at the triangle boundaries and corners respectively. The position of the slip plane normal and slip direction on the stereographic plot is kept fixed and the rotations are indicated by a movement of the stress axis.

Figure 27 shows a portion of a stereographic plot of a face-centered cubic crystal. In one of the unit triangles contours of equal resolved shear stress for the slip system active in this particular triangle are drawn. The numerical value of the resolved shear stress at any point in the triangle is given by $\cos \chi \cos \lambda$, where χ and λ are respectively the angles which the slip direction and the slip plane normal make with the particular position of the applied stress, Ta. The slip direction and the slip plane normal for the most favorable slip system for a grain of applied tension in this unit triangle of Figure 27 are indicated by S and N respectively. Thus the value of the resolved shear stress for point a would be 0.46, obtained by substituting the measured angle between a and S for χ and of angle between a and N for λ in the function, $\cos \chi \cos \lambda$. For orientation a, slip on a single slip system will occur when the resolved shear stress equals the value of the critical resolved shear stress Cs, i.e., when $0.46\ Ta = C_s$. If the value of applied stress Ta becomes greater than $C_s/0.46$ without the occurrence of any slip, then it is apparent that the effective stress Te must have moved away from position a to a point of lower $\cos \chi \cos \lambda$ value, i.e, moved down the contour gradient. The general direction of this movement is assumed to take the path of quickest descent, i.e., perpendicular to the contours. Thus with increasing values of Ta, when no slip is

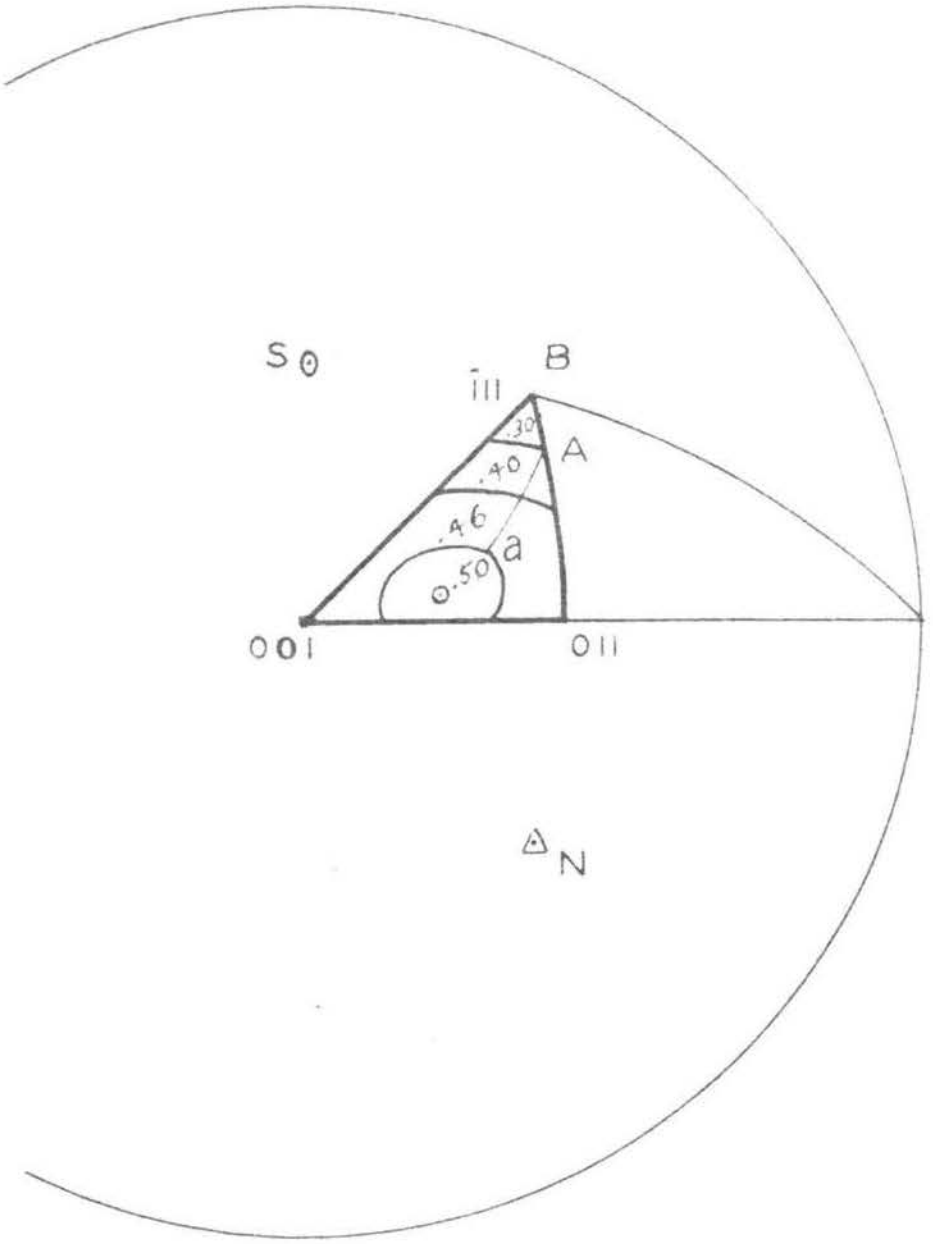

FIGURE 27. Resolved shear stress contours in a stereographic unit triangle of a face-centered cubic metal.

taking place, the position a tends to reach the orientation A on the boundary of the unit triangle. Any further increase of Ta will cause either duplex slip at A or movement of Te along the direction of decreasing cos χ cos λ until it reaches the corner position B. The corner of the unit triangle being a minimum position of the resolved shear stress, any further increase in Ta results in multiple slip which produces deformation without any immediate separation of the common surface between adjacent grains. As the various slip systems are symmetrically disposed around this position, the individual rotations cancel each other, thus maintaining the end orientation. If the value of Te in a grain cannot reach the corner point due to insufficient lateral stresses, slip occurs and rotations are produced in the usual directions of single or duplex slip, the latter taking place if Te has reached a boundary of the unit triangle. Greatest lateral stresses are required by those grains which are furthest removed from the appropriate corner points, and thus are the grains most likely to rotate. The reverse is true for grains oriented near the corners. Thus it is apparent that each grain and in some cases different parts of the same grain, because of the different positions of Ta as plotted in the unit triangle, will have different amounts and directions of movement of Te. When slip occurs the lateral stresses are released; Te returns to the new position of Ta and the process starts all over again. Thus the deformation process is considered as slip-like in character and the texture resulting can be determined by considering the probability of the various steps.

B. DEVELOPMENT OF THE DOUBLE FIBRE TEXTURE IN COLD-DRAWN NICKEL

As explained in chapter II, the drawing stresses can be approximated by tension in the direction of drawing and uniformly distributed radial compression in a plane perpendicular to this direction. Thus it is apparent, that before any attempt is made to rationalize the drawing texture, it is necessary to consider the textures developed during tension and compression.

Tension texture in nickel. Slip in single crystals of nickel at 20°C is reported to occur on the (111) family of planes and in the $[10\bar{1}]$ direction[44]. In Figure 28, four of the twenty four equivalent unit triangles on a stereographic plot of a face-centered cubic crystal are outlined with heavy lines. The most favorable slip system for each of the four triangles is listed in table VI. It has been proposed earlier that rotation will occur only if deformation takes place before Te has reached a corner position of a unit triangle. Rotations corresponding to single or duplex slip occur according as Te is within the triangle or on one of the common boundaries between two triangles. In Figure 29, unit triangle I of Figure 28 has been redrawn to a larger scale, and the lines of quickest descent to the corners, to the $[\bar{2}11]$ direction, and to the maxima on the triangle sides are shown. The rotations for duplex slip are indicated by arrowheads along the

---

44 E. Schmid, "International conference on Physics, Vol. II, The solid state of matter", Physical Society, London, 1935.

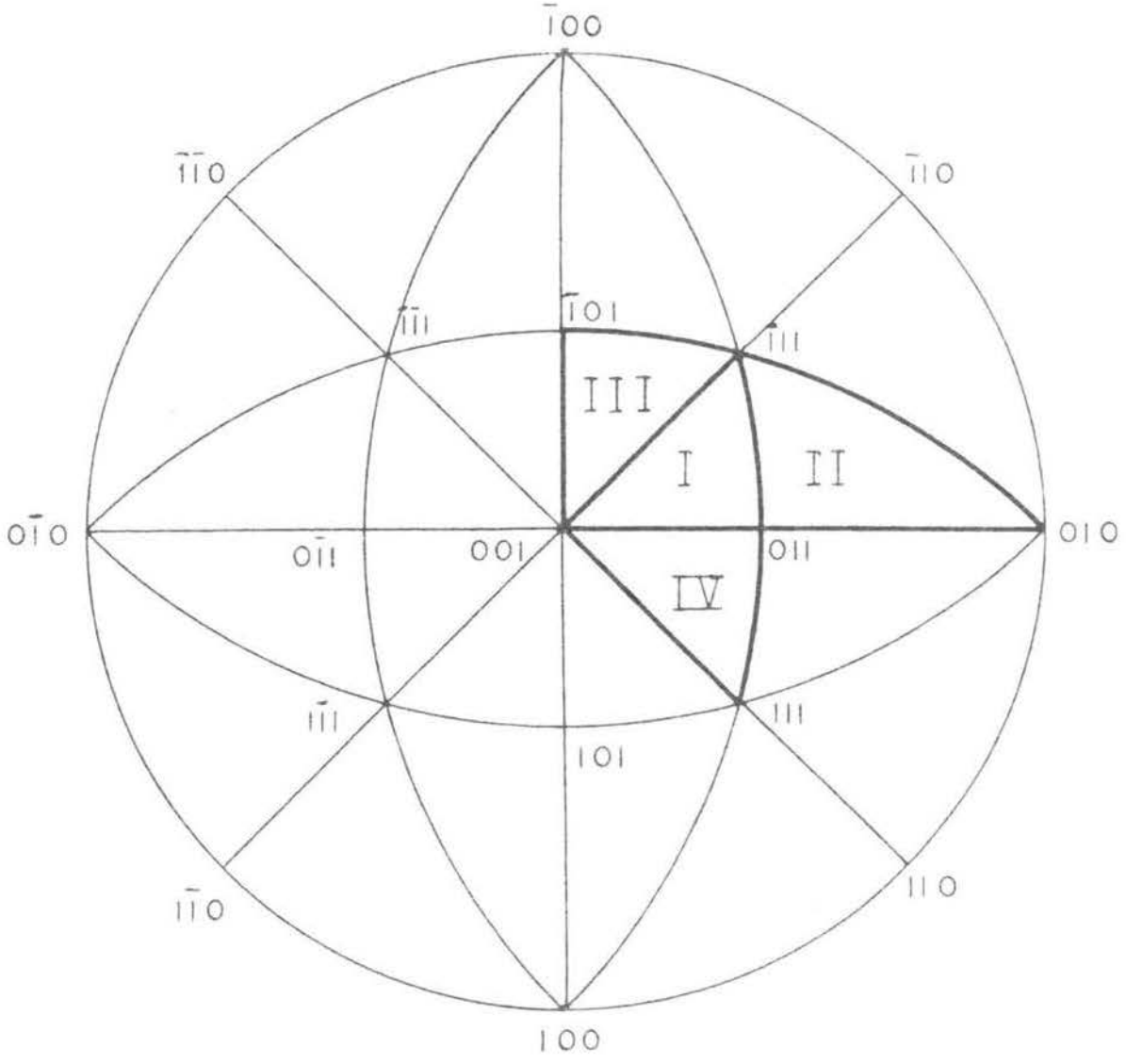

FIGURE 28. Stereographic unit triangles for a face-centered cubic metal.

TABLE VI

MOST FAVORED SLIP SYSTEM IN TENSION FOR THE UNIT TRIANGLES OUTLINED IN FIGURE 28.

Unit Triangle	Most Favored Slip System
I	$(111)\,[\bar{1}01]$
II	$(111)\,[\bar{1}10]$
III	$(\bar{1}\bar{1}1)\,[011]$
IV	$(\bar{1}11)\,[101]$

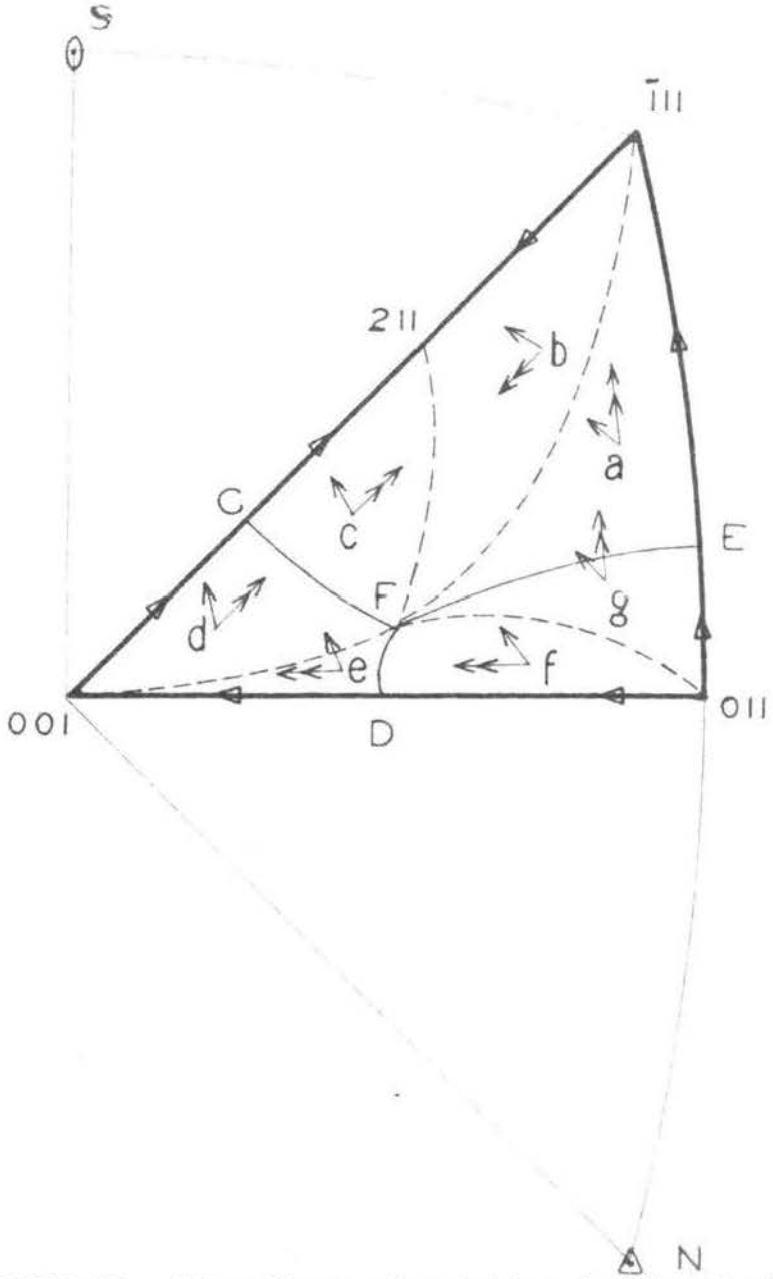

FIGURE 29. Directions of rotation due to single slip (→) and duplex slip (↠) for nickel in tension.

triangle sides.

To predict a deformation texture, the possible rotations due to single and duplex slip for various typical points in a unit triangle are considered. Thus, for a position of applied stress a, if deformation occurs before Te reaches a triangle boundary, the rotation due to single slip is in the direction S, as indicated by a single-headed arrow at a. However, if there is no deformation, Te moves down the stress gradient to reach the [$\bar{0}$11 - $\bar{1}$11] triangle boundary between [$\bar{1}$11] and point D which represents the maximum shear stress value on this boundary. Here again, if deformation takes place before Te reached the $\bar{1}$11 corner, the rotation due to duplex slip occurs in the direction shown by the arrowhead on the boundary, producing the rotation of a shown by the double-headed arrow. The single and duplex rotations for other typical points b, c, d, e, f and g are deduced from similar reasoning. It will be noted that all points lying within the area bounded by the two lines of quickest descent [F - 011] and [F - $\bar{1}$11], and by the [$\bar{0}$11 - $\bar{1}$11] triangle boundary exhibit similar rotations due to single and duplex slip. Since all orientations within these boundaries behave similarly, it is convenient to consider them as a group and to mark off such areas by dashed lines as shown in Figure 29.

It is apparent from the directions of rotation at different points that, as deformation proceeds, the orientation representing a particular grain or part of a grain will move across the unit triangle. But once an orientation moves into a region near a triangle corner, the likelihood for further rotation is decreased,

as explained in the previous section of this report. This holds true for grains oriented near the $\bar{1}11$ corner in the EF$[\bar{1}11]$ region, and those near the 001 corner in the DF$[00\bar{1}]$ region, but not for those near the 011 corner in the DF$[0\bar{1}1]$ and EF$[01\bar{1}]$ regions or those near the 001 corner in the CF$[00\bar{1}]$ region. This can be easily explained by considering two orientations: one, similar to a near the $\bar{1}11$ corner; the other, similar to f near the 011 corner. Any rotation due to single or duplex slip at the orientation near the $\bar{1}11$ corner moves the position of the point toward $[\bar{1}11]$, thus decreasing the likelihood of further rotation. The reverse is true for the orientation near the 011 corner, i.e., the probability of further rotation increases with the occurrence of single or duplex slip. In this region between $[\bar{1}11]$ and $[\bar{2}11]$, although the rotations tend to lead the orientation away from the $\bar{1}11$ corner, the nearness of the end point of rotations, the $[\bar{2}11]$, reduces the probability of further rotations.

The general trend of rotations in different regions of the unit triangle as deduced from this treatment are shown in Figure 30. Thus, the tension texture of nickel may be considered as concentration of orientations near $[\bar{1}11]$, $[\bar{2}11]$, and $[\bar{1}00]$ directions. As no experimental work on pure tension textures has been encountered in the review of published literature, the validity of the predicted tension textures cannot be verified.

Compression texture in nickel. The directions of rotations for single and duplex slip in compression may be determined in the

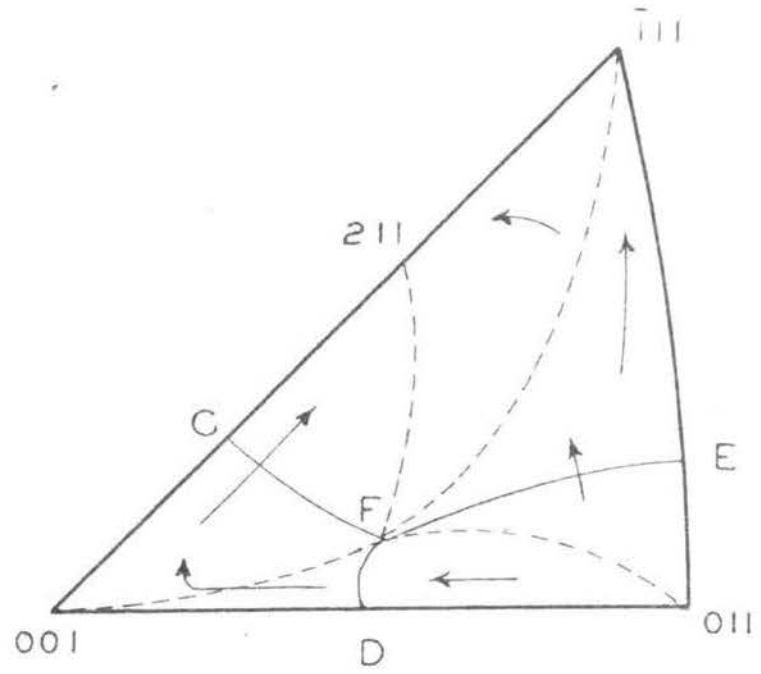

FIGURE 30. General trend of rotation in different regions of a unit stereographic triangle for nickel in tension.

same manner as described above. It should however be kept in mind that single slip during compression moves the position of the applied stress toward the operative slip plane normal while duplex slip causes it to move toward the great circle joining the two poles of the simultaneously operating slip planes. The directions of rotations in compression for various typical orientations in different regions of a unit triangle are shown in Figure 31. It will be noted that all orientations within the region F $[\bar{1}11][011]$, and an appreciable proportion of those in the CF$[\bar{1}11]$ region will move toward the line F$[011]$, thus depleting the region around the $\bar{1}11$ corner. It is apparent from a consideration of the various rotation directions that the orientations have a general tendency to move into the DF$[011]$ region, as shown in Figure 32. As the path of the effective stress in this region is along the line D$[011]$ and toward the corner 011, duplex rotation toward $[011]$ is the more probable. Thus a strong concentration of orientations in the $[011]$ direction is expected. At the same time some residual concentration of orientations near $[001]$ may be expected due to the tendency of the orientations lying on the CF$[001]$ region to rotate toward the 001 corner. The prediction of $[011]$ compression texture in nickel is confirmed by the experimental work of Layland[45].

Drawing texture in nickel. As proposed earlier, the drawing

---

45 E. L. Layland, unpublished senior thesis at Carnegie Institute of Technology, 1941.

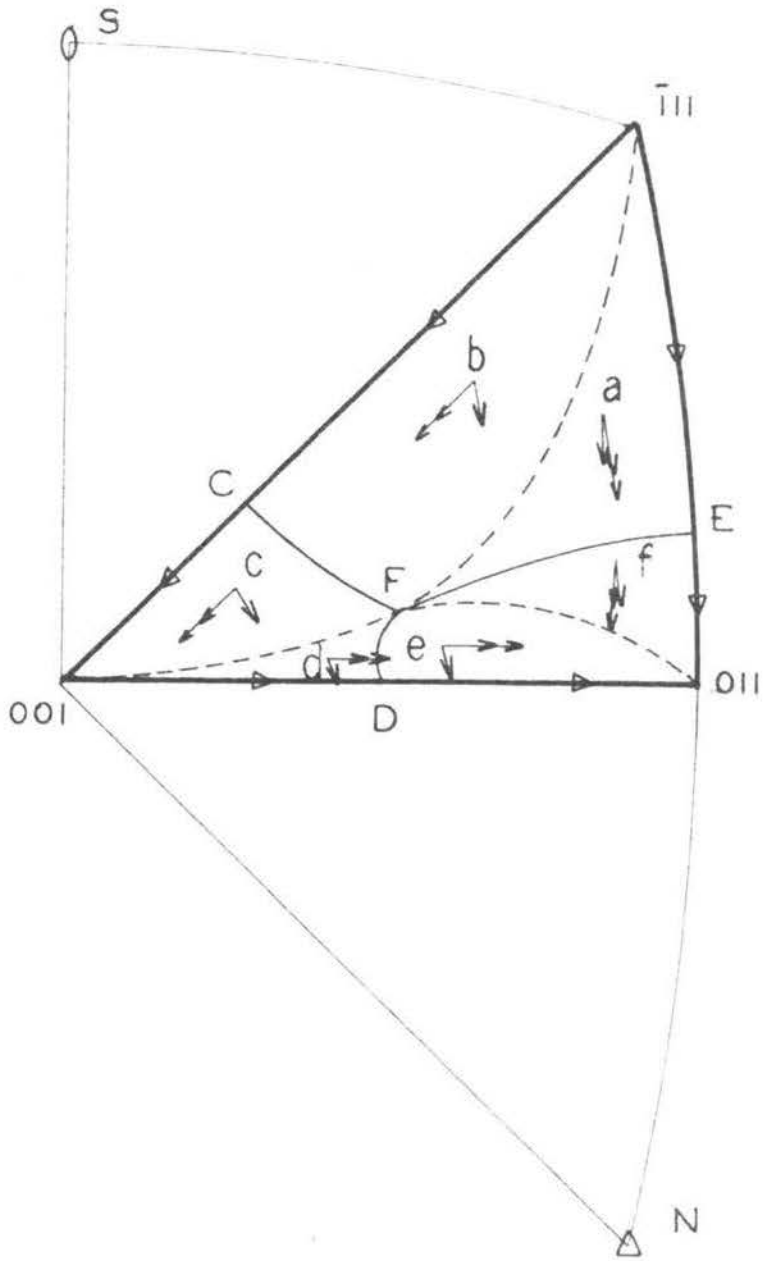

FIGURE 31. Directions of rotation due to single slip (⟶) and duplex slip (⟶⟶). for nickel in compression.

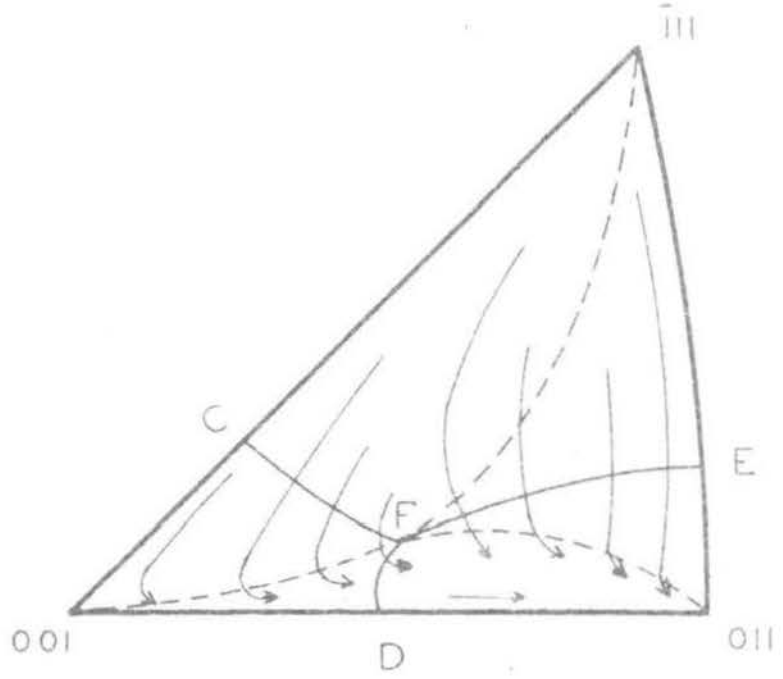

FIGURE 32. General trend of rotation in different regions of a unit stereographic triangle for nickel in compression.

stresses can be approximated by tension in the direction of drawing and uniformly distributed radial compression in a plane perpendicular to this direction. The end orientation in drawing can be predicted by examining the ways in which both tension and compression end conditions may be satisfied simultaneously. The longitudinal tension, assumed to be the predominating influence, causes concentration of the orientations near $[\bar{1}11]$, $[211]$ and $[001]$ directions (Figure 33). For simplicity the compression texture in nickel can be considered as a predominantly $[011]$ texture. These compression directions, which must be 90° from the $[\bar{1}11]$, $[211]$ and $[001]$ tension directions, lie on great circles C_1, C_2 and C_3 respectively. Compression at any point on these great circles will tend to bring the $[011]$ compression direction in alignment with itself whilst retaining the tension textures. The amount of rotation to effect this alignment for points on each of the three circles is as follows: On c_1, a rotation of not more than 30° to the $[\bar{1}\bar{1}0]$, $[0\bar{1}1]$ and $[\bar{1}01]$; on c_2, a rotation of as much as 90° to $[\bar{1}\bar{1}0]$ or $[\bar{1}10]$ and on c_3, a rotation of not more than 45° to $[\bar{1}\bar{1}0]$ or $[\bar{1}\bar{1}0]$. Because of the large rotation required for reaching $[\bar{1}\bar{1}0]$, the orientations on c_2 tend to rotate toward the nearby $[0\bar{1}1]$ and $[\bar{1}01]$. This results in a decrease of concentration of orientations around the $[211]$ and a corresponding strengthening of the 111 texture. Thus a double fibre texture with $[\bar{1}11]$ and $[\bar{1}00]$ in the fibre axis is produced. This predicted texture is found to agree with the experimental results discussed in chapter V.

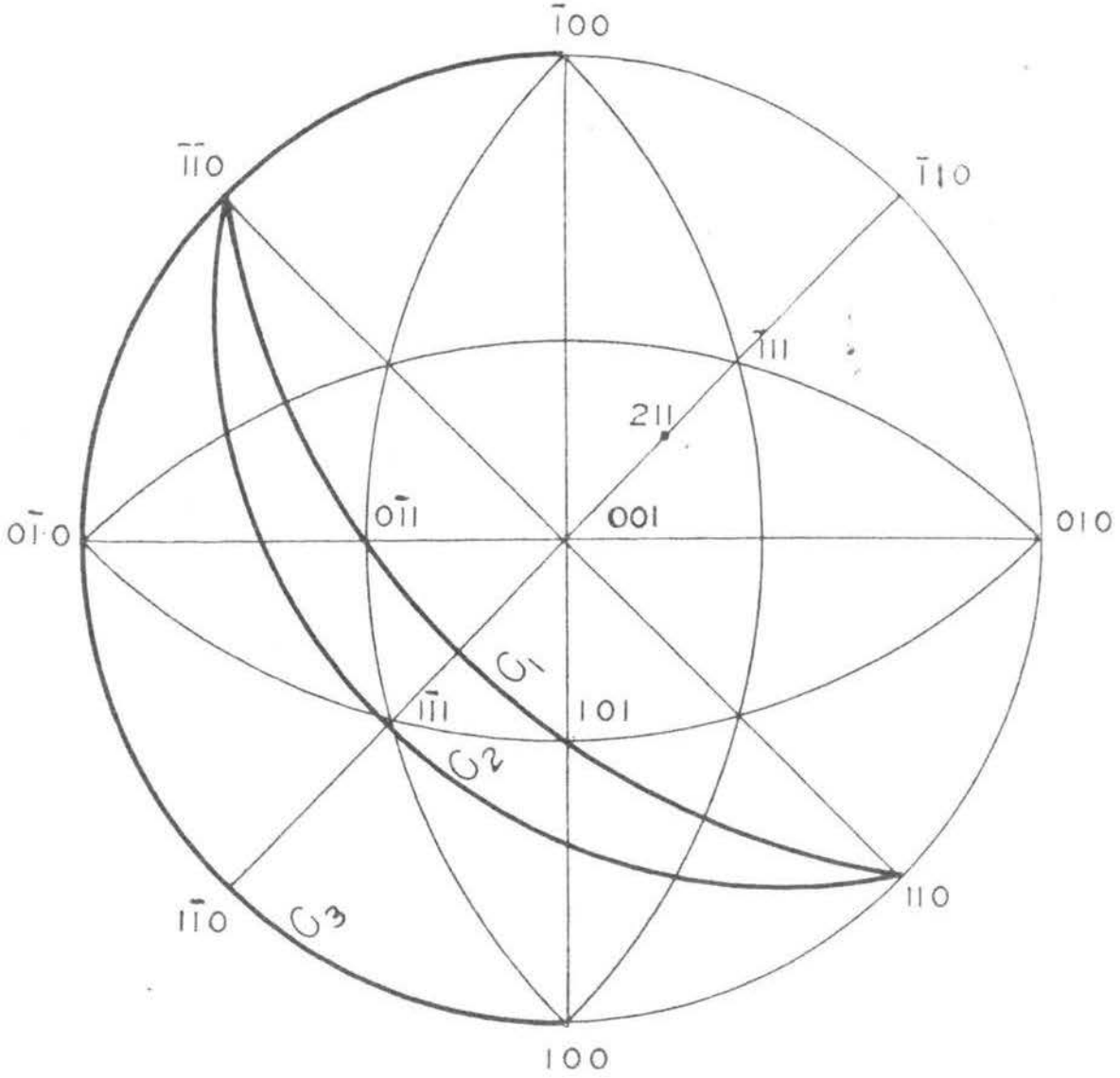

FIGURE 33. Ideal tension texture and the corresponding range of compression directions.

CHAPTER VII

VALIDITY OF THE POLE FIGURE DATA FOR COLD-DRAWN METALS

For obtaining the pole figure data for cold drawn nickel, the following two assumptions were made: first, that the distribution of crystals with the favored direction (the direction that tends to align itself along the fibre axis during the drawing process) at any one angle of inclination around the fibre axis is uniform; second, that the deformation within the body of the drawn metal and thus the resultant deformation texture is uniform. This chapter deals with the experimental work done to investigate the validity of these assumptions.

Distribution of orientations for any one angle of inclination around the fibre axis of a drawn metal. During the drawing process, the crystallites of a polycrystalline metal rotate to align their favored crystallographic directions along the fibre axis. This alignment becomes more and more perfect with progressively increasing amounts of cold-drawing. As discussed earlier, the stresses developed during the drawing process can be approximated by tension in the direction of drawing and uniformly distributed radial compression in a plane perpendicular to this direction. Therefore, at any stage of the drawing process before the ideal end orientation is reached, the distribution of crystals with the favored directions at any one angle of inclination around the fibre axis can be expected to be uniform.

The distribution of the 111 direction for various angles of inclination around the fibre axis of a 60 per cent cold-drawn nickel rod was determined by measuring the intensity of 111 reflection for various angles of rotation---α and revolution---ϕ of a spherical x-ray diffraction specimen. A detailed description of the experimental procedure is given in Appendix II.

X-ray diffraction charts showing the variation of 111 intensity due to rotation of the specimen at every ten degree interval of ϕ are shown in Figure 34. The portions of the charts to the right of the vertical line drawn at the zero value of α show the variation in intensity registration due to the instrument itself. Sample calculations for the determination of maximum percentage variation for a given value of ϕ are included in Appendix II. The net maximum variation in I_{111} intensity due to rotation at various angles of revolution in a 60 per cent cold-drawn nickel rod (item no. 3) are given in table VII. Because the axis of rotation at $\phi = 0$, is perpendicular to the diffracting planes, a negligible variation in intensity is observed. The variation in intensity at other ϕ values is seen to be as high as 51 per cent. This variation in intensity can be explained by considering the hot-rolled stock which is used for the production of cold-drawn rods. The alternate passes in the hot-rolling process are usually diamond and oval and the last pass is oval to round. The reduction along the major axis of the oval is very large. Thus, the working of the rod from the oval to the round on the last pass may be considered as an upsetting action along the major axis. This

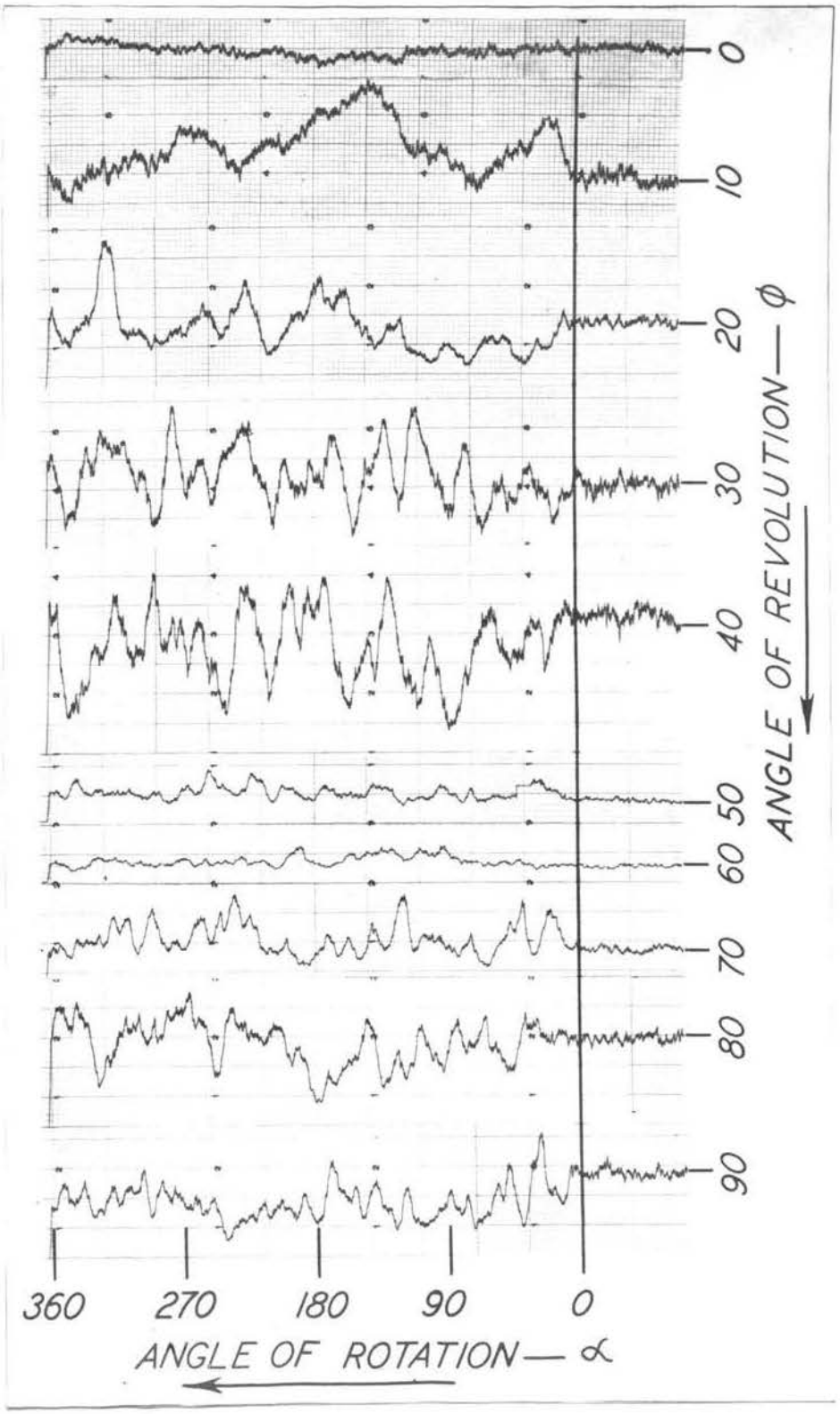

FIGURE 34. Variation of 111 intensity due to rotation of the spherical specimen machined for a 60 per cent cold-drawn nickel rod.

TABLE VII

MAXIMUM VARIATION IN I_{111} DUE TO ROTATION

AT TEN DEGREE INTERVALS OF ϕ

Angle of Revolution ϕ	Average Recorded I_{111} (intensity units on chart)	Recorded Maximum Variation in I_{111} $\pm$ percent	Recorded Maximum Variation in I_{111} due to the instrument $\pm$ percent	Net Maximum Variation $\pm$ percent
0	7.45	4.0	2.0	2.0
10	4.55	23.1	6.3	16.8
20	1.72	62.2	11.1	51.1
30	4.3	26.8	7.5	19.3
40	2.7	50	11	39
50	0.63	44.5	12.5	32
60	0.4	37.5	16.6	20.9
70	1.18	18.7	11.7	7.0
80	1.8	52.7	10.2	42.5
90	1.7	50	11.9	38.1

results in a characteristic "Cross Fibre" texture[46]. During the cold-drawing of this hot-rolled stock, it is expected that some residual cross fibre texture may be retained, thus explaining the variation in diffracted intensity during rotation of the specimen. Thus, the residual nature of this secondary texture superimposed on the drawing texture and also the fact that only one reference direction--the direction along the fibre axis--in a rod can be outlined, makes it necessary to obtain an average value of intensity at any angle ϕ by fast rotation of the x-ray diffraction specimen.

Uniformity of texture in the body of a drawn metal. There exists a difference of opinion among various investigators as to the uniformity of deformation produced within the body of a metal during the drawing process. The opinions of Weiss[47] and Beck[48] are of interest in exemplifying different points of views. In 1928, as a result of his x-ray analysis by photographic technique, Weiss reported that the outer layers in drawn materials undergo non-uniform and increased degree of deformation. In 1936, Beck investigated the hardness penetration effected by the cold drawing of steel rods. He concluded:

---

46 N. P. Goss, Working of Metals, (A.S.M. Publication, 1937), p. 995.

47 L. Weiss, Z. Metallkunde, Vol. 20 (1928), p. 118-121.

48 J. E. Beck, Working of Metals, (A.S.M. Publication, 1937), p. 111.

> "There are those who maintain that the change of physical characteristics effected by cold drawing is only skin deep, or at best extends only a short distance under the bar surface. Such an idea is entirely erroneous. In general, it might be said that the effect of cold drawing is uniformly distributed over the cross-section even in the largest diameters cold-drawn."

It was shown in chapter V that the degree of alignment of [111] direction along the fibre axis in cold-drawn nickel increases as the amount of cold-reduction is increased. Thus, if uniform deformation is assumed, it is evident that at any particular stage of the cold-drawing process, the distribution of crystals with [111] direction along the fibre axis will also be uniform. As the (111) planes are perpendicular to the [111] direction and thus the fibre axis, measurement of 111 reflection intensities from various regions on the cross-section of the rod provide a means of investigating the nature of distribution of the deformation texture. Such intensity measurements for the 111 reflections on the cross-section of a 60 per cent cold-drawn nickel rod were found to show a maximum variation of approximately 800 per cent. The order of magnitude of this variation indicates that the texture within the drawn rod is not uniform and therefore uniform deformation during the drawing process cannot be assumed.

Because of the uniformity of radial compression developed when a metal is drawn through a die, the drawn rod can be divided into concentric regions centered on the fibre axis and having approximately similar deformation characteristics. Figure 35 shows the relation of the spherical specimen to the rod from which it was machined. Regions of approximately similar deformation characteris-

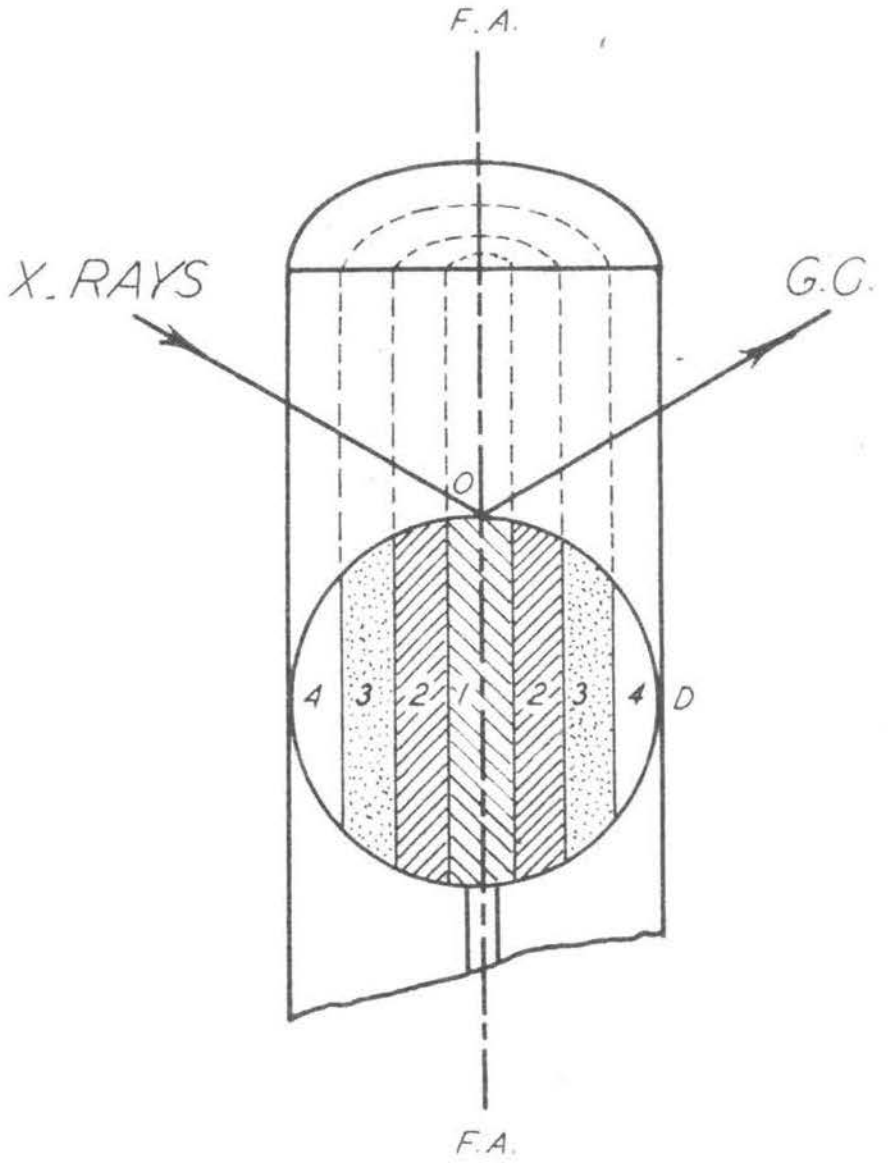

FIGURE 35. Relation of the spherical specimen to drawn rod from which it is machined.

tics are shown by areas 1, 2, 3 and 4. Positions of the x-ray source and the Geiger counter are also indicated. The axis of rotation is perpendicular to the plane of the figure and passes through the centre of the specimen. It is seen, that a 90 degree rotation of the specimen causes the x-ray beam to traverse regions 1 through 4. Thus, the data obtained for drawing different regions of a pole figure can be considered to correspond to specimens with different deformation characteristics. Similar arguments also hold true for other methods of pole figure determinations for drawn materials.

It is evident from the above discussion that pole figure method for describing the textures of drawn materials is not quantitatively reliable. Therefore, the drawn texture should be described only as alignment of specific crystallographic directions along the fibre axis.

CHAPTER VIII

VARIATION OF TEXTURE IN COLD DRAWN NICKEL

As shown in Chapter VII, inhomogeneous deformation of the metal occurs during the cold drawing process. As a result the deformation texture varies in different concentric regions around the fibre axis. In this chapter results of a quantitative determination of variation in deformation texture of the cold drawn nickel rods are presented. The effect of annealing at various temperatures on the distribution of texture is also discussed. Only basic principles of the x-ray diffraction technique used for texture variation study are included in this chapter and the experimental details are discussed in Appendix III.

A. X-RAY TECHNIQUE FOR DETERMINATION OF TEXTURE VARIATION

The variation of texture in various concentric regions of the cold drawn and also of the cold drawn and subsequently annealed nickel rods was studied by an x-ray diffraction technique employing circular disc specimens. A special specimen mount, called hereafter the "Disc specimen mount" was constructed for this purpose (for details see Appendix III).

Preparation of x-ray disc specimens. Five, 1/4" thick discs from each of the three cold drawn nickel rods with 20.6 (item no. 1), 40.5 (item no. 2) and 60 (item no. 3) per cent cold reduction were machined on a lathe. Their faces were smoothed and made parallel by

taking very light cuts. The specimens were continuously cooled with water during machining.

The fifteen specimens thus obtained were divided into five batches of three specimens each, the three degrees of cold reduction mentioned above being represented in each batch. One batch was used for investigations of the as drawn metal and the remaining four were annealed for one hour at 400°, 600°, 800° and 1000°C respectively. All the specimens were then mechanically polished and etched in a 40 per cent nitric acid solution to remove the surface layers of the metal disturbed due to machining and polishing operations.

Basic principles of the x-ray technique. As explained in chapter VII, a cold drawn rod can be divided into concentric regions of approximately similar deformation characteristics. The drawing texture in nickel can be described as an alignment of [111] and [100] directions along the fibre axis. The degree of this alignment depends upon the amount of cold deformation produced. The (111) and (100) planes, being perpendicular to the [111] and [100] directions respectively in nickel, lie in a plane perpendicular to the fibre axis of the drawn rod. Thus a quantitative determination of the variation in texture can be made by measuring the 111 and 100 reflection intensities from various concentric regions on the cross-section of the rod.

In Figure 36 essential elements of the 'disc specimen mount' are shown. The circular disc specimen (1) is fixed centrally on the face plate (2) provided with a shaft (3). The axis of rotation aa' coin-

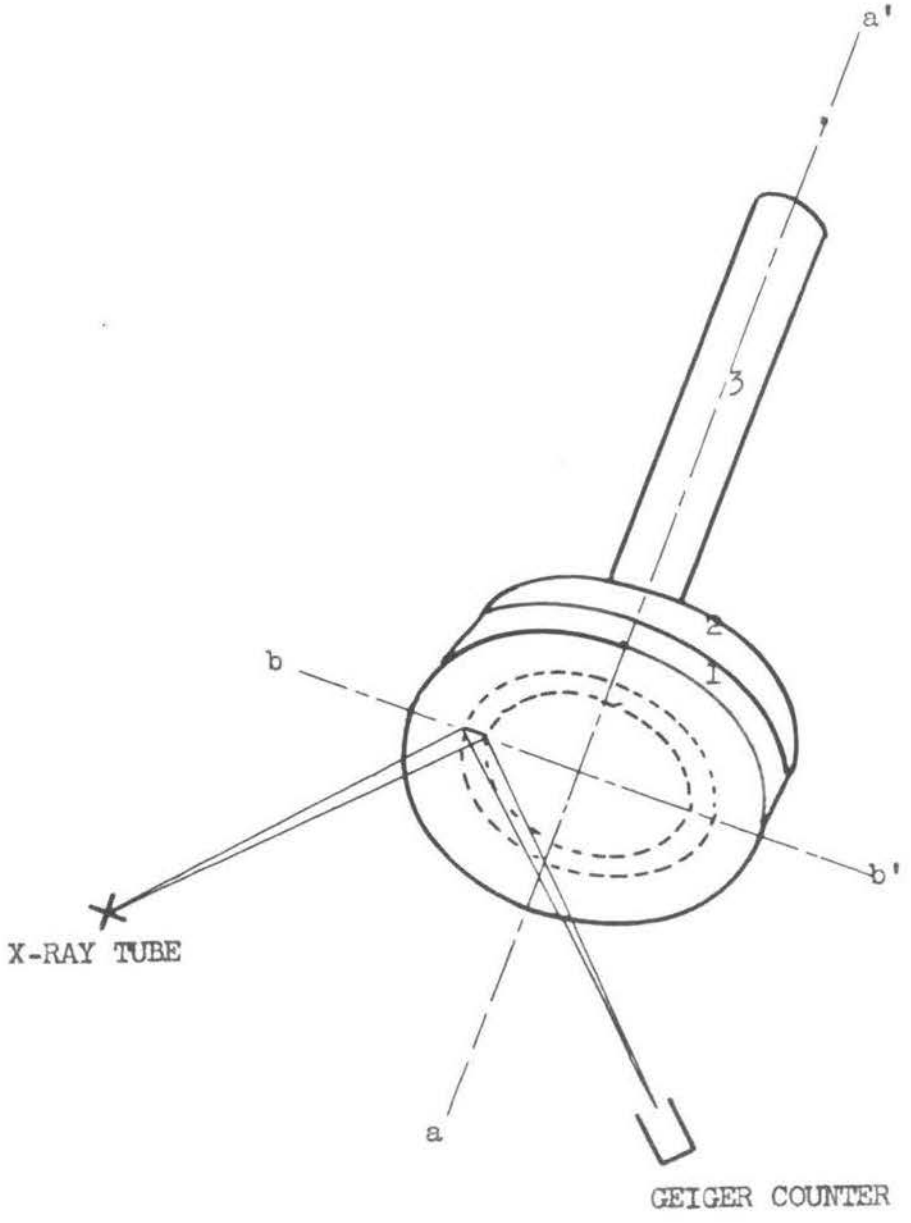

FIGURE 36. Essential Elements of the 'Disc-specimen Mount'.

cides with the fibre axis of the specimen. The position of the x-ray source and the Geiger counter are also indicated. Means are also provided for lateral movement of the specimen in a direction at right angles to the fibre axis. Thus different regions of the specimen can be irradiated with the x-ray beam. By rotating the specimen at 60 rpm, an average value of (111) and 2(100) reflections from any concentric region of the rod may be obtained.

Measurement of x-ray intensity. Measurements of the (111) and 2(100) reflection intensities at the fibre axis and at 0.05 inch intervals on the radii of the disc specimens were made. No one system of slits and amplitude setting could be used to register both (111) and 2(100) reflections satisfactorily for the following reason. The different intensity of the two reflections is so great that the slit system which gave a maximum (111) intensity within ten units on the chart, caused the 2(100) lines to drop within one unit, thus increasing the probability of error in their values. Therefore it was found necessary to prepare the following three sets of x-ray diffraction charts: the first and second sets were made with different slit systems and amplitude settings to obtain accurate data for the (111) and 2(100) reflections respectively, the third set was made to obtain comparitive values of (111) and 2(100) reflections by using the same slit system and amplitude setting. The smallest tube slit (0.075 centimeter) was used for all the three sets, and the Geiger tube slit and the amplitude settings were adjusted to obtain satisfactory readings for each individual set. With the given tube slit, the shape of

the area on the surface of the specimen irradiated by the x-ray beam was a square of 0.1 inch--one side.

B. EXPERIMENTAL RESULTS

The (111) and 2(100) reflections from disc specimens of 20.6 (item no. 1), 40.5 (item no. 2) and 60 (item no. 3) per cent cold drawn nickel rods were measured. Similar intensity measurements on the specimens annealed at various temperatures, as described in a previous section, were also made. For preparation of the three cold drawn nickel rods representing approximately 20, 40 and 60 per cent cold reductions, stock materials annealed at 927°C after having received varying amounts of cold work, were used. This is readily seen from the flow sheet of cold drawing operation (Figure 15). It is known that the orientations generated by forming processes on subsequent annealing of the deformed metal, may result either in retention of the deformation texture or developement of a new recrystallization texture. In some metals, however, especially on annealing at high temperatures, the deformation texture is returned to a random state. As shown in a later section, the cold drawn texture of nickel, though retained on subsequent annealing at 800°C, is rendered very weak. Thus, the presence of this residual texture due to previous cold work on the stock materials used, though very weak in nature, must be kept in mind when making a comparative study of the effect on orientation of increasing cold deformation to which the metal is subsequently subjected.

Variation of texture in cold drawn nickel. The relative in-

tensity values of I_{111} and $I_{2(100)}$ reflections from the three sets of x-ray diffraction charts mentioned in the previous section are listed in tables VIII through X. These intensity values have been plotted on ordinates of graphs at their corresponding distances from the fibre axis as shown in Figures 37 through 45. Relative intensity of (111) and 2(100) reflections from annealed nickel powder are also indicated on the graphs. These intensity values thus correspond to a randomly oriented specimen.

Figures 37, 38 and 39 show the relative concentration of crystals with [111] direction aligned along the fibre axis in different concentric regions of the 20.6 (item no. 1), 40.5 (item no. 2) and 60 (item no. 3) per cent cold drawn nickel rods respectively. For economy of words and convenience of discussion, crystals with a favored crystallographic direction [hkl] aligned along the fibre axis are hereafter called '[hkl] oriented crystals'. It is seen from figures 37 through 39 that the concentration of [111] oriented crystals is largest at the fibre axis and steadily decreases with increasing distance from the fibre axis till it reaches a minimum value near the mid-radius of the rods. The rate of decrease of this concentration increases with increasing degrees of cold deformation. Concentric regions in the vicinity of the mid-radius of the rod do not show any significant change of concentration. In the outermost regions, however, a slight increase in concentration is noted. In these regions of the rods, the concentration of [111] oriented crystals is seen to steadily decrease with increasing degree of deformation. In contrast to this, the concentration at the fibre axis increases by

TABLE VIII

RELATIVE (111) INTENSITY AT VARIOUS DISTANCES FROM THE FIBRE AXIS ON THE CROSS-SECTION OF COLD DRAWN NICKEL RODS

Concentric region No.	Distance from fibre axis (inches)	20.6% cold reduced	40.5% cold reduced	60% cold reduced
1	0	4.43	7.45	8.6
2	0.05	3.2	5.87	8.6
3	0.1	2.47	4.08	6.4
4	0.15	1.7	2.1	3.0
5	0.2	1.16	0.75	0.85
6	0.25	0.8	0.55	0.22
7	0.3	0.75	0.38	0.05
8	0.35	0.9	0.45	0.05
9	0.4	1.35	0.58	0.12

TABLE IX

RELATIVE 2(100) INTENSITY AT VARIOUS DISTANCES FROM THE FIBRE AXIS OF THE CROSS-SECTION OF COLD DRAWN NICKEL RODS

Concentric region No.	Distance from fibre axis (inches)	20.6% cold reduced	40.5% cold reduced	60% cold reduced
1	0.	4.1	2.8	2.75
2	0.05	3.6	2.2	2.75
3	0.1	2.73	1.65	2.0
4	0.15	2.2	1.2	1.17
5	0.2	1.85	1.16	0.87
6	0.25	1.4	1.05	0.62
7	0.3	1.35	1.03	0.61
8	0.35	1.55	1.4	0.9
9	0.4	2.15	1.73	1.2

TABLE X

RELATIVE (111) AND 2(100) INTENSITY AT VARIOUS DISTANCES FROM THE FIBRE AXIS ON THE CROSS-SECTION OF COLD DRAWN NICKEL RODS

Concentric region No.	Distance from fibre axis (inches)	20.6% cold reduced		40.5% cold reduced		60% cold reduced	
		I_{111}	$I_{2(100)}$	I_{111}	$I_{2(100)}$	I_{111}	$I_{2(100)}$
1	0	11	1.07	13.31	0.89	13.75	0.72
2	0.05	10.5	0.9	12.54	0.77	13.75	0.86
3	0.1	8.46	0.88	11.0	0.58	11	0.55
4	0.15	5.46	0.62	6.6	0.4	5.06	0.28
5	0.2	3.75	0.52	3.3	0.33	1.45	0.17
6	0.25	2.72	0.46	1.95	0.22	0.52	0.17
7	0.3	2.63	0.42	1.55	0.22	0.44	0.11
8	0.35	2.8	0.5	1.87	0.33	0.61	0.22
9	0.4	4.09	0.6	2.33	0.44	0.79	0.33

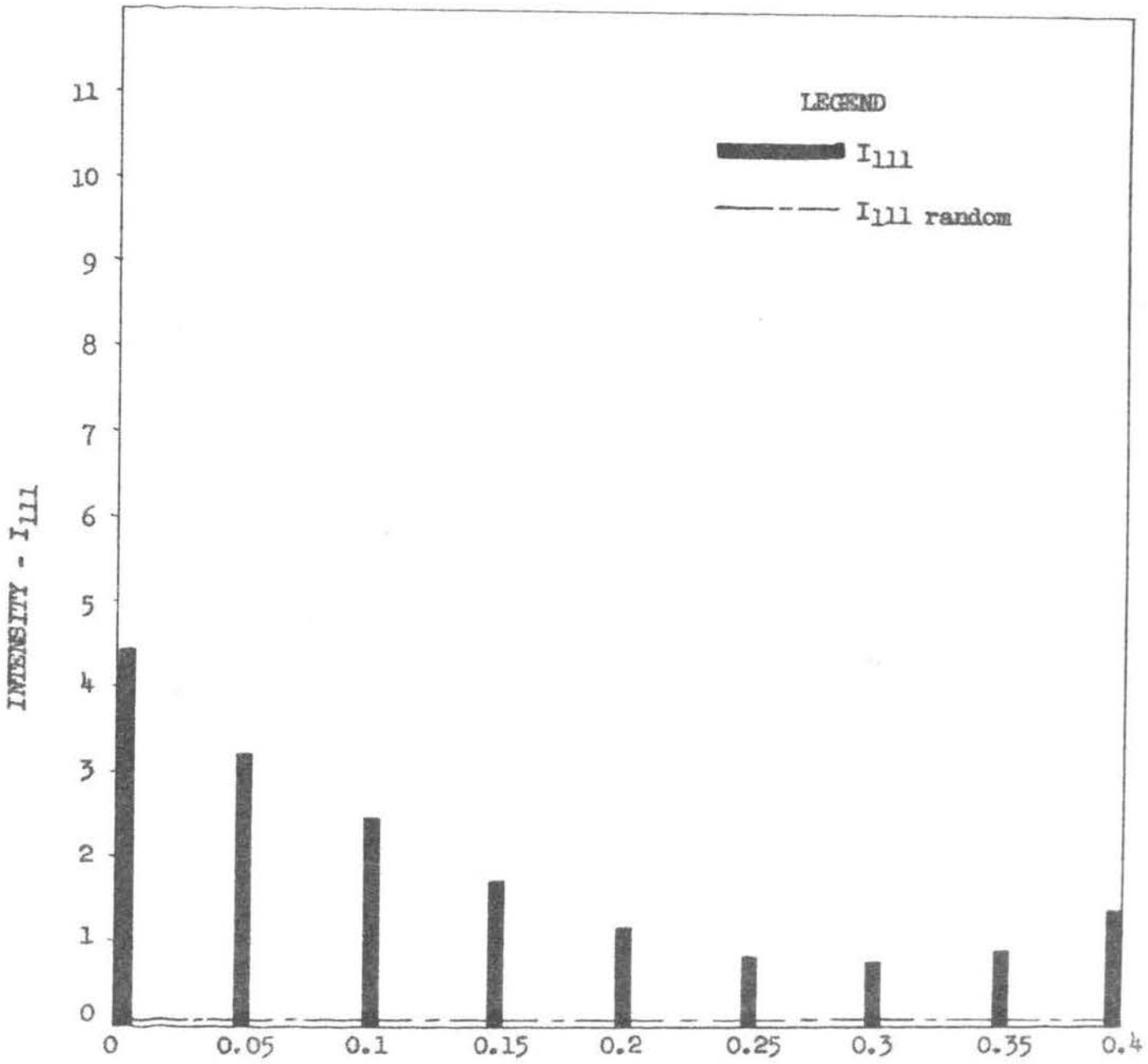

Distance (in inches) of the center of the area irradiated by the x-ray beam from the center of the specimen.

FIGURE 37. Relative (111) intensity from concentric regions at various distances from the fibre axis of a 20.6 per cent cold drawn (item no. 1) one inch diameter nickel rod.

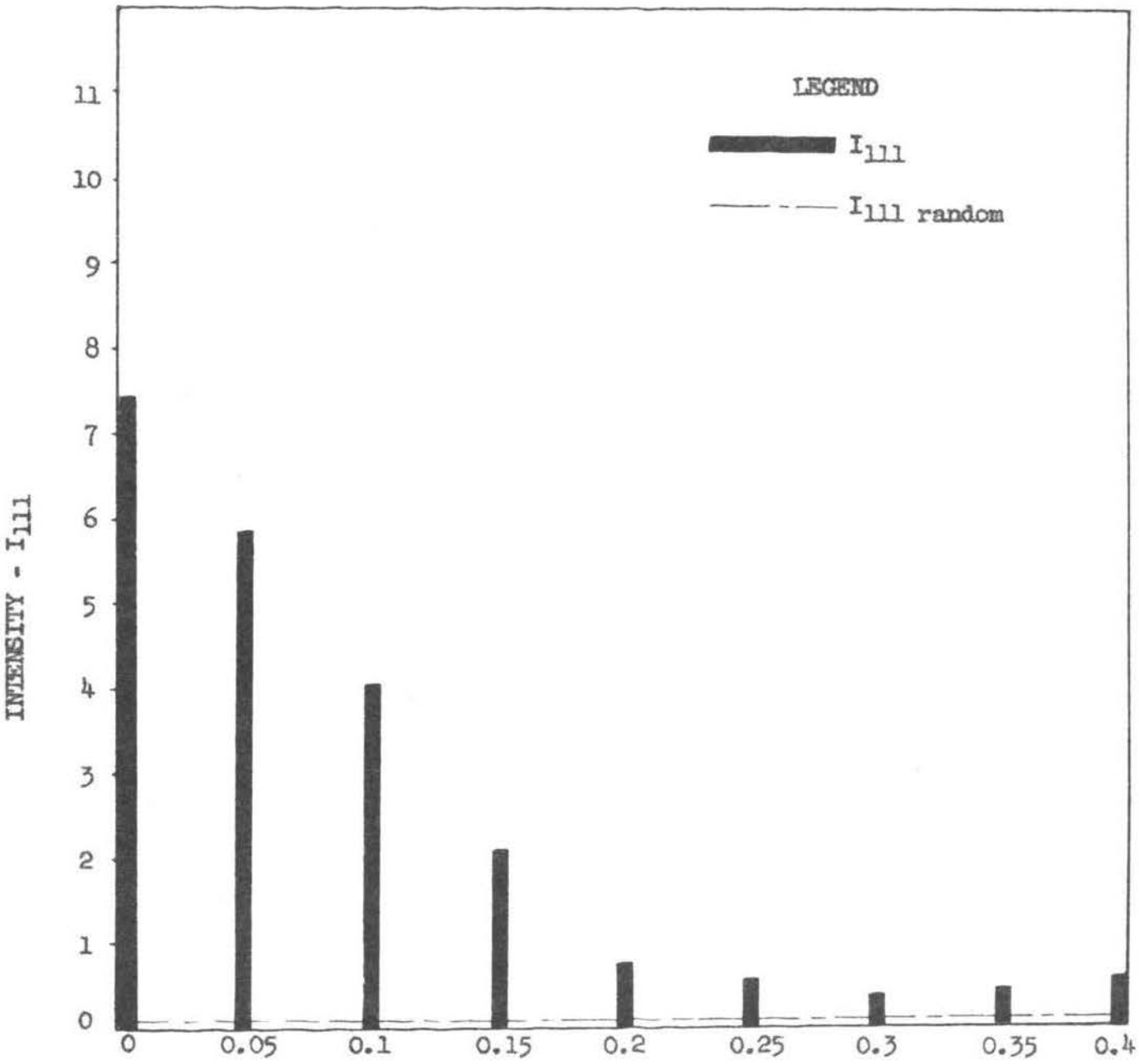

Distance (in inches) of the center of the area irradiated by the x-ray beam from the center of the specimen.

FIGURE 38. Relative (111) intensity from concentric regions at various distances from the fibre axis of a 40.5 per cent cold drawn (item no. 2) one inch diameter nickel rod.

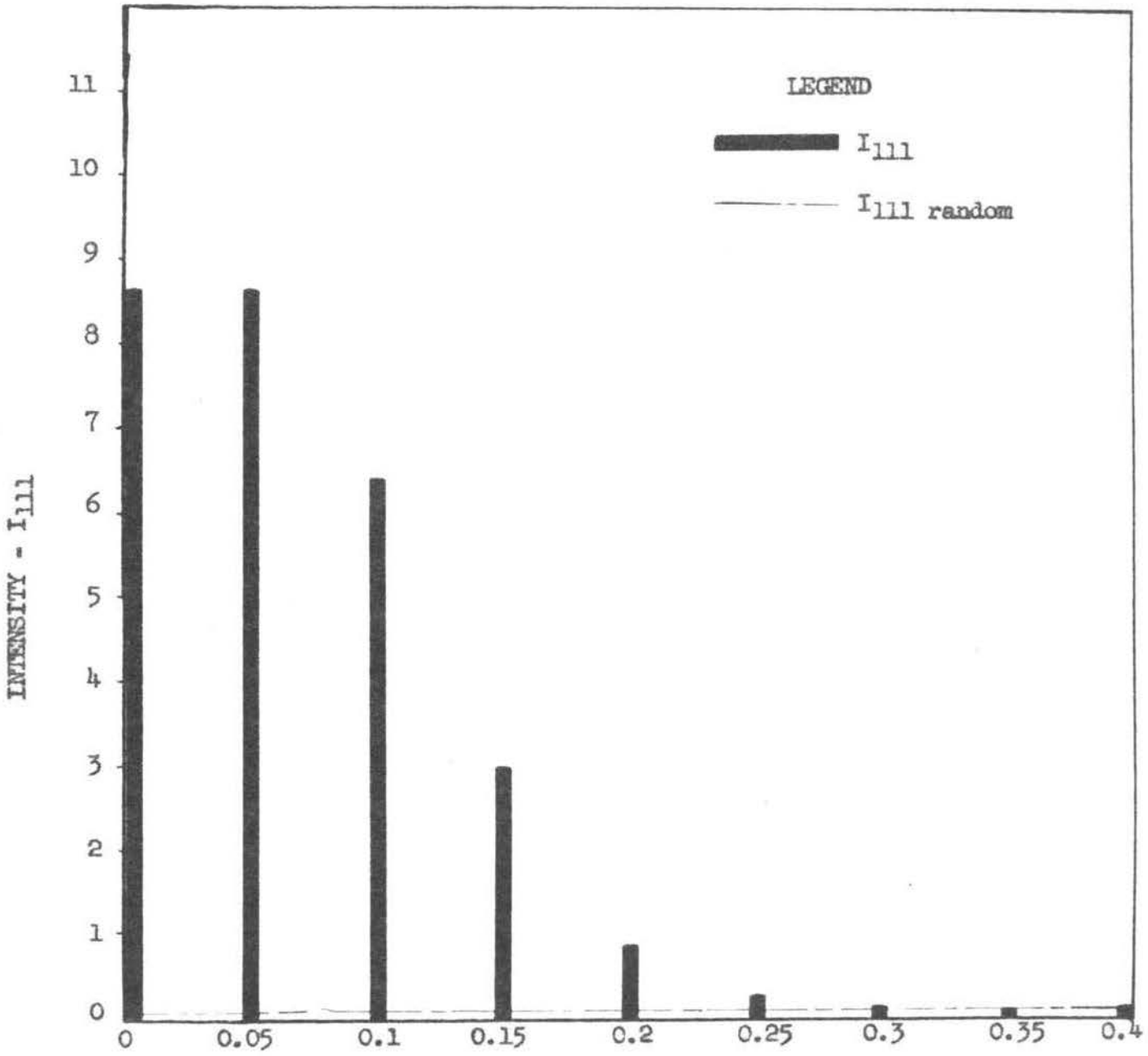

Distance (in inches) of the center of the area irradiated by the x-ray beam from the center of the specimen.

FIGURE 39. Relative (111) intensity from concentric regions at various distances from the fibre axis of a 60 per cent (item no. 3) one inch diameter nickel rod.

sixty eight per cent when the cold deformation is increased from 20.6 to 40.5 per cent, whereas a further 20 per cent increase in cold reduction produces only fifteen per cent increase in the concentration of [$\bar{1}$11] oriented crystals.

Figures 40, 41 and 42 show the relative concentration of [$\bar{1}$00] oriented crystals in different concentric regions of the 20.6 (item no. 1), 40.5 (item no. 2) and 60 (item no. 3) per cent cold drawn nickel rods. Unlike the [$\bar{1}$11] oriented crystals, the concentration of [$\bar{1}$00] oriented crystals in the inner regions of the cold drawn rods decreases with increased degree of cold reduction. But for this difference in behaviour, the general characteristics of concentration distribution of [$\bar{1}$11] and [$\bar{1}$00] oriented crystals are similar, as seen in Figures 37 through 42.

The relative concentration of [$\bar{1}$11] and [$\bar{1}$00] oriented crystals in various regions of the different nickel rods is shown in Figures 43 through 45, and the values at the fibre axis are listed in table XI. It is seen that approximately ten per cent of the crystals are aligned with their [$\bar{1}$00] directions along the fibre axis of the 20.6 per cent (item no. 1) cold drawn rod, and this number decreases to about five per cent as the cold reduction is increased to 60 per cent. Thus, it is apparent that in cold drawn nickel, increasing amounts of cold reductions tend to produce a predominately [$\bar{1}$11] texture. This conclusion is further strengthened by the observation that the concentrations of [$\bar{1}$00] oriented crystals in all regions of the cold drawn rods decrease with increasing deformation, as seen in Figures 40 through 42.

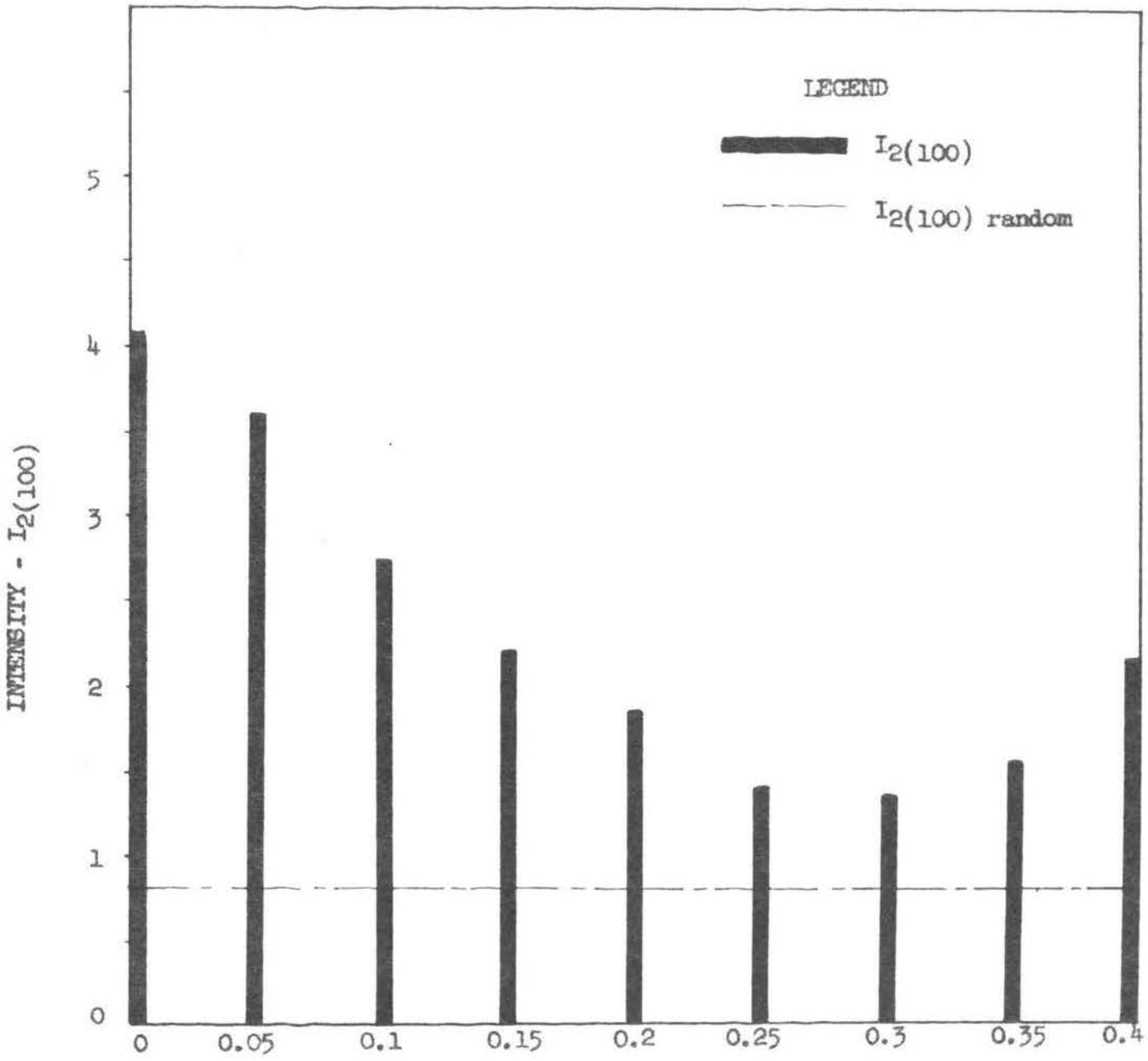

Distance (in inches) of the center of the area irradiated by the x-ray beam from the center of the specimen.

FIGURE 40. Relative 2(100) intensity from concentric regions at various distances from the fibre axis of a 20.6 per cent cold drawn (item no. 1) one inch diameter nickel rod.

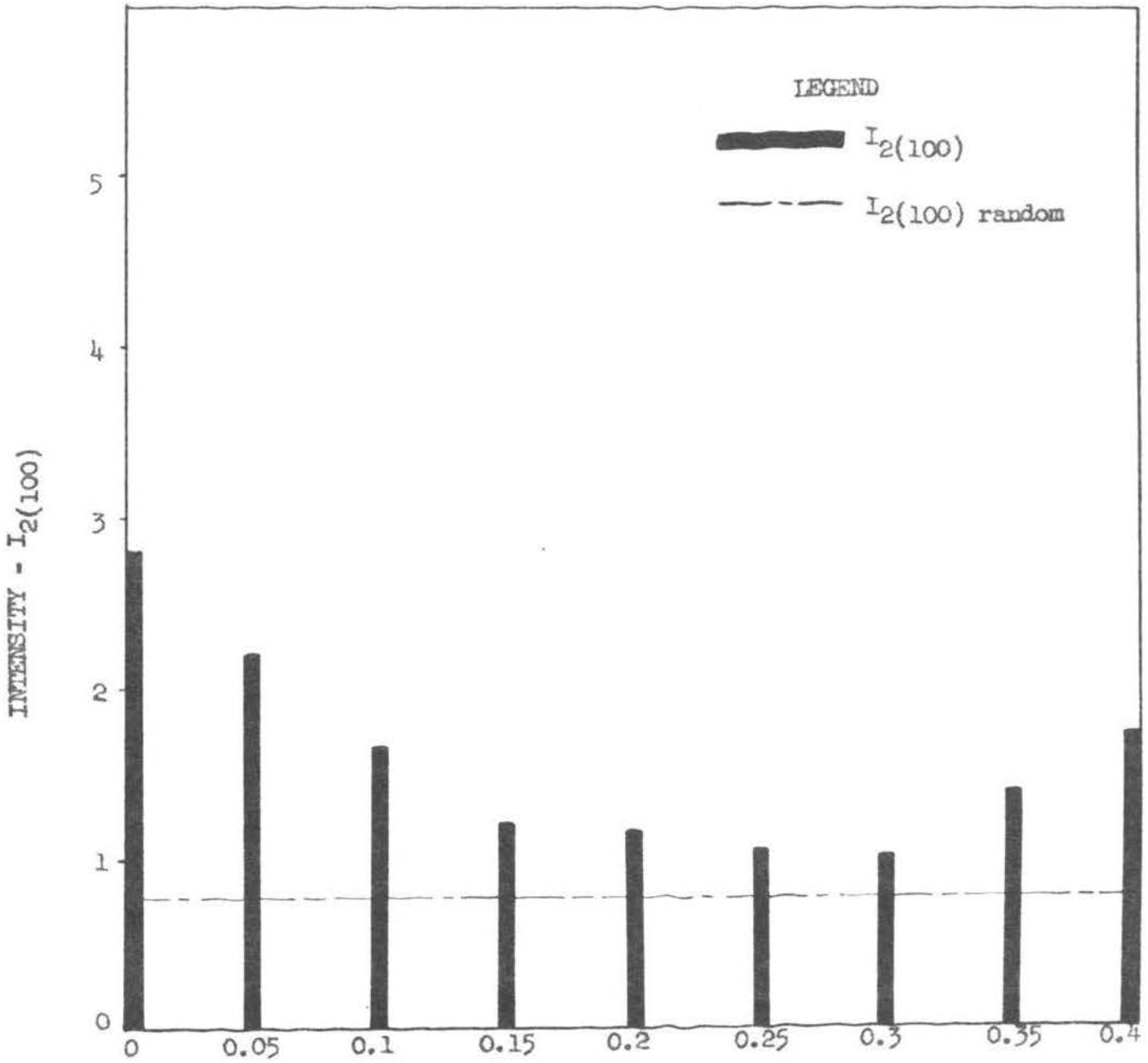

Distance (in inches) of the center of the area irradiated by the x-ray beam from the center of the specimen.

FIGURE 41. Relative 2(100) intensity from concentric regions at various distances from the fibre axis of a 40.5 per cent cold drawn (item no. 2) one inch diameter nickel rod.

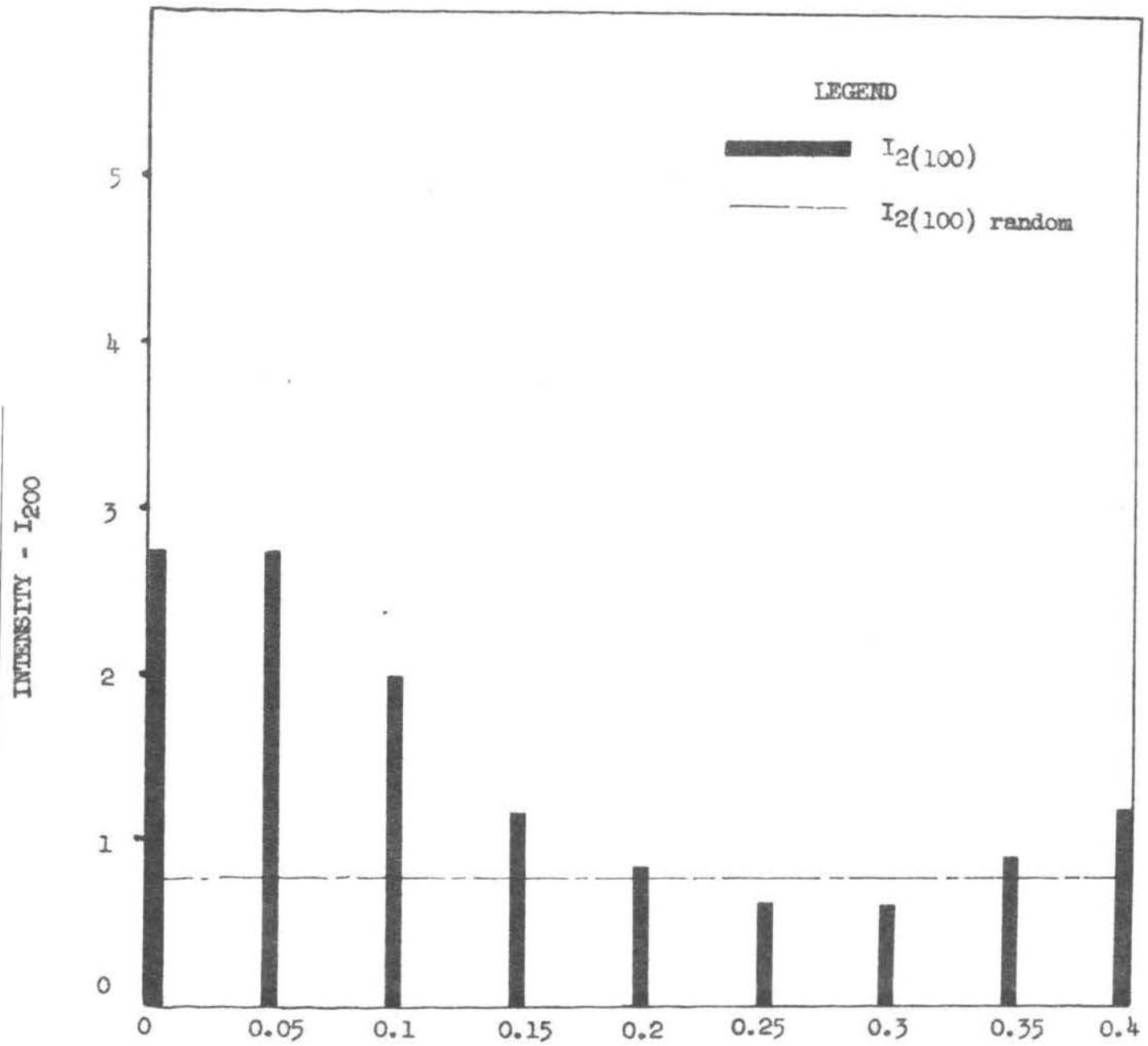

FIGURE 42. Relative 2(100) intensity from concentric regions at various distances from the fibre axis of a 60 per cent cold drawn (item no. 3) one inch diameter nickel rod.

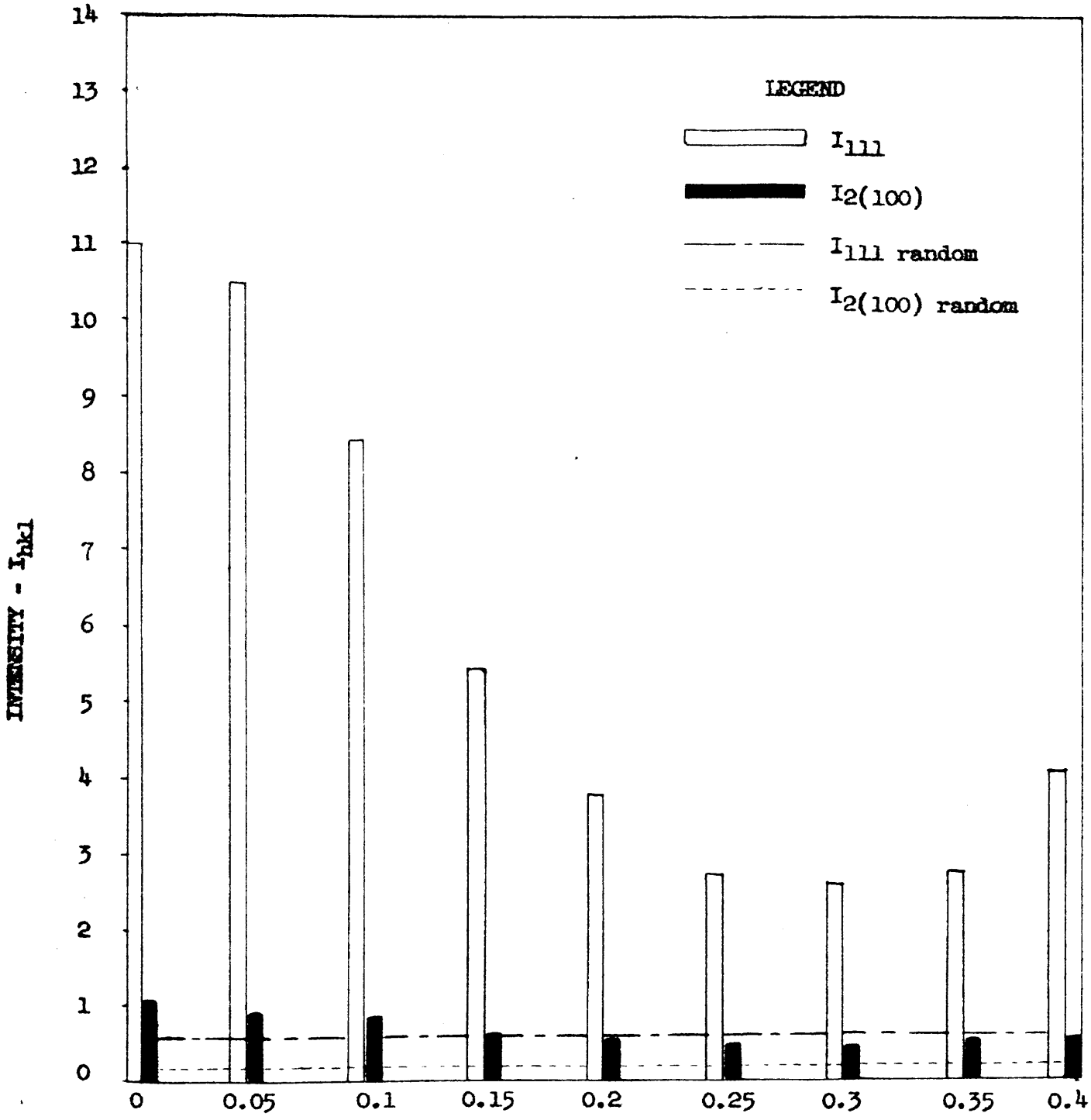

Distance (in inches) of the center of the area irradiated by the x-ray beam from the center of the specimen.

FIGURE 43. Relative (111) and 2(100) intensity from concentric regions at various distances from the fibre axis of a 20.6 per cent cold drawn (item no. 1) one inch diameter nickel rod.

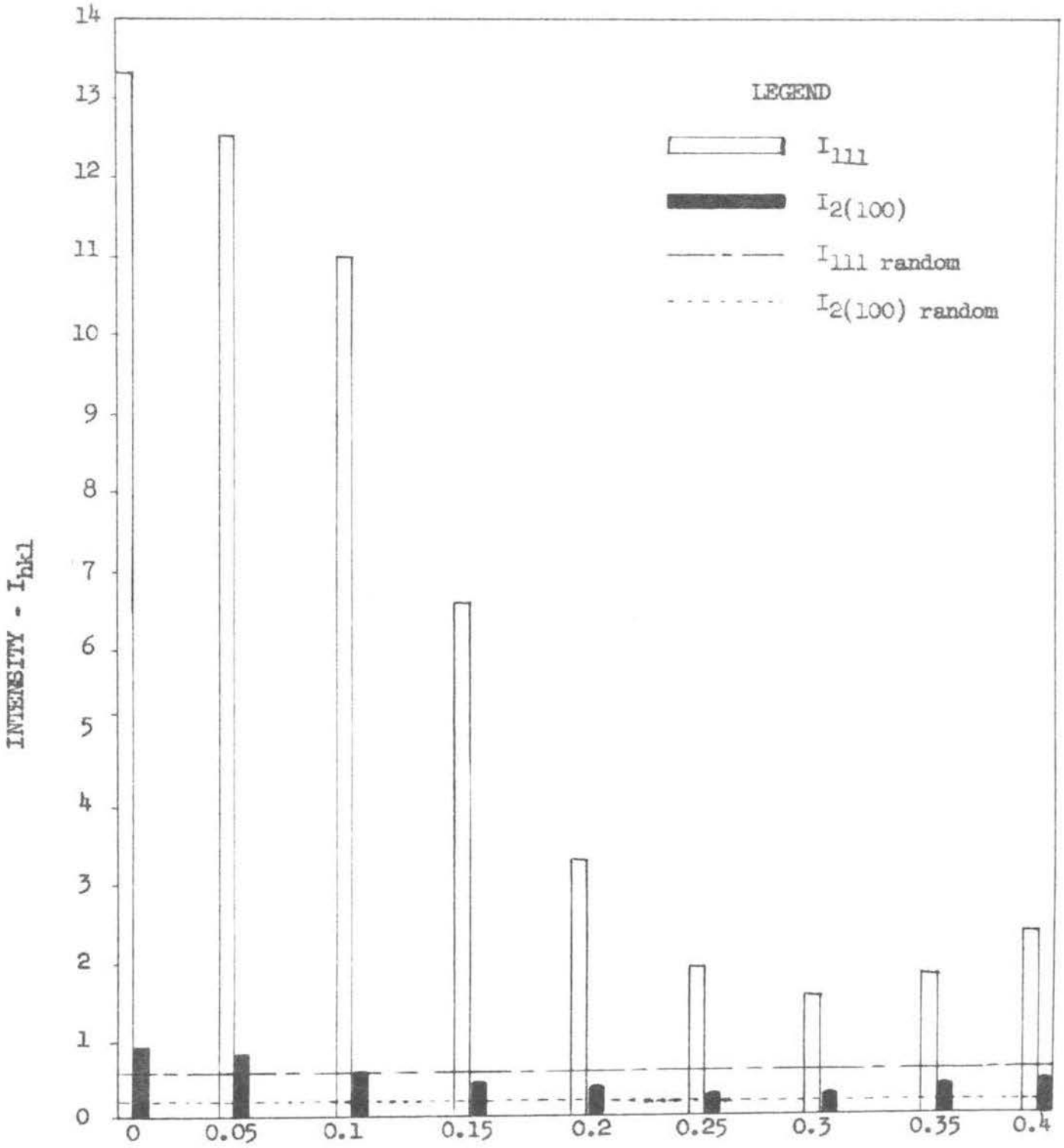

Distance (in inches) of the center of the area irradiated by the x-ray beam from the center of the specimen.

FIGURE 44. Relative (111) and 2(100) intensity from concentric regions at various distances from the fibre axis of a 40.5 per cent cold drawn (item no. 2) one inch diameter nickel rod.

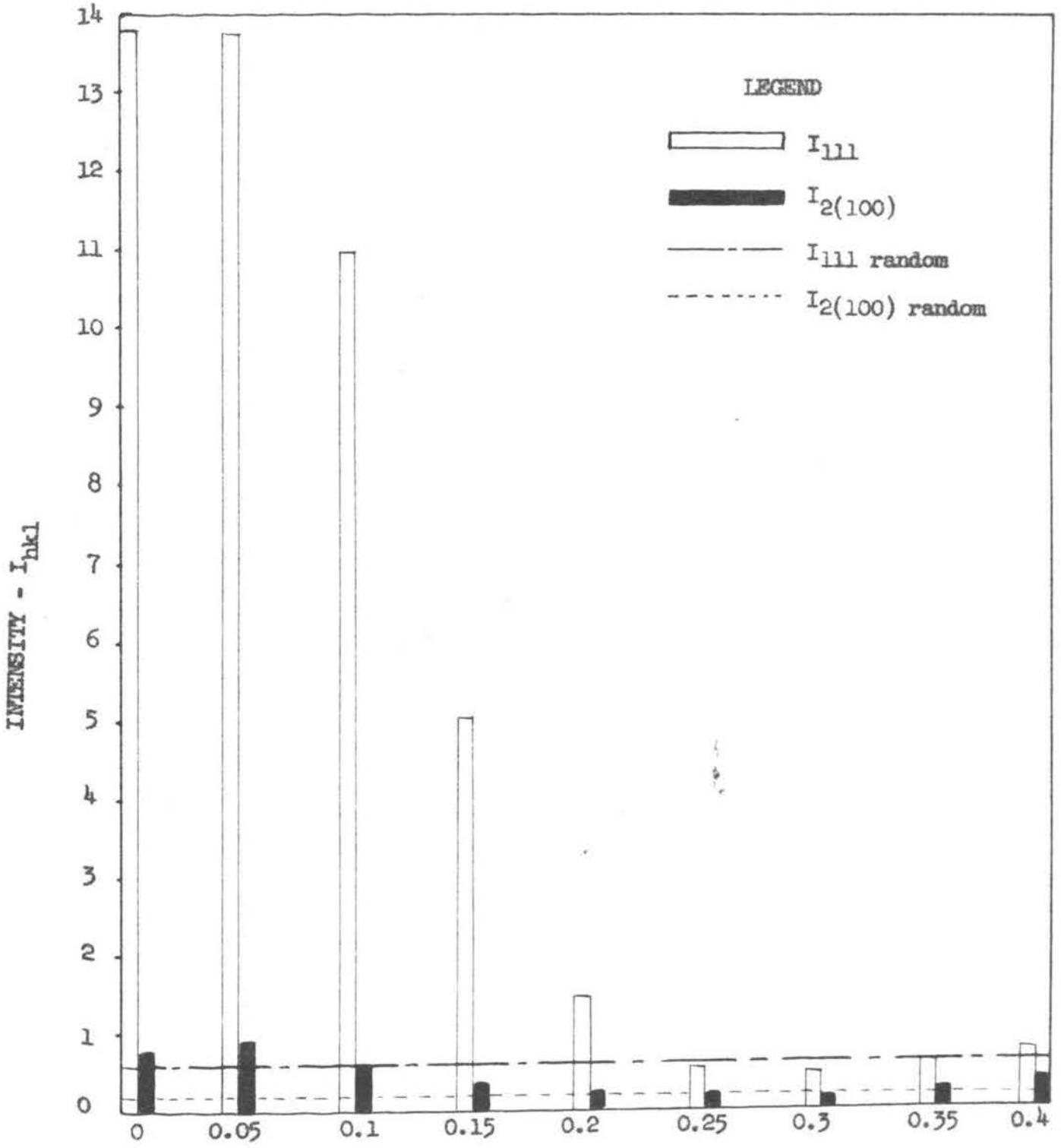

Distance (in inches) of the center of the area irradiated by the x-ray beam from the center of the specimen.

FIGURE 45. Relative (111) and 2(100) intensity from concentric regions at various distances from the fibre axis of a 60 per cent cold drawn (item no. 3) one inch diameter nickel rod.

TABLE XI

RELATIVE CONCENTRATION OF [111] AND [100] ORIENTED CRYSTALS AT THE FIBRE AXIS OF COLD DRAWN NICKEL RODS

Percent cold reduction	Relative concentrations (~~percent~~) of	
	[111] oriented crystals	[100] oriented crystals
20.6	100	9.7
40.5	100	6.7
60	100	5.2

Figure 46 shows the relation of variation in I_{111} intensity for different concentric regions to the amount of cold reduction in cold drawn nickel rods. It is seen that the intensity for the inner regions 1 through 4 increases with increased deformation, whereas region 5 shows a decrease upto 40 per cent cold reduction and then a slight increase as 60 per cent cold reduction is produced. In contrast to this, the intensity in the outer regions 6 through 9 steadily decreases with increasing cold reduction. Thus, the deformation characteristics of the groups of regions 1 through 4 and 6 through 9, though somewhat similar within each group, are different from each other.

During cold drawing of a metal all fibres undergo the same overall extension in the direction of the rod axis, still the amount of deformation in various regions around the fibre axis is seen to be different. This apparent anomaly can be explained in the following manner. If a metallic rod is subjected to pure tension, a uniform distribution of tensile stresses on the cross-section may be assumed. But when a metal is drawn through a die, the distribution of tensile stresses is modified by the radial compression developed during the drawing operation. The compressive stresses are maximum near the die walls and decrease as the fibre axis of the rod is approached. Thus the [111] texture in nickel, characteristic of deformation by tension, is expected to become more and more weak at increasing distances from the fibre axis. This fact is borne out by experimental x-ray diffraction data, shown in Figures 37 through 39.

Due to the tensile stresses predominant in the central regions

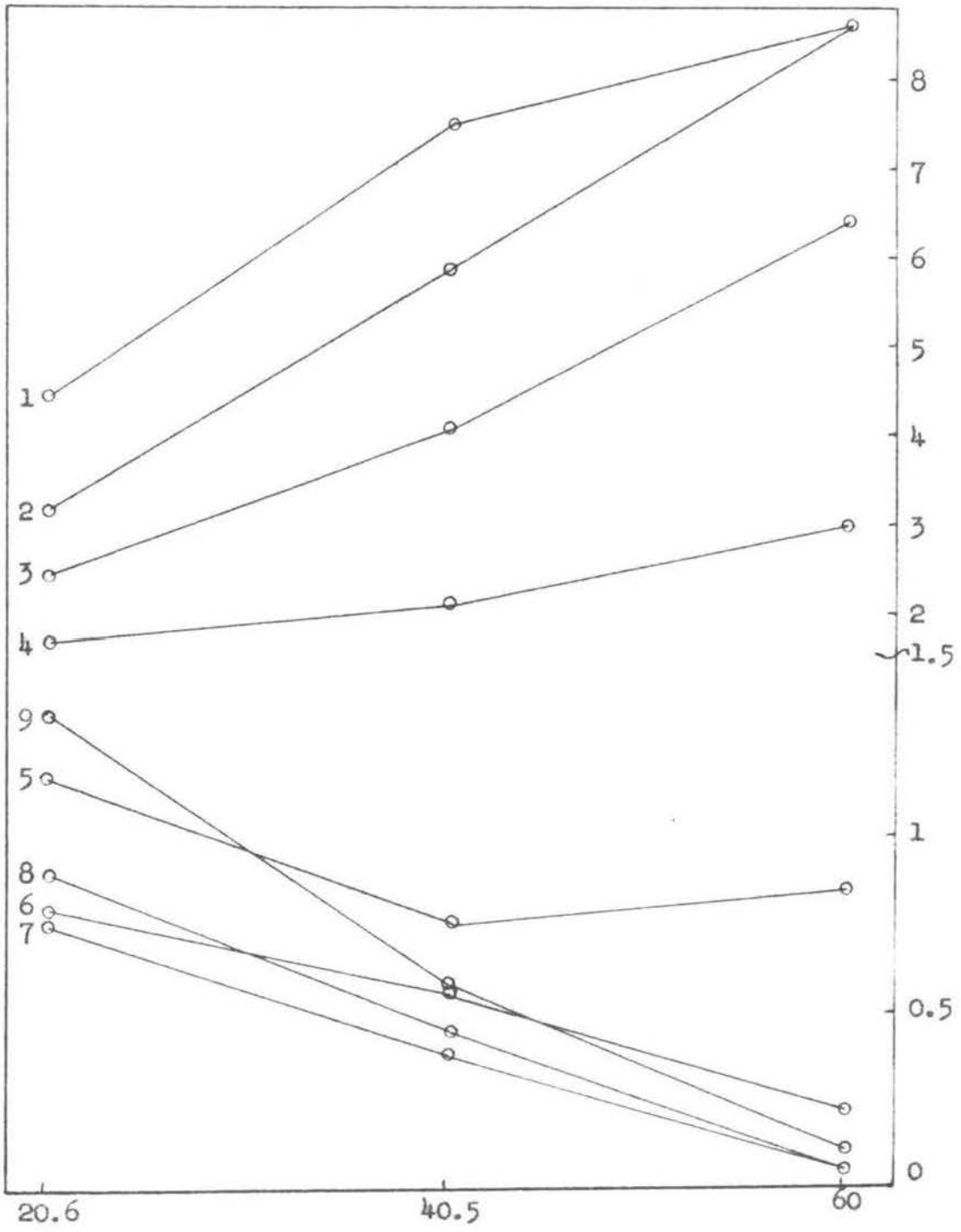

Percent cold reduction.

FIGURE 46. Relation of variation in (111) intensity for different concentric regions to the amount of cold reduction in cold drawn nickel rods.

of the rod, the crystals rotate to align their body diagonals--the largest dimension of the cube--along the tension direction. Whereas, due to superimposition of compressive and tensile stresses in the outer regions, the rotations are more complex and the body diagonals of the crystals do not align along the rod axis. Thus, even though the over-all extension of the fibres in a rod is the same, the degree of deformation increases with increasing distances from the fibre axis. A slight decrease in the amount of deformation in the outermost region of the rod, as indicated by increased concentration of [111] oriented crystals, is probably due to the effect of the drawing die which seems to hinder rotations of the crystals near the surface in directions other than parallel to its walls. It is easily seen that rotations in a direction parallel to the die walls tend to align the body diagonals along the fibre axis.

From the discussion given above, it may be concluded that the total deformation in a drawn rod first increases with increasing distance from the fibre axis almost to the surface where a slight decrease is observed.

Effect of annealing on variation in texture. Intensity data from the x-ray diffraction charts of the disc specimens annealed at 400°, 600°, 800° and 1000°C, as described previously, is listed in tables XII through XVII. Graphs of relative intensities of (111) and also of 2(100) reflections at various distances from the fibre axis on the disc specimens are shown in Figures 47 through 70. The specimens annealed at 800°C show a recrystallized fine grained struc-

TABLE XII

RELATIVE (111) INTENSITY AT VARIOUS DISTANCES FROM THE FIBRE AXIS OF 20.6 PERCENT (ITEM NO. 1) COLD DRAWN AND ANNEALED DISC SPECIMENS OF NICKEL

Distance from fibre axis (inches)	Annealing Temperature °C				
	As drawn	400	600	800	1000
0	4.43	6.4	4.76	0.87	2.15
0.05	3.2	4.16	3.95	0.49	1.45
0.1	2.47	2.97	2.69	0.35	1.02
0.15	1.7	1.97	1,85	0.25	1.3
0.2	1.16	1.3	1.4	0.15	1.25
0.25	0.8	0.95	0.91	0.3	1.1
0.3	0.75	0.95	0.9	0.43	0.85
0.35	0.9	1.05	0.9	0.43	0.5
0.4	1.35	1.55	1.2	0.6	0.7

TABLE XIII

RELATIVE (111) INTENSITY AT VARIOUS DISTANCES FROM THE FIBRE AXIS OF 40.5 PERCENT (ITEM NO. 2) COLD DRAWN AND ANNEALED DISC SPECIMENS OF NICKEL

Distance from fibre axis (inches)	Annealing Temperature °C				
	As drawn	400	600	800	1000
0	7.45	6.4	7.0	0.8	1.58
0.05	5.87	4.5	6.55	0.82	1.6
0.1	4.08	3.45	5.03	0.75	1.02
0.15	2.1	2.0	2.73	0.55	0.62
0.2	0.75	1.0	1.4	0.3	0.82
0.25	0.55	0.44	0.7	0.23	1.0
0.3	0.38	0.33	0.45	0.33	0.85
0.35	0.45	0.43	0.5	0.3	0.69
0.4	0.58	0.65	0.6	0.45	0.73

TABLE XIV

RELATIVE (111) INTENSITY AT VARIOUS DISTANCES FROM THE FIBRE AXIS OF 60 PERCENT (ITEM NO. 3) COLD DRAWN AND ANNEALED DISC SPECIMENS OF NICKEL

Distance from fibre axis (inches)	Annealing Temperature °C				
	As drawn	400	600	800	1000
0	8.6	9.8	10.2	0.25	0.12
0.05	8.6	8.35	9.1	0.45	0.15
0.1	6.4	7.0	5.0	0.4	0.45
0.15	3.0	3.28	1.75	0.26	0.35
0.2	0.85	1.12	0.71	0.37	0.56
0.25	0.22	0.38	0.1	0.22	0.6
0.3	0.05	0.1	0.05	0.1	0.75
0.35	0.05	0.06	0.1	0.15	0.8
0.4	0.12	0.12	0.2	0.22	0.35

TABLE XV

RELATIVE 2(100) INTENSITY AT VARIOUS DISTANCES FROM THE FIBRE AXIS OF 20.6 PERCENT (ITEM NO. 1) COLD DRAWN AND ANNEALED DISC SPECIMENS OF NICKEL

Distance from fibre axis (inches)	Annealing Temperature °C				
	As drawn	400	600	800	1000
0	4.1	5.1	3.8	2.3	1.65
0.05	3.6	3.95	3.15	1.4	1.63
0.1	2.73	3.1	2.4	1.1	1.87
0.15	2.2	2.15	2.0	0.7	2.0
0.2	1.85	1.6	1.6	1.2	1.0
0.25	1.4	1.55	1.5	1.0	2.2
0.3	1.35	1.5	1.5	0.84	1.6
0.35	1.55	2.0	1.65	0.85	1.18
0.4	2.15	2.5	2.25	1.0	0.7

TABLE XVI

RELATIVE 2(100) INTENSITY AT VARIOUS DISTANCES FROM THE FIBRE AXIS OF 40.5 PERCENT (ITEM NO. 2) COLD DRAWN AND ANNEALED DISC SPECIMENS OF NICKEL

Distance from fibre axis (inches)	Annealing Temperature °C				
	As drawn	400	600	800	1000
0	2.8	3.65	3.4	2.45	1.35
0.05	2.2	2.43	3.0	1.8	0.8
0.1	1.65	1.75	1.9	1.43	1.0
0.15	1.2	1.15	1.4	0.93	1.25
0.2	1.16	1.0	1.15	1.15	0.75
0.25	1.05	0.9	1.1	1.15	1.0
0.3	1.03	0.9	1.0	0.95	1.22
0.35	1.4	1.35	1.2	1.3	1.2
0.4	1.73	1.7	1.62	1.2	1.8

TABLE XVII

RELATIVE 2(100) INTENSITY AT VARIOUS DISTANCES FROM THE FIBRE AXIS OF 60 PERCENT (ITEM NO. 3) COLD DRAWN AND ANNEALED DISC SPECIMENS OF NICKEL

Distance from fibre axis (inches)	Annealing Temperature °C				
	As drawn	400	600	800	1000
0	2.75	3.1	3.5	1.5	1.4
0.05	2.75	3.25	3.3	1.55	1.7
0.1	2.0	2.45	2.4	1.25	2.5
0.15	1.17	1.4	1.39	1.06	1.4
0.2	0.87	0.9	0.93	1.05	2.2
0.25	0.62	0.7	0.7	1.35	2.6
0.3	0.61	0.6	0.63	1.35	2.4
0.35	0.9	0.81	0.8	0.72	2.1
0.4	1.2	1.14	1.2	1.48	1.8

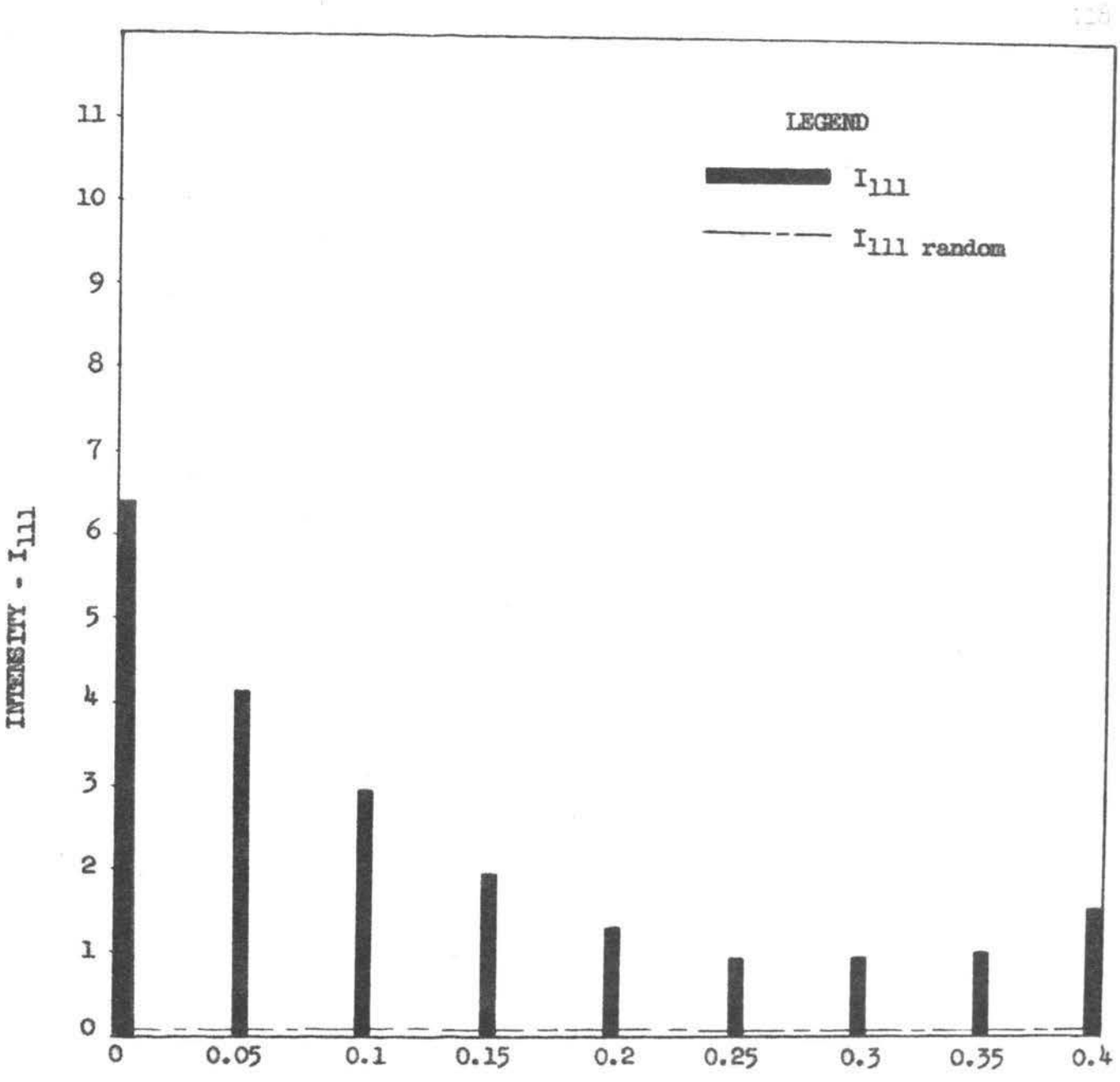

Distance (in inches) of the center of the area irradiated by the x-ray beam from the center of the specimen.

FIGURE 47. Relative (111) intensity from concentric regions at various distances from the fibre axis of a 20.6 per cent cold drawn one inch diameter nickel rod annealed at 400°C for one hour.

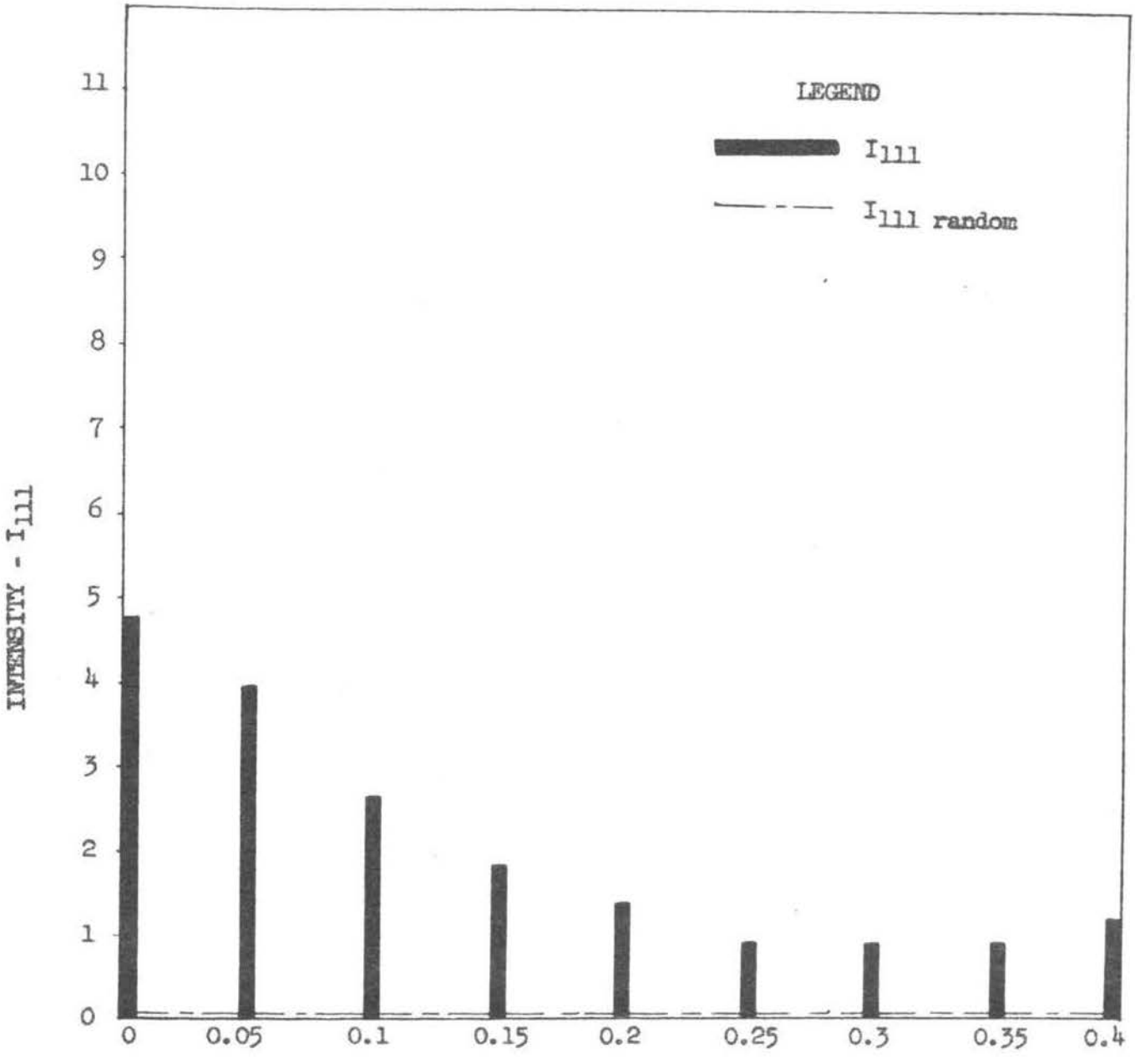

Distance (in inches) of the center of the area irradiated by the x-ray beam from the center of the specimen.

FIGURE 48. Relative (111) intensity from concentric regions at various distances from the fibre axis of a 20.6 per cent cold drawn one inch diameter nickel rod annealed at 600°C for one hour.

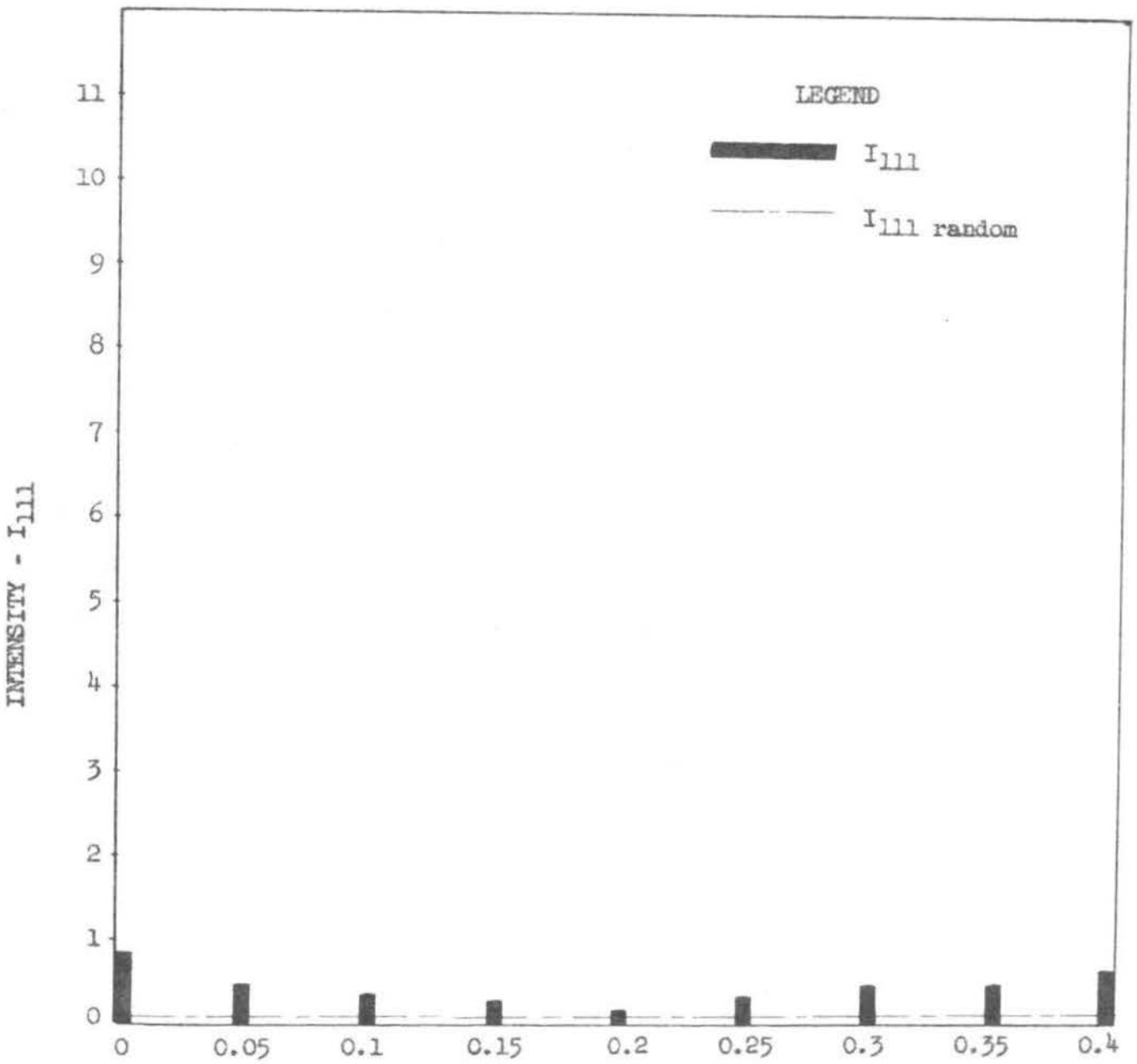

Distance (in inches) of the center of the area irradiated by the x-ray beam from the center of the specimen.

FIGURE 49. Relative (111) intensity from concentric regions at various distances from the fibre axis of a 20.6 per cent cold drawn one inch diameter nickel rod annealed at 800°C for one hour.

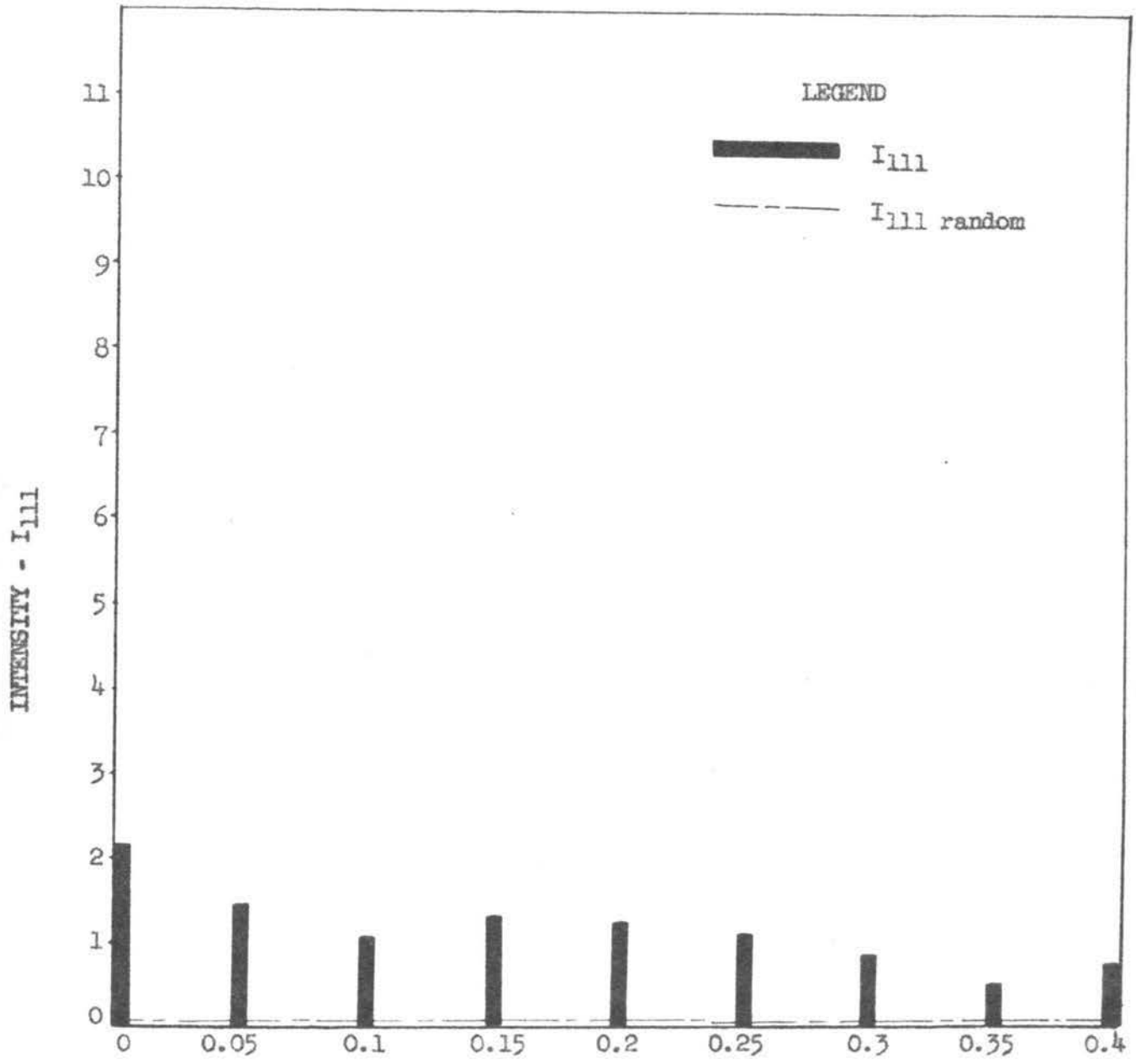

Distance (in inches) of the center of the area irradiated by the x-ray beam from the center of the specimen.

FIGURE 50. Relative (111) intensity from concentric regions at various distances from the fibre axis of a 20.6 per cent cold drawn one inch diameter nickel rod annealed at 1000°C for one hour.

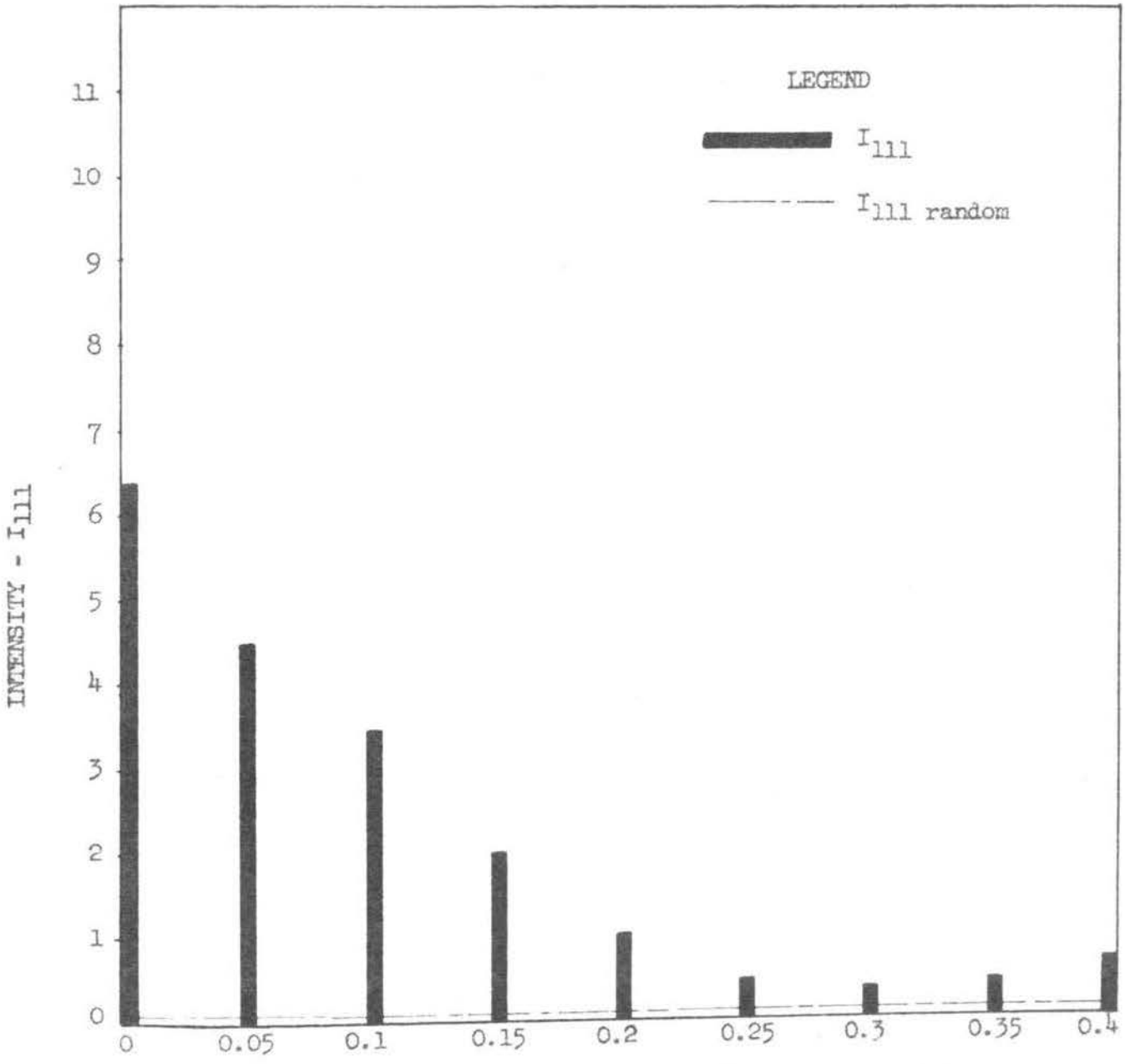

Distance (in inches) of the center of the area irradiated by the x-ray beam from the center of the specimen.

FIGURE 51. Relative (111) intensity from concentric regions at various distances from the fibre axis of a 40.5 per cent cold drawn one inch diameter nickel rod annealed at 400°C for one hour.

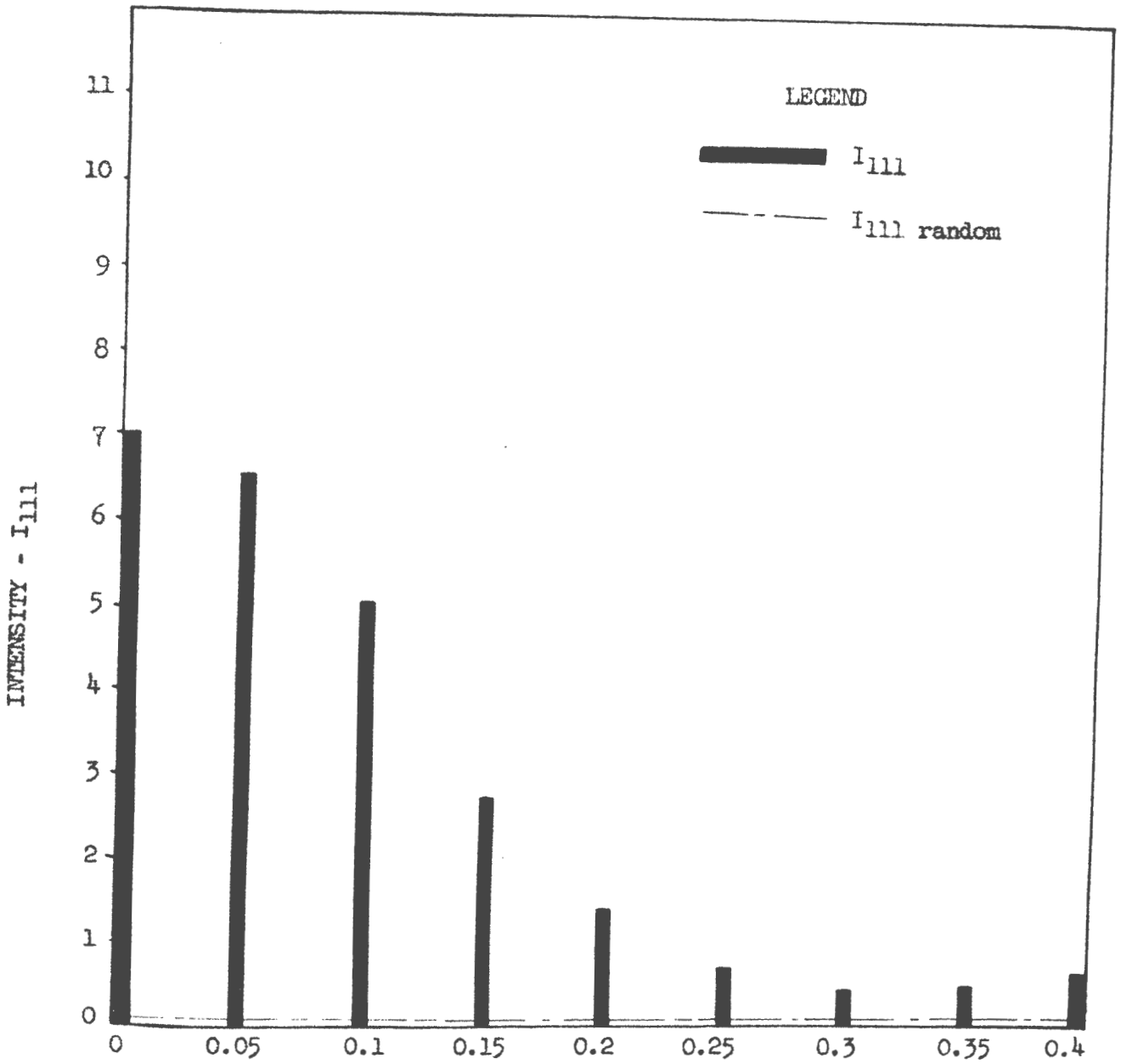

Distance (in inches) of the center of the area irradiated by the x-ray beam from the center of the specimen.

FIGURE 52. Relative (111) intensity from concentric regions at various distances from the fibre axis of a 40.5 per cent cold drawn one inch diameter nickel rod annealed at 600°C for one hour.

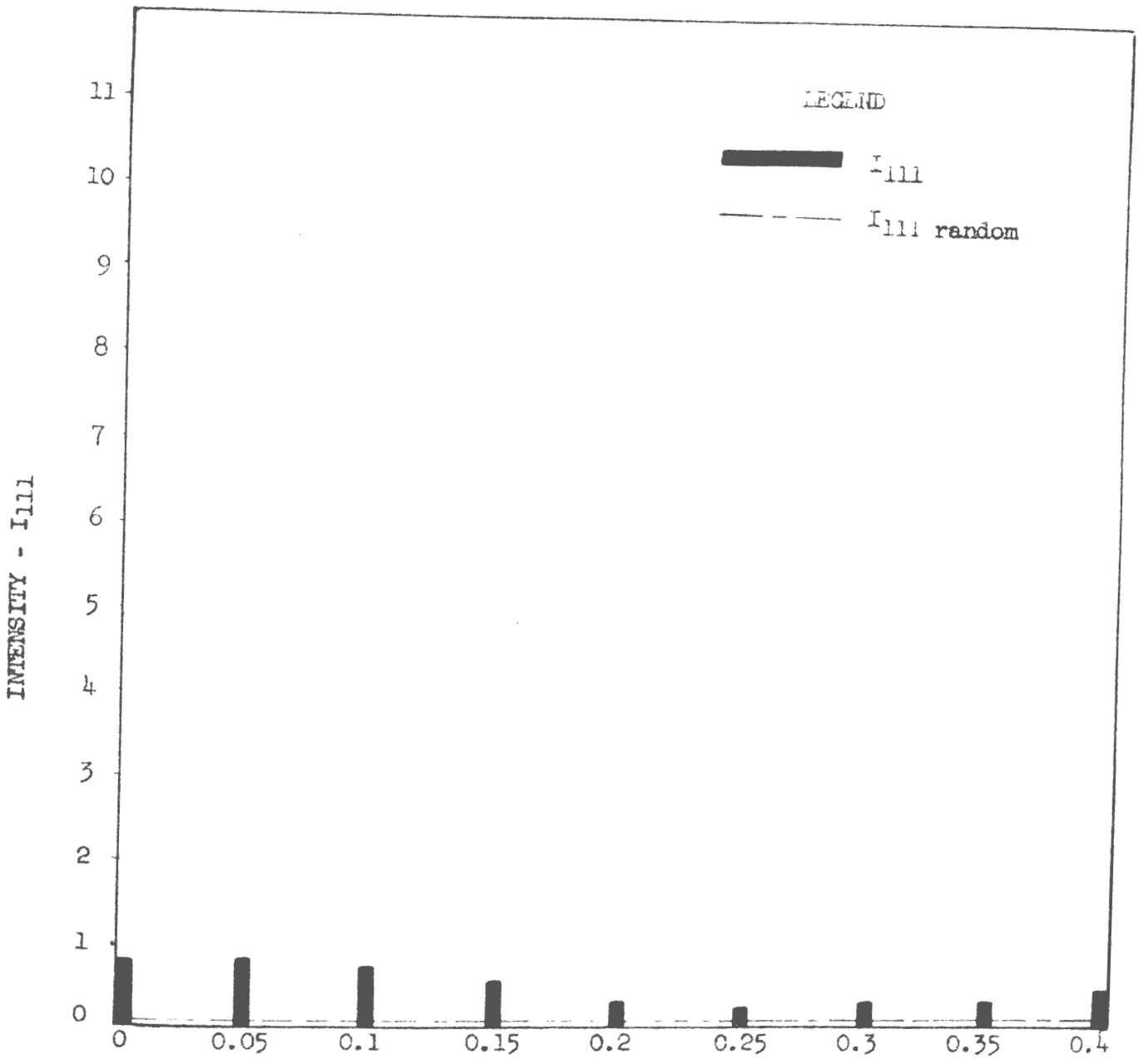

Distance (in inches) of the center of the area irradiated by the x-ray beam from the center of the specimen.

FIGURE 53. Relative (111) intensity from concentric regions at various distances from the fibre axis of a 40.5 per cent cold drawn one inch diameter nickel rod annealed at 600°C for one hour.

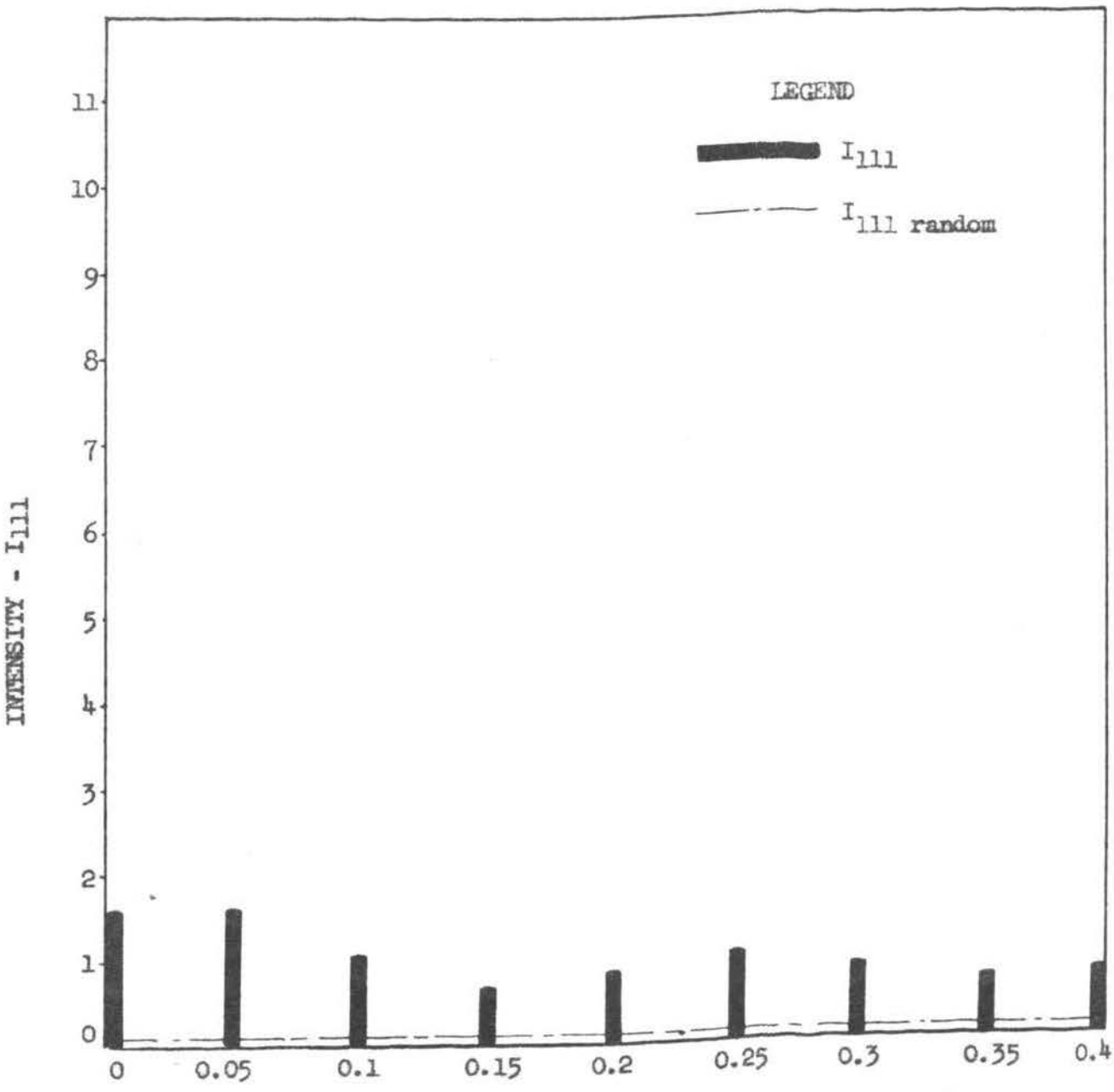

Distance (in inches) of the center of the area irradiated by the x-ray beam from the center of the specimen.

FIGURE 54. Relative (111) intensity from concentric regions at various distances from the fibre axis of a 40.5 per cent cold drawn one inch diameter nickel rod annealed at 1000°C for one hour.

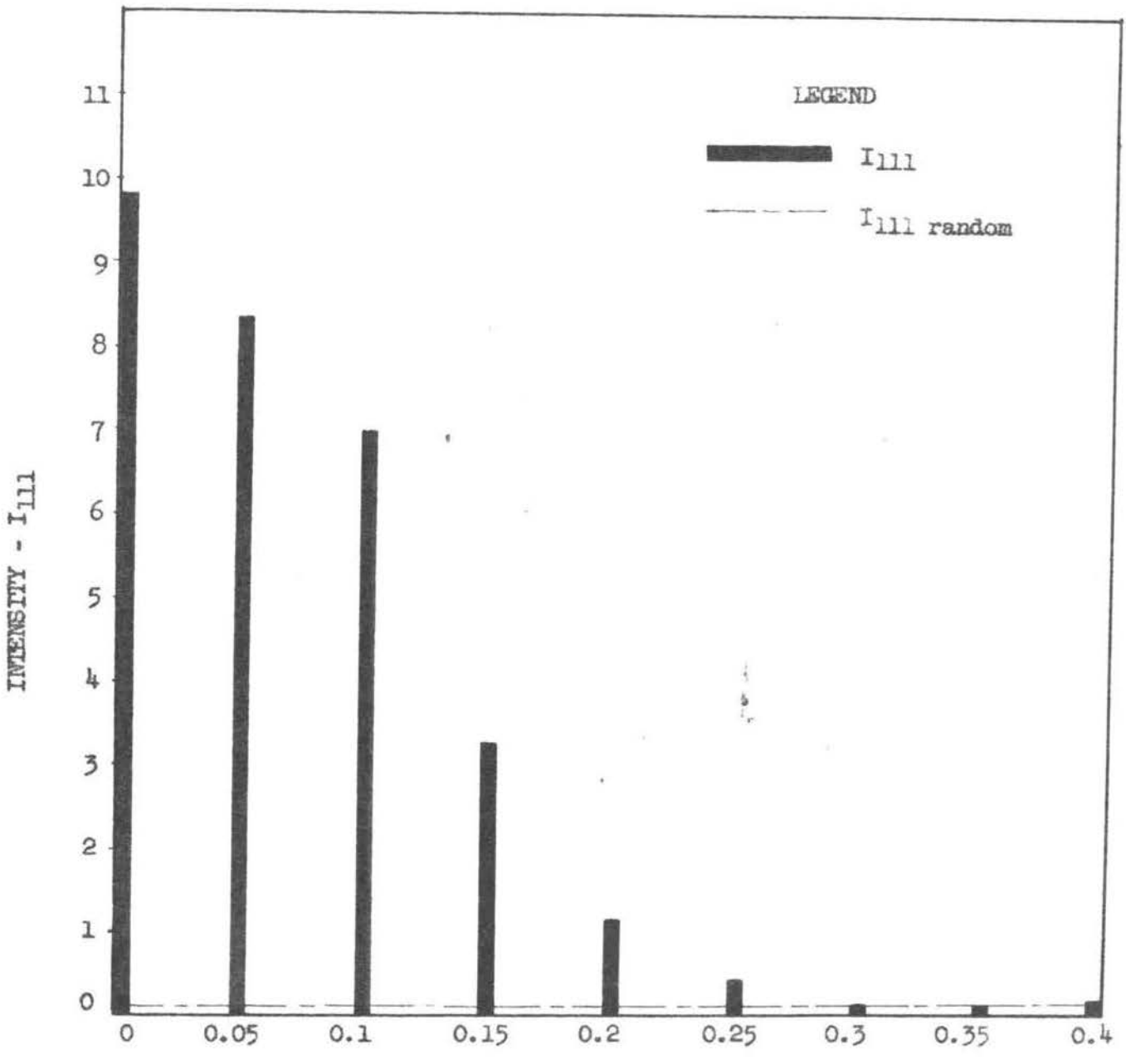

Distance (in inches) of the center of the area irradiated by the x-ray beam from the center of the specimen.

FIGURE 55. Relative (111) intensity from various concentric regions at various distances from the fibre axis of a 60 per cent cold drawn one inch diameter nickel rod annealed at 400°C for one hour.

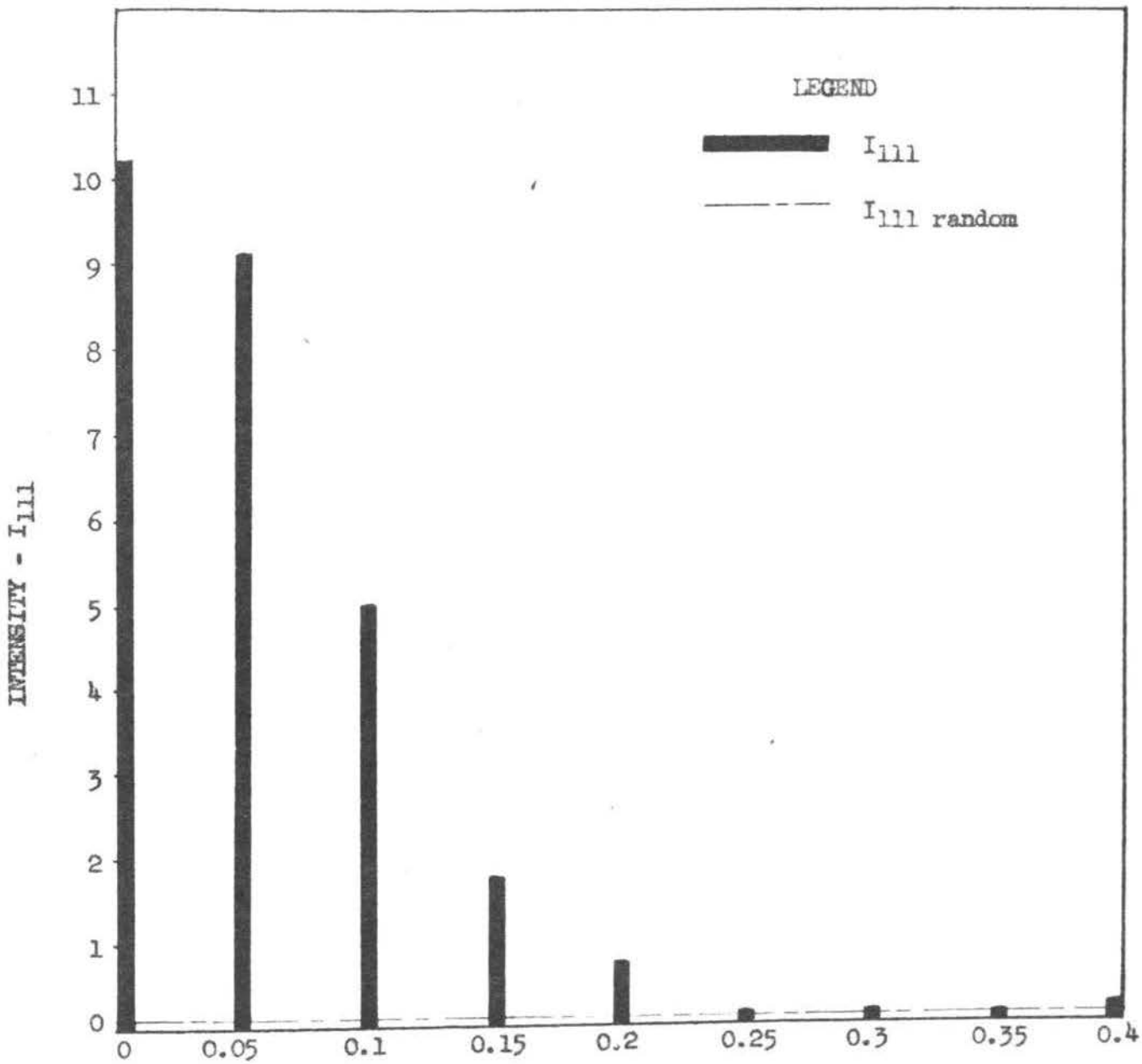

Distance (in inches) of the center of the area irradiated by the x-ray beam from the center of the specimen.

FIGURE 56. Relative (111) intensity from concentric regions at various distances from the fibre axis of a 60 per cent cold drawn one inch diameter nickel rod annealed at 600°C for one hour.

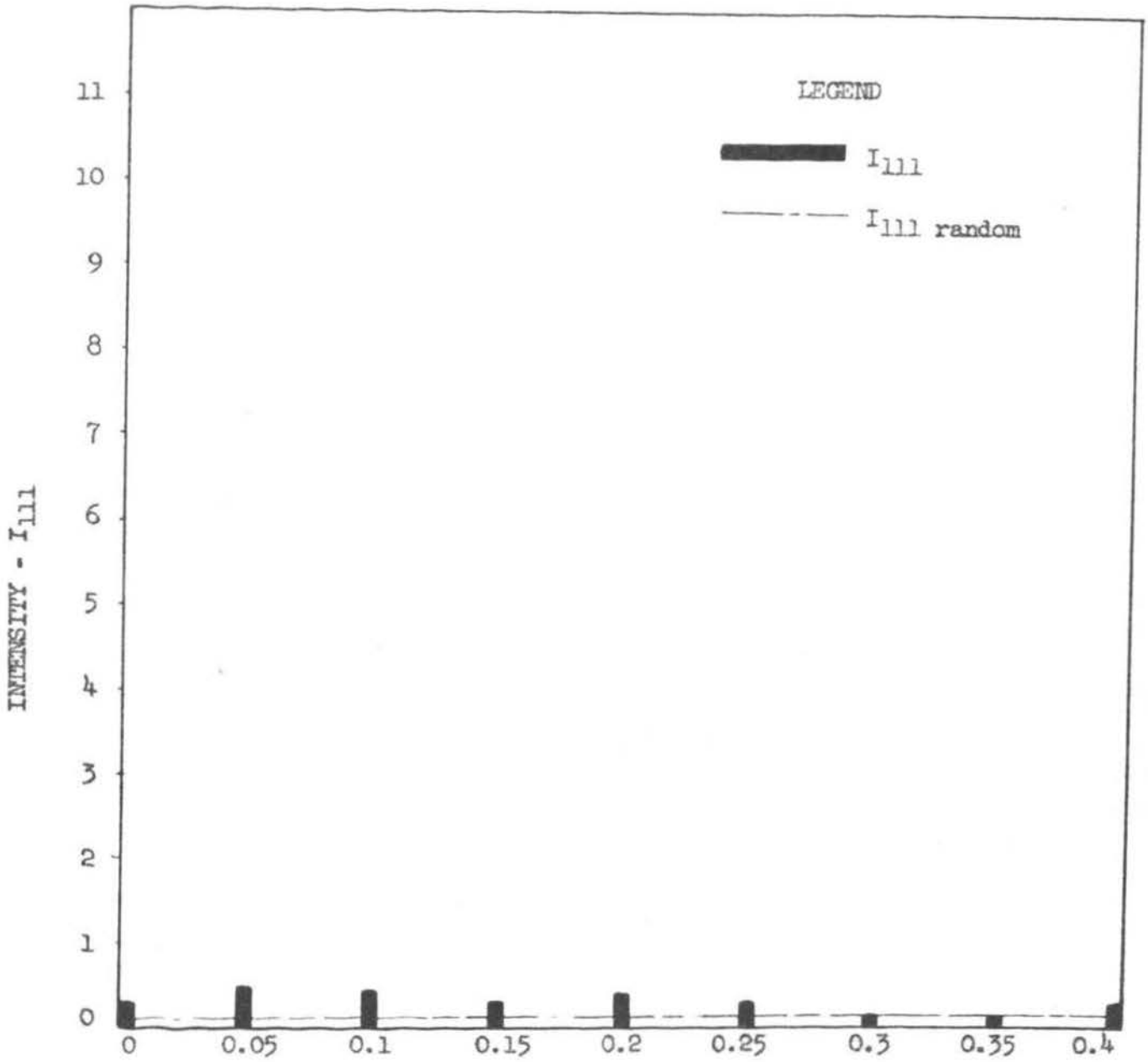

FIGURE 57. Relative (111) intensity from concentric regions at various distances from the fibre axis of a 60 per cent cold drawn one inch diameter nickel rod annealed at 800°C for one hour.

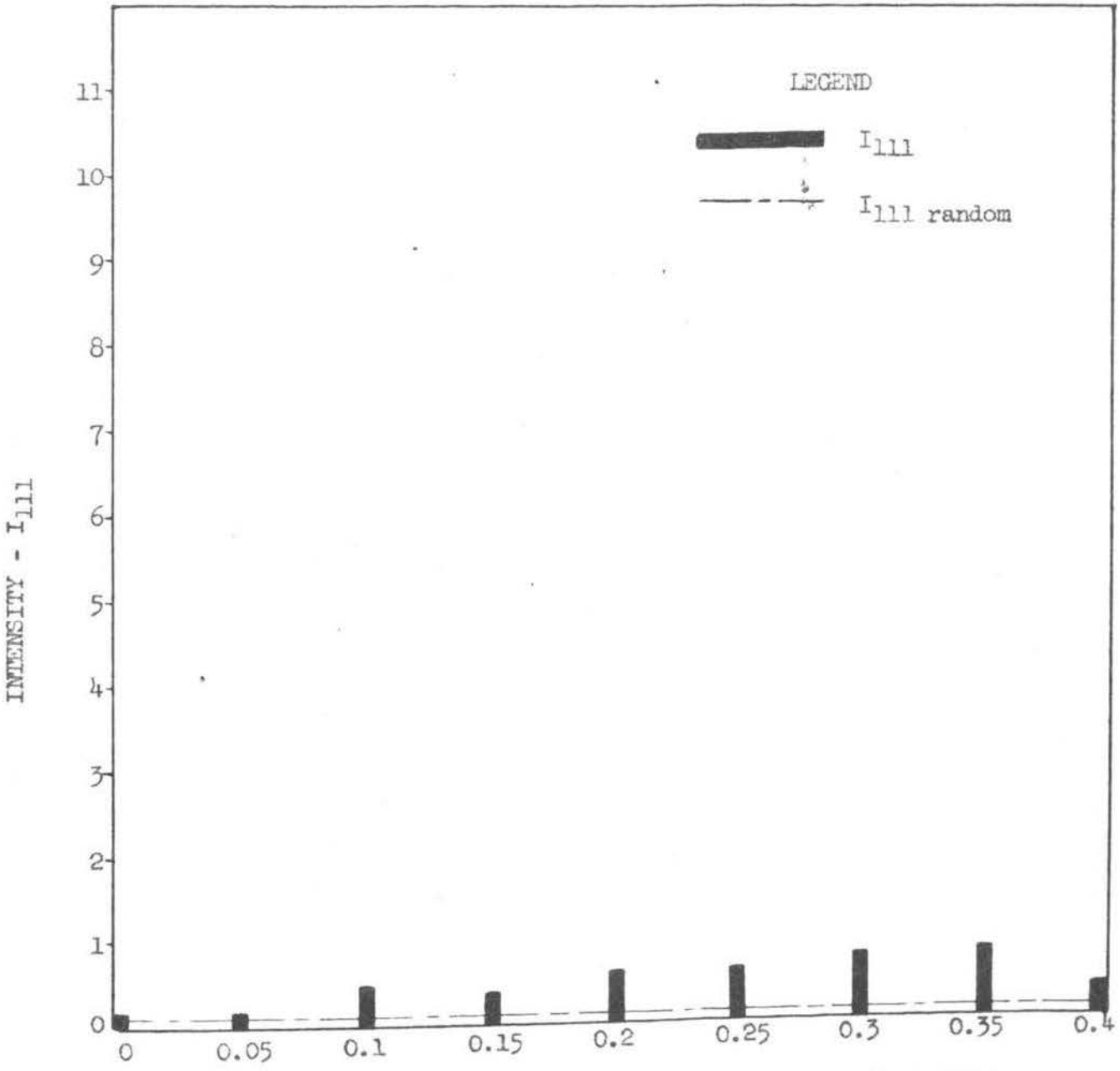

FIGURE 58. Relative (111) intensity from concentric regions at various distances from the fibre axis of a 60 per cent cold drawn one inch diameter nickel rod annealed at 1000°C for one hour.

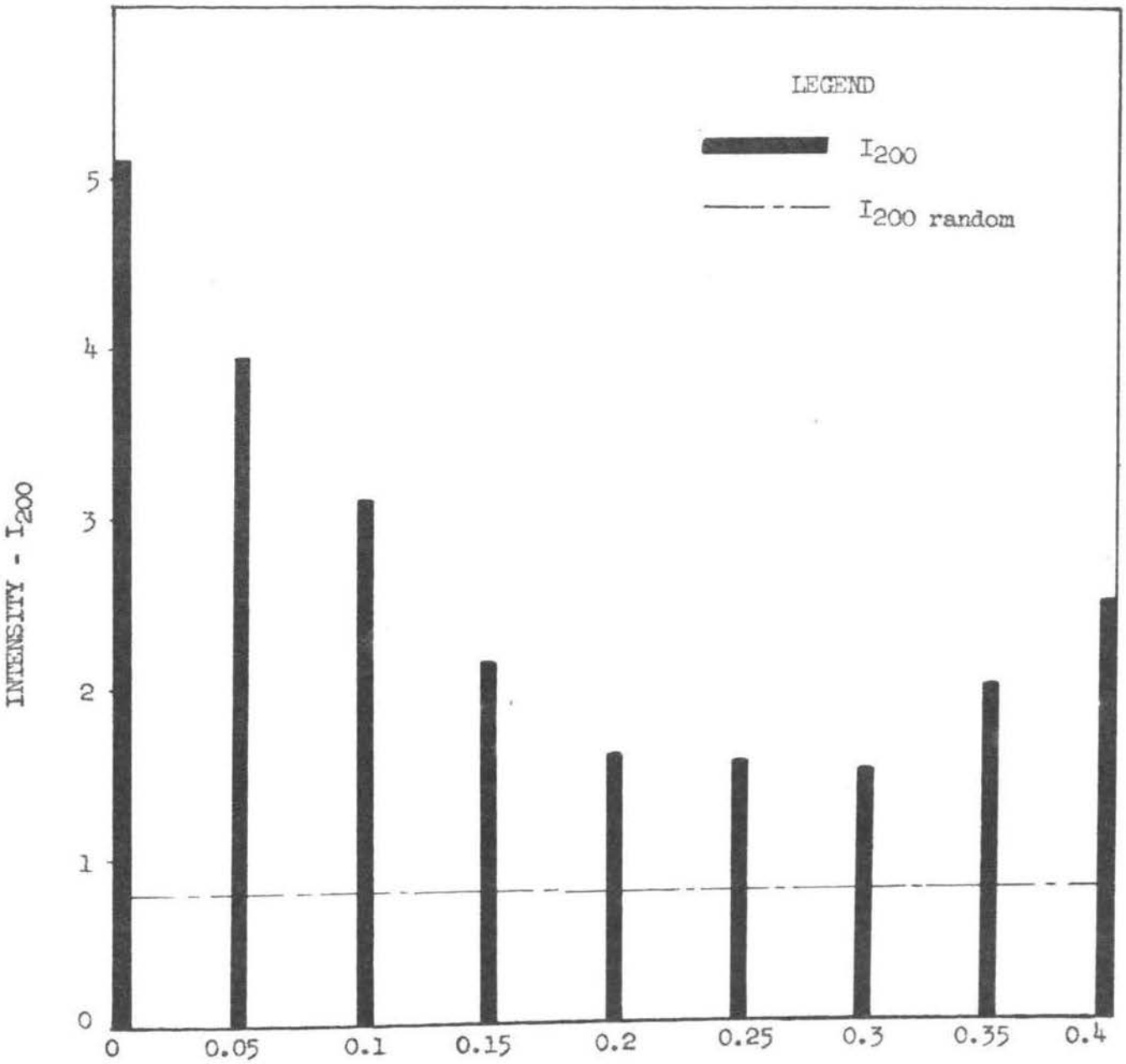

Distance (in inches) of the center of the area irradiated by the x-ray beam from the center of the specimen.

FIGURE 59. Relative 2(100) intensity from concentric regions at various distances from the fibre axis of a 20.6 per cent cold drawn one inch diameter nickel rod annealed at 400°C for one hour.

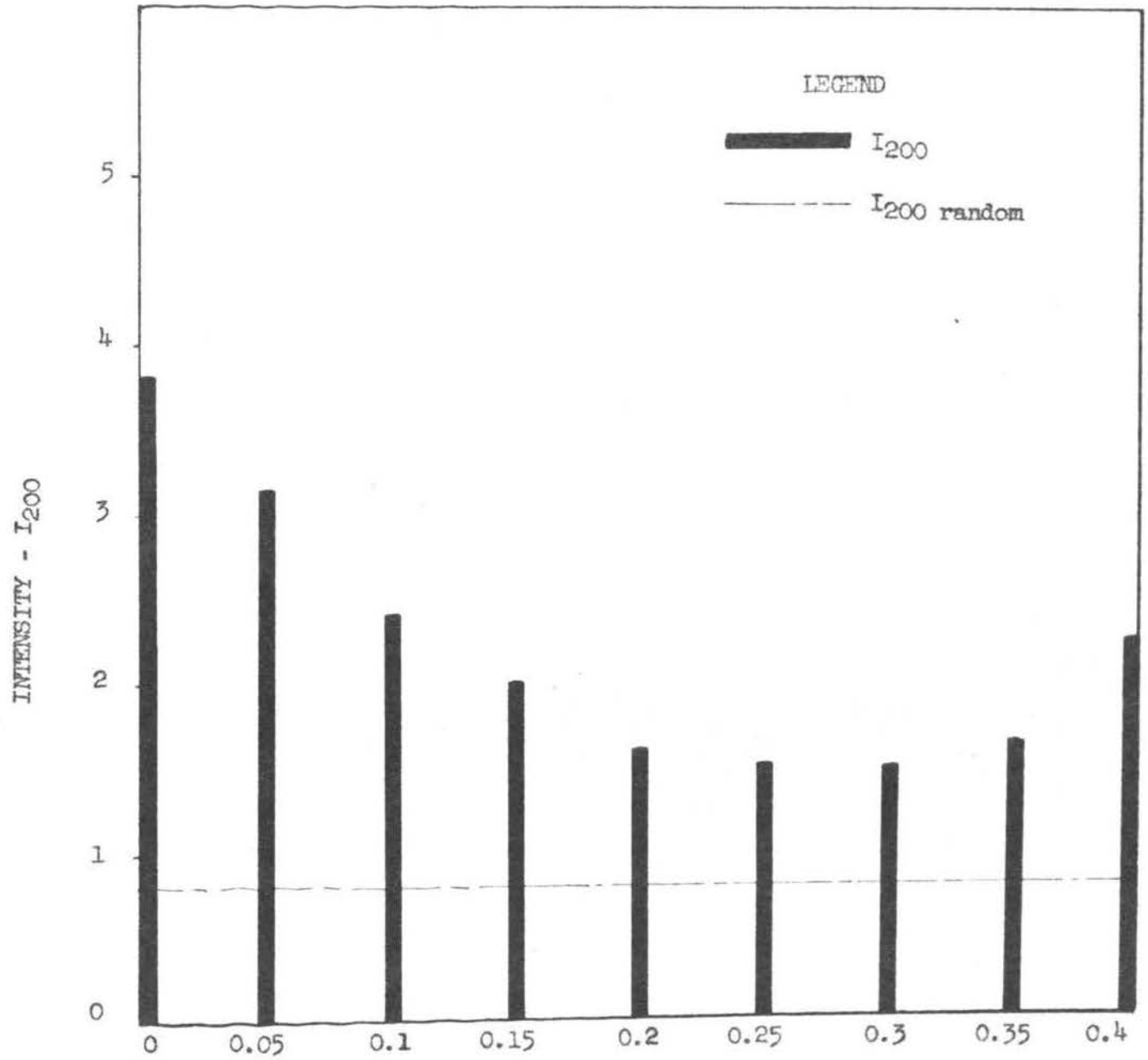

Distance (in inches) of the center of the area irradiated by the x-ray beam from the center of the specimen.

FIGURE 60. Relative 2(100) intensity from concentric regions at various distances from the fibre axis of a 20.6 per cent cold drawn one inch diameter nickel rod annealed at 600°C for one hour.

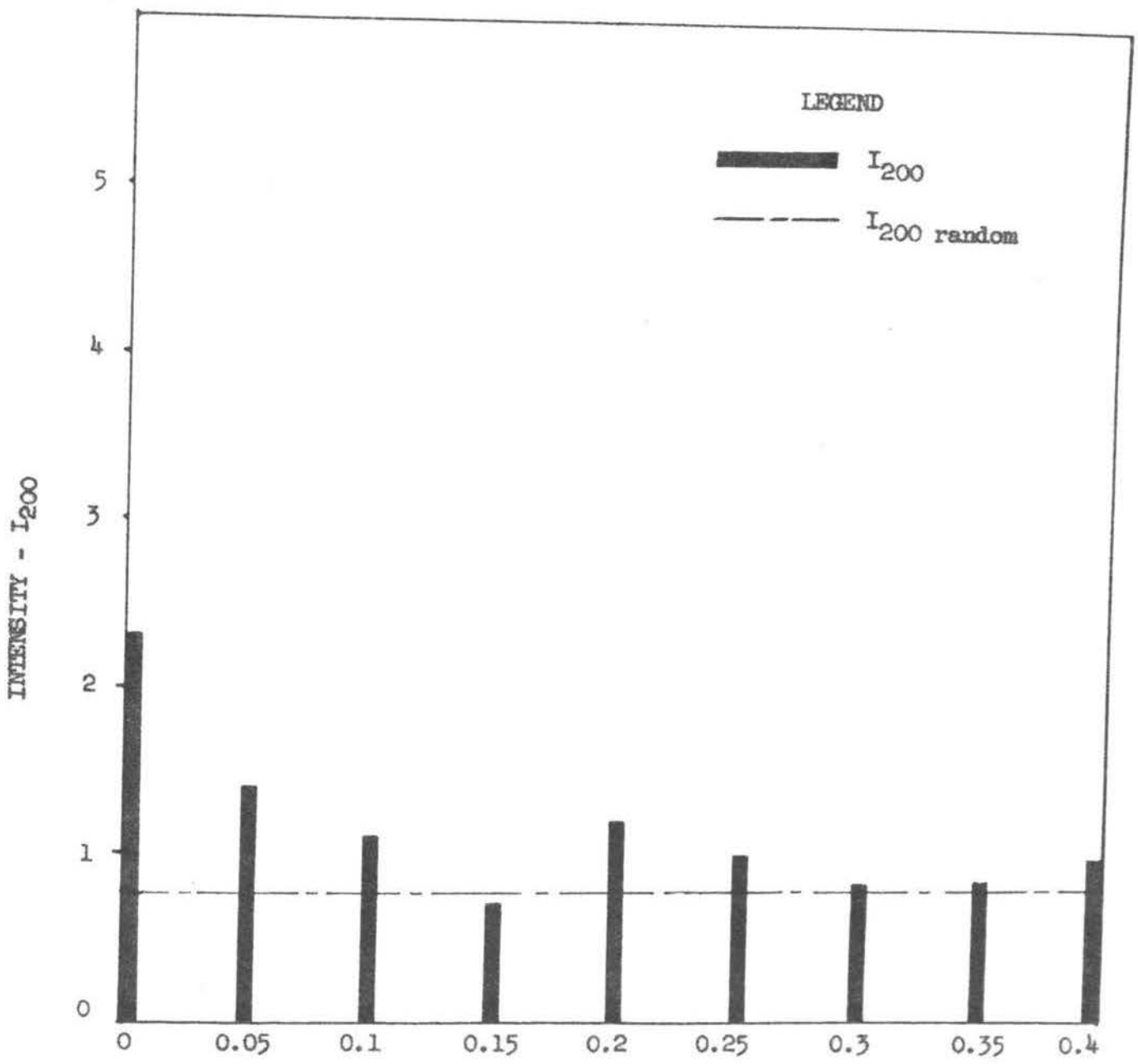

FIGURE 61. Relative 2(100) intensity from concentric regions at various distances from the fibre axis of a 20.6 per cent cold drawn one inch diameter nickel rod annealed at 800°C for one hour.

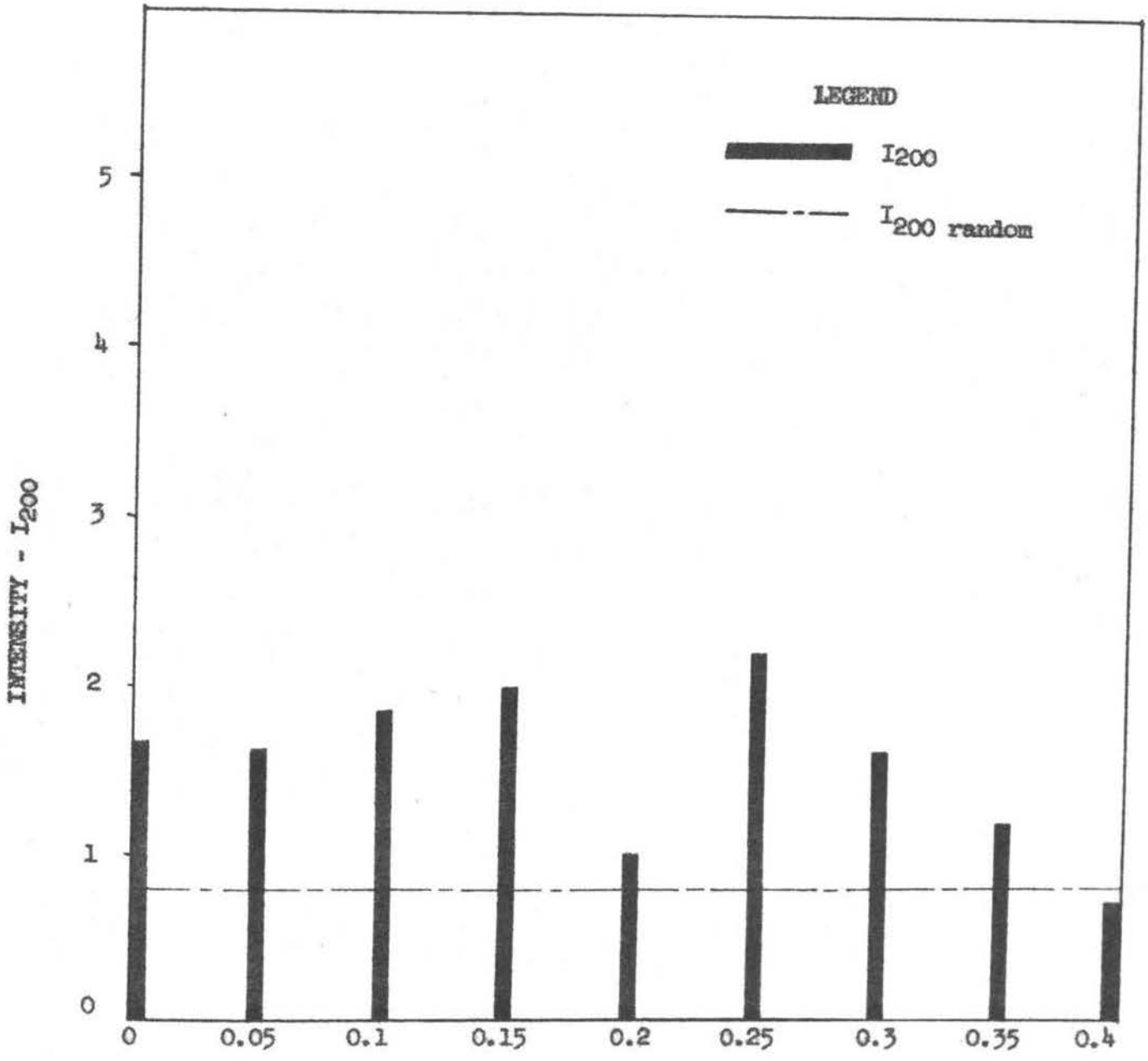

Distance (in inches) of the center of the area irradiated by the x-ray beam from the center of the specimen.

FIGURE 62. Relative 2(100) intensity from concentric regions at various distances from the fibre axis of a 20.6 per cent cold drawn one inch diameter nickel rod annealed at 1000°C for one hour.

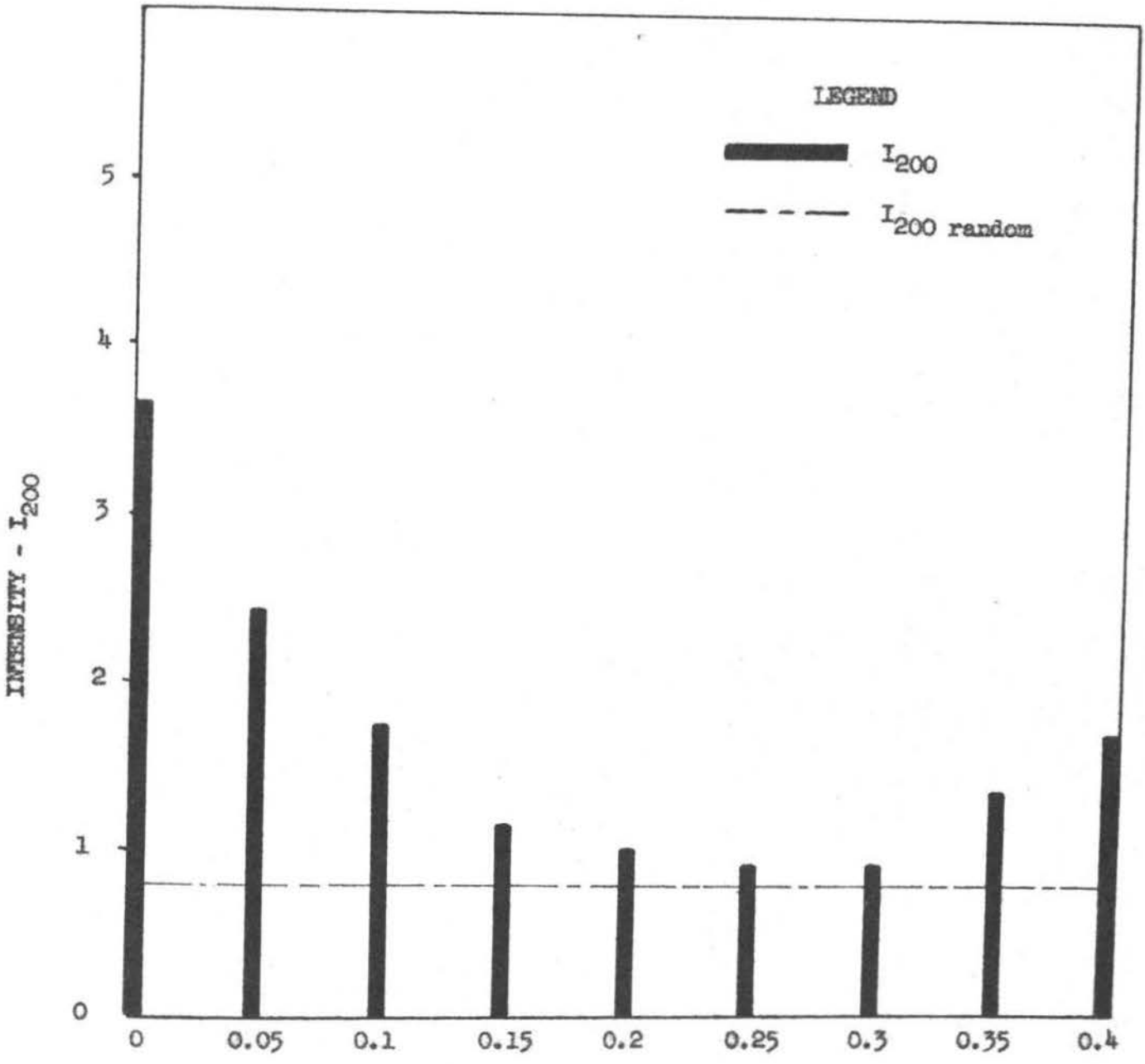

FIGURE 63. Relative 2(100) intensity from concentric regions at various distances from the fibre axis of a 40.5 per cent cold drawn one inch diameter nickel rod annealed at 400°C for one hour.

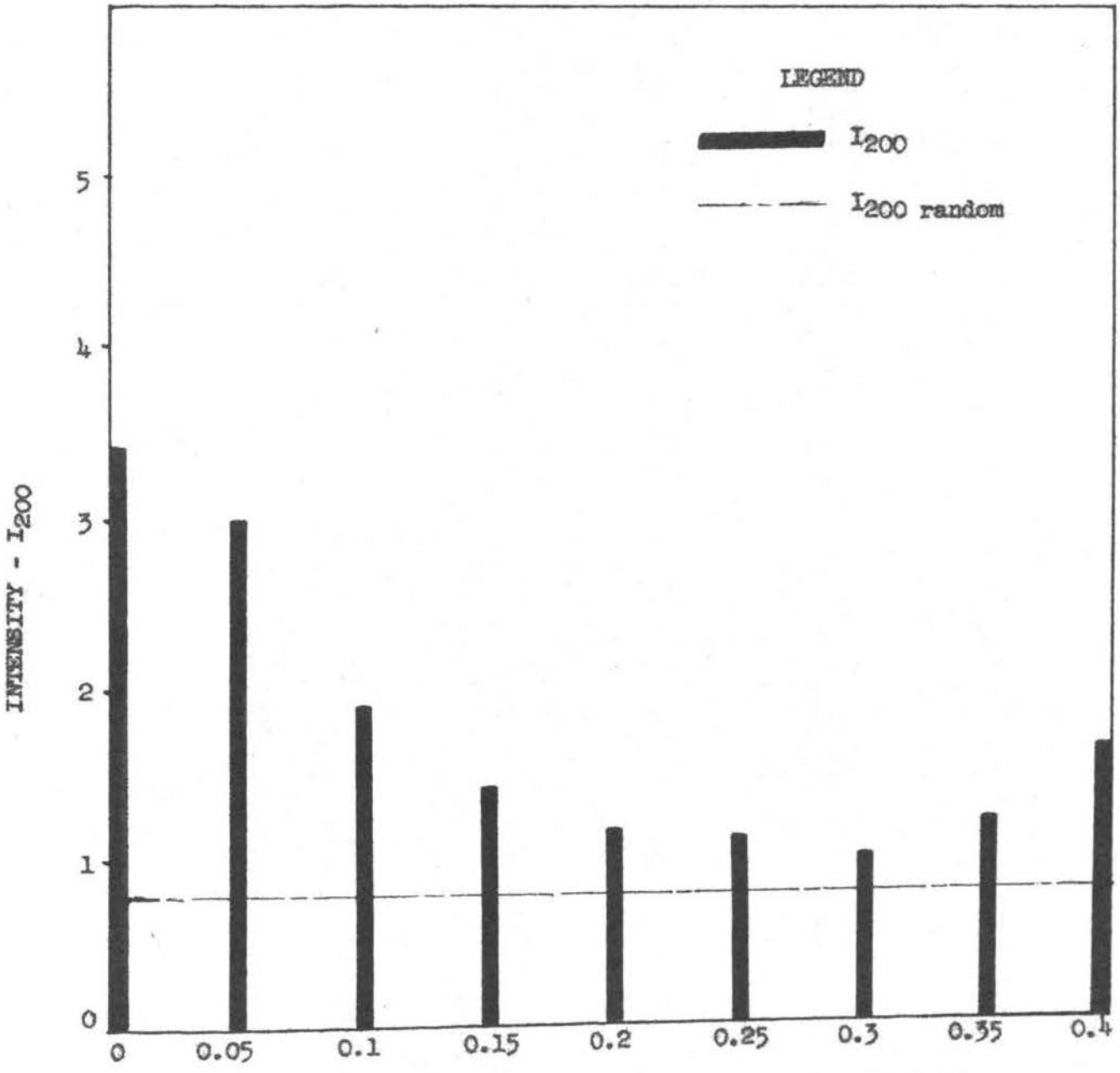

FIGURE 64. Relative 2(100) intensity from concentric regions at various distances from the fibre axis of a 40.5 per cent cold drawn one inch diameter nickel rod annealed at 600°C for one hour.

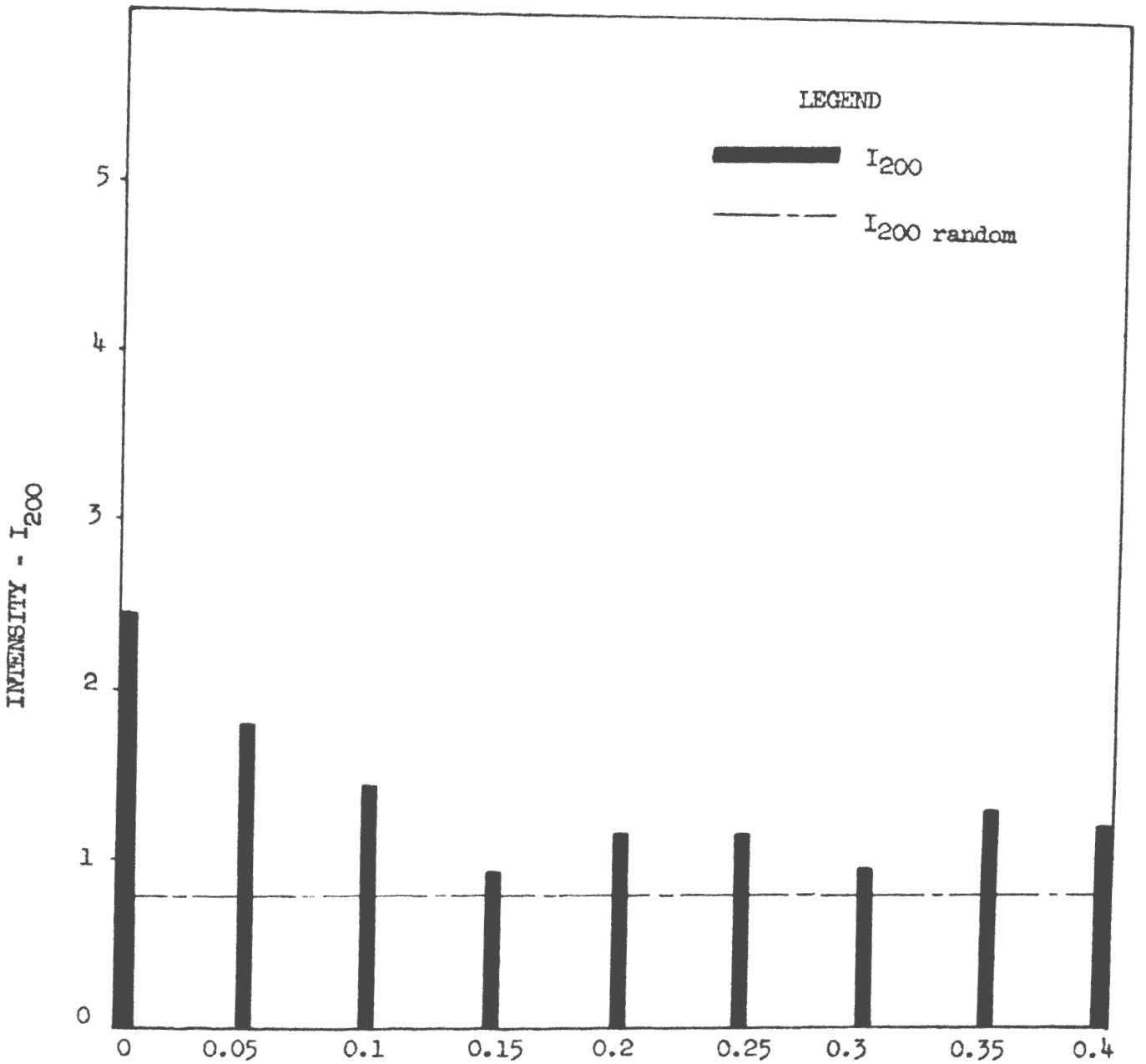

Distance (in inches) of the center of the area irradiated by the x-ray beam from the center of the specimen.

FIGURE 65. Relative 2(100) intensity from concentric regions at various distances from the fibre axis of a 40.5 per cent cold drawn one inch diameter nickel rod annealed at 800°C for one hour.

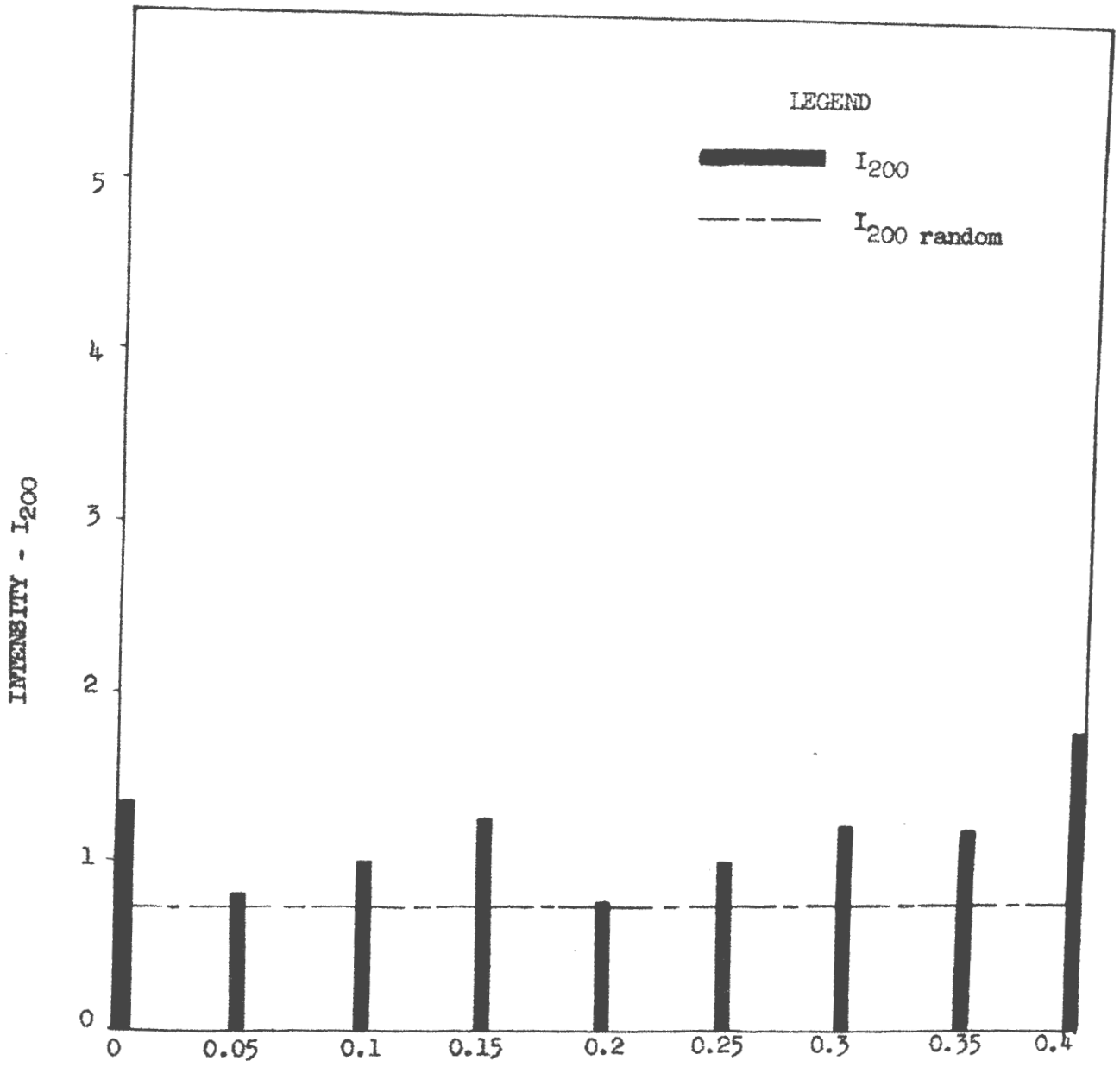

Distance (in inches) of the center of the area irradiated by the x-ray beam from the center of the specimen.

FIGURE 66. Relative 2(100) intensity from concentric regions at various distances from the fibre axis of a 40.5 per cent cold drawn one inch diameter nickel rod annealed at 1000°C for one hour.

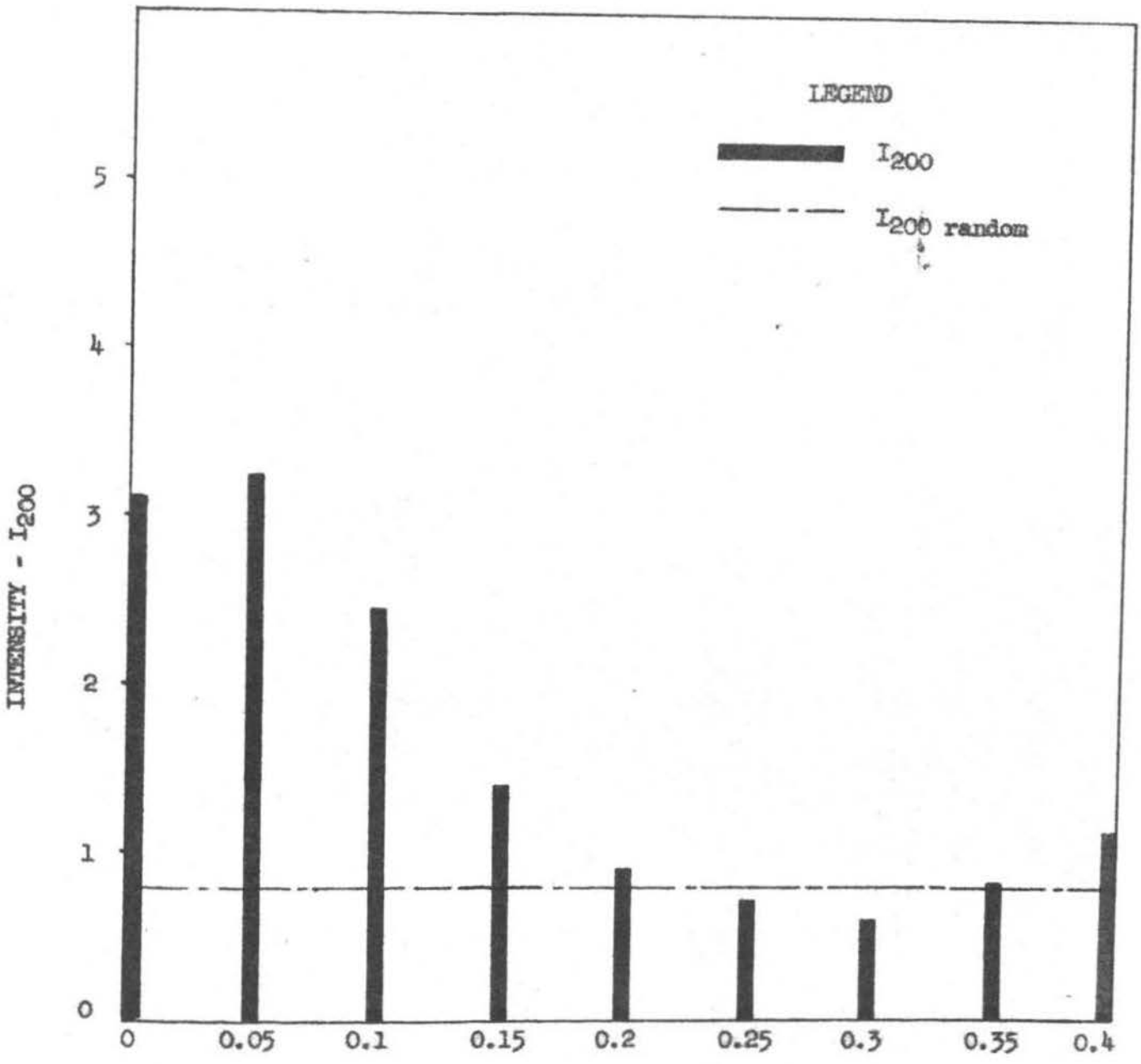

FIGURE 67. Relative 2(100) intensity from concentric regions at various distances from the fibre axis of a 60 per cent cold drawn one inch diameter nickel rod annealed at 400°C for one hour.

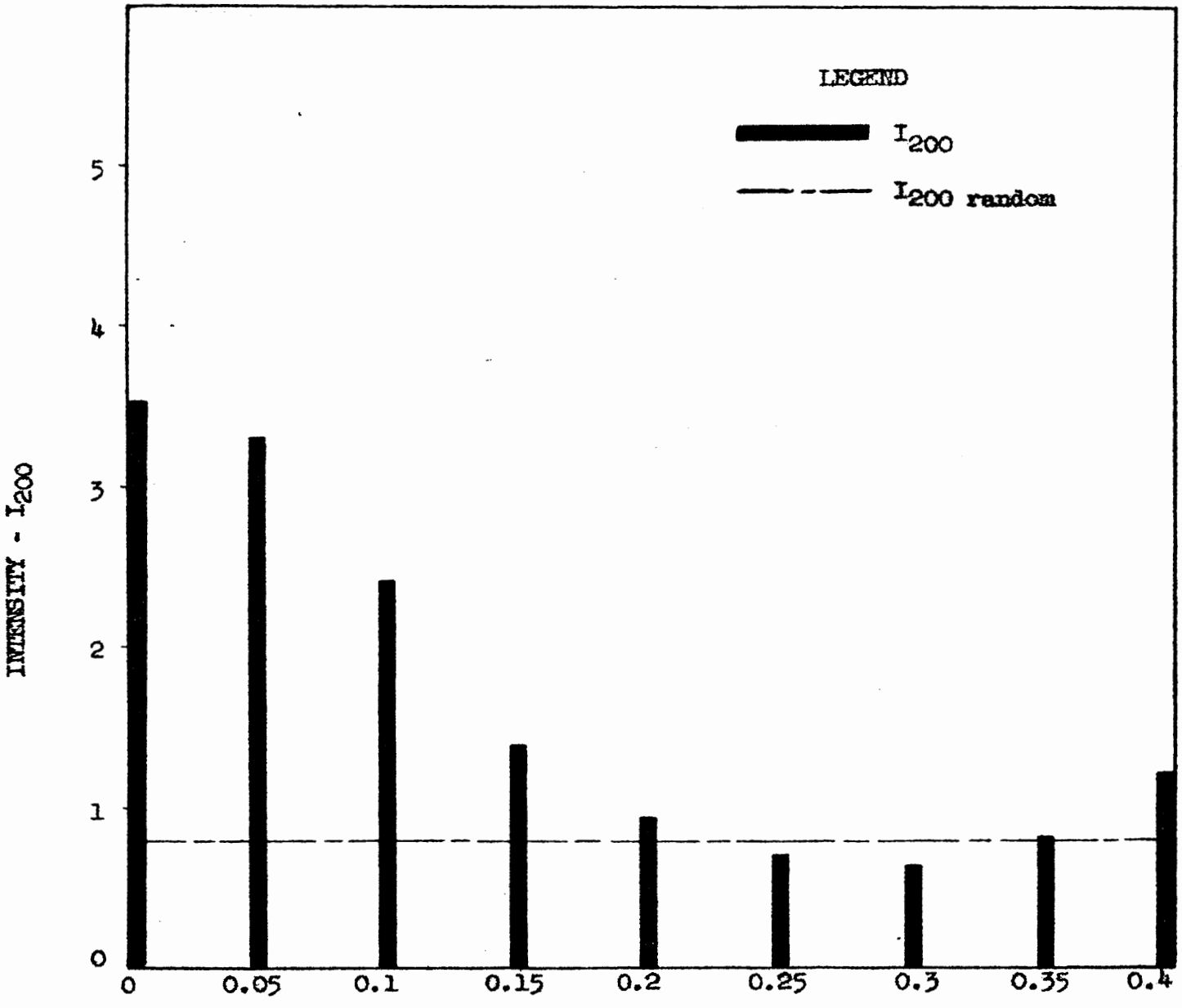

Distance (in inches) of the center of the area irradiated by the x-ray beam from the center of the specimen.

FIGURE 68. Relative 2(100) intensity from concentric regions at various distances from the fibre axis of a 60 per cent cold drawn one inch diameter nickel rod annealed at 600°C for one hour.

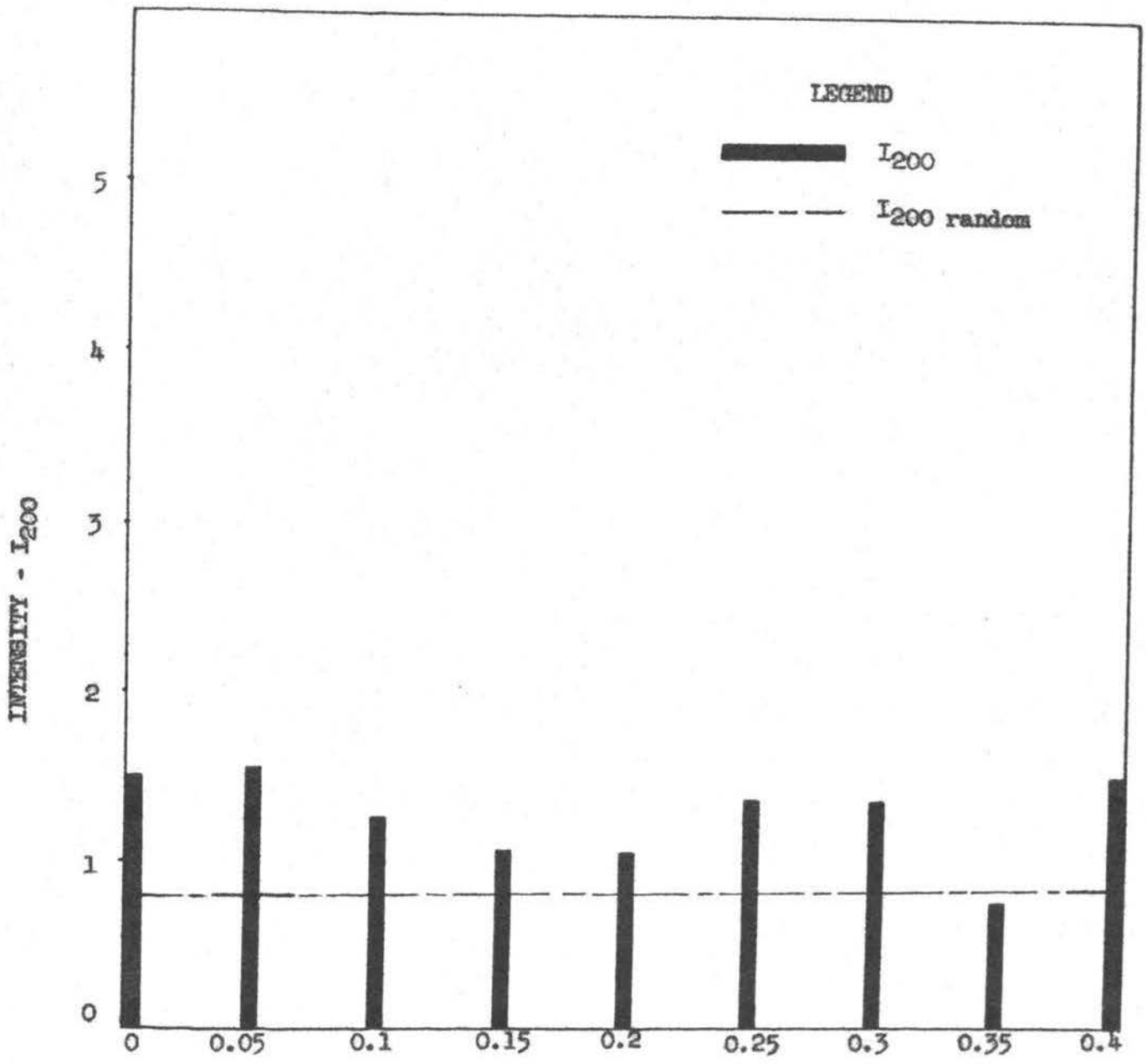

Distance (in inches) of the center of the area irradiated by the x-ray beam from the center of the specimen.

FIGURE 69. Relative 2(100) intensity from concentric regions at various distances from the fibre axis of a 60 per cent cold drawn one inch diameter nickel rod annealed at 800°C for one hour.

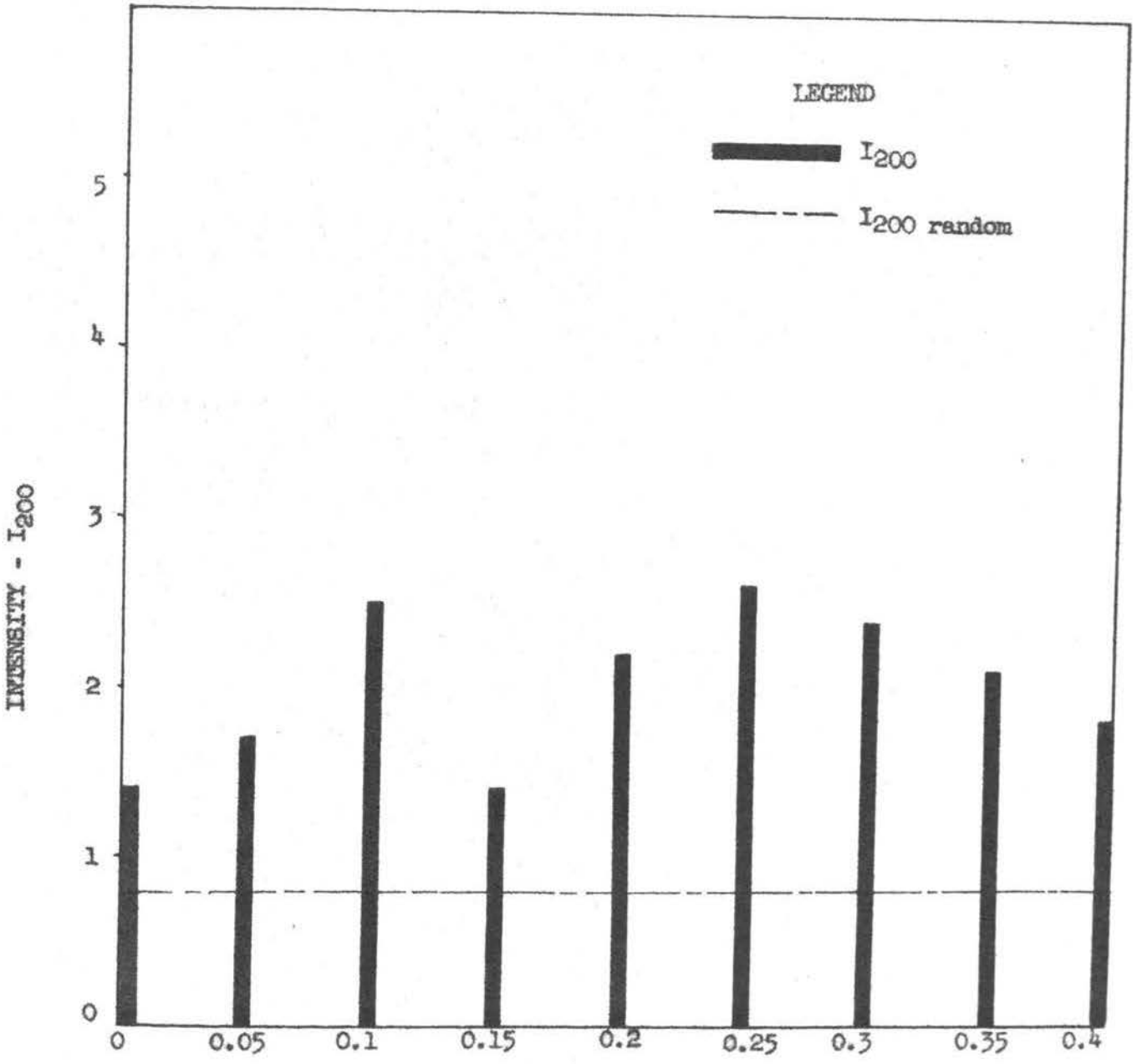

Distance (in inches) of the center of the area irradiated by the x-ray beam from the center of the specimen.

FIGURE 70. Relative 2(100) intensity from concentric regions at various distances from the fibre axis of a 60 per cent cold drawn one inch diameter nickel rod annealed at 1000°C for one hour.

ture, as shown in the photomicrographs presented in chapter X. Standard x-ray diffraction patterns made on the surface of these specimens show the presence of only (111) and 2(100) reflections, indicating that no new orientation is developed during recrystallization of cold drawn nickel.

As seen in Figures 37, 40, 47 and 59, sharpening of the [$\bar{1}$11] and [$\bar{1}$00] drawing textures in 20.6 per cent cold drawn nickel (item no. 1) is observed on annealing at 400°C. With further increase in the annealing temperature the two orientations are progressively weakened to a minimum at 800°C (Figures 48 and 49; 60 and 61). On annealing at 1000°C, a slight strengthening of the texture is noted (Figures 50 and 62). Thus, it is seen that both [$\bar{1}$11] and [$\bar{1}$00] orientations on annealing the 20.6% cold drawn specimen behave in a similar manner. In contrast to this [$\bar{1}$11] orientation in 40.5 per cent cold drawn nickel (item no. 2) is first weakened and then strengthened on annealing at 400° and 600°C respectively (Figures 38, 51 and 52), whereas, [$\bar{1}$00] orientation is first strengthened and then weakened after similar annealing operations (Figures 41, 63 and 64). Annealing at 800°C weakens both the [$\bar{1}$11] and [$\bar{1}$00] textures (Figures 53 and 65). On annealing at 1000°C, while the [$\bar{1}$11] texture is sharpened, the [$\bar{1}$00] texture is rendered weak (Figures 54 and 66). The effect of annealing on the [$\bar{1}$11] and [$\bar{1}$00] textures in 60 per cent cold drawn nickel (item no. 3) is similar to that in item 1 (20.6% cold drawn), as shown in Figures 39, 55, 56, 57 and 58; 42, 67, 68, 69 and 70. However, the following difference in the case of item no. 3 (60% cold drawn) should be noted. As seen in Figures 39, 55 and 56;

42, 67 and 67, the [111] and [100] textures in item no. 3 (60 per cent cold drawn) are progressively sharpened on annealing at 400° and 600°C respectively, while this sharpening of deformation textures in 20.6% cold drawn nickel (item no. 1) is observed at 400°C after which weakening of the texture ensues. Similar sharpening of texture in 99.95 per cent cold drawn aluminum wire recrystallized at 600°C has been reported by Schmid and Wasserman[49 50)]. Though the general trend of distribution of 111 texture in cold drawn nickel is retained on annealing at 800°C, the intensity of (111) reflections is reduced almost to the point of annihilation of the preferred orientation, as seen in Figures 49, 53 and 57. In contrast to this, the distribution of 100 texture becomes random on annealing at 800°C as shown in Figures 61, 65 and 69. The distribution of 111 texture becomes random on annealing at 1000°C as seen in Figures 50, 54 and 58.

It may be pointed out that the x-ray diffraction technique discussed above is ideally suited for studying the effect of different mill variables, e.g., the die angles, number of draws, intermediate anneals etc. on the distribution of deformation in a metal during cold drawing. A proper choice of the mill practice to produce cold drawn materials with greatest possible uniformity can thus be made.

[49 50] E. Schmid and G. Wasserman, Z. Physik, Vol. 9 (1928), p. 106.

CHAPTER IX

INVESTIGATION ON VARIATION IN HARDNESS AND MACROSTRUCTURE OF COLD DRAWN NICKEL

This chapter deals with the study of hardness variation in drawn nickel rods produced due to non-uniform distribution of the cold-working effect during the drawing process. Photomacrographs of the cross-sections on the drawn rods are included and the macrostructures discussed.

A. HARDNESS VARIATION IN DRAWN NICKEL RODS

It has been shown in chapter VIII that the cold-working effect during the drawing process is not evenly transmitted throughout the cross-section of the drawn rods. Thus, variation in hardness, depending upon the size of the rod and the extent of cold reduction given to the material, is expected.

Although it is well known that the hardness of a cold drawn rod increases with the amount of cold drawing effected, it is perhaps not quite so generally realized that the resulting hardness may vary over the cross-section of the drawn rod. In industry, routine hardness tests are usually carried out on the mid-radius or center of the cross-section, or on filed flats on the surface of the rod, and the results are commonly accepted as indicating the hardness of the rod as a whole. Such tests, without regard to the variation in hardness according to the position at which the tests are made, are obviously unsatisfactory. This is specially true when machines employing small

indenters, which make the hardness tests very local in character, are used. The increased tendency to carry out hardness tests on drawn rods, and to include hardness values in specifications, increases the significance of this hardness variation over the cross-section.

Choice of method for hardness testing. Hardness in metals is commonly measured by the 'Rockwell' or the 'Armstrong-Vickers' hardness tests. Brinell hardness tests on large sections have also been used in the past. In the Rockwell hardness test, either a 1/16-in-diameter hardened-steel ball or a spheroconical diamond penetrator (designated as 'Brale') is used. The standard Vickers indenter consists of a diamond in the form of a square-based pyramid with an included angle of 136 degrees between opposite faces.

The useful range of 1/16-in-diameter ball indenter is from Rockwell B 0 to B 100. The hardness of wrought nickel is from Rockwell B 95 upwards, depending on the degree of cold deformation to which the metal is subjected. In the upper range of the Rockwell B scale, the ball indenter is known to show some tendency to distort, thus introducing errors in the hardness measurements. Notwithstanding distortion of the indenter, the 1/16-in-diameter ball would still be inappropriate for studying the variation in hardness owing to the lack of sensitivity of the spherical-shaped indenter to small differences in hardness, specially when the depth of impression is shallow [49][50].

---

[50] [49] George L. Kehl, The Principles of Metallographic Laboratory Practice (New York: McGraw-Hill Book Company, Inc., 1949), p. 230.

It is evident that large impressions do not permit a satisfactory number of hardness measurements on the cross-section of a one inch diameter rod and thus are undesirable. In view of the reasons enumerated above, the use of a spherical indenter for this investigation was not considered.

Trial tests for determining a suitable load for Vickers hardness test were made as follows. Diamond pyramid hardness measurements on different radii on the cross-section of the 40.5 per cent cold drawn nickel rod (item no. 2) were carried out at 5, 10, 20 and 30 kg loads respectively. The hardness at the center of the specimen was determined with a 10-kg load. A representative set of data from such a test is listed in table XVIII. It was found that consistently reproducible values are not obtained with the various loads investigated. Moreover, the scatter in values from an ideal hardness-variation curve which is expected to show an increase in hardness with increasing distances from the fibre axis and a decrease near the surface of the rod, is appreciable for loads up to 20-kg as seen in table XVIII. Although the values obtained with 30-kg load agree with the expected manner of hardness variation, its use was considered unsatisfactory owing to non-reproducibility of the results as mentioned above. However, to complete the record, DPH measurements with 30-kg load on 20.6 (item no. 1) and 60 (item no. 3) per cent cold drawn nickel rods were also carried out. As the hardness varies with the position of the test spot on the cross-section of the rod, values for different radii of a specimen were not averaged to avoid introduction of errors due to errors in exact positioning of the specimen under the indenter. A representa-

TABLE XVIII

DPH (VICKERS) VALUES ON DIFFERENT RADII ON THE CROSS-SECTION OF 40.5 PERCENT COLD DRAWN NICKEL ROD (ITEM NO. 2) WITH VARIOUS LOADS ON THE PENETRATOR

Distance from fibre axis (inches)	Diamond Pyramid Hardness Number			
	5-kg load	10-kg load	20-kg load	30-kg load
0	--	249	--	--
0.05	254	249	257	252
0.1	265	260	256	254
0.15	274	264	271	254
0.2	268	251	261	264
0.25	260	279	254	274
0.3	268	272	271	275
0.35	274	274	261	276
0.4	268	279	269	270
0.45	239	264	260	268

tive set of Vickers hardness data for the three cold drawn nickel rods is listed in Table XIX. The hardness variation in 20.6 and 40.5 per cent cold drawn specimens (items no. 1 and 2 respectively) is seen to follow the expected trend of variation fairly closely, whereas the values for the 60 per cent cold drawn specimen (item no. 3) show a considerable scatter. It seems that 30-kg load is not sufficient to obtain hardness values representative of the wrought metal, specially for the 60 per cent cold drawn specimen. The relation of the size of the impression to the grain size at the mid-radius on the cross-section of 20.6, 40.5 and 60 per cent cold drawn nickel rods (items nos. 1, 2 and 3 respectively) is shown in Figures 71 through 73 respectively. It is seen that the impression due to indentation covers approximately thirty and twenty five grains in the 20.6 and 40.5 per cent cold drawn specimens respectively, whereas, in the 60 per cent cold drawn specimen only six to eight grains are covered. The small size of the impression on the 60 per cent cold drawn specimen indicates that hardness measurements representative of the metal may not be obtained due to increased importance of variation in surface effects.

To investigate the use of higher loads, Rockwell hardness tester was used due to ease of its operation. Rockwell hardness scales A, C and D (Brale penetrator with 60, 100 and 150-kg loads respectively) were tried. As the size of impression with 100 and 150-kg loads was too great to permit a satisfactory number of hardness measurements on the radius of one inch diameter specimens, a load of 60-kg was finally selected. Relation of the size of impression with a Brale indenter under 60-kg load to the grain size

TABLE XIX

DPH (VICKERS) VALUES ON RADII ON THE CROSS-SECTION OF 20.6 (ITEM NO. 1), 40.5 (ITEM NO. 2) AND 60 (ITEM NO. 3) PERCENT COLD DRAWN NICKEL RODS WITH 30-KG LOAD ON THE PENETRATOR

Distance from fibre axis (inches)	Diamond Pyramid Hardness Number		
	20.6% cold drawn	40.5% cold drawn	60% cold drawn
0	205	249	269
0.05	211	252	252
0.1	212	254	258
0.15	210	254	269
0.2	209	264	269
0.25	210	274	268
0.3	205	275	274
0.35	205	276	270
0.4	205	270	274
0.45	216	268	262

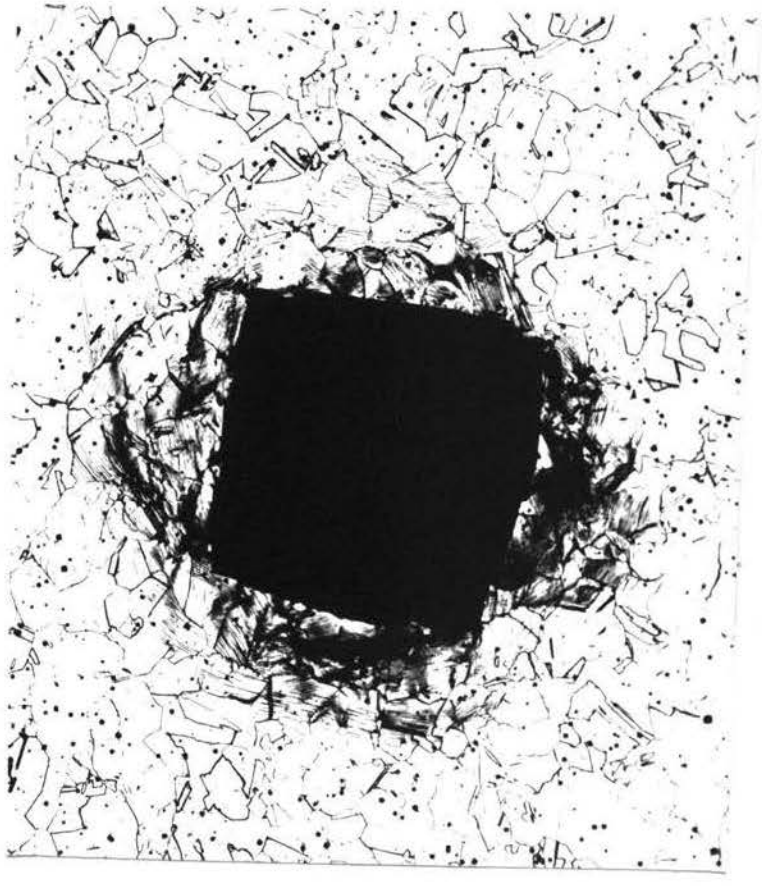

FIGURE 71. Relation of the size of impression (for diamond pyramid indenter under 30-kg load) to the grain size at mid-radius on the cross-section of a 20.6 per cent cold drawn one inch diameter nickel rod. (x100).

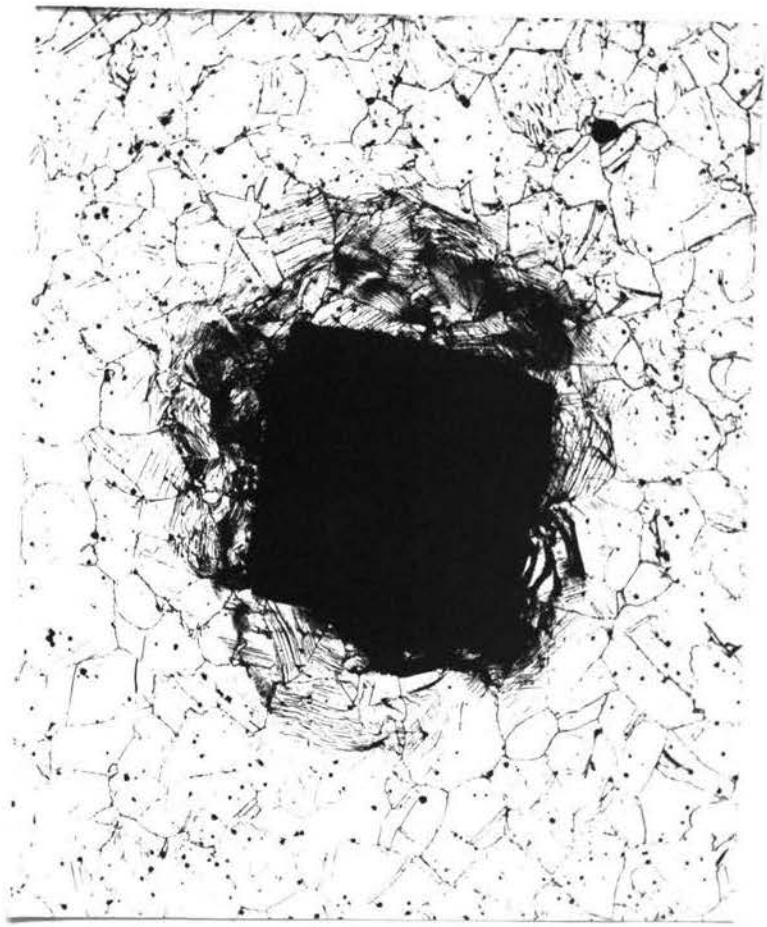

FIGURE 72. Relation of the size of impression (for diamond pyramid indenter under 30-kg load) to the grain size at mid-radius on the cross-section of a 40.5 per cent cold drawn one inch diameter nickel rod. (x100).

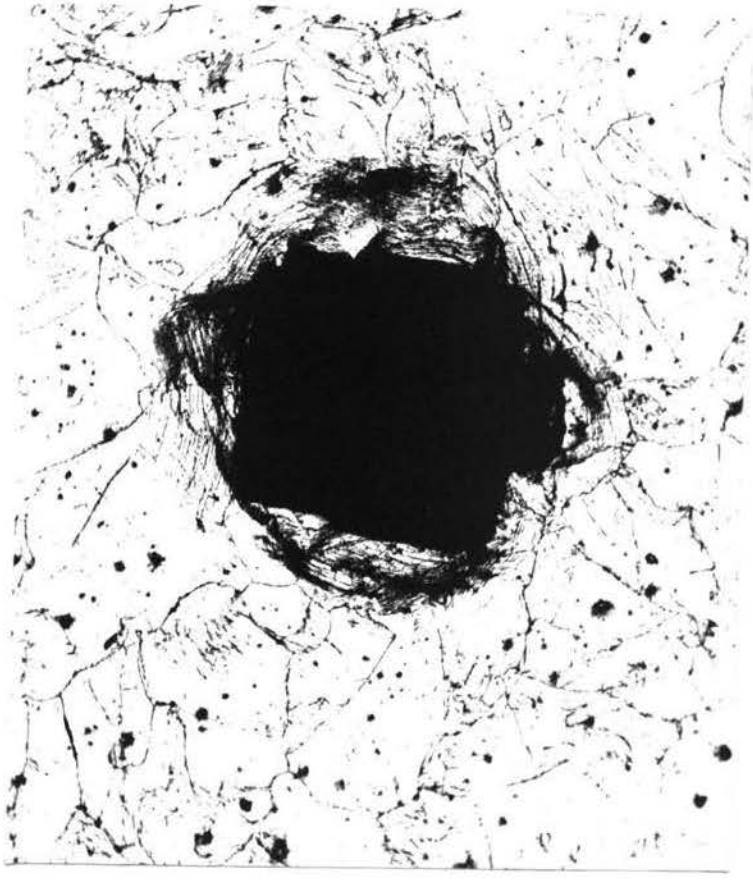

FIGURE 73. Relation of the size of impression (for diamond pyramid indenter under 30-kg load) to the grain size at mid-radius on the cross-section of a 60 per cent cold drawn one inch diameter nickel rod. (x100).

at mid-radius on the cross-section of 20.6 (item no. 1), 40.5 (item no. 2) and 60 (item no. 3) per cent cold drawn nickel rods is shown if Figures 74 through 76. A comparitive study of Figures 71 through 73 and 74 through 76 shows that the size of impression due to a Brale under 60-kg load is approximately double that of the diamond pyramid indenter under a 30-kg load. The average diameter of the Brale impression and the metal deformed due to indentation as seen under the microscope were determined with a measuring eyepiece. The average diameters thus determined for the 20.6 (item no. 1), 40.5 (item no. 2) and 60 (item no. 3) per cent cold drawn nickel specimens were 0.047", 0.042", and 0.04" respectively. In view of the above observation, Rockwell hardness 'A' measurements at 0.1" intervals on the radii of the above mentioned specimens were carried out.

Experimental results. Rockwell-A hardness values at 0.1" intervals on the radii on cross-sections of the three cold drawn nickel rods (items 1, 2 and 3) are listed in table XX. Hardness measurements at a distance of 0.45 inch from the fibre axis are also recorded. Plots of Rockwell-A hardness versus distance from the fibre axis of the 20.6, 40.5 and 60 per cent cold drawn nickel specimens are shown in Figures 77 through 79. Diamond pyramid hardness values from table XIX are also indicated on these plots to show the relative degree of their scatter.

Values of Rockwell-A hardness measurments at a distance of 0.45 inch from the fibre axis are probably in error due to close proximity of the neighbouring impression toward the center on the

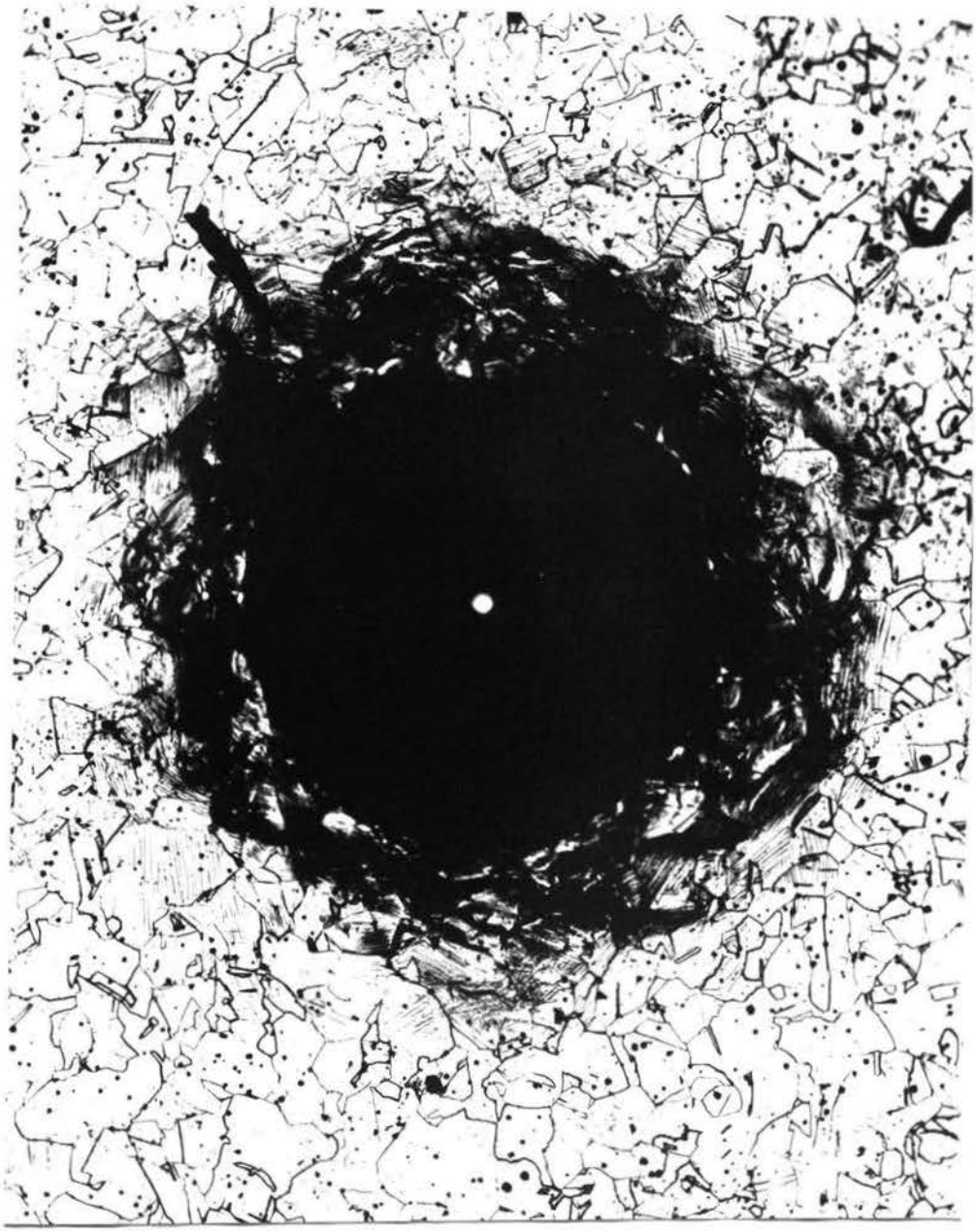

FIGURE 74. Relation of the size of impression (for Brale indenter under 60-kg load) to the grain size at mid-radius on the cross-section of a 20.6 per cent cold drawn one inch diameter nickel rod. (x 100).

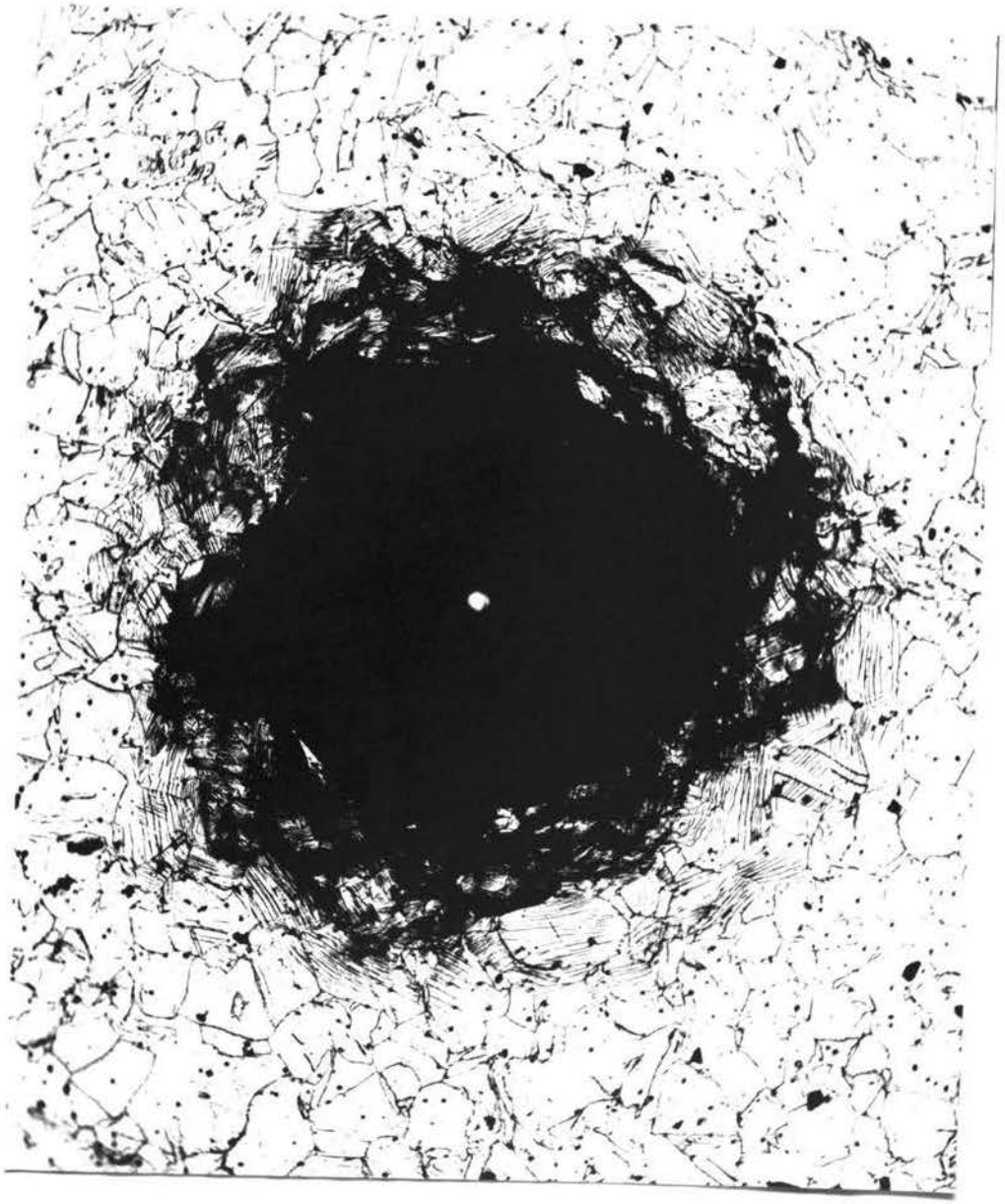

FIGURE 75. Relation of the size of impression (for Brale indenter under 60-kg load) to the grain size at mid-radius on the cross-section of a 40.5 per cent cold drawn one inch diameter nickel rod. (x 100).

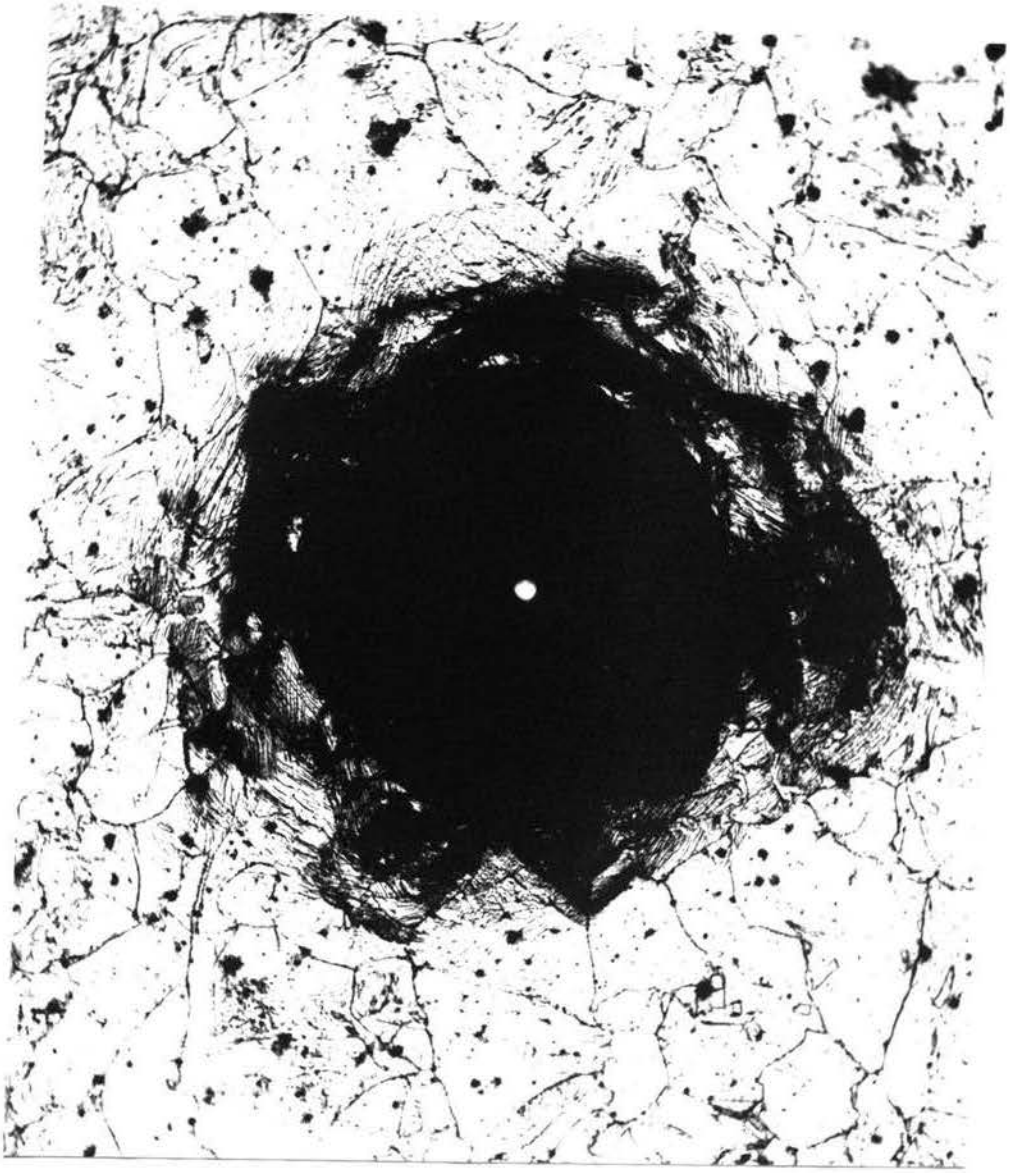

FIGURE 76. Relation of the size of impression (for Brale indenter under 60-kg load) to the grain size at mid-radius on the cross-section of a 60 per cent cold drawn one inch diameter nickel rod....(x 100).

TABLE XX

ROCKWELL HARDNESS VALUES ('A' SCALE--BRALE PENETRATOR AND 60-KG LOAD) ON RADII ON THE CROSS-SECTION OF 20.6 (ITEM NO. 1), 40.5 (ITEM NO. 2), AND 60 (ITEM NO. 3), PERCENT COLD DRAWN NICKEL RODS

Distance from fibre axis (inches)	Rockwell Hardness Values--'A' Scale		
	20.6% cold drawn	40.5% cold drawn	60% cold drawn
0	49.5	55.5	56
0.1	54	57.8	59.1
0.2	54	58.2	59.8
0.3	54.1	58.2	60.5
0.4	54	56.9	58
0.45	52.8	56	55.2

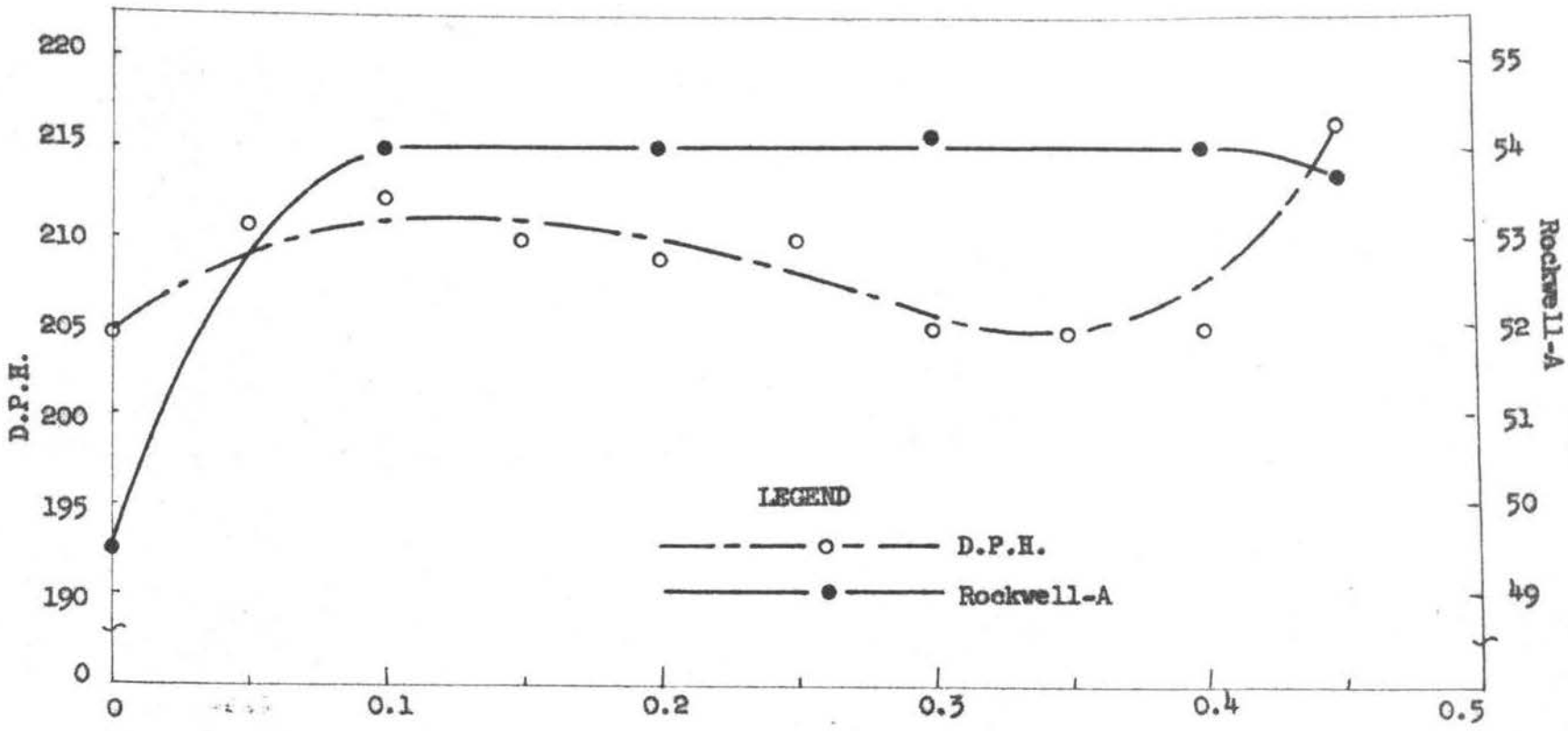

FIGURE 77. Variation in Rockwell-A and diamond pyramid hardness (30-kg) with distance from the fibre axis of a 20.6 per cent cold drawn one inch diameter nickel rod.

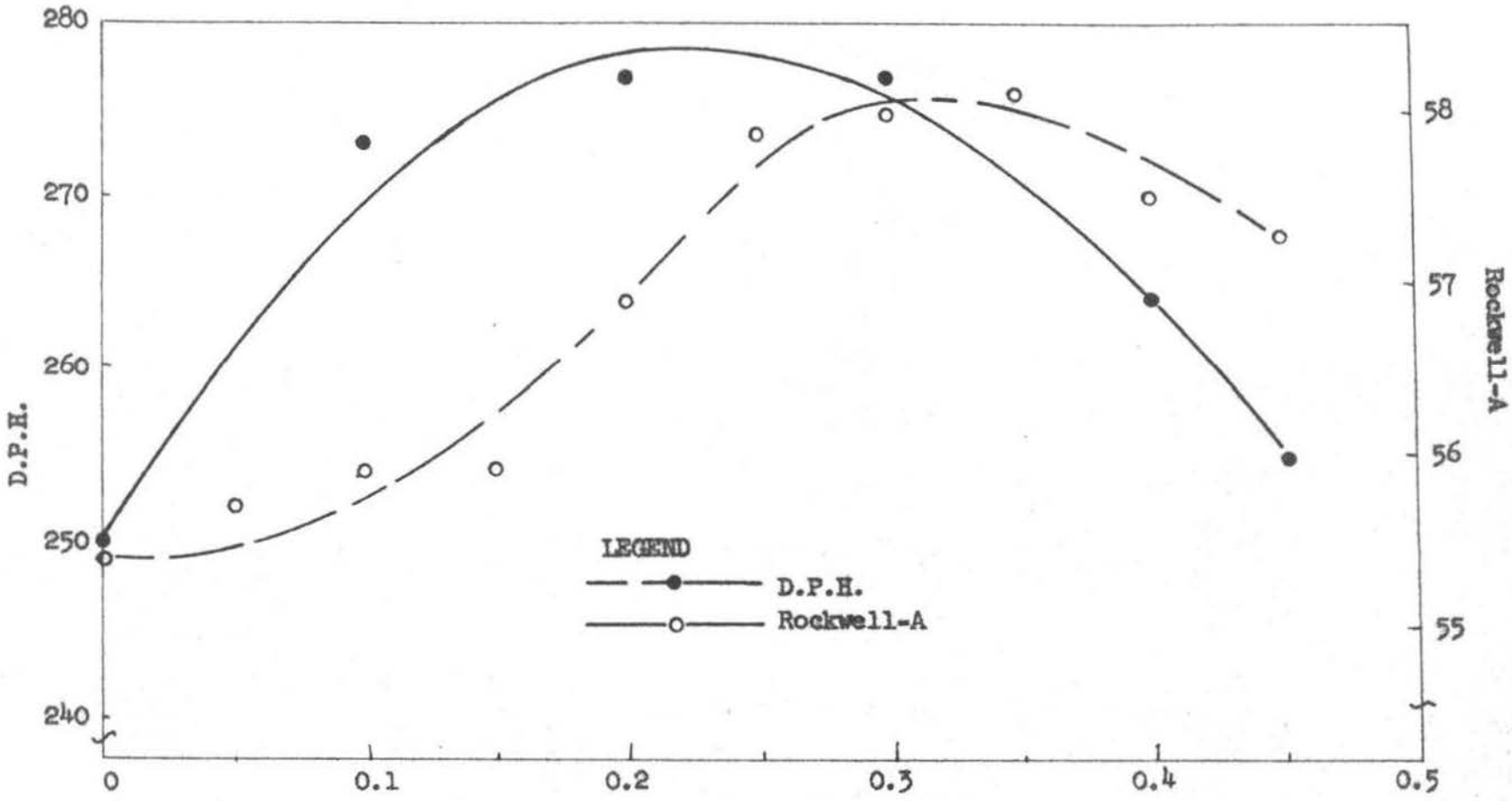

FIGURE 78. Variation in Rockwell-A and diamond pyramid hardness (30-kg load) with distance from the fibre axis of a 40.5 per cent cold drawn one inch diameter nickel rod.

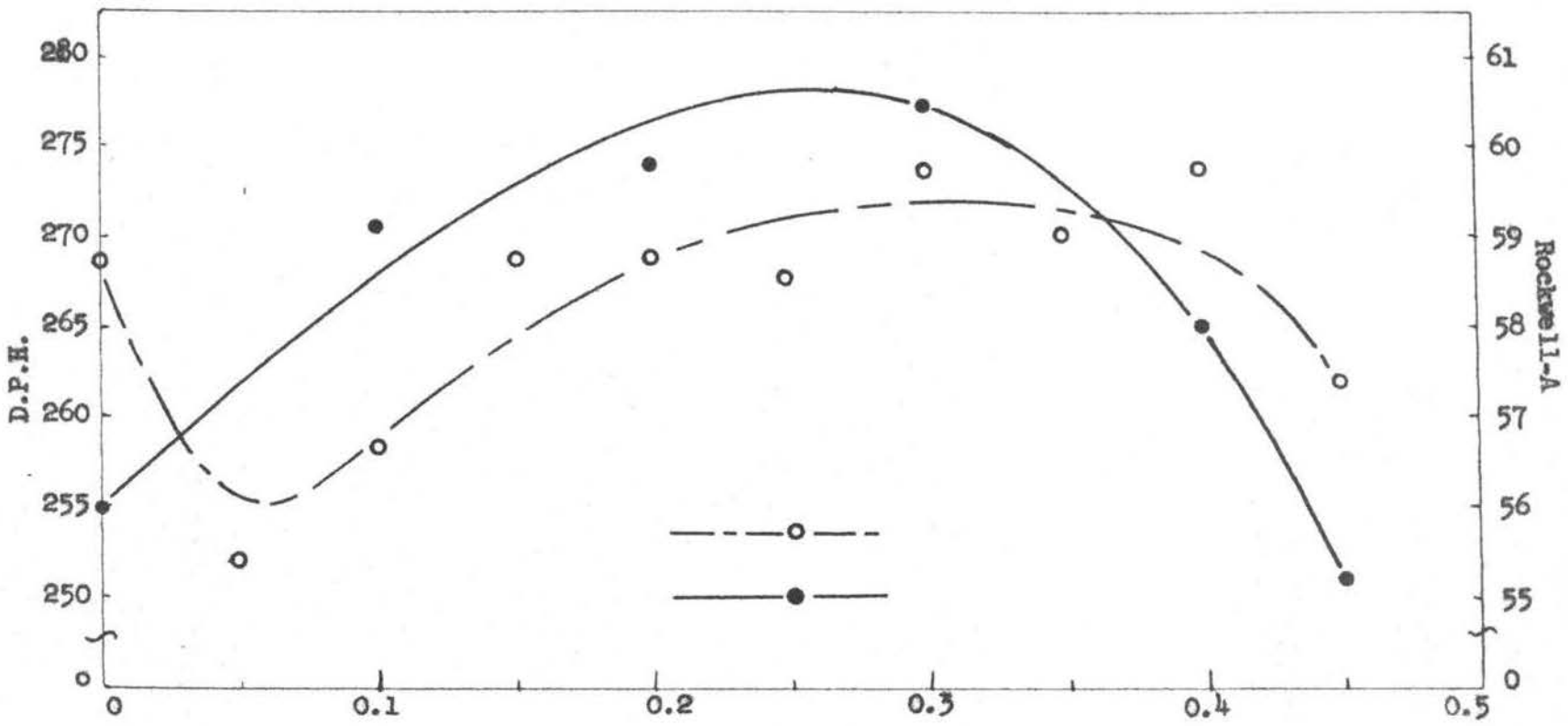

FIGURE 79. Variation in Rockwell-A and diamond pyramid hardness (30-kg load) with distance from the fibre axis of a 60 per cent cold drawn one inch diameter nickel rod.

same radius and the edge of the specimen, and therefore will be discarded. As seen in Figure 77, the hardness of 20.6 per cent cold drawn nickel rod (item no. 1) increases from the center to a distance of 0.1 inch from the fibre axis. No significant change in hardness is noted with further increase in distance from the center of the specimen. Whereas, in 40.5 (item no. 2) and 60 (item no. 3) per cent cold drawn nickel rods hardness increases from a minimum at the center to a maximum at the mid-radius and then decreases as the surface of the rod is approached (Figures 78 and 79). To show the effect of increasing degrees of cold drawing on the hardness at various distances from the fibre axis of the three nickel rods (items 1, 2 and 3), the Rockwell-A hardness data from table XX was combined and replotted in Figure 80. As expected, the hardness throughout the cross-section of the drawn rod increases with increasing degrees of cold drawing.

The variation of hardness at different distances from the fibre axis of the drawn rods, as seen in Figure 80, shows that the cold-working effect during the drawing operation is not evenly transmitted throughout the cross-section of the drawn metal. The fact that maximum hardness is observed at the mid-radius indicates that the cold working effect is greatest in this region. This is in conformity with the x-ray diffraction data on texture variation presented in chapter VIII, which shows that complex slip rotations of crystals due to superimposition of compressive and tensile stresses in the outer concentric regions of the rod during the drawing operation are produced, while near the surface of the rod the crystal rotations are hindered due to the effect of the die walls. This investigation being a minor

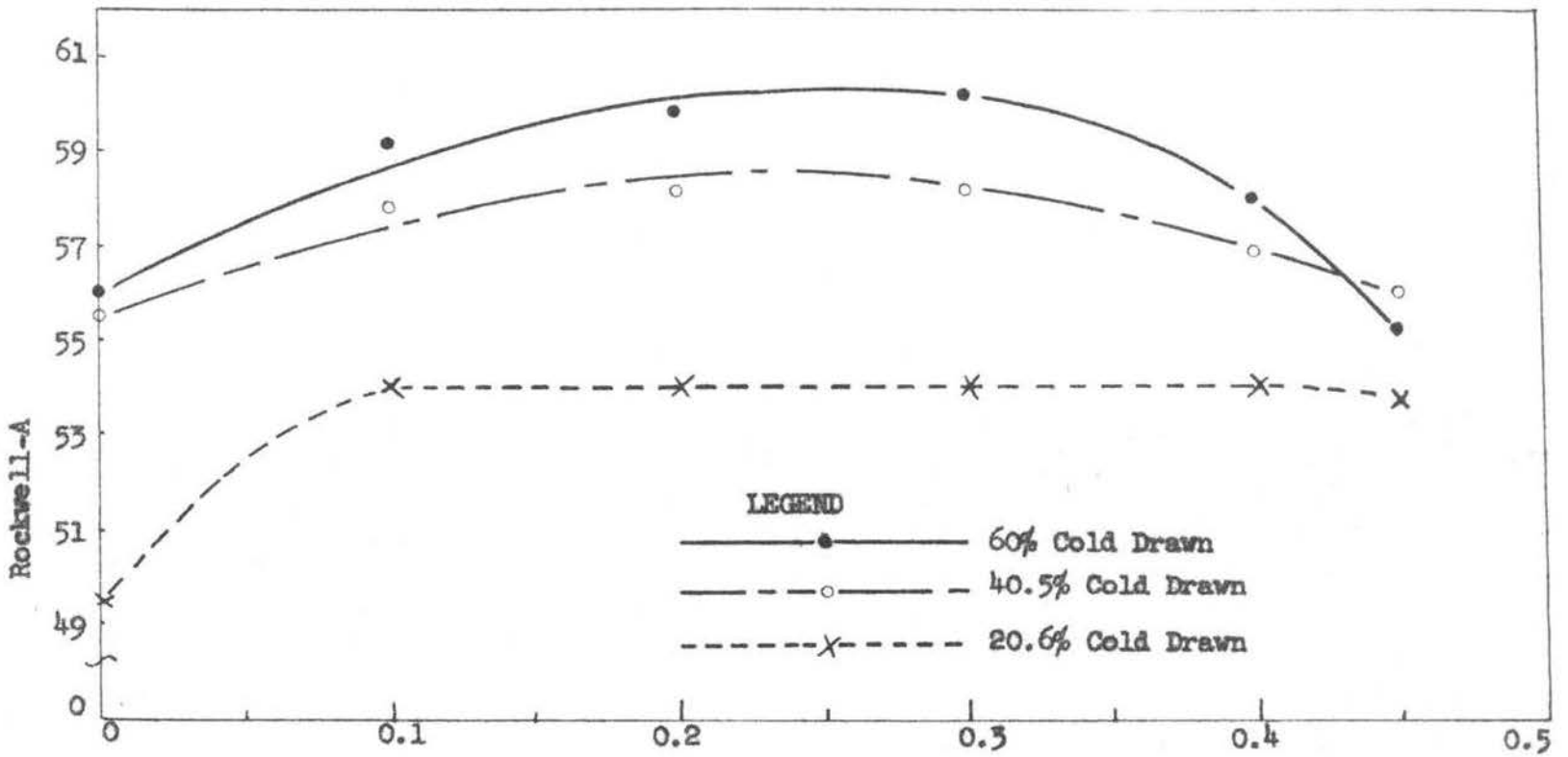

FIGURE 80. The effect of increasing degrees of cold drawing on the hardness at various distances from the fibre axis of one inch diameter cold drawn nickel rods.

phase of the problem under study, enough data was not obtained to justify any attempt at correlating the observed texture and hardness variations.

B. MACROSTRUCTURE OF COLD DRAWN NICKEL

The rate of attack of acids on a metal is known to depend, among many other things, on the ammount of cold work to which the metal is subjected. Thus, if the cold-working effect on the cross-section of a drawn rod is non-uniform, regions undergoing the greatest amount of cold deformation will be selectively dissolved by the acid.

Preparation and etching of macro-specimens. Two circular specimens, like the x-ray disc specimens described in chapter VIII, were machined from each of the 20.6, 40.5 and 60 per cent cold drawn (item nos. 1, 2 and 3) one inch diameter nickel rods. The six specimens were divided into two sets of three specimens each, the three degrees of cold drawing mentioned above being represented in each set. The specimens were mechanically polished and etched in concentrated nitric acid. One set of specimens were etched for five minutes, whereas, the etching time for the second set was increased to fifteen minutes. The etchant was agitated at one-minute intervals.

Experimental results. Photomacrographs of the two sets of specimens discussed in the previous section, made with vertical illumination, are shown in Figures 81 and 82. It is evident that the rate of dissolution of metal in the outer concentric regions of the rods is greater than that at central regions. Figure 81 shows the

20.6% Cold Drawn

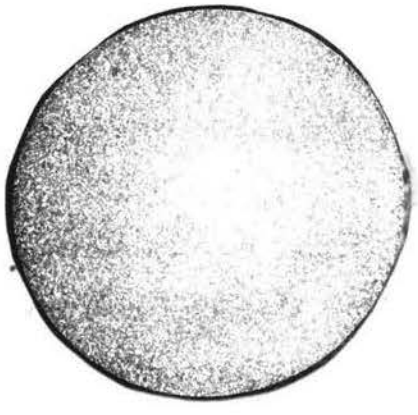

40.5% Cold Drawn

60% Cold Drawn

FIGURE 81. Macrophotographs of cross-section of cold drawn one inch diameter nickel rods. (etched for 5 minutes in concentrated nitric acid)....x2.

20.6% Cold Drawn

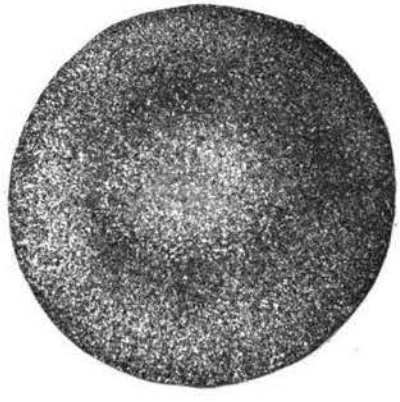

40.5% Cold Drawn

60% Cold Drawn

FIGURE 82. Macrophotographs of cross-section of cold drawn one inch diameter nickel rods. (etched for 15 minutes in concentrated nitric acid)...x2.

progressive increase in depth of penetration of the cold-working effect with increasing amounts of cold drawing. With increased etching time, regions in the vicinity of mid-radius of the specimens (Figure 82) show increased etching of the metal, indicating that the deformation in these regions is greatest.

CHAPTER X

MICROSTRUCTURE OF COLD DRAWN AND ANNEALED NICKEL

Photomicrographs at the center, and at distances of 0.125, 0.25 and 0.49 inches from the fibre axis on the cross-section of 20.6, 40.5 and 60 per cent cold drawn one inch diameter nickel rods (items no. 1, 2 and 3) were made to determine whether any possible variation in their microstructure existed. Similar photomicrographs at the center, mid-radius, and near the edge on the cross-section of the three items (20.6, 40.5 and 60 per cent cold drawn) were made after one hour anneals at 400°, 600°, 800° and 1000°C.

A. MICROSTRUCTURE OF COLD DRAWN NICKEL

Microstructures at the center, and at distances of 0.125, 0.25 and 0.49 inches from the fibre axis on the cross-section of 20.6, 40.5 and 60 per cent cold drawn one inch diameter nickel rods (items no. 1, 2 and 3) are shown in Figures 83, 84 and 85 respectively. It is seen that no significant change in the grain size at various spots on the cross-section of any one of the three items exists. Thus it appears that metallographic studies on the cross-section of a cold drawn rod are not well suited for detection of inhomogeneous deformation that is known to occur during the drawing process.

B. MICROSTRUCTURE OF ANNEALED NICKEL

Photomicrographs at the center, mid-radius, and near the edge

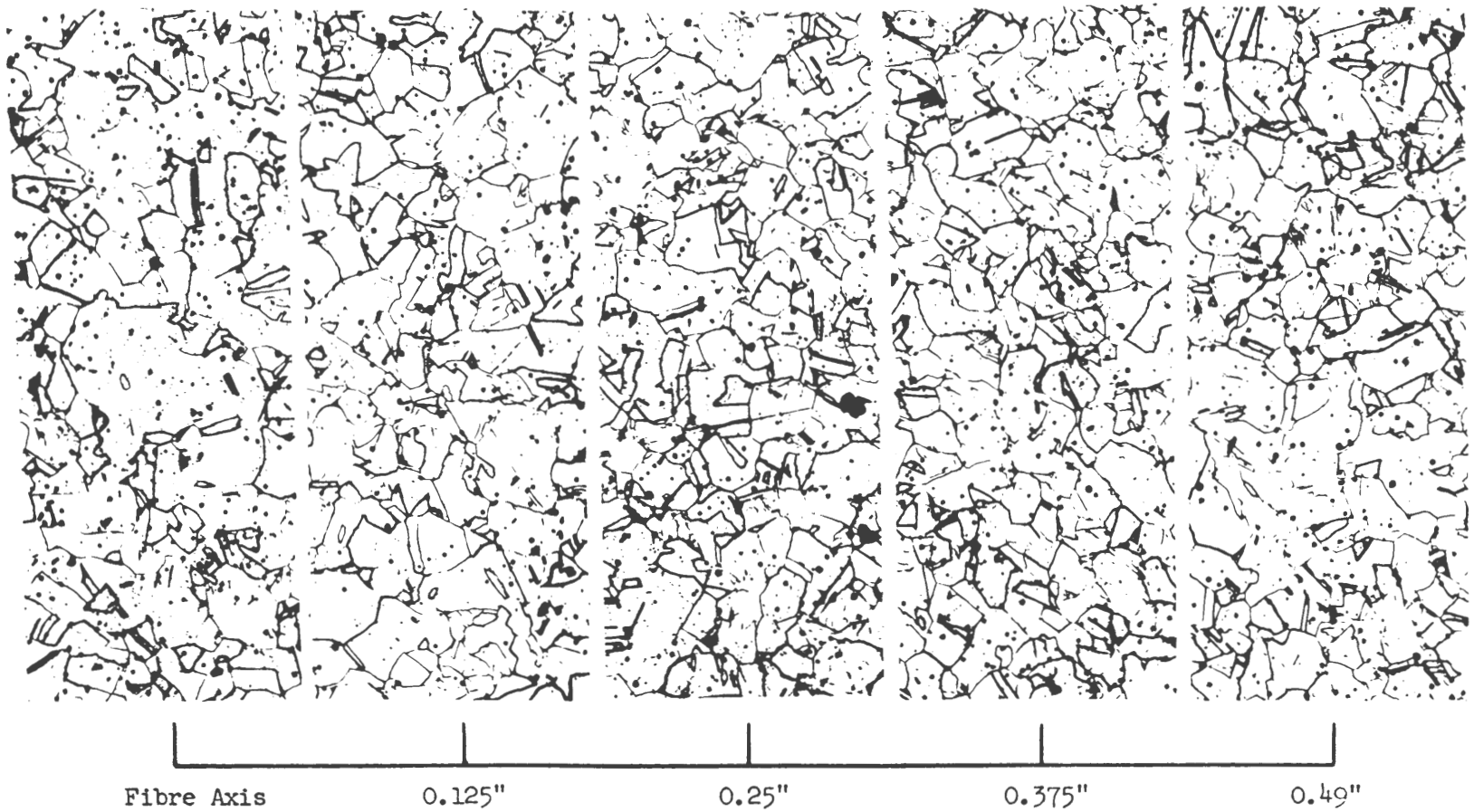

FIGURE 83. Microstructure at various distances from the fibre axis on the cross-section of a 20.6 per cent cold drawn one inch diameter nickel rod. X 100

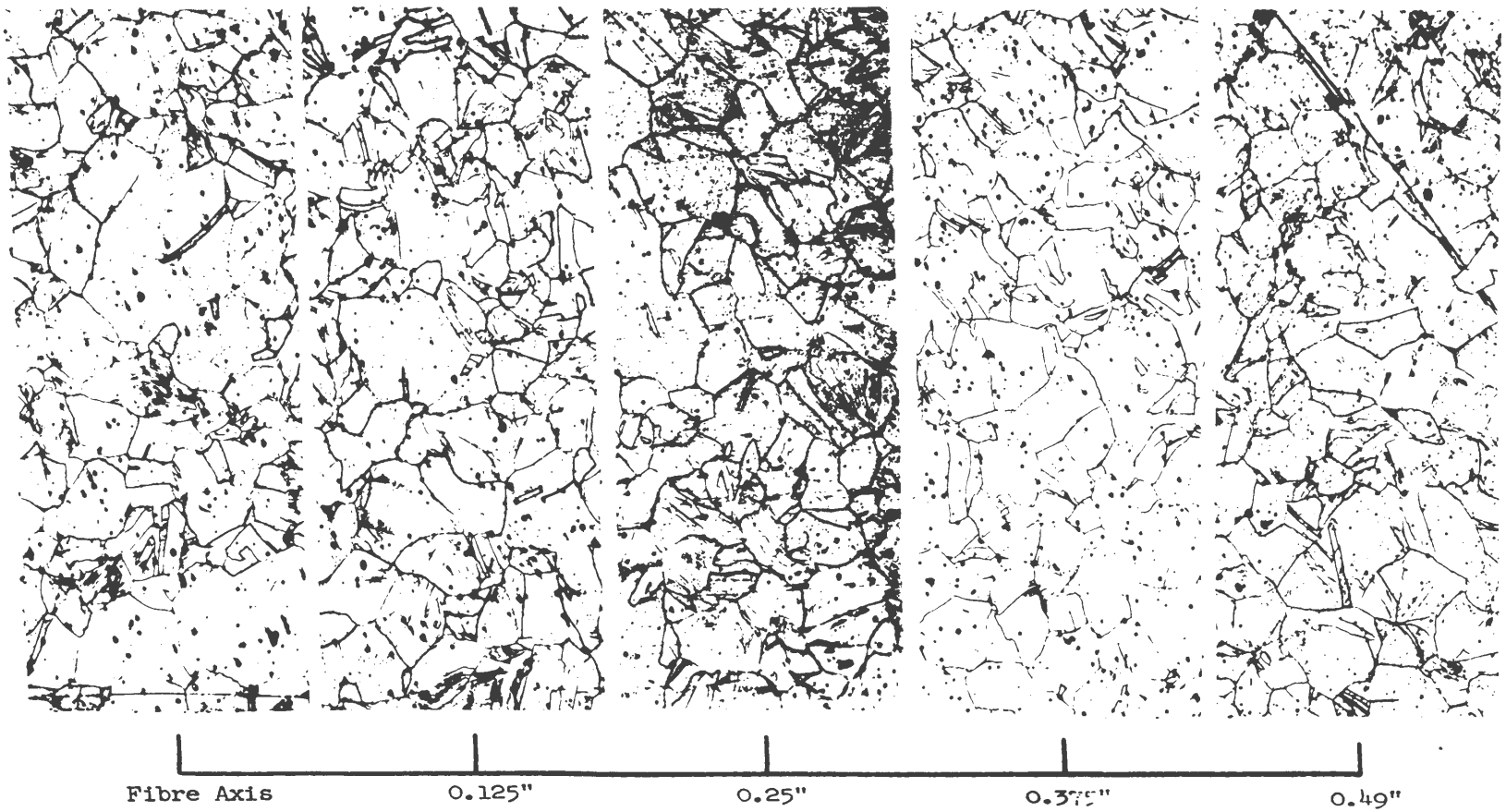

FIGURE 84. Microstructure at various distances from the fibre axis on the cross-section of a 40.5 per cent cold drawn one inch diameter nickel rod. X100

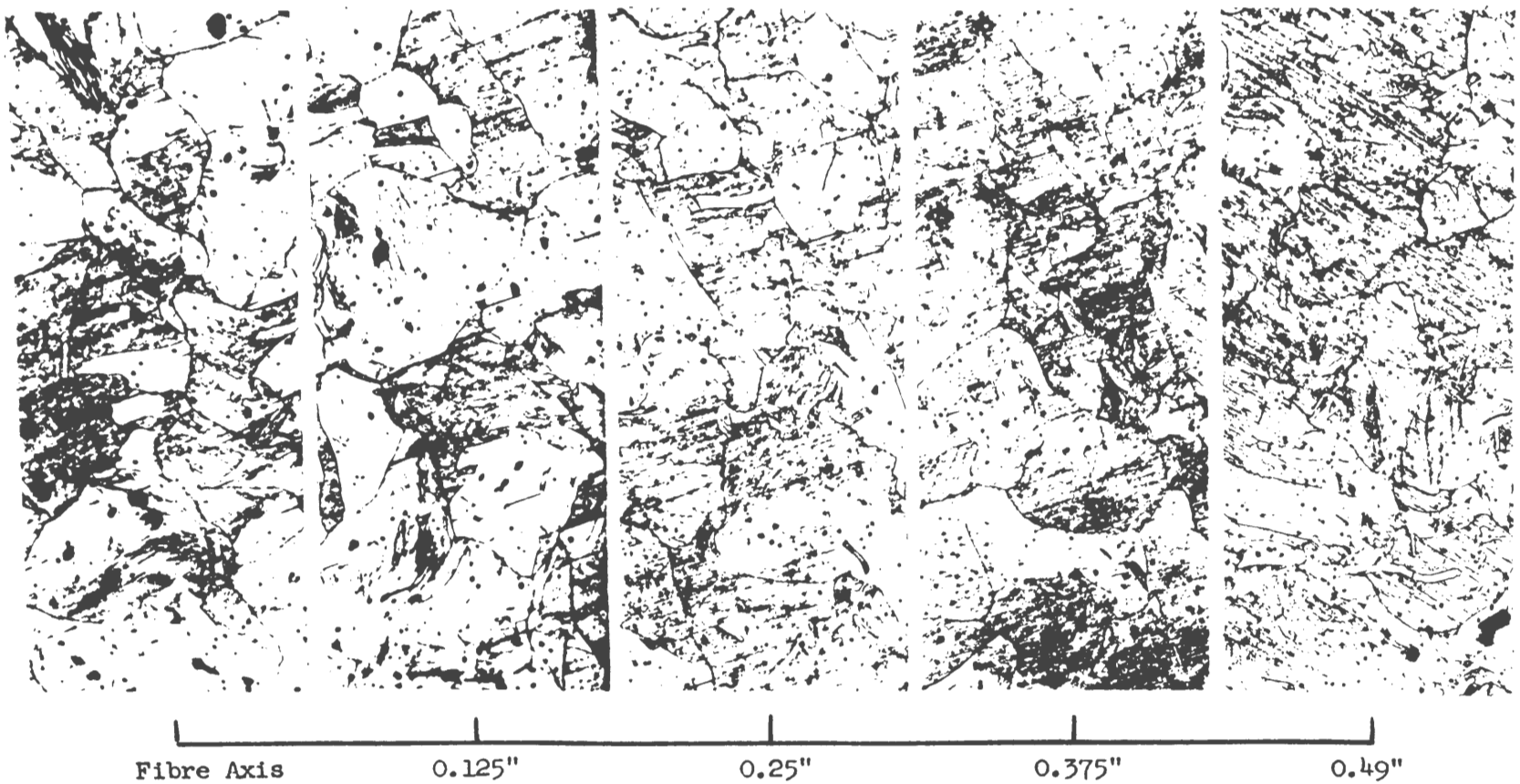

FIGURE 85. Microstructure at various distances from the fibre axis on the cross-section of a 60 per cent cold drawn one inch diameter nickel rod. X 100

on the cross-section of 20.6, 40.5 and 60 per cent cold drawn one inch diameter nickel rods (items no. 1, 2 and 3) after one hour anneals at 400°, 600°, 800° and 1000°C are shown in Figures 86, 87 and 88 respectively.

As seen in Figures 86 through 88, one hour anneals at 400° and 600°C do not produce any significant change in the microstructure of all three items (20.6, 40.5 and 60 per cent cold drawn). On annealing at 800°C, item no. 1 (20.6 per cent cold drawn) does not show any grain refinement (Figure 86), whereas, in item no. 2 (40.5 per cent cold drawn) a noticeable refinement of grains is observed after a similar annealing treatment (Figure 87). Considerable grain refinement in item no. 3 (60 per cent cold drawn) is observed after an 800°C anneal, as seen in Figure 88. After annealing at 1000°C, all three items (20.6, 40.5 and 60 per cent cold drawn) show a considerable coarsening of the grains due to excessive grain growth. Triangular and square shaped etch pits indicating the presence of (111) and (100) planes respectively at approximately right angles to the fibre axis in the cold drawn rods are seen in different grains (Figures 86 through 88).

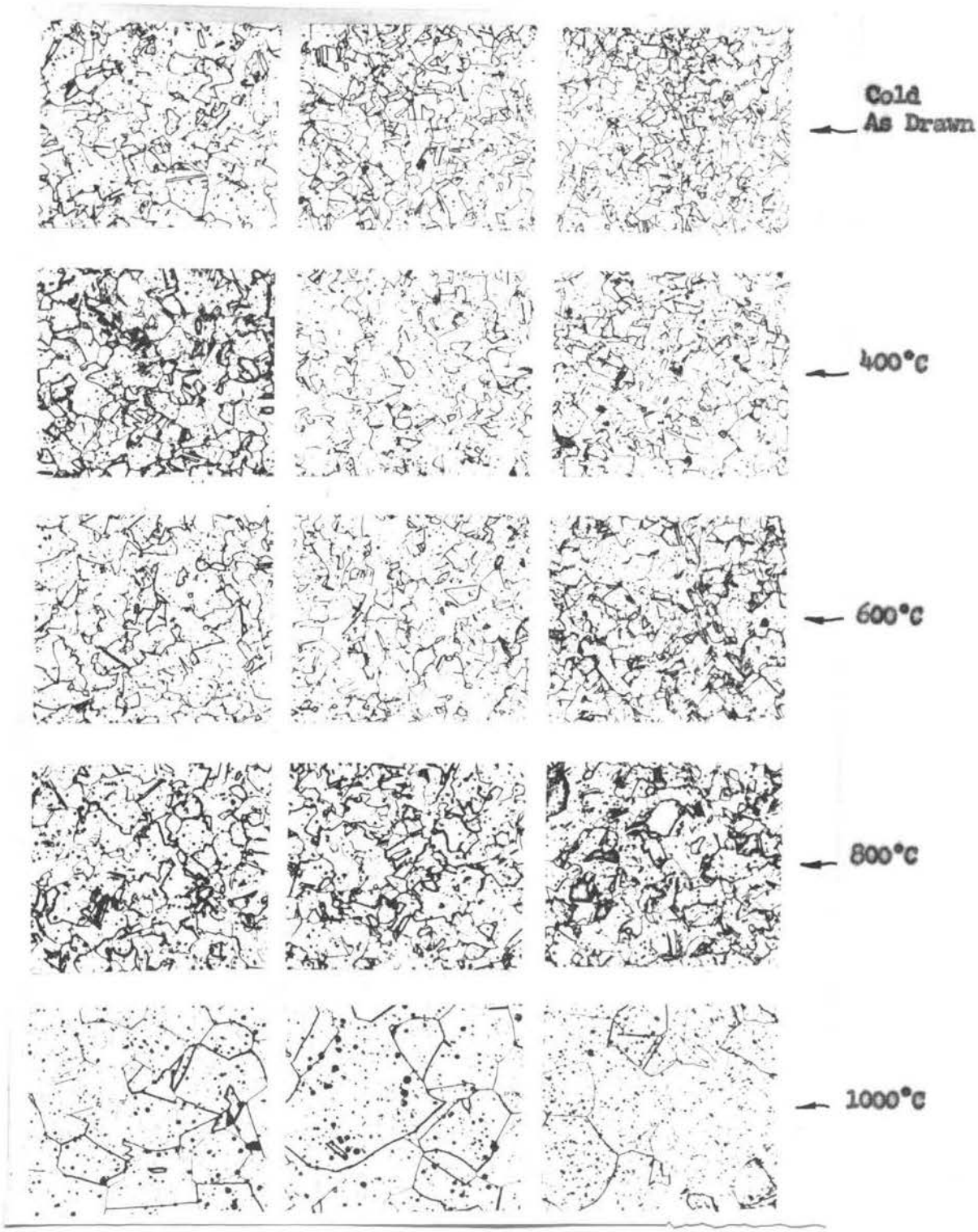

FIGURE 86. Microphotographs of 20.6 per cent cold drawn and annealed one inch diameter nickel rod.....x50.

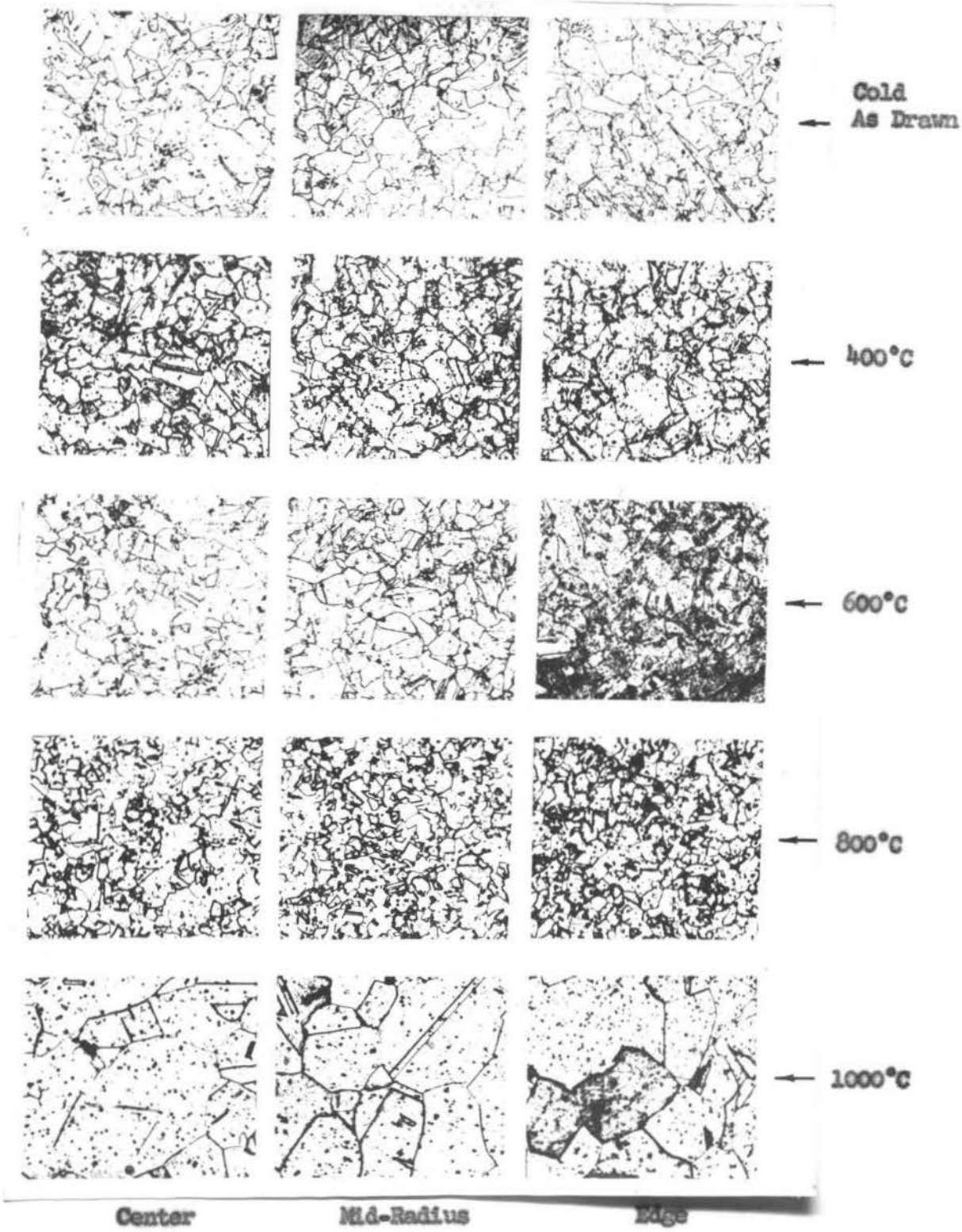

FIGURE 87. Microphotographs of 40.5 per cent cold drawn and annealed one inch diameter nickel rod....x50.

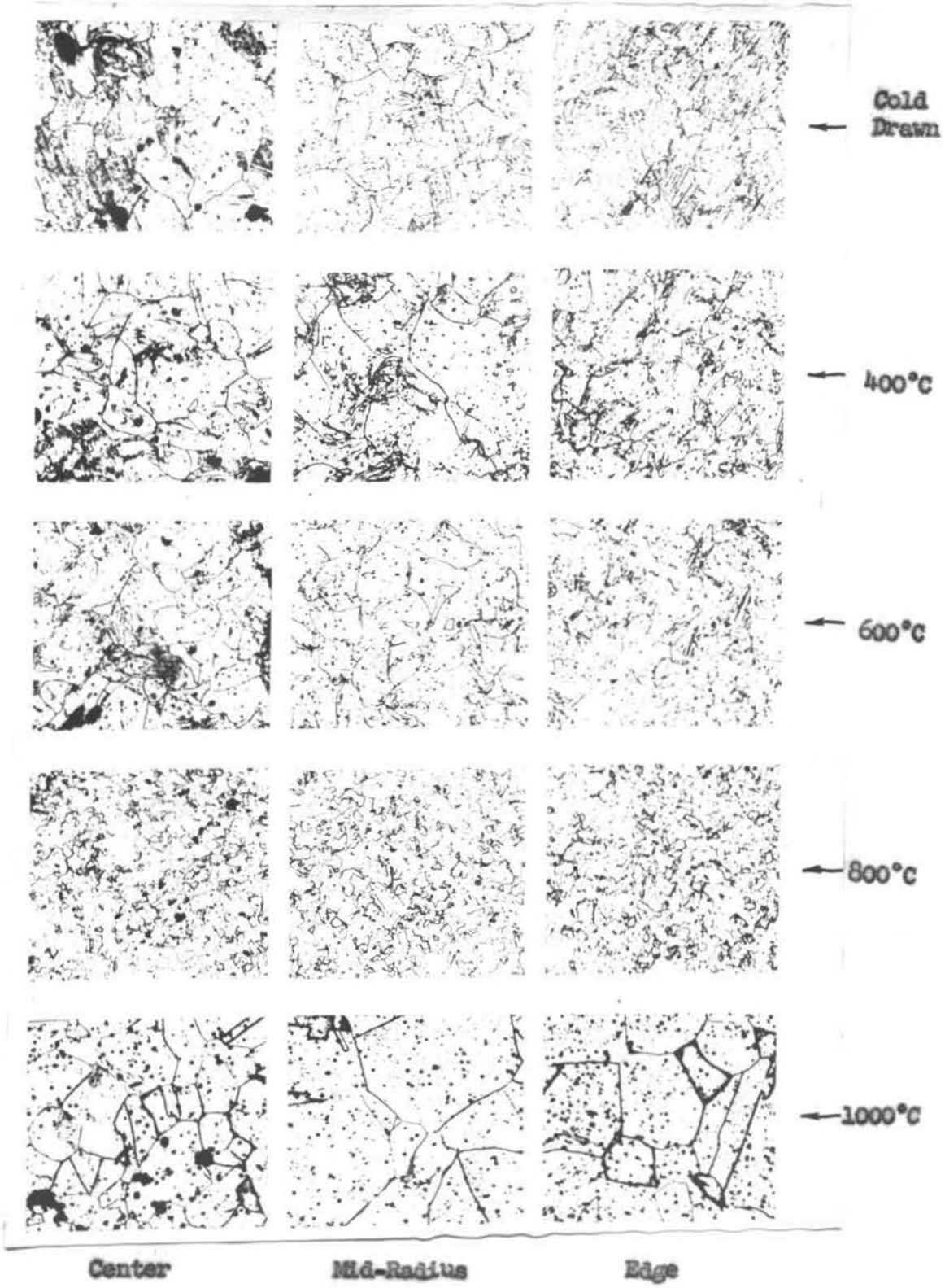

FIGURE 88. Microphotographs of 60 per cent cold drawn and annealed one inch diameter nickel rod....x50.

CHAPTER XI

SUMMARY AND CONCLUSIONS

A. SUMMARY

A new x-ray diffraction technique for pole figure determination, which permits complete pole figure coverage with only one spherical x-ray specimen, was developed. The thickness of the metal layer disturbed due to machining and polishing the spherical specimen was determined by an x-ray diffraction method.

Deformation textures in 20.6, 40.5 and 60 per cent cold drawn one inch diameter nickel rods (items no. 1, 2 and 3 respectively), were determined and corresponding pole figures were drawn.

A critical examination of the validity of assumptions generally made for the determination of pole figures, especially in the case of cold drawn nickel, was made. A new method for diagrammatic representation of the texture data for drawn metals was proposed.

The Calnan and Clews method of deformation texture analysis was examined and used to determine the probable origin of the tension, compression, and cold drawn texture of nickel.

An x-ray diffraction technique for quantitative determination of texture variation in cold drawn metals was developed and the variation of texture in 20.6, 40.5 and 60 per cent cold drawn one inch diameter nickel rods (items no. 1, 2 and 3) was determined.

Hardness measurements on the cross-section of all three items (20.6, 40.5 and 60 per cent cold drawn) were made. Macrographs on

the cross-section of the three specimens were also prepared.

Microstructure studies at various distances from the fibre axis on the cross-section of the as drawn nickel rod (items no. 1, 2 and 3) and also after subsequent annealing at 400°, 600°, 800° and 1000°C were carried out.

B. CONCLUSIONS

The preferred orientation in cold drawn nickel can be described as a double fibre texture with [111] and [100] directions aligned along the fibre axis of the drawn rod. The degree of alignment of [111] direction was much greater than that of the [100] direction, which showed a considerable amount of scatter from the ideal end orientation.

The concentration of [111] orientation in the 20.6 per cent cold drawn nickel (item no. 1) increased to twice as much with an additional 20 per cent increase in cold reduction. Further cold drawing did not increase the concentration of the orientation to any appreciable extent. In contrast to this, [100] orientation did not show any significant change with increasing cold work, however, a slight tendency for its decrease at higher reductions was noted.

The generally accepted assumption, that distribution of orientations for any one angle of inclination around the fibre axis is uniform, was found to be incorrect due to the presence of residual textures in the stock metal used for cold drawing.

The texture within the cold drawn nickel rods was found to vary considerably, indicating that non-uniform deformation occurs

during the cold drawing process. The total deformation was found to increase with increasing distance from the fibre axis almost to the surface of the rods where a slight decrease was observed.

On annealing, no new orientations due to recrystallization in cold drawn nickel were developed. Sharpening of the [111] and [100] textures in the 20.6 per cent cold drawn nickel (item no. 1) was shown on annealing at 400°C. Similar sharpening of the two textures in item no. 3 (60 per cent cold drawn) was observed after 400° and 600°C anneals. However, item no. 2 (40.5 per cent cold drawn) indicated a weakening of the [111] texture and strengthening of the [100] texture on annealing at 400°C. After annealing at 800°C all three items (20.6, 40.5 and 60 per cent cold drawn) showed a very considerable weakening of the [111] and [100] textures.

The concentration of [111] and [100] orientations in cold drawn nickel rods first decreased from a maximum at the fibre axis to a minimum near the mid-radius, and then showed a slight increase with increasing distance from the fibre axis. Though this general trend of distribution of [111] texture was retained on annealing the cold drawn metal at 800°C, the concentration of this orientation was decreased almost to the point of annihilation of the preferred fibre texture. In contrast to this, the distribution of [100] texture becomes random on annealing at 800°C. Random distribution of the [111] texture was produced only after annealing the cold drawn rods at 1000°C.

Hardness on the cross-section of 20.6 per cent cold drawn one inch diameter nickel rod (item no. 1) increased from the center to a distance of 0.1 inch from the fibre axis. No significant change in

hardness was noticed with further increase in distance from the center of the specimens. Whereas, in 40.5 and 60 per cent cold drawn rods (items no. 2 and 3 respectively) hardness increased from a minimum at the center to a maximum near the mid-radius and then decreased, as the surface of the rod was approached.

Outer concentric regions of the cold drawn nickel rods showed a maximum rate of dissolution in concentrated nitric acid, indicating that these regions suffered the maximum deformation during the cold drawing process.

No significant change in the microstructure at various distances from the fibre axis on the cross-section of 20.6, 40.5 and 60 per cent cold drawn nickel rods (items no. 1, 2 and 3) was observed. Recrystallization indicated by development of equiaxed fine grains in the metal was observed on annealing the three rods (items no. 1, 2 and 3) at 800°C, whereas a 1000°C anneal resulted in considerable grain growth.

BIBLIOGRAPHY

Barrett, C. S., "The stereographic projection". Trans AIME, Vol. 124, p. 52, 1937.

_____, and L. H. Levenson, "Determination of orientation by etch pits". Trans AIME, Vol. 137, p. 76, 1940.

_____, "The crystallographic mechanisms of translation, twinning, and banding". Cold working of metals, Cleveland: American Society for metals, 1949.

_____, The Structure of Metals, New York: McGraw-Hill Book Company, 1952. 661 pp.

Beck, J. E., Working of Metals, A.S.M. Publication, 1937. 228 pp.

Becker, K., R. O. Herzog, W. Jancke, and M. Polanyi, "Methods for the arrangement of crystal elements". Z. Physik, Vol. 5, p. 61, 1921.

Boas, W. and E. Schmid, "The interpretation of deformation textures in metals". Z. Tech. Physik, Vol. 12, p. 71, 1931.

Calnan, E. A. and C. J. B. Clews, "Deformation textures in face-centered cubic metals". Phil. Mag., Vol. 41, p. 1085, 1950.

_____, and C. J. B. Clews, "The development of deformation textures in metals. Part II. Body-centered cubic metals". Phil. Mag., Vol. 42, p. 616, 1951.

_____, and C. J. B. Clews, "The development of deformation textures in metals. Part III. Hexagonal metals". Phil. Mag., Vol. 42, p. 919, 1951.

Cook, M. and T. L. Richards, "Fundamental aspect of cold working of metals". J. Inst. Met., Vol. 78, p. 463, 1951.

Decker, B. F., "Validity of pole figures," J. Appl. Phy., Vol. 16, p. 309, 1945.

_____, E. T. Asp, and D. Harker, "Preferred orientation determination using a Geiger counter x-ray diffraction goniometer". J. Appl. Phy., Vol. 19, p. 388, 1948.

Ettisch, M. Polanyi, and K. Weissenberg, Z. Physik., Vol. 7 (1921), p. 181.

_____, M. Polanyi, and K. Weissenberg, "Faserstruetur hartgezogener Metalldrähte", Z. Phys. Chemie, Vol. 99 (1921), pp. 332-337.

Greenwood, Gilbert, "Fibre texture in nickel wires", Z. Krist., Vol. 72 (1929), pp. 309-317.

_____, "On the cold working of platinum wires and the fibrous texture thereby produced", Z. Kristal., Vol. 78 (1931), pp. 242-250.

Göler, G. v. and G. Sachs, Z. Physik, Vol. 41 (1927), pp. 873, 889.

Goss, N. P., Working of Metals, A.S.M. Publication, 1937. pp. 228.

Hibbard, W. R., Jr., and M. K. Yen, "Wire textures of copper and its binary and solid solution alloys with aluminum, nickel and zinc". Trans AIME, Vol. 175, p. 126, 1948.

_____, "A theory of deformation textures in metals", Rev. Met., p. 131, Feb. 1951.

Hill, R., The mathematical theory of plasticity, London: Oxford University Press, 1950.

Hofman, W., Röntgenuntersuchungen an Bleilegierungen, Z. Metallkunde, Vol. 29 (1937), p. 266-267.

Jetter, L. K., and B. S. Borie, Jr., "A Method for the Quantitative Determination of Preferred Orientation", J. App. Phy., Vol. 24 (1953), pp. 532-535.

Kehl, George L., The Principles of Metallographic Laboratory Practice, New York: McGraw-Hill Book Company, Inc., 1949. pp. 520.

Mark, H., M. Polanyi, and E. Schmid, "Processes in the stretching of zinc crystals", Z. Physik, Vol. 12 (1923), pp. 58-72; 78-110; 111-116.

Mazza, L., and A. G. Magini, "The crystal structure of nickel", Phil. Mag., Vol. 7 (1929), p. 301.

Mises, R. v., Z. angew. Math. Mech., Vol. 8 (1928), p. 161.

Navarro, F. R. N., "The influence of grain boundaries on the plastic properties of metals". United Trade Press (London), p. 38, 1950.

Neil, D. J., "A sheet specimen scanner for x-ray diffraction". Can. Inst. of Tech., Vol. 29, p. 84, 1951.

Norton, J. T., "A technique for quantitative determination of textures of sheet metals". J. Appl. Phy., Vol. 19, p. 1176, 1948.

Obermayer, A. V., Versuche uber den Ausfluss plastischen Tones, Ber. d. Kaiserl. Akad. d. Wissensch., Wein 1868, p. 737.

Pickus, M. R. and C. H. Mathewson, "On the theory of the origin of rolling textures in face-centered cubic metals". J. Inst. Met., Vol. 64, p. 237, 1939.

Polanyi, M., "Structure changes in metals through cold working". Z. Physik, Vol. 17, p. 42, 1923.

_____, "Deformation, rupture, and hardening of crystals". Trans. Far Soc., Vol. 24, p. 72, 1928.

Pomp, A., E. Siebel and E. Houdremont, "Uber den Kraft-und Arbeitsbedarf beim Kaltziehen von Drahten", Mitt. K. W. Inst. Eisenforsch., Vol. 11 (1929), p. 53.

Sachs, G. and Van Horn, Practical Metallurgy, A.S.M. Publication, 1940. 567 pp.

_____, Fundamentals of the Working of Metals. London: Permagon Press, 1954. 156 pp.

Schmid, E., and G. Wassermann, "Uber die Unterschiede von Kern-und Mantelzonen gezogener Drähte", Z. Metallkunde, Vol. 19 (1927), pp. 325-327.

_____, and G. Wassermann, Z. Physik., Vol. 42 (1927), p. 779.

_____, and G. Wassermann, Z. Physik., Vol. 9 (1928), p. 106.

_____, and G. Wassermann, Naturwissenschaft, Vol. 17 (1929), p. 321.

_____, "International conference on Physics, Vol. II, The solid state of matter", Physical Society, London, 1935.

_____, and W. Boas, Plasticity of crystals, London: F. A. Hughes and company, 1950, (English translation).

Siebel, E., "The plastic forming of metals", Steel, Vol. 94 (1934), No. 12, p. 28.

_____, The plastic forming of metals", Steel, Vol. 94 (1934), No. 12, pp. 28-30; No. 13, p. 38.

Schulz, L. G., "Determination of preferred orientation in flat transmission samples using a Geiger counter x-ray spectrometer". J. Appl. Phy., Vol. 20, p. 1033, 1949.

_____, "A direct method of determining preferred orientation in flat reflection samples using a Geiger counter x-ray spectrometer". J. Appl. Phy., Vol. 20, p. 1030, 1949.

Taylor, G. I., "Resistance to shear in metal crystals". Trans. Far. Soc., Vol. 24, p. 121, 1928.

_____, Mechanism of plastic deformation of crystals". Proc. Royal Soc., Vol. A 145, p. 362, 1934.

_____, "Plastic strain in metals". J. Inst. Met., Vol. 62, p. 307, 1938.

_____, and H. Quinney, "The distortion of wires on passing through a draw plate", J. Inst. Metals (London), Vol. 49 (1932), pp. 187-202.

"Tentative method for preparing quantitative pole figures of metals". ASTM, E 81 - 49 T, 1949.

Tresca, H., Memoires sur L'ecoulement des corps solides; Ann. du conservatoire des arts et metiers, 1865; Comptes rendus, 1867.

Unkel, H., "Einiges uber die fleissbewegung beim Pressen von stengen und Rohren sowie beim Ziehen", Z. Metallk., Vol. 20 (1928), p.325.

_____, Uber die fleissbewegung in Plastischen Material. Berlin: J. Springer, 1928.

Vargha, G. v., and G. Wassermann, "Uber den Einfluss des Formgebungsverfahrens auf die Kristallgleichrichtung in Drähten, Z. Metallkunde, Vol. 25 (1933), pp. 310-313.

Wassermann, G., Textures of metallic materials, Berlin: Julius Springer, 1939.

Wever, F., "The structure of cubically crystallizing metals after rolling". Z. Physik, Vol. 28, p. 69, 1924.

_____, and W. E. Schmid, "Texture of cold-deformed metals". Z. Metallkunde, Vol. 22, p. 133, 1930.

_____, "Texture of metals after cold deformation". Trans AIME, Vol. 93, p. 51, 1931.

Weiss, L., Die Entstehung und Folgen von Spannungsunterschieden in den Querschnitten Kaltgezogener Kupferstangen, Z. Metallkunde, Vol. 20 (1928), p. 118-121.

Wensch, Glen W., "Electrolytic Polishing of Nickel", Metals Progress, November 1950, pp. 735-36.

Williams D. H., and D. S. Eppelsheimer, "Universal specimen mount for pole figure determination using the Schulz-Decker Technique", Univ. of Mo. Tech. Series, Bulletin No. 79.

Wood, J. K., "An analytical discussion of the construction of pole figures". J. Appl. Phy., Vol. 19, p. 784, 1948.

Yeu, M. K., Interim report to Watertown Arsenal, WHL 401 - 14/4, March 20, 1950.

APPENDIX

APPENDIX I

X-RAY MEASUREMENT OF THE THICKNESS OF METAL LAYER DISTURBED DURING MACHINING OF THE X-RAY DIFFRACTION SPECIMENS.

During machining of a metal the cutting tool produces considerable distortion and fragmentation of crystal grains in the surface layers. Back-reflection x-ray photographs of such a surface show a broadening of the lines or diffusion of the diffraction spots. By etching away successive layers of the worked surface, x-ray photographs corresponding to the condition of the metal at various depths can be obtained. When the disturbed metal is completely etched away, no further change in the diffraction patterns is observed.

This x-ray technique does not satisfactorily work with cold-worked metals, as their diffraction patterns show a non-uniform intensity of lines due to presence of preferred orientation. Though the depth to which a metal is disturbed during machining depends on its previous state (cold worked or annealed), a rough approximation of the thickness of this layer in a cold worked metal can be made by its measurement in the annealed state.

THICKNESS OF DISTURBED LAYER IN MACHINED NICKEL

An annealed sample of 40.6 per cent cold drawn nickel (item no. 2) was subjected to a similar machining operation as that employed for the preparation of the x-ray diffraction specimens. Back-reflection x-ray patterns of the surface as machined, and after etching

away successive surface layers were obtained by conventional methods with cobalt radiation. Beam diameter of 1.0 mm and film-specimen distance of 3 cm was used. At 35 k.v. and 9 m.a. current on the x-ray tube, a 3-hour exposure was required to obtain satisfactory patterns. The etching solution used consisted of two parts by volume of water and one part by volume of concentrated nitric acid.

Figures 89 through 96 show back-reflection x-ray patterns from the as machined, and after successive etching away of 0.0002, 0.0009, 0.0016, 0.0021, 0.0026, 0.0031 and 0.0034 inches of the surface of the specimen. It is seen that the degree of diffuseness of reflection spots decreases as successive layers to a depth of 0.0026 inches are etched away (Figures 89 through 94). Further etching of the metal does not produce any change in the sharpness of reflection spots (Figures 95 and 96), thus showing that the thickness of surface layer disturbed due to this specific machining operation is approximately 0.0026 inches.

FIGURE 89. Back-reflection x-ray pattern from machined nickel. (Co radiation).

FIGURE 90. Back-reflection x-ray pattern from machined nickel after etching away 0.0002 inch of the surface. (Co radiation).

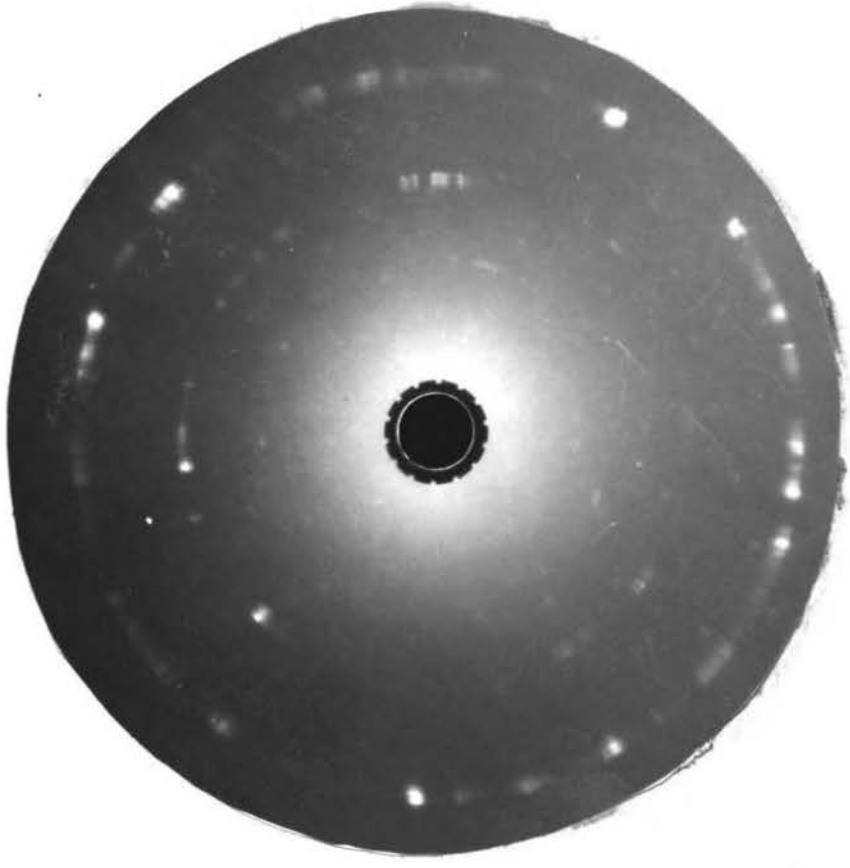

FIGURE 91. Back-reflection x-ray pattern from machined nickel after etching away 0.0009 inch of the surface. (Co radiation).

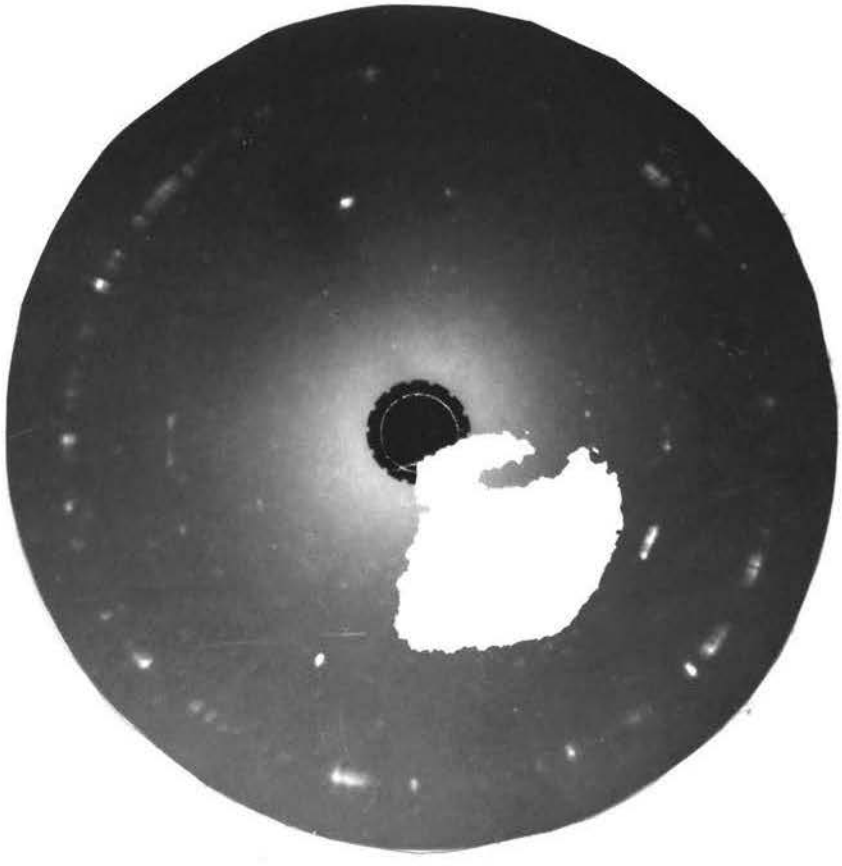

FIGURE 92. Back-reflection x-ray pattern from machined nickel after etching away 0.0016 inches of the surface. (Co radiation).

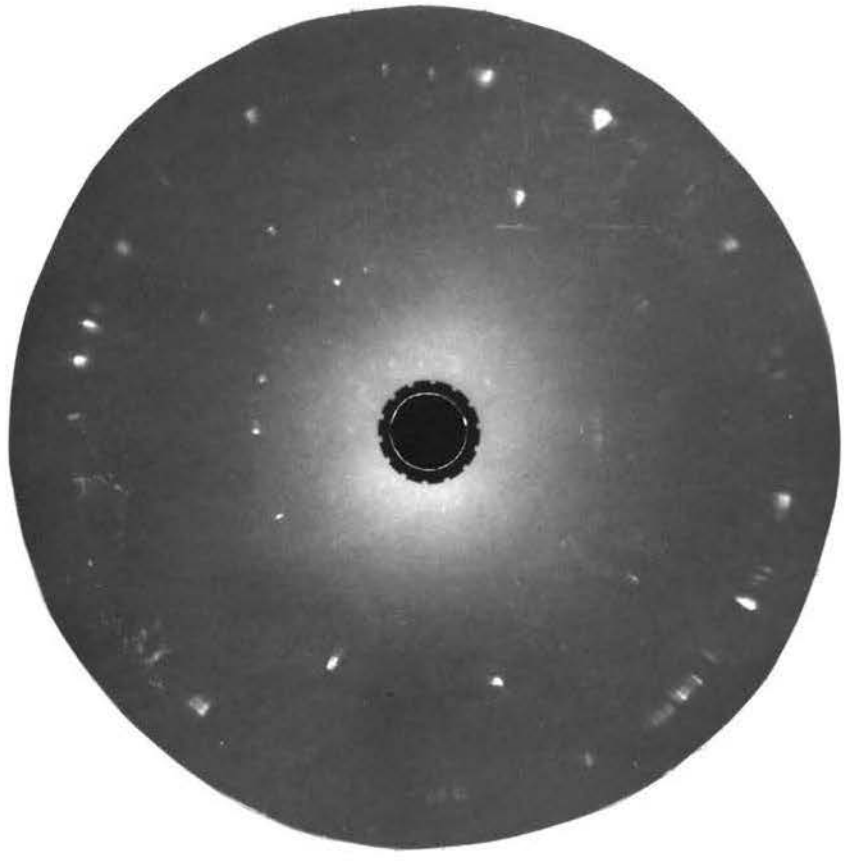

FIGURE 93. Back-reflection x-ray pattern from machined nickel after etching away 0.0021 inch of the surface. (Co radiation).

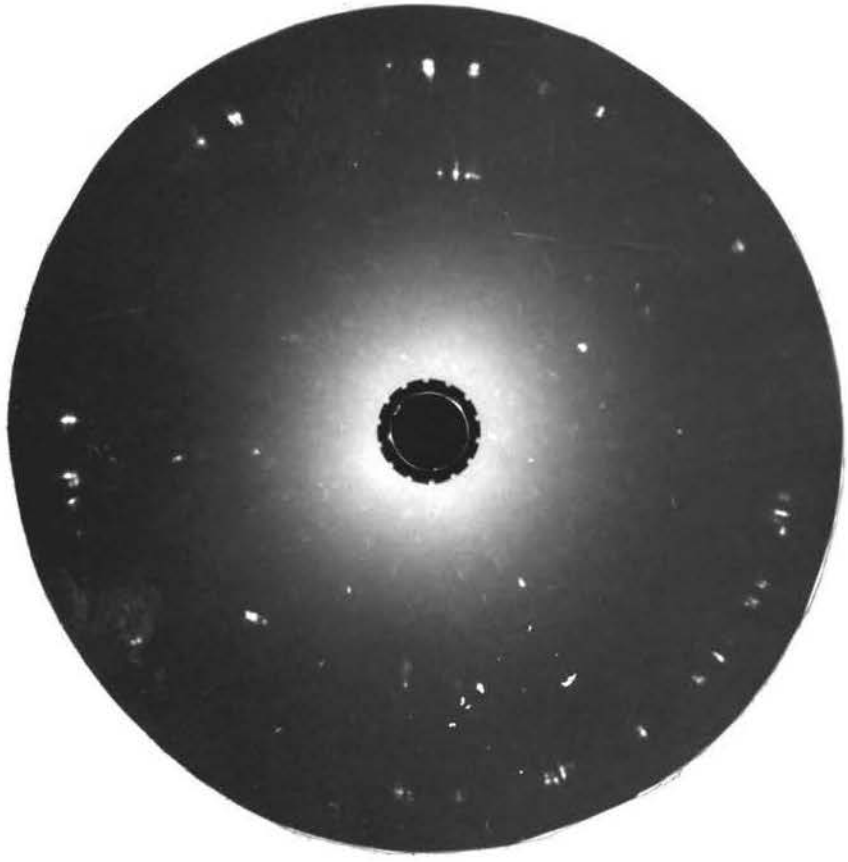

FIGURE 94. Back-reflection x-ray pattern from machined nickel after etching away 0.0026 inch of the surface. (Co radiation).

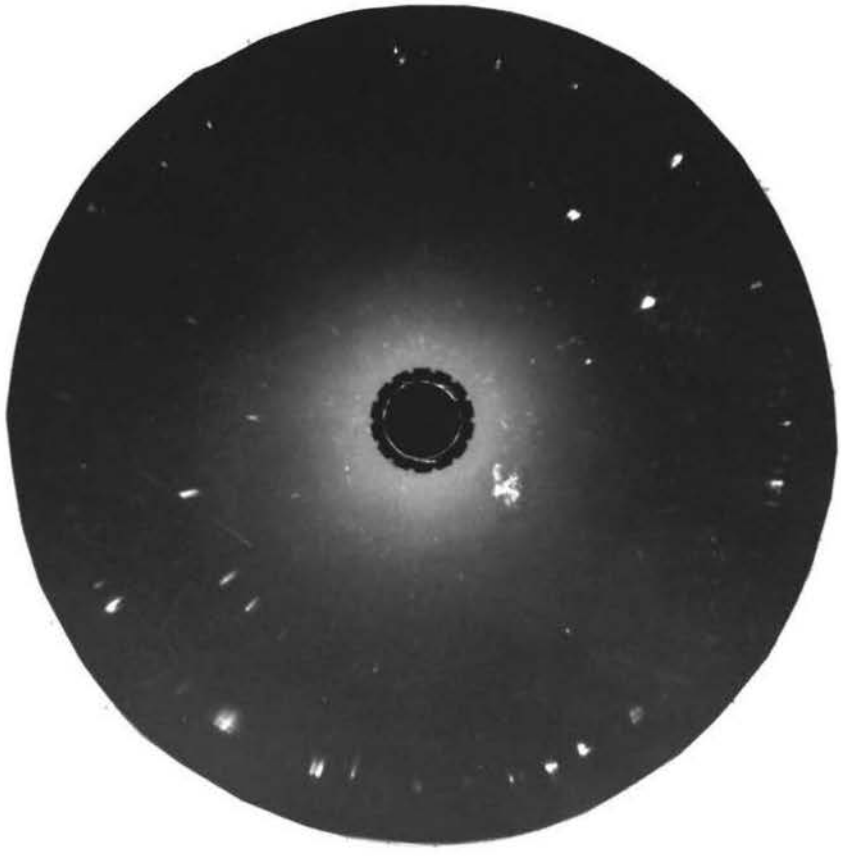

FIGURE 95. Back-reflection x-ray pattern from machined nickel after etching away 0.0031 inch of the surface. (Co radiation).

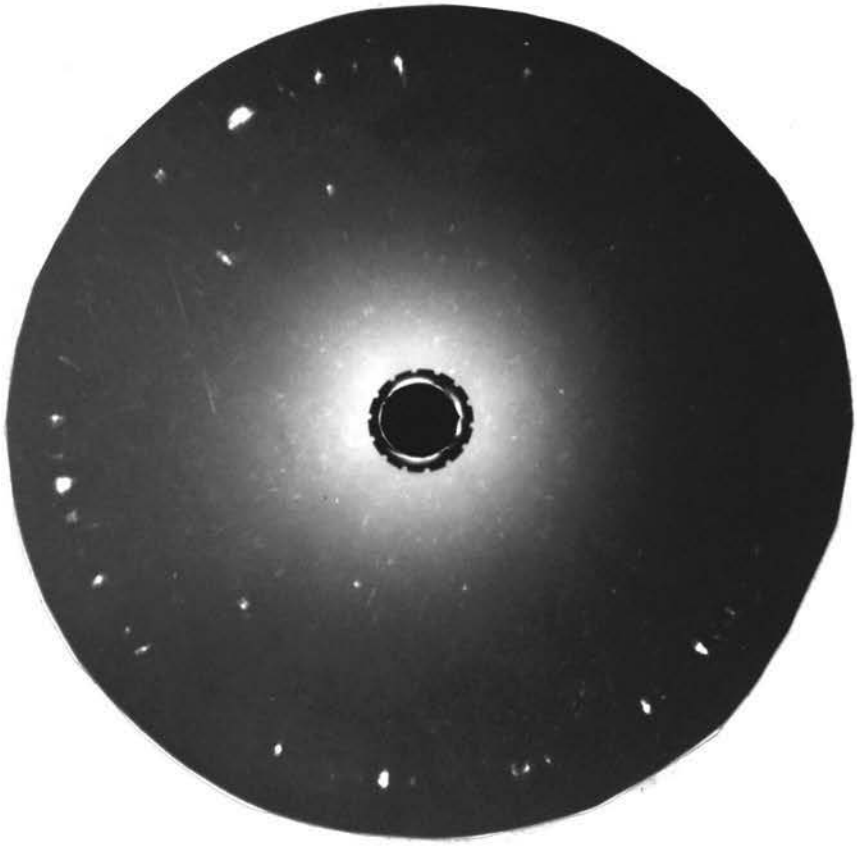

FIGURE 96. Back-reflection x-ray pattern from machined nickel after etching away 0.0034 inch of the surface. (Co radiation).

APPENDIX II

X-RAY TECHNIQUE FOR POLE FIGURE DETERMINATION

A 'spherical specimen mount' was developed for use in the pole figure studies conducted. Because a spherical specimen is employed, the intensity of reflections may be plotted directly on a stereographic net without geometry or absorption corrections. For complete pole figure coverage with one diffraction specimen, two mutually perpendicular axes of rotation are required to vary the orientation of the specimen on the x-ray beam. One axis is defined by a cylindrical stem appended to the spherical specimen. This axis is usually a principal direction of the specimen, as for example, the fibre axis in a drawn rod. The second axis, which is perpendicular to the first axis and is parallel to the spectrometer axis, passes through the center of the spherical specimen. For simplicity, the axis which allows angular changes around any of the concentric latitude circles in the polar net drawn on the projection plane will be referred to as the axis of rotation. The axis which allows angular changes which change the diameter of the concentric latitude circles will be referred to as the axis of revolution. Similarly, the corresponding angles will be referred to as the angles of rotation (α) and revolution (ϕ) respectively.

A. CONSTRUCTION OF THE 'SPHERICAL SPECIMEN MOUNT'

The spherical specimen mount consists of the following four major parts.

i) The mounting standard

ii) The base quadrant

iii) The graduated sector

iv) The specimen holder

The mounting standard and various components of the 'spherical specimen mount' are shown in Figures 97 and 98, whereas, an assembled view is given in Figure 99. The mounting standard consists of a cylindrical stem (1) pressed into a brass disc (2). Around this disc is a concentric brass ring (3) provided with a hole (4) corresponding to the locating pin on the spectrometer base. This ring can be rotated around the brass disc and can be fixed in any position by means of set screw (5). This arrangement permits the correct positioning of the spherical-specimen mount on the x-ray spectrometer.

The base quadrant (6) is mounted on the mounting standard by fixing the brass disc of the mounting standard to the base quadrant with two machine screws countersunk into the brass disc. The upper surface of the base quadrant is fitted with a 'revolution axis' gauge. This gauge consists of a pin (7) mounted vertically on a slide (8) which in turn is mounted in recessed ways (9). The gauge is calibrated along one of the ways (10) and the index mark is placed on the upper surface of the slide. The center of the pin (7) is aligned with the axis of revolution of the spherical specimen.

Along the left hand edge of the base quadrant is mounted a stop (11) which fixes the position of the graduated sector (22) which is mounted over the pin (7) and lies on top of the base quadrant. An adjusting screw (13) mounted through a hole in the left hand edge

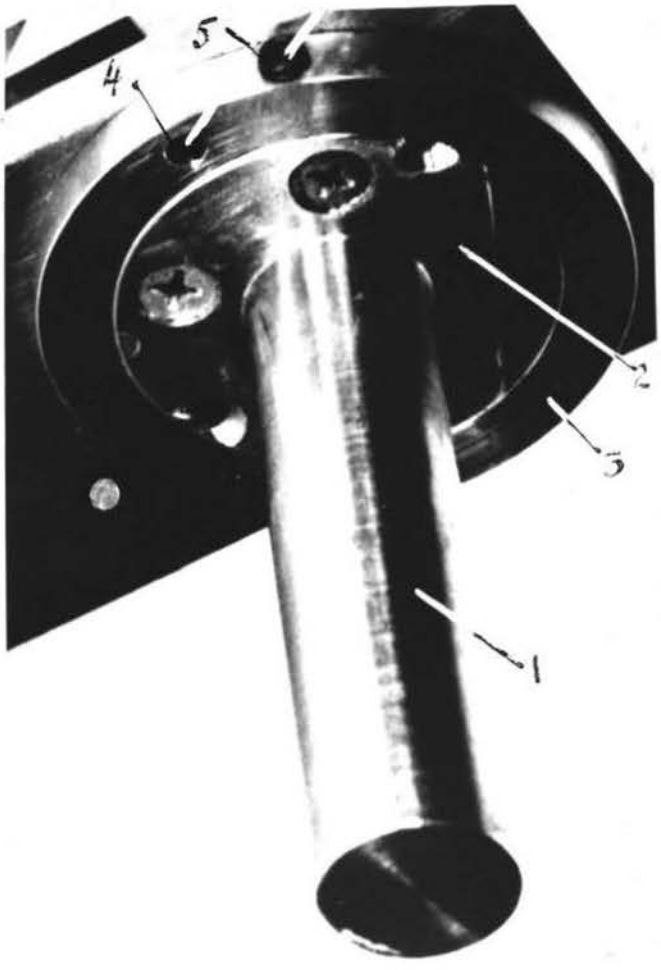

FIGURE 97. Mounting standard of the 'spherical specimen mount'.

FIGURE 98. Various components of the 'spherical specimen mount'.

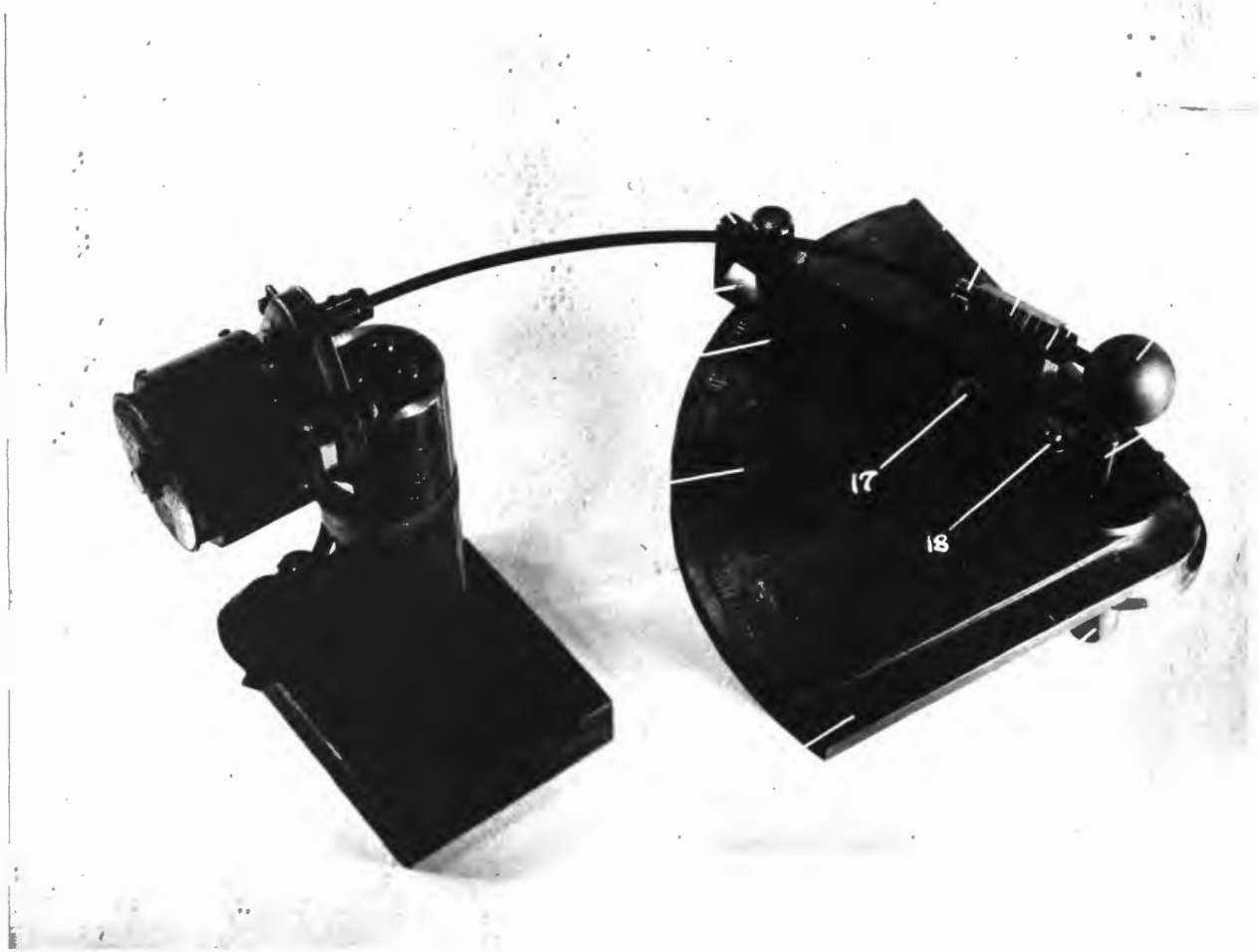

FIGURE 99. The 'spherical-specimen mount'.

of the base quadrant and threaded into the slide of the 'revolution axis' gauge, allows the pin and thus the axis of the revolution of the specimen to be set at a distance equal to the radius of the specimen, from the path of the x-ray beam.

The graduated sector is divided into degrees along its circumference. The specimen holder consists of a base plate (14) which mounts on the pin (7) on top of the graduated sector. An index edge (15) is machined on the outer edge of the base plate to indicate the angle of revolution ϕ on the graduated sector. A bearing stand (16) is mounted on the base plate with screws (17, 18) passing through slotted holes on the bottom of the stand. This permits alignment of the axis of rotation in such a way that it passes through the axis of revolution and also that it bisects the angle contained between the incident and the diffracted beam when the specimen holder is set at $\phi = 0$. In this bearing (16) sits a sleeve, to the outer and (19) of which is attached a flexible shaft driven from a motor mounted on a separate base. A stem machined on the spherical specimen (21) fits into the other end (20) of the sleeve and can be fixed in any longitudinal position with a set screw. The specimen holder can be locked at any desired angle of revolution by means of 'C' clamp (22). Figure 100 shows the 'spherical specimen mount' in operation on an x-ray diffraction spectrometer.

B. USE OF THE SPHERICAL SPECIMEN MOUNT

The specimen held in the spherical specimen mount may be given five independent motions. For their explanation in the description

FIGURE 100. 'Spherical Specimen Mount' in operation on an x-ray diffraction spectrometer.

below refer to Figures 98--99 on pages 198--199 and their accompanying numbering system. The five independent motions of the specimen are as follows:

1. It rotates through an angle θ about the vertical spectrometer axis as the Geiger counter arm is rotated through 2θ, θ being the Bragg angle for the family of planes under investigation.

2. The specimen can be moved linearly along the axis of rotation either by sliding the stem appended to the specimen in its bearing sleeve (20), or by moving the 'revolution axis gauge' in the recessed ways (9) provided on the base quadrant (6).

3. Lateral movement of the rotation axis of the specimen (defined by the axis of its stem) may be achieved by adjusting the position of the bearing stand (16) on the base plate (14).

4. Rotation of the spherical specimen around the rotation axis defined by the stem axis of the specimen.

5. Revolution of the spherical specimen around the revolution axis defined by the perpendicular spectrometer axis.

Some of the above mentioned motions are necessary for alignment of the spherical specimen on the 'spherical specimen mount' before any measurement of preferred orientation is made.

Alignment of the spherical specimen. The alignment of the spherical specimen comprises the following steps:

1. The axis of revolution of the specimen is set at a distance equal to the radius of the specimen from the path of the x-ray beam by adjusting the slide (8) in the 'ways' (9), as accurately as the

calibration (10) would permit. This position of the revolution axis is temporarily fixed by means of the adjusting screw (13).

2. The axis of rotation is then made to intersect the axis of revolution and also bisect the angle between the incident and diffracted x-ray beams. This is done by first setting a dial indicator gauge on the specimen surface, with the specimen holder set at ϕ equals zero. The specimen holder is then revolved through 180°. In order to obtain the same reading on the dial indicator gauge at both positions, adjustments are made by means of screws (17) and (18).

3. Again, using the dial indicator, the specimen is accurately centered on the revolution axis by sliding the specimen stem in its bearing sleeve (20). The position of the specimen is then fixed by a set screw.

4. The final positioning of the specimen in the x-ray beam is then accomplished by further linear adjustment of the specimen along the rotation axis. This is done by observing the position of any strong peak in the diffraction pattern and adjusting the specimen by moving the 'revolution axis gauge' in the recessed ways (9) after loosening the adjusting screw (13), until the diffracted line appears at its proper 2θ value. This 2θ value of the selected line is determined by making a standard x-ray diffraction pattern from a flat specimen of the metal under investigation.

The final aligned position of the specimen is then fixed by tightening the adjusting screw (13).

Measurement of preferred orientation. As discussed in chapter

IV, complete coverage of a pole figure can be obtained by measuring the intensity of reflection from the family of planes under investigation at various α and ϕ settings of the spherical specimen. Changes in the position of the diffracting plane normal on the polar net corresponding to changes in the orientation of the specimen are shown in Figure 17 on page 45. For the specimen setting at ϕ equals zero, constant intensity readings should occur on rotation of the specimen as the diffracting plane normal lies along the axis of rotation. This intensity reading corresponds to the center of the polar net. It is easily seen that a 45°, counter-clockwise revolution of the specimen, as one looks down on the specimen, gives intensity reading corresponding to a point 45° to the right of the center of the polar net. Keeping the angle of revolution fixed, a 30° clockwise rotation of the specimen, as one looks towards the x-ray tube, causes a 40° counter-clockwise movement on the 45° latitude circle on the polar net. Thus, if a specimen is revolved ϕ° counter-clockwise and then rotated about the axis of rotation, successive readings along the circumference of the ϕ° latitude circle are obtained.

The orientation around the fibre axis in the ideal case of a cold drawn rod is supposed to be random. Thus, an average value of the reflection intensity for any latitude circle is obtained by rotating the specimen at 60 rpm. Angle of revolution is changed for settings of 10° latitude intervals. If some area of the pole figure warrants increased coverage, it is easily done by using settings of 5° latitude intervals in that region. With the specimen rotating continuously, intensities of a reflection and its background for different ϕ

settings are obtained by running the Geiger counter a few degrees to cover the angle at which the reflection appears.

Slit system for pole figure determination in cold drawn nickel. Standard slit system was used for the determination of pole figures of cold drawn nickel. To minimize the background intensity and the surface area of the specimen irradiated by the x-ray beam, a small tube slit (0.075 centimeter) was employed. As the diffraction lines of nickel are widely separated, a wide slit on the Geiger counter was used to obtain reflections of satisfactory intensity.

Plotting of the data. As the rotation or revolution of the specimen does not bring about any change in the diffraction geometry, no intensity correction is required. Thus, the data on reflection intensities may be plotted directly on a polar net.

The intensity contour system for presenting the data was used in this thesis. The maximum reflection intensity from the plane under investigation was taken as fifty units and all intensity values were then expressed in terms of this base. The intensity contours were designated as follows: up to ten units--1, eleven to twenty--2, twenty one to thirty--3, thirty-one to forty--4, and forty-one to fifty--5.

Determination of the distribution of orientations for any one angle of inclination around the fibre axis of a drawn rod. At any stage of the drawing process before the ideal end orientation is reached, the distribution of crystals with favored direction (the direction that tends to align itself along the fibre axis during the

drawing process) at any one angle of inclination around the fibre axis is expected to be uniform. However, due to the residual texture that might be present due to previous cold working of the stock metal used for drawing, a variation in this distribution may be expected. The distribution of a favored [hkl] direction for various angles of inclination around the fibre axis of a cold drawn metal in the cubic system may be determined by measuring the intensity of corresponding (hkl) reflections for various angles of rotation α and revolution ϕ of a spherical x-ray diffraction specimen. The procedure used for scanning the spherical specimen of cold drawn nickel was as follows:

After proper alignment of the specimen as discussed in a previous section, the background intensity and the angle (2θ) of maximum intensity for (111) planes was determined by scanning the diffracted beam in the usual manner. The Geiger counter was then held stationary at this value of angle 2θ. With the sphere held constant at 10° intervals of ϕ, the specimen was rotated at a speed of 3 rph. The rotation of the specimen was synchronized with the movement of the potentiometer recorder chart. Reference marks on the stem of the specimen and its bearing sleeve were made to correspond to zero degrees rotation of the specimen. For every ϕ setting of the specimen, the potentiometer chart was first allowed to run for four minutes without rotation of the specimen to record the variation in intensity registration due to the instrument itself, and then a rotation of 360° was given to the specimen. X-ray diffraction charts thus prepared for a spherical specimen of 60 per cent cold drawn nickel (item no. 3) are shown in Figure 34 on page 83.

Sample calculations for maximum percentage variation for the specimen setting ϕ equals 80°. First, maximum percentage variation in reflection intensity recorded during rotation of the specimen is calculated. This value is then corrected for variation in intensity registration due to the instrument itself. A sample calculation for the specimen setting ϕ equals 80° is given below.

a) Maximum I_{111} on the chart---------2.75 intensity units

Minimum I_{111} on the chart----------0.85 intensity units

Average I_{111} for ϕ equals 80°-----$\frac{2.75 + 0.85}{2}$

$= 1.8$ intensity units

Maximum variation in I_{111}---------$\frac{2.75 - 0.85}{2}$

$= \pm 0.95$ intensity units

Maximum % variation in I_{111}-------$\frac{0.95}{1.8} \times 100 = 52.7\%$.

b) The maximum percentage variation in I_{111} for the instrument can be calculated in a similar manner from the portions of the charts appearing on the right hand side of the vertical line drawn at α equals zero. This value is found to be 10.2%.

c) Thus, from (a) and (b), the net variation due to rotation of the specimen is: 52.7 - 10.2 = 42.5%.

APPENDIX III

X-RAY TECHNIQUE FOR DETERMINATION OF TEXTURE VARIATION IN COLD DRAWN NICKEL RODS.

It was shown in chapter VII, that inhomogeneous deformation of the metal occurs during the cold drawing process. As a result the deformation texture varies in different concentric regions around the fibre axis.

The drawing texture in nickel can be described as an alignment of [111] and [100] directions along the fibre axis. The degree of this alignment depends upon the amount of cold deformation produced. The (111) and (100) planes, being perpendicular to the [111] and [100] directions respectively in nickel, lie in a plane perpendicular to the fibre axis of a drawn rod. Thus a quantitative determination of the variation in texture can be made by measuring the 111 and 100 reflection intensities from various concentric regions on the cross-section of the rod. A specimen mount, called hereafter the "Disc specimen mount', was constructed for this purpose.

A. CONSTRUCTION OF THE DISC SPECIMEN MOUNT

The Disc-Specimen Mount consists of the following three major parts:

1) the mounting standard
2) the alignment assembly
3) the specimen holder

The bottom, rear and front views of the 'Disc specimen mount'

are shown in Figures 101, 102 and 103 respectively. The mounting standard consists of a stem (1) pressed into a brass disc (2). Around this disc is a concentric brass ring (3) provided with a hole (4) corresponding to the locating pin on the spectrometer base. This ring can be rotated around the brass disc and can be fixed in any position with a set screw (5). This arrangement permits the correct positioning of the Disc-Specimen Mount on the x-ray spectrometer. A rectangular base plate (6) is mounted on the brass disc (2) with machine screws countersunk into it,

The alignment assembly consists of three dove-tail machine slides. The base slide (7) is mounted on the plate (6) and has a male dove-tail machined on each side. The center slide (8) is a female dove-tail to fit the male dove-tail (7). This provides the means of lateral movement on the base slide (7). This movement is controlled by an adjusting screw (9) fastened to the side of the female slide (8) by means of a thrust bearing and screwed into the base slide. The female slide can be locked in any lateral position on the male slide with a set screw (10) on the back of the female slide. This lateral displacement of the female slide can be measured with a scale (11) marked on the front side of this slide and an index mark on the top of the base plate. On the upper surface of the female slide is machined another female dove-tail slot at 90° to that on its bottom. The top male slide (12) is fitted similar to the base male slide so that it slides forward and backward in the female slot on the slide (8). The forward and backward movement, as in the case of the lateral movement, is controlled by another adjusting screw (13) and

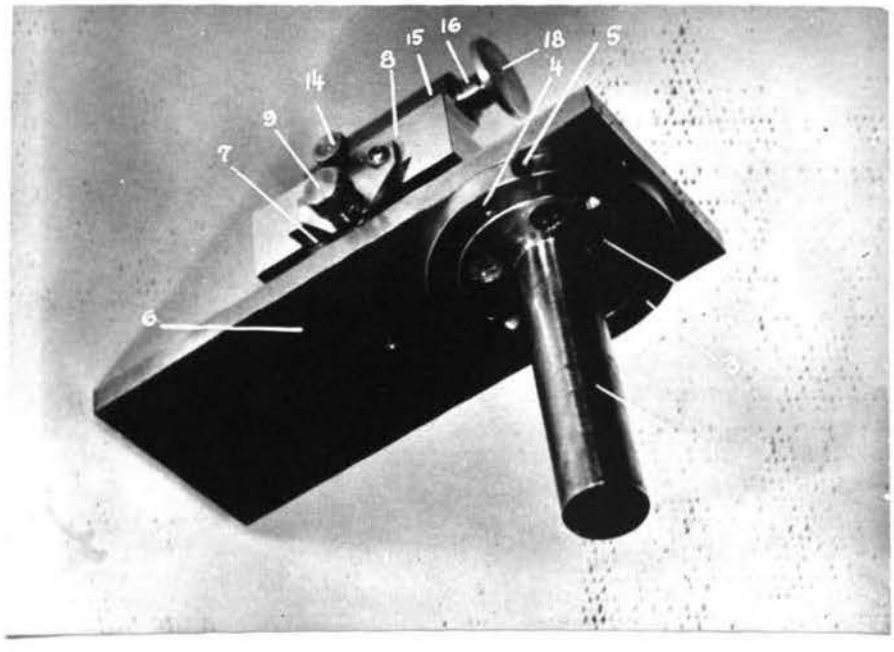

FIGURE 101. Bottom view of the Disc-Specimen Mount.

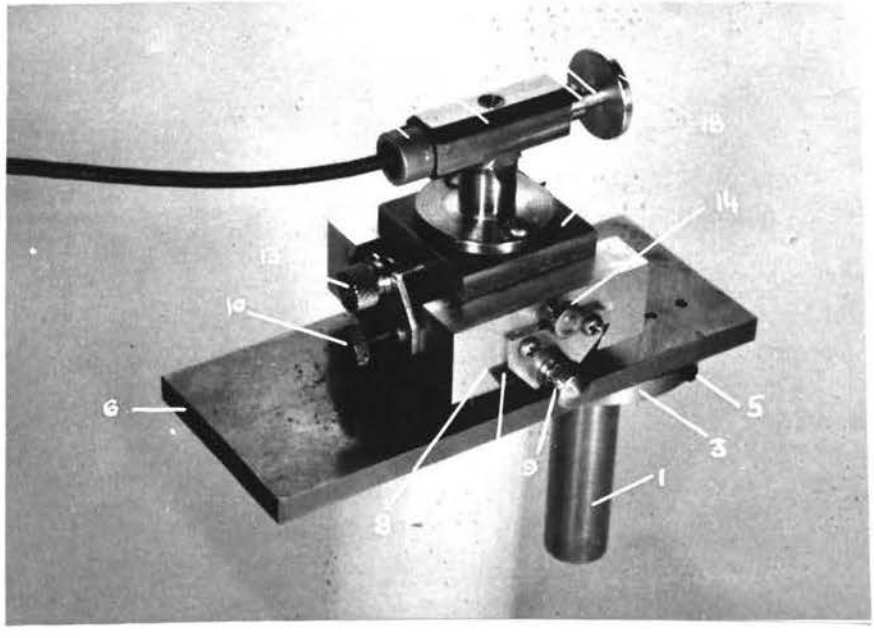

FIGURE 102. Rear view of the Disc-Specimen Mount.

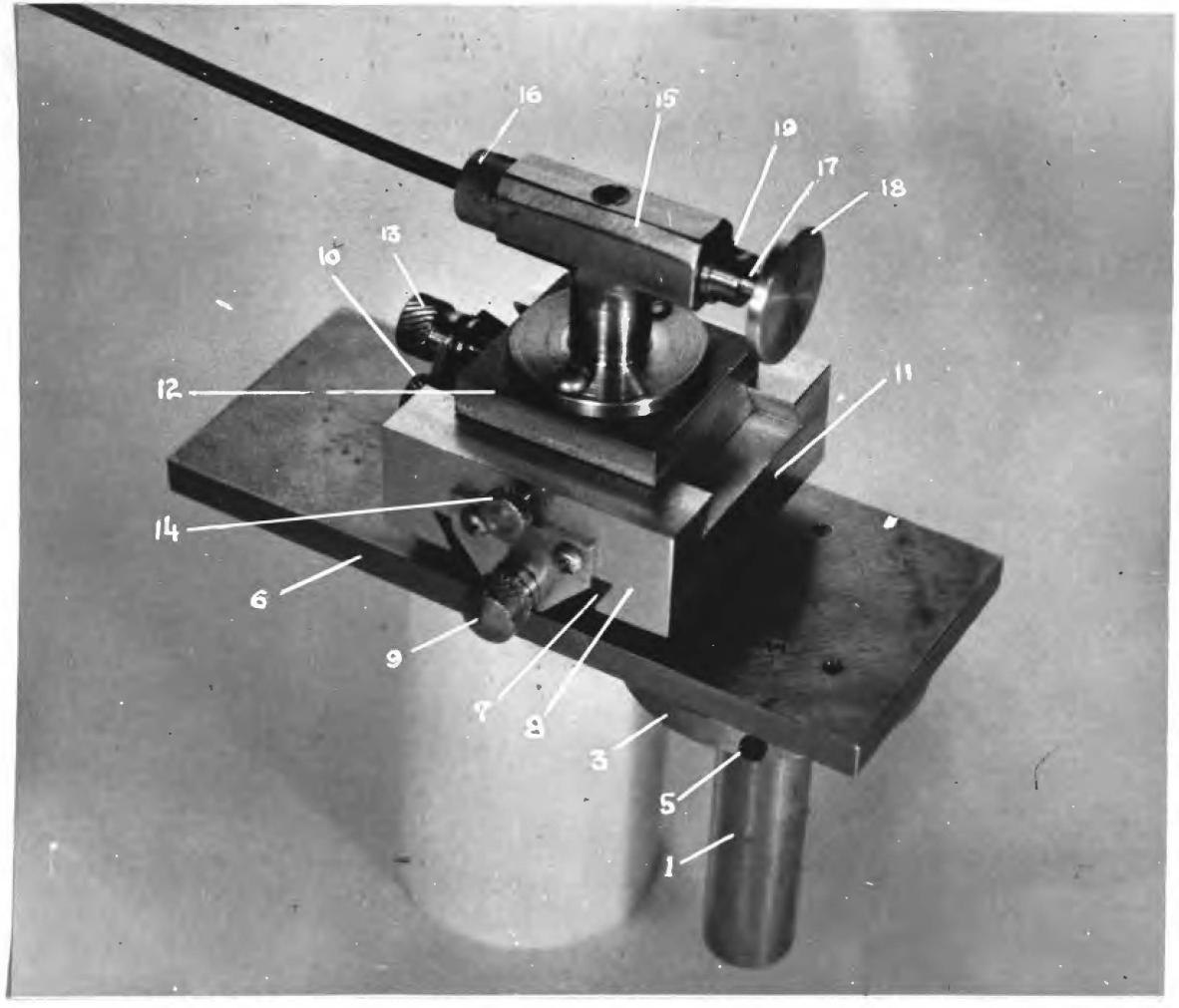

FIGURE 105. Front view of the Misc-Specimen Mount.

can be locked in any desired position with another set screw (14).

The specimen holder consists of a bearing (15) and journal (16) attached to the top slide (12). To the back end of the journal is attached a flexible shaft which is driven with a motor mounted on a separate base. Into the front part of the journal fits a shaft (17) which is provided with a face-plate (18) onto which the flat specimen can be fastened with any kind of cement. This shaft can be fixed in the journal in any required longitudinal position with a set screw (19). Figure 104 shows the 'Disc specimen mount' in operation on an x-ray diffraction spectrometer.

The x-ray disc specimen held in the Disc specimen mount may be given four independent motions. For their explanation in the description below refer to Figures 101-103, on pages 210-212 and their accompanying numbering system.

1. It rotates through an angle θ about the vertical spectrometer axis as the Geiger counter arm is rotated through 2θ, θ being the Bragg angle for the family of planes under investigation.

2. Rotation of the specimen around the axis of the shaft (17), and hereafter called the axis of rotation.

3. Lateral movement of the rotation axis of the specimen may be achieved by a lateral displacement of the center slide (8).

4. The specimen can also be moved linearly along the axis of rotation either by sliding the shaft (17) in the journal (16) or by a forward and backward movement of the top slide (12). This last movement is necessary for aligning the specimen in the x-ray beam.

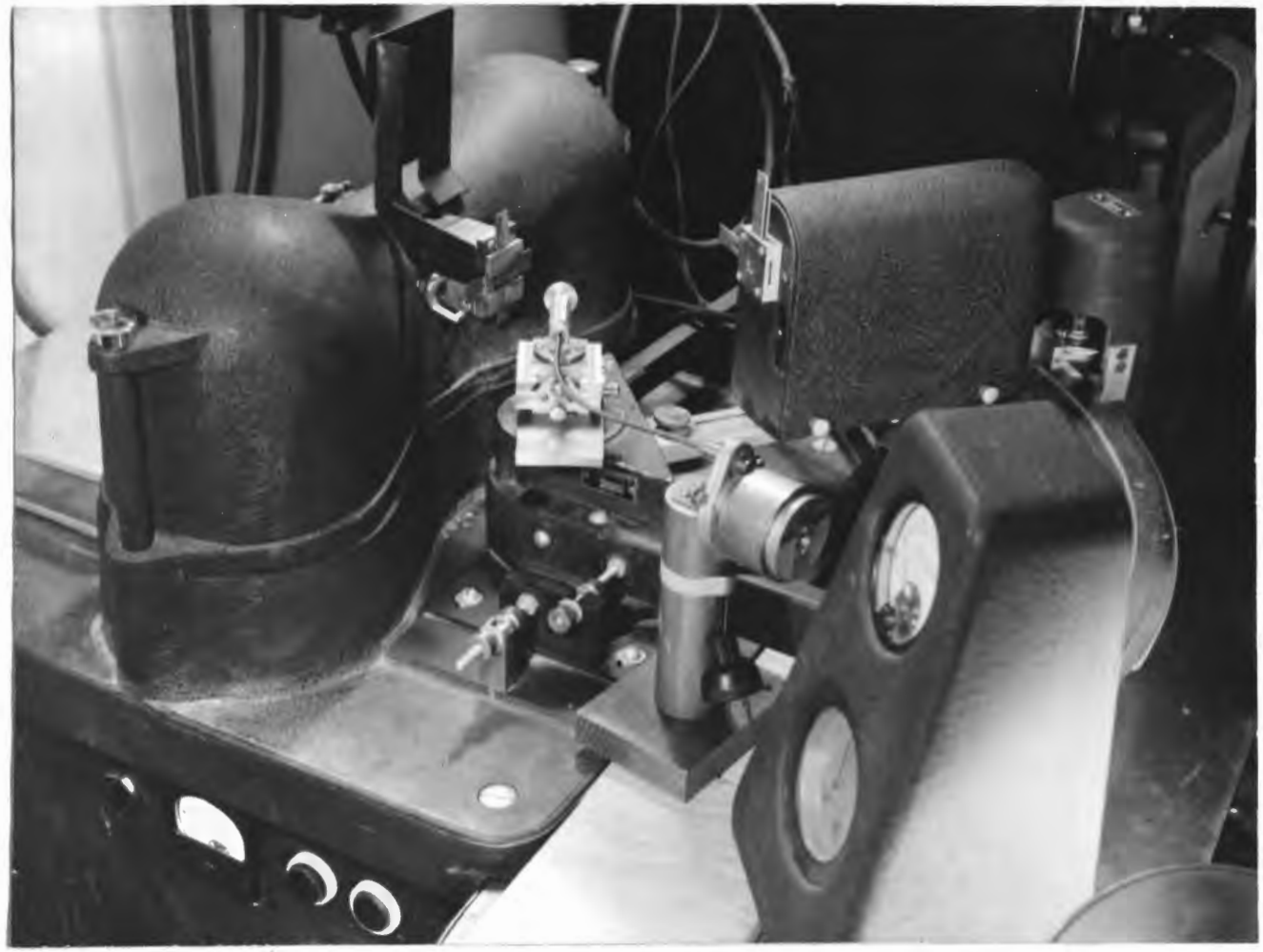

FIGURE 10b. 'Disc Specimen Mount' in operation on an x-ray diffraction spectrometer.

B. USE OF THE DISC SPECIMEN MOUNT

Before any x-ray intensity measurements are made, alignment of the specimen in the incident x-ray beam is necessary.

Alignment of the disc specimen. The disc specimen is fixed centrally on the face plate (18) with any metal cement. A rough adjustment to bring the x-ray specimen in the x-ray beam can be made by a linear movement of the shaft (17) in the journal (16). The final positioning of the specimen in the x-ray beam is then accomplished by further linear adjustments along the axis of rotation. This is done by observing the position of any strong peak in the diffraction pattern and adjusting the specimen by a forward and backward motion of the top slide (12), until the diffracted line appears at its proper 2θ value. This 2θ-value of the selected line is determined by making a standard x-ray diffraction pattern of the specimen being studied.

The final aligned position of the specimen is then fixed by tightening the set screw (14).

Slit system for study of texture variation in cold drawn nickel. Standard slit system of the x-ray diffraction spectrometer was used for the measurement of line intensities. The smallest x-ray tube slit (0.075 centimeter) was employed for the various nickel specimens and the Geiger counter slit was adjusted to obtain readings of satisfactory intensity. With the given tube slit, the shape of the area on the surface of the specimen irradiated by the x-ray beam was a square 0.1 inch on a side.

Measurement of x-ray intensity. After proper alignment of the specimen as discussed in a previous section, the x-ray beam can be made to irradiate any desired area on the surface of the specimen. This is done by a lateral displacement of the center slide (8). The exact position of the area irradiated by the x-ray beam can be determined by means of the scale (11) marked on the front side of the center slide (8) and an index mark on top of the base plate (6). The specimen is rotated at 60 rpm and the Geiger counter is allowed to run few degrees before and through the proper 2θ angle of the planes under investigation. Thus average intensity of reflections from various concentric regions of the specimen are obtained.

Measurements of (111) and 2(100) reflection intensities at the center and at 0.05 inch intervals on the radii of the nickel disc specimens were made in the above described manner. These intensity values were plotted on ordinates of graphs at their corresponding distances from the fibre axis.

APPENDIX IV

LIMITATIONS OF THE POLE FIGURE METHOD FOR ORIENTATION STUDIES IN METALS SHOWING INHOMOGENEOUS TEXTURE

A majority of the techniques for pole figure determination are based on the assumption that the texture developed in a metal during deformation is homogeneous. It was shown in chapter VIII, that considerable variation in texture exists in cold drawn nickel. Similar texture variation in extruded or swaged metals may be expected. Some investigations of textures in drawn, extruded and swaged metals have been reported in the literature, as for example, the study of deformation textures in extruded aluminum rod reported by Jetter and Borie in the May 1953 issue of the Journal of Applied Physics. Unfortunately the existence of texture variation in the metals investigated was not recognized. It seems that a word of caution is warranted for the use of pole figure method for texture studies in metals in which the texture is inhomogeneous.

VITA

The author was born in Lahore, Panjab, India, March 15, 1925. After receiving the B.Sc. degree from The Panjab University in 1944, he joined the College of Mining and Metallurgy B.H.U., where he received his B.Sc. (Met.) degree in 1948.

After working for two and one-half years as a technical supervisor with the Indian Smelting and Refining Company, Bombay, India, he came to the United States and joined the Missouri School of Mines and Metallurgy at Rolla, Missouri, in February 1951. He received a degree of Master of Science from this institution in May 1952. In February, 1952, he received The International Nickel Company Research Fellowship at the Missouri School of Mines and Metallurgy.